

TUNING NITRIC OXIDE SYNTHASE:
INVESTIGATING THE THIOLATE “PUSH”
AND NO RELEASE

Thesis by

Charlotte A. Whited

In Partial Fulfillment of the Requirements for the

Degree of

Doctor of Philosophy

CALIFORNIA INSTITUTE OF TECHNOLOGY

Pasadena, California

2011

(Defended April 25, 2011)

© 2011

Charlotte A. Whited

All Rights Reserved

ACKNOWLEDGEMENTS

First and foremost, I have to thank Harry. I wouldn't have made it through this process without the support and encouragement he gave throughout the five years I've spent in his group. He let me pursue my project wherever that took me scientifically and it is this freedom that lead completion of my thesis. He even sent me all over the country and even to Japan to talk about my work. I cannot thank you enough Harry, I will never forget you! And where there is Harry, there is Jay. Thanks for making our science better and for always pushing us to work harder and to be more thorough.

Thank you to my committee members, Jackie Barton, Doug Rees, and Theo Agapie. Your ideas have been incredibly helpful. I do not deserve all the support you have given me. Thank you for all the time you have invested in me and my work.

Several collaborators have helped significantly with this work. Dr. Emily Weinert (a postdoc with Prof. Michael Marletta at Berkeley) helped me with all of the stopped-flow data found in Chapters 4 and 5. This has been an incredibly fruitful collaboration, with each of us assisting the other. She is a joy to work with. Many insightful discussions with her and with Michael Winter, also in the Marletta lab, deepened my understanding of the more biological side of bioinorganic chemistry. Dr. Jawahar Sudhamsu in the lab of Prof. Brian Crane sent me the plasmid for gsNOS and a detailed protocol for its expression. The ability to work on a thermophilic enzyme made all the difference. Sudhamsu was also kind enough to carefully answer several emails from me with some issues to troubleshoot. Other members of the Crane lab are currently working on crystallizing my protein samples. I am grateful for all their efforts and still have my fingers crossed! I want to also thank Mike Hill at Occidental and several undergraduates who have worked for him (particularly Katie

Lavoie and Bryan Hunter). Mike taught me most of what I know about electrochemistry and Bryan is currently working on finishing up voltammetric studies of my protein samples. Thank you, Mike, for all your instruction and support throughout the past few years. Working with Katie both at Oxy and at Caltech was a wonderful experience — good luck in grad school, Katie!

The majority of my instruction during graduate school came from my peers in the Gray Group. Kyle Lancaster taught me everything I know about molecular biology and protein expression (and collected my EPR spectra). Thank you, Kyle, for not only being a great teacher, but for being an awesome friend! Keep hosting parties and getting everyone out of the lab for a few drinks. Science needs more people like you. Good luck — I know you'll be some big famous guru of bioinorganic chemistry some day! I also want to thank Alec Durrell and Gretchen Keller. It's been a long five years and you guys have not only put up with me but encouraged me, helped me with various things around lab, and commiserated with me when things got bad. Thank you so much for your support, friendship, and company at conferences. I can't believe how much we've been through together and that it's finally coming to an end. Good luck guys — and keep Jay on his toes! Many other members of the Gray Group have been good friends through the years (Paul Oblad, Matt Hartings, Maraia Ener, and Jeff Warren to name a few). There are really too many to list here. This has been a wonderful place to work. Grad school can be hard, but we struggled through our time here together and I am better for it. Thank you.

Jillian Dempsey is an incredible scientist and friend. Jill, you fielded all my lame questions, you trained me on the laser, you listened to all my complaints and frustrations, and somehow you're still friends with me. I knew I would be ok at Caltech when I saw that

Garth CD in your car. I'm really going to miss the days we rocked out to country music in 321 Noyes. I love you dearly and can't wait to see how successful you and Alex will be at UNC over the next few years.

Dad, you inspired me to go into science from the time I was a little girl. I haven't forgotten the rubber band that you froze in liquid nitrogen and shattered on the floor all those years ago. Thank you for all your patience, encouragement, and advice. You understand this whole process so well. I wouldn't be here today if it weren't for you. I love that I am so much like you. And Jim, you're the best big brother a girl could ask for. You supported me, toughened me up, and kept me laughing even when things weren't going well. Thank you, Gayle, for loving and taking care of all of us. Thank you all for being here for my defense, I love you very much and can't wait to move back closer to home!

And my final thank you goes to Matt Whited. I didn't know you were waiting here for me when I decided to come to Caltech, but I'm so glad that you were. Thank you for answering my silly questions, drying my tears, and for sharing this journey with me. Without your constant encouragement I know that I would not have made it to the end of this PhD. I'm looking forward to our next adventure in Minnesota and many more years together.

ABSTRACT

All heme thiolate enzymes have conserved hydrogen bonding networks surrounding the axial thiolate ligand. In order to understand the role of this proximal hydrogen bonding network in nitric oxide synthases (NOS), three mutants of the NOS enzyme from *Geobacillus stearothermophilus* were expressed and characterized. The wild type enzyme has a tryptophan residue at position 70 that π -stacks with the porphyrin ring and donates a long hydrogen-bonding interaction to the thiolate ligand of the heme iron. The native Trp was replaced with His, Phe, and Tyr. These three residues were selected to investigate the two effects of the Trp, H-bonding and π -stacking. Several different spectroscopic techniques were used to investigate the stability and properties of these mutant enzymes. The identity of each mutant was confirmed by mass spectrometry. Both UV-visible absorption and circular dichroism spectroscopies were used to assess the stability of the new proteins. It was shown using binding assays, generation of the ferrous-CO species, and redox titrations that the σ -donating abilities of the thiolate are increased after removal of the hydrogen bonding group in the Trp. Finally, electron paramagnetic resonance spectroscopy and Evans method nuclear magnetic resonance spectroscopy were used to characterize the spin state of the iron center in each mutant, reflecting the increased σ -donating capabilities of the thiolate upon removal of the hydrogen bonding group. The reduction potential of wild type and W70H were determined by chemical titration to be -362 and -339 mV vs. NHE, respectively. This is the first report of the reduction potential of any bacterial nitric oxide synthase.

The reactivity of each the wild type enzyme and the three new mutants was tested using stopped-flow mixing coupled with UV-visible absorption spectroscopy and the

Griess Assay. Autoxidation rates measured by stopped-flow suggest that the Tyr and Phe mutants do indeed have significantly more negative reduction potentials, but that the His mutant is particularly slow to oxidize. The Griess Assays showed that all four enzymes produce nitrite in solution, when provided with substrate, cofactor and hydrogen peroxide (as a source of reducing equivalents). In single turnover experiments, however, only three of the four enzymes showed evidence of ferric-NO production. The His mutant showed no intermediate absorbance near 440 nm (which would be indicative of ferric-NO formation), suggesting that it releases NO^- rather than the radical species NO^\bullet . The role of this hydrogen bond is concluded to be an electronic one, rather than playing any part in positioning the heme. It prevents formation of the inactive P420 species, and tunes the reduction potential to one high enough to be reduced by a reductase but low enough to still deliver an electron to the redox active cofactor, tetrahydrobiopterin, at the end of catalysis.

The rate at which NO is released by each NOS enzyme varies greatly among isoforms and species, over nearly two orders of magnitude. One residue (an isoleucine located above the heme in bacterial enzymes) involved in the gating of NO release has been previously identified by Stuehr. However, this single residue does not account for the entirety of the differences among the forms of NOS. Another residue, a histidine at position 134 in NOS from *Geobacillus stearothermophilus* (gsNOS), was hypothesized to also participate in gating NO release based on an observed correlation between rates of NO release and the bulk of side chains at this position. Each single point mutation, H134S and I223V, and the double mutant were expressed in gsNOS and their reactivity toward the diatomic molecules CO and NO were studied. CO rebinding was investigated using laser flash photolysis and NO release using stopped flow UV-visible spectroscopy. The presence

of both monomer and dimer was observed in solution, and position 134 was shown to be another key residue in gating NO release. Wild type gsNOS contains both the bulkier Ile223 and His134 and has the slowest measured NO release (0.039 s^{-1}) of all NOS enzymes. A new, more accurate kinetics model for turnover is proposed. Each single mutation increased NO release substantially, while the double mutant has a rate constant of 1.0 s^{-1} , nearly as fast as mammalian iNOS at 2.3 s^{-1} , identifying position 134 as another important factor determining rate constants for NO release.

TABLE OF CONTENTS

Acknowledgements	iii
Abstract	iv
Table of Contents	ix
List of Figures	xi
List of Schemes	xiii
List of Tables	xiv
Chapter 1: Introduction and Background	1
Nitric Oxide Synthases	2
Mechanism of NO Production	6
Bacterial Nitric Oxide Synthases	9
An Interest in Heme-Thiolates	15
Tools of the Bioinorganic Chemist	19
Conclusion	21
References	23
Chapter 2: An Interest in Thiolate Coordination	27
Introduction	29
Materials and Methods	45
Results and Discussion	50
Concluding Remarks and Discussion	60
References	65
Chapter 3: Hydrogen Bonding Mutants: Thermodynamics	69
Introduction	71
Materials and Methods	82
Results and Discussion	92
Conclusions	109
References	111
Chapter 4: Hydrogen Bonding Mutants: Kinetics	116
Introduction	118
Materials and Methods	124
Results and Discussion	127
Conclusions	138
References	141
Chapter 5: Pathway Mutations and NO Release	143
Introduction	145
Experimental Methods	150
Results	153
Discussion	162
Conclusions	174
References	176
Chapter 6: Electrochemistry of gsNOS	180

Introduction.....	182
Materials and Methods	187
Results.....	188
References.....	196
Chapter 7: Conclusions and Future Work.....	198
Roles of Hydrogen-Bond Donating Groups	199
Gating Diatomics in NOS	202
Future Directions	203
Appendix I: Wires Review	A1
Appendix II: Labeling gsNOS.....	A18

LIST OF FIGURES

<i>Number</i>	<i>Page</i>
1.1 Domains of NOS	5
1.2 Structure of bsNOS and iNOS	10
1.3 Structure of gsNOS	14
1.4 Rhenium wire in binding pocket.....	18
1.5 Absorption spectra of several forms of NOS.....	20
2.1 Electronic states of a DBA molecule.....	31
2.2 Tunneling timetables	34
2.3 Potential energy curves for electron transfer	35
2.4 Rhenium wire in binding pocket.....	38
2.5 Absorption spectra of iNOS:wire complexes	40
2.6 Luminescence spectra of iNOS and iNOS:wire	41
2.7 Transient difference spectra of reduced iNOS	42
2.8 Transient absorption spectra of iNOS.....	43
2.9 Absorbance spectra of ascorbate and TMPD	49
2.10 Transient absorbance spectra of quenched tmRu-F ₉ bp	50
2.11 Transient luminescence of Ru(bpy) ₃ ²⁺	51
2.12 Luminescence decay of wire bound to iNOS	53
2.13 Transient absorbance of iNOS:wire complex.....	54
2.14 Transient absorbance of quenched iNOS:wire complex.....	55
2.15 Transient generation of Fe(III/II) difference spectrum	56
2.16 Transient absorbance of iNOS:wire complex.....	57
2.17 Transient absorbance of iNOS:wire complex.....	57
2.18 Steady-state reduction of iNOS	59
2.19 The heme center to NOS	62
3.1 Close up of heme center	77
3.2 Thermal denaturation curve of gsNOS	80
3.3 Crystal structure of gsNOS	81
3.4 Cuvette used for Hemochromagen Assay	86
3.5 Apparatus used for redox titrations.....	91
3.6 Thermal denaturation curves for all four NOS mutants.....	92
3.7 Ferrous-CO complex of wild type gsNOS	94
3.8 Ferrous-CO complex of W70F gsNOS	94
3.9 Spectral changes induced by imidazole.....	96
3.10 Calculation of dissociation constants from gsNOS.....	97
3.11 Absorbance changes upon introduction of arginine	97
3.12 Formation of the gsNOS “hemochrome”	99
3.13 Absorbance spectra of gsNOS mutants	100
3.14 EPR spectra of four gsNOS mutants	101–102
3.15 Spectroelectrochemistry of Ru(acac) ₃	106

3.16 Redox titration of wild type gsNOS	107
3.17 Redox titration of W70F gsNOS	107
4.1 Close up of heme-thiolate with Trp70	124
4.2 Autoxidation of W70F ferrous gsNOS	128
4.3 Autoxidation of W70H ferrous gsNOS with substrate	129
4.4 Single turnover reaction of wild type gsNOS.....	135
4.5 Single turnover reaction of W70Y gsNOS	136
4.6 Single turnover intermediates of W70Y gsNOS	136
4.7 Single turnover reaction of W70H gsNOS	137
5.1 Absorption spectra of gsNOS	154
5.2 Steady-state Fe(II)-CO/Fe(II) difference spectrum	155
5.3 Transient generation of five-coordinate Fe(II)	156
5.4 Transient difference spectrum of gsNOS	157
5.5 Kinetics traces for each of four mutant enzymes	158
5.6 Single turnover experiment with gsNOS.....	161
5.7 Generated fits for both single and double exponential.....	163
5.8 Spectra of intermediates for H134S/I223V	168
5.9 Spectra of intermediates for wild type.....	169
5.10 Spectra of intermediates for five-state model.....	173
6.1 Depictions of proteins in films	184
6.2 Method of attachment of gsNOS	189
6.3 Cyclic voltammograms of attached gsNOS	189
6.4 Voltammetric response at 100 mV/s.....	190
6.5 Fit of scan rate dependence to Equation 6.1	191
6.6 Cyclic voltammogram of gsNOS, attached with PEG linker	192
6.7 Background-subtracted cyclic voltammograms	192
6.8 Cyclic voltammograms of gsNOS in DDAB film	193
6.9 Cyclic voltammograms of W70F gsNOS in DDAB film	194

LIST OF SCHEMES

<i>Number</i>	<i>Page</i>
1.1 Production of NO by NOS	3
1.2 Electron transfer cofactors in NOS	4
1.3 Reaction mechanism of NOS	8
2.1 Photosynthesis and respiration	29
2.2 Flash/quench schemes	36
2.3 Reaction mechanism of NOS	37
2.4 tmRu-F ₉ bp	45
2.5 Reversible flash/quench experiment	52
2.6 Oxidation of TMPD	53
3.1 Five-electron oxidation of arginine	72
3.2 Reaction mechanism of NOS	74
4.1 Production of NO by NOS	119
4.2 Reaction mechanism of NOS	120
4.3 Electron transfer cofactors	121
4.4 Reaction scheme for the Griess Assay	122
4.5 Reaction of oxygen with ferrous NOS	127
4.6 Reaction of reduced NOS with oxygenated buffer	133
5.1 Reaction mechanism of NOS	146
5.2 Model for conversion of ferrous to ferric NOS	160
5.3 Standard kinetics model for recombination	162
5.4 Modified kinetics model for CO	166
5.5 Five-state model for NO kinetics	170
6.1 Surfactants for making films	185
6.2 Maleimide-terminated thiol	188

LIST OF TABLES

<i>Number</i>	<i>Page</i>
2.1 Ru and Re wires that bind to iNOS.....	39
3.1 Spectral dissociation constants of imidazole and arginine.....	98
3.2 Molar absorptivities of four NOS mutants	99
3.3 EPR g-tensors of each mutant.....	102
3.4 Number of unpaired electrons by Evans method	103
4.1 Rate constants for autoxidation of NOS	130
4.2 Nitrite production rates by gsNOS mutants.....	131
5.1 CO recombination rates.....	158
5.2 Percentage of each rate constant by mutant.....	159
5.3 Rate constants for NO release	161
5.4 Effects of concentration on relative amplitudes	164
5.5 Power dependence	165
5.6 Full kinetics details for single turnover of each mutant	171
6.1 Reduction potentials of cytochrome P450-BM3	182
6.2 Measured reduction potentials of four NOS mutants.....	194

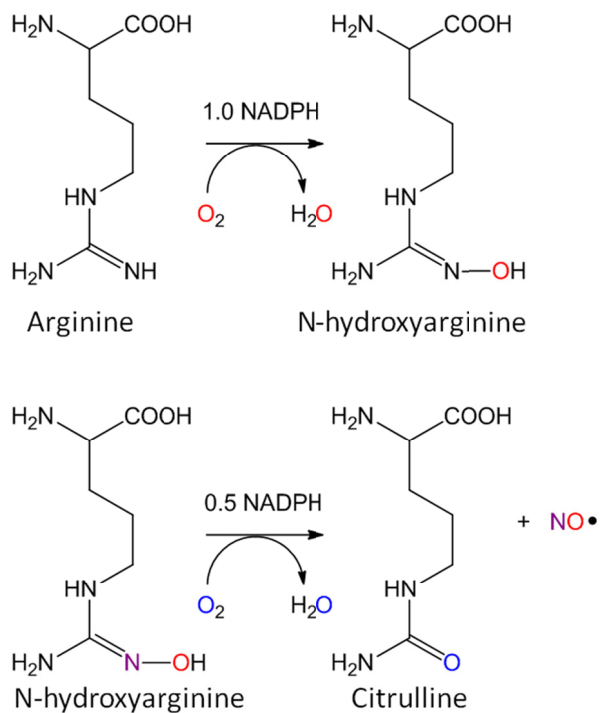
Chapter 1

Introduction and Background

1.1 Nitric Oxide Synthases

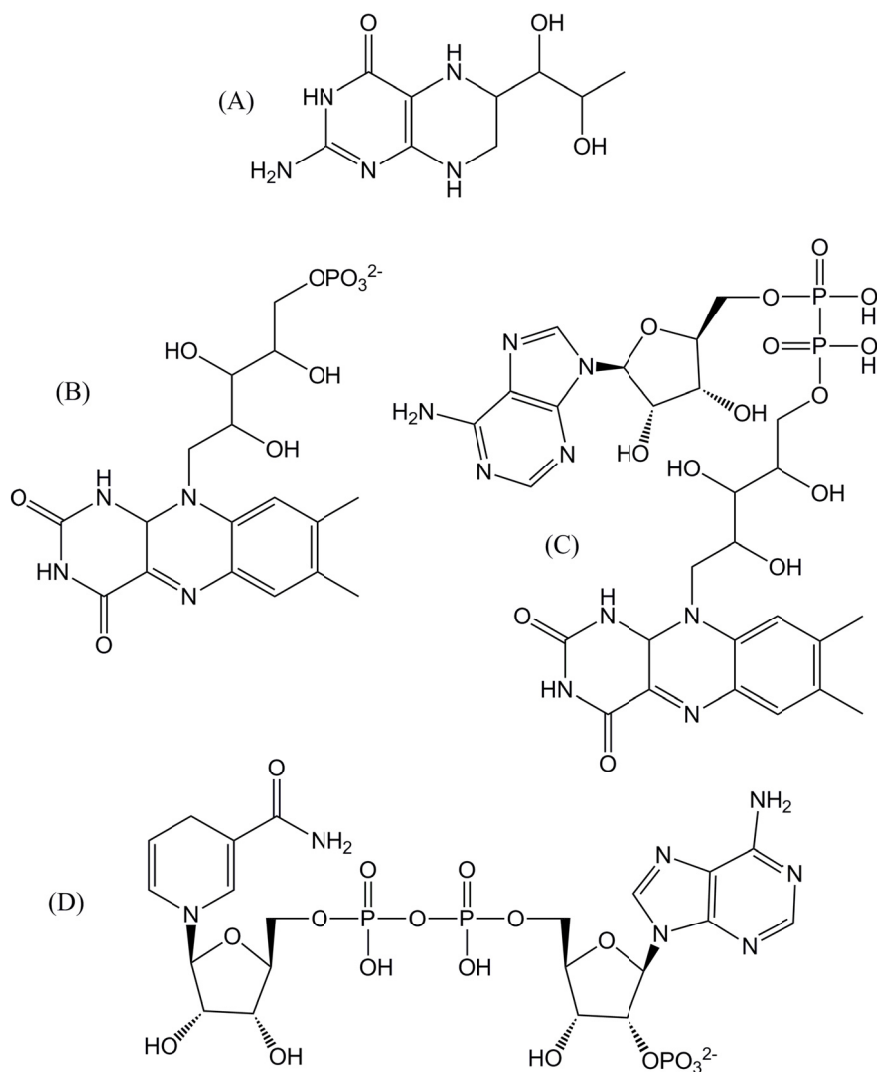
Salvador Moncada and colleagues reported in 1987 that the molecule responsible for relaxation of blood vessels is nitric oxide (NO).¹ This publication marked the beginning of a new area of chemical and biological research, now with thousands of articles published each year. Long known as a cytotoxic agent in pathological processes and a major component of smog, NO is now recognized as a key signaling molecule in the cardiovascular, immune, and nervous systems.²

Nitric oxide synthases (NOSs) are responsible for the production of NO in living systems.³ The three (mammalian) isoforms of the enzyme are named for the tissues in which they are found: endothelial NOS (eNOS), neuronal (nNOS), and an inducible form found in macrophages (iNOS).⁴ NOS enzymes have been identified in some bacterial species as well, such as *Bacillus subtilis* and *Sorangium cellulosum*.⁵⁻⁶ NOS catalyzes the oxidation of L-arginine (Arg) to L-citrulline in two turnovers, with N-hydroxy-L-arginine (NOHA) as an enzyme-bound intermediate (the product of the first turnover). The overall reaction is shown in **Scheme 1.1**.



Scheme 1.1. Production of NO by nitric oxide synthases from the starting material arginine.

Each mammalian enzyme forms a homodimer of two identical polypeptide chains.⁷ Each single, long (1000+ residue) chain contains a reductase domain, a calmodulin linker, and an oxygenase domain (**Figure 1.1**). The reductase domain contains binding sites for NADPH (nicotinamide adenine dinucleotide phosphate) and the flavins FMN (flavin mononucleotide or riboflavin 5'-phosphate) and FAD (flavin adenine dinucleotide), all cofactors are shown in **Scheme 1.2**.⁸ The calmodulin linker is a calcium responsive agent that causes structural changes in the presence/absence of Ca²⁺. The oxygenase domain binds the substrates (arginine and N-hydroxy-L-arginine), a heme cofactor, and a redox-active tetrahydrobiopterin cofactor. It is at the heme cofactor in the oxygenase domain where oxidation of substrate occurs.



Scheme 1.2. Cofactors involved in electron transfer in NOS: (A) tetrahydrobiopterin, (B) FMN, (C) FAD, and (D) NADPH.⁹

The mammalian isoforms are regulated through a complicated system of checks and balances. The functions of eNOS and nNOS are regulated by calcium ions and a calmodulin linker, while iNOS is calcium ion independent.¹⁰ Calmodulin is a polypeptide chain, in this case literally fused to the chain of the NOS enzyme, and is very sensitive to the presence of calcium regulating eNOS and nNOS by preventing electron transfer to the oxygenase domain in the absence of Ca.¹¹ On the other hand, the levels of expression of inducible NOS is regulated very carefully within white blood cells.¹⁰ Further, the

reduction potential of iNOS is also controlled by the presence of substrate in order to prevent release of reactive oxygen species. (When Fe(II) is produced in the absence of substrate, oxygen binds, oxidizes the iron to Fe(III), and is released as superoxide.)¹²

The oxygenase domain (NOSoxy) contains a thiolate-ligated heme (protoporphyrin IX, or P-IX) as in cytochromes P450 (P450) and (6R)-5,6,7,8-tetrahydrobiopterin (pterin, H₄B). NO is produced when this domain is supplied with electrons from the reductase domain to activate dioxygen, in the presence of fully reduced pterin cofactor. In the absence of H₄B no NO is produced, but rather other NO_x species.¹³ Although structural characterization of full-length NOS has not been reported to date, structures of individual domains are known.¹⁴⁻¹⁵

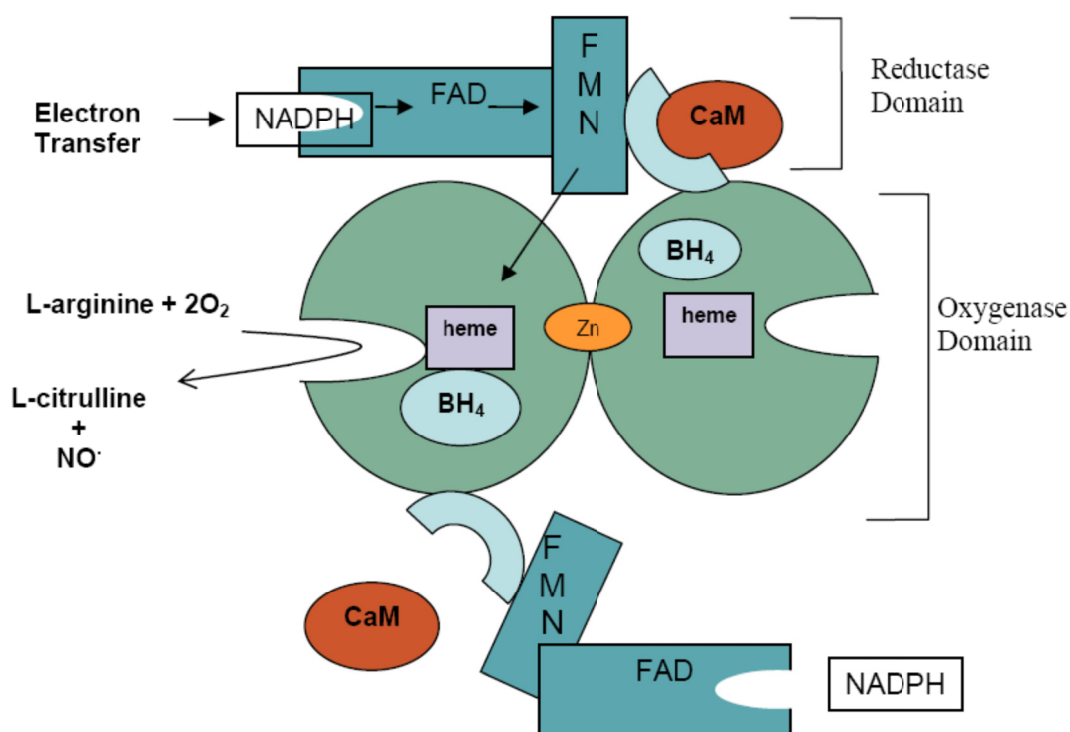


Figure 1.1. Graphical representation of the domains and geometry of nitric oxide synthases. (YHL Nguyen, PhD thesis from Caltech). (Note: No crystal structure of any full-length mammalian nitric oxide synthase has ever been reported, only the separate domains, thus it is still unclear how and where the two domains interact.)

1.2 Mechanism of NO Production

Arginine is oxidized to nitric oxide in two full turnovers, through the intermediate N-hydroxy-L-arginine. The intermediate actually has a higher binding affinity than arginine, preventing it from leaving the binding pocket, where it is positioned above the heme.¹⁶ The first turnover is a two-electron oxidation of substrate, formally a hydroxylation of one of the guanidinium nitrogens.² The stoichiometry of this reaction is identical to that of hydroxylations carried out by the extensively-studied cytochromes P450.¹⁷⁻¹⁸ The second reaction, however, is unique in biology. The use of the tetrahydrobiopterin in a redox-active manner (**Scheme 1.3**) is unique to NOS. Also, the second turnover is formally a three-electron oxidation of NOHA to citrulline and NO, specifically the radical species and not any other nitrogen oxide.³

The mechanism of NO production is not completely understood. The resting state of the enzyme is a six-coordinate ferric heme with a water molecule occupying the sixth ligand position (four positions are occupied by N donors from the porphyrin and one by a sulfur atom from an axial cysteine, Cys194).⁸ Although neither Arg nor NOHA ligates the heme, substrate binding shifts both the Soret absorption maximum and the heme spin state. The presence of substrate in the binding pocket sterically excludes water, forcing a high-spin five-coordinate heme complex.¹⁸ One-electron reduction of the NOS:substrate complex gives a five-coordinate ferrous heme that readily binds dioxygen, forming a ferrous-oxy species (equivalent to ferric superoxide), the last observed intermediate in the catalytic cycle.¹⁹

The role of pterin has been extensively investigated. This molecule binds in a pocket alongside the heme, forming a hydrogen bond with a protoporphyrin-IX carboxylate, thereby coupling it to the active site.²⁰ It is known that a pterin-based radical forms and is reduced during the catalytic cycle, as determined by analysis of results from rapid-freeze EPR experiments.²¹⁻²³ Production of NO has never been observed without fully reduced pterin cofactor, such conditions produce cyano-ornithine and nitrite rather than citrulline and NO.¹³

The NOS reaction cycle bears many similarities to that of cytochromes P450 (cyt. P450). Cyt. P450s contain thiolate-heme active sites and hydroxylate substrates via two-electron oxidation processes.¹⁸ The cyt. P450 cycle also begins with substrate binding followed by heme reduction, dioxygen binding, and another reduction step leading to the formation of a high-valent iron-oxo complex (Compound I) that hydroxylates the substrate (**Scheme 1.3**). Separate enzymes serve as reductases for most cyt. P450s, but substrate hydroxylation can be driven using external sources of electrons.¹⁷ It is of note that one cytochrome P450 has been found with an attached reductase domain: cyt. P450 BM3.²⁴ The reductase domain of this enzyme also shuttles electrons from NADPH through two flavins to the heme cofactor just like mammalian NOS, although it does not need to dimerize to function as NOS does. Owing to these similarities, the mechanism of the first turnover of NOS is postulated to be the same as that of cyt. P450s. However, the second turnover, a three-electron oxidation, is thought to employ a unique mechanism.²⁵ It has been suggested that a protonated ferric hydroperoxide may act as the nucleophile in the second turnover rather than Compound I, which is a ferryl P-IX radical cation.¹⁶

Another similarity between cyt. P450s and NOSs is the presence of three universally-conserved hydrogen bond donors to the axial thiolate ligand. All three come from backbone amide groups in P450, but in NOS only two come from amides, the third donor being the N-H group on a tryptophan residue.²⁶⁻²⁷ This Trp is conserved in every NOS identified to date.²⁸ In P450, there is a phenylalanine in that position which π -stacks with the porphyrin ring, just as this Trp does, although it is in no way involved in hydrogen bonding. The role of these hydrogen bond donors and π -stacking in tuning the electronics of the thiolate donor and porphyrin ring has not previously been fully investigated. The fact that these donors come from amides in the backbone make

mutagenesis nearly impossible (one was replaced by a proline residue, removing the amide group, but also shifting an entire loop within the protein, confusing results).

Steps in the mechanistic cycle borrowed from cyt. P450 are shown in **Scheme 1.3**. Although several intermediates in the cyt. P450 cycle already have been observed, there can be no doubt that “the hunt for an unambiguous experimental identification of the ephemeral active oxygen species will most certainly continue”.²⁹ In fact, after several decades of research on cyt. P450s it was only within the past year that the elusive, high-valent Compound I was positively characterized and shown to be the active hydroxylating oxidant.³⁰ If that is the case for cyt. P450, then we may conclude that work on the NOS catalytic cycle is just beginning.

1.3 Bacterial Nitric Oxide Synthases

The function of inducible nitric oxide synthase in mammalian macrophage cells is predominantly to kill the cells of invading bacteria by pumping them full of nitric oxide.¹⁰ NO is a radical species and therefore reacts rapidly with many parts of cells causing extensive damage. Given its usefulness in killing bacterial cells, it was surprising when researchers discovered NO synthase-like proteins in prokaryotic systems in the early 2000s.³¹⁻³² Since then, NOS-like proteins have been identified in all kingdoms of life, with examples in archaea and bacteria, emphasizing their biological importance.⁵ Their presence in several pathogenic species is of particular interest. The bacterial NO synthases from three phyla of Gram-positive bacteria (actinobacter, deinococcus, and firmicutes) in particular share high levels of homology with the oxygenase domains of eukaryotic enzymes.⁶

Bacterial enzymes share many similarities with their mammalian counterparts. First, they share surprising sequence homology, with about 45% of their peptide sequences being identical and 50–60% similar.³³ Comparison of their overall three-dimensional folds reveals strikingly similarities (**Figure 1.2**); nearly every helix and loop is mirrored in each system studied to date.⁵ All important residues are maintained, those involved in hydrogen bonds with the substrate and cofactors, and the cysteine providing iron ligation, to highlight a few. All NOS oxygenase domains, regardless of species of origin, contain binding sites for the heme cofactor (protoporphyrin-IX), substrate, and the necessary pterin. All of these overlay exactly when aligning multiple structures, if one simply centers the structures around the iron atom in the heme.^{32, 34} Every NOS requires substrate, both cofactors, reducing equivalents and dioxygen to function. When these pieces are combined, NO is produced catalytically.

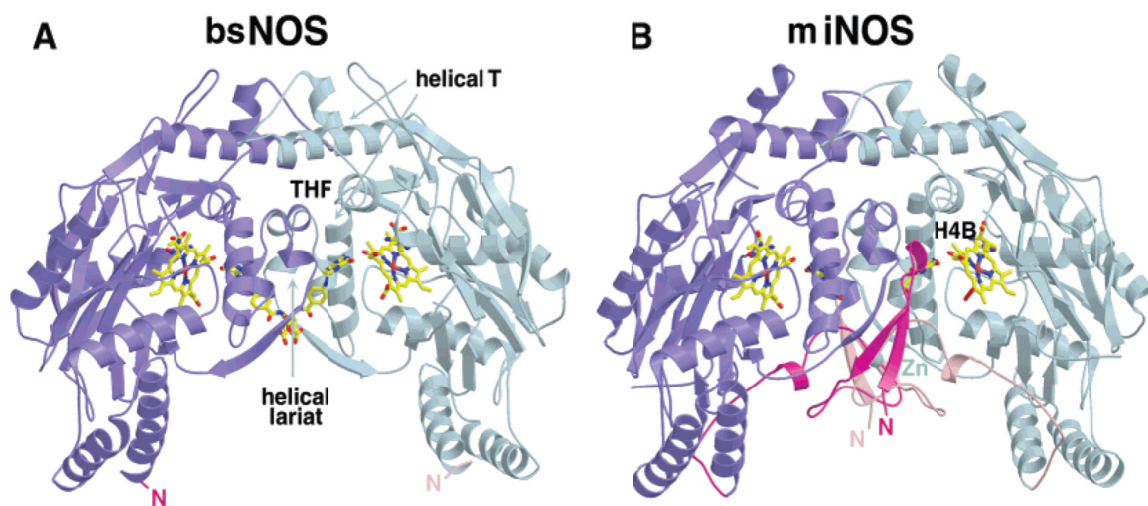


Figure 1.2. A crystallographic comparison of the three-dimensional folds of a bacterial NOS (A, from *Bacillus subtilis*) and a mammalian NOS (B, from inducible NOS found in mammalian macrophages). Note that all NOS oxygenase domains crystallize as a dimer. The missing N-terminal Zn-binding loop is highlighted in fuchsia, B.³²

There are also, however, some striking differences between bacterial and eukaryotic systems. The largest difference is that only one bacterial NOS (bNOS) has been identified to date that contains a fused reductase domain within its amino acid sequence.³⁵ Nearly all bNOS enzymes are made up of only the oxygenase domain where the chemistry of NO production occurs (the NOS from *Sorangium cellulosum* being the only exception). This raises the question of how reducing equivalents can be delivered. bNOS is also missing a zinc-binding loop contained in all the mammalian isoforms. This loop is necessary for the dimerization of mammalian systems, a requirement for function because a reductase domain from one monomer of enzyme provides the reducing equivalents for the oxygenase domain of the other monomer.³⁶ Truncation of the peptide chain in order to remove this loop results in the abolishment of catalytic activity. This loop partially obstructs the pterin cofactor binding site, protecting it from solvent.³⁷ Some bacteria cannot synthesize tetrahydrobiopterin, they simply lack the necessary sequences in their genomes.⁶ It has been proposed that removal of this loop allows room to accommodate the larger pterin, tetrahydrofolate, which all these bacteria are able to synthesize.⁵ The final major difference is a single point mutation near the heme. This position is a conserved valine among eukaryotic systems, while in bacteria it is an isoleucine.³⁸ It has been shown previously that this residue, situated right above the iron atom and within Van der Waals contact distance of Fe-NO species (Ile), affects the rate of NO release from the enzyme.³⁹ These differences may highlight key functional differences among species.

Given these few but striking differences, it was necessary to prove that bacterial NO synthase-like proteins did in fact produce nitric oxide, and using the same chemistry

as their eukaryotic counterparts. One landmark study required the collaboration of three groups, those of Stephen Lippard, Dennis Stuehr and Evgeny Nudler.³³ It is a complicated process to definitively prove that an enzyme functions and produces NO, not any other species, *in vivo*. In oxygenated aqueous solution, NO is oxidized rapidly to nitrite and nitrate. Reagents have been developed that can colorimetrically detect these NO metabolites in solution (Griess Assay, Cayman Chemicals). As NO transforms to NO_2^- and NO_3^- in solution, the concentration of these in solution is proportional to the amount of NO produced.³⁴ This team of researchers used both the Griess Assay to detect NO in the extracellular environment of the cells of *B. subtilis* and *B. anthracis* and an NO-specific fluorescent probe called CuFL that allows for intracellular NO detection. These techniques, in combination with creative use of an arabinose promoter, allowed them to prove that NO is indeed produced in these cells by their NOS enzymes.

The demonstration of NO synthesis within bacterial cells raises the question of why NO is produced.⁶ The signaling functions of NO in eukaryotic systems are mediated by the NO receptor, soluble guanylate cyclase (sGC).⁴⁰ A bacterial homolog of sGC has been identified as a family of H-NOX proteins found by Michael Marletta and coworkers.⁴¹ Interestingly, though, no H-NOX protein has been found in the genome of any bacteria that also code for NOS.⁴² No other NO receptors have been identified. It has been proposed that in pathogenic bacteria the synthesis of NO promotes resistance to oxidative stress caused by the host immune system.⁴³ NO may also promote antibiotic resistance, due to its ability to chemically modify many compounds used as antibacterial agents.⁴⁴ While these hypotheses may explain the role of NO in pathogenic strains such

as *Staphylococcus aureus* and *Bacillus anthracis*, the role of NO in non-pathogenic bacteria remains a mystery.

The NOS (gsNOS) from a non-pathogenic bacterial thermophile, *Geobacillus stearothermophilus*, is the focus of this majority of this work. Only one chapter deals with the mammalian inducible isoform, the rest focus on this unique bacterial enzyme. gsNOS is noted for the particularly stable ferrous-oxy complex it forms.³⁴ This complex lasts only a few seconds at most in other enzymes, but is stable on the order of a minute in gsNOS at 4 °C. It is not incredibly surprising that the kinetics of this enzyme are slower at standard temperatures than other enzymes, given it comes from a thermophilic organism and must function properly at significantly elevated temperatures. It is this stability that makes this a useful system to study. This enzyme was originally expressed, characterized, and crystallized by Brian Crane and coworkers at Cornell.³⁴ The protein fold as revealed by X-ray crystallography is shown in **Figure 1.3**, with a close-up on the heme-thiolate active site.

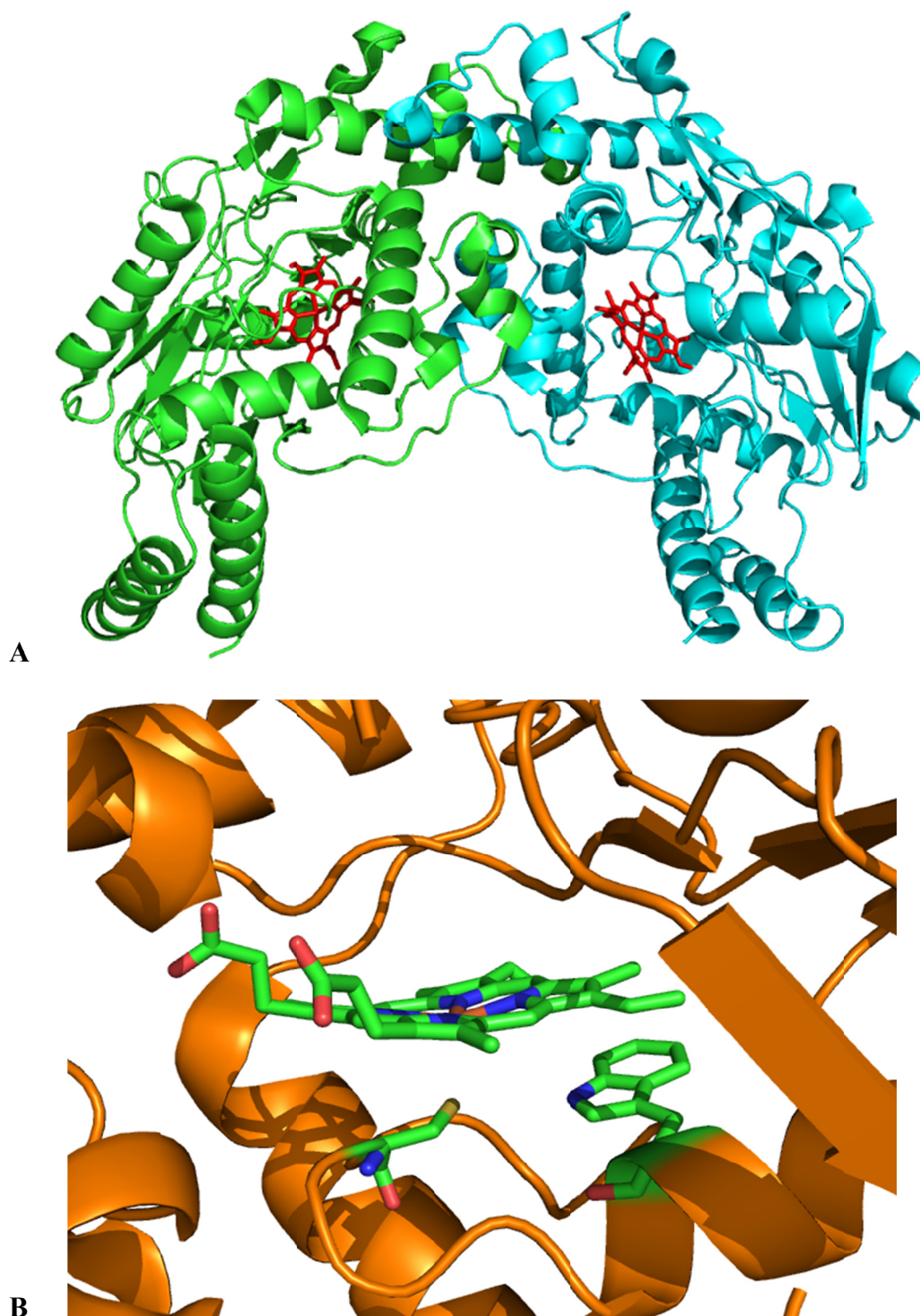


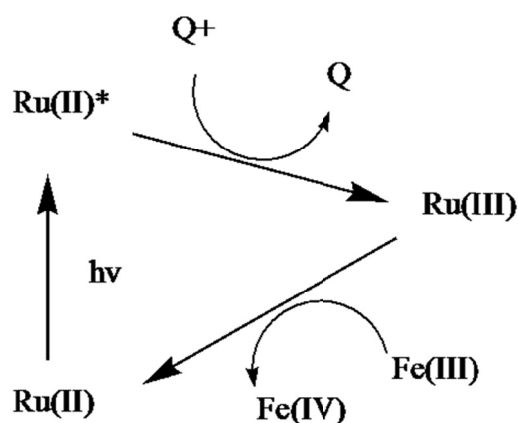
Figure 1.3. (A) Three-dimensional fold of gsNOS: the two peptide chains are shown in green and teal, with the heme highlighted in red. Note the strikingly similarity to the folds of bsNOS and iNOS (**Figure 1.2**). (B) An expanded view of the heme-thiolate active site of gsNOS, showing the axial cysteine ligand and a conserved tryptophan residue that hydrogen bonds to the thiolate and stacks with the porphyrin rings (PDB file 2FLQ).

1.4 An Interest in Heme-Thiolates

The Gray group has had a long-standing interest in heme-thiolate systems, specifically high-valent iron-oxo species long believed (and only recently proven) to be the active hydroxylating species in cytochromes P450. Our work on high-valent iron hemes actually began in the mid to late 1990s. The group had developed a technique called flash/quench, a general scheme of which is shown in **Scheme 1.4**.⁴⁵ In this process, a photosensitizer such as ruthenium(II) tris(2,2'-bipyridine (or bpy)) is excited by illumination with visible light (into its metal to ligand charge transfer band) creating an excited state with a lifetime of more than 600 μ s (the flash). Interestingly, this excited state has a significant driving force to either gain or lose an electron, about 0.8 V.⁴⁶ In the presence of another reactant, such as ruthenium(III) hexaammine, the excited state reacts (is quenched) to form Ru(II) hexaammine and Ru(III)(bpy)₃. This Ru(III)(bpy)₃ species is an incredibly potent oxidant, with a driving force of nearly 1.3 V (in aqueous solution). Not only does flash/quench provide a more potent reactant, but often the further separation of charges produces a longer lifetime for the oxidizing species, allowing more time for the desired reaction to occur. (This same flash/quench scheme can be performed using a reductive quencher such as octacyano molybdate to produce the strong reductant Ru(I)(bpy)₃.)

Both reversible and irreversible quenchers can be used. In reversible systems, the quencher eventually reacts with either Ru(III) or another oxidized species to reform all of the original species in their resting oxidation states. For irreversible systems, once the quencher reacts with the excited photosensitizer it undergoes further chemistry,

preventing any back reactions; the system can never return to its resting state and with each laser pulse the reactants are consumed. Co(III) complexes are typical irreversible oxidative quenchers — once reduced, the ligands become labile and are replaced by water to form the hexaaquoCo(II) complex, which is much more difficult to oxidize again. The development of this technique has allowed the Gray group to study several interesting reactions that cannot occur on the timescale of the Ru(II)^* excited state.



Scheme 1.4. An oxidative flash/quench scheme, where Ru represents the photosensitizer Ru(bpy)_3 , Fe represents the iron within the heme cofactor, and Q is an oxidative quencher such as ruthenium hexaammine (so named because of its effect on the photosensitizer).

One such reaction viewed only using flash/quench involves the heme system microperoxidase-8 (MP8).⁴⁷ MP8 is a peptide containing only 8 amino acids, including two cysteines which form thioether links to a *c*-type heme. Remarkably, this tiny peptide and cofactor can still carry out peroxidation reactions. In an attempt to generate high-valent iron species in this histidine-ligated heme, researchers combined MP8, Ru(bpy)_3 and $\text{Ru(NH}_3)_6$ in buffered aqueous solution. Upon irradiation with a 10 ns pulse of 470 nm light from an Nd:YAG-pumped OPO (optical parametric oscillator), the Ru(II)(bpy)_3^* excited state forms. This then reacts with the $\text{Ru(NH}_3)_6$ on the nanosecond timescale to form Ru(III)(bpy)_3 . This Ru(III) species then oxidizes the iron atom of MP8

to form an oxidized, formally Fe(IV) species. Both Compound II (ferryl) and Compound I (ferryl + porphyrin radical cation) were observed. This process was repeated with the enzyme horse radish peroxidase (HRP).⁴⁸ With this system, and irreversible oxidative quencher was needed in order to afford enough time to transfer an electron from the heme center to the Ru(III) species. The characterization of these species furthered our understanding of their catalytic cycle.

The group then wished to extend this process to generate high-valent iron species in more complex systems, particularly cytochromes P450. Unfortunately, this afforded no detectable reaction. In fact, the use of irreversible quenchers led only to the degradation of their protein systems. The highly oxidized Ru(III) will find something to react with, even if it cannot perform the desired reaction with the iron, effectively leading to oxidative destruction of the protein.

In an effort to observe these elusive high-valent species in a cyt. P450, the group then began developing what later came to be called “wires”. Wires are modified photosensitizers, similar to the traditional Ru(bpy)₃ but with an additional component.⁴⁹ In examining the crystal structures of HRP and cyt. P450s, it became clear that while the heme of HRP was exposed to solvent (and therefore solution) on one edge, the heme of cyt. P450 was completely buried by the protein backbone. Researchers needed a way to promote interaction between the photosensitizer and the active site. The second component of these wires addressed this issue of coupling to the protein by attaching a tail group to the photosensitizer head (**Figure 1.4**). The tail group typically resembled the substrate of the particular cyt. P450 under study, bringing the Ru moiety closer to the heme, in effect, wiring the two together.

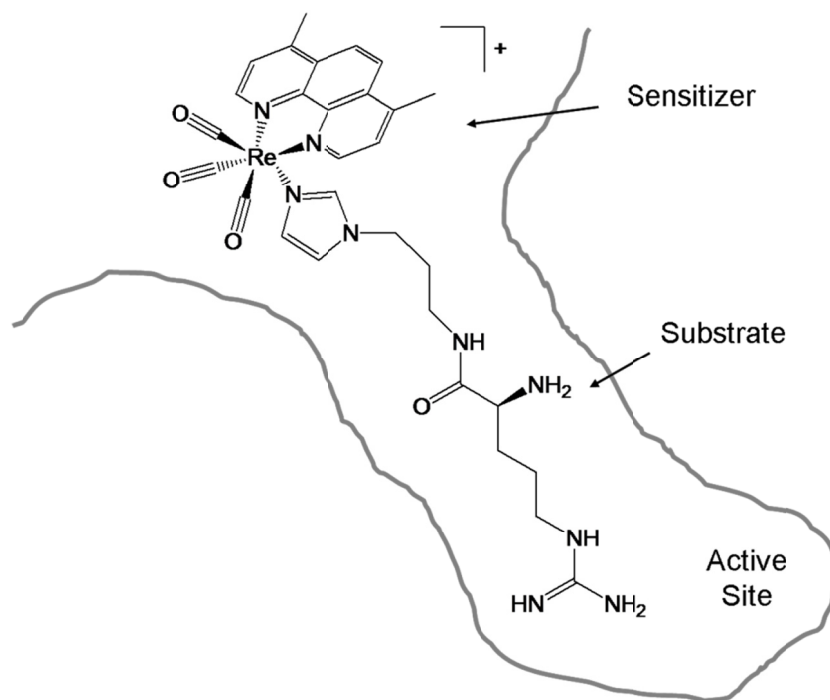


Figure 1.4. Schematic representation of a rhenium wire linked to an arginine-like tail binding within the NOS substrate binding pocket.⁴⁹

While these wires were never successfully used to generate high-valent iron, they were shown to photochemically reduce the iron centers of both cyt. P450 BM3 and iNOS.⁵⁰ Several systems were developed for each enzyme and their binding thoroughly characterized, but while forward electron transfer to the heme was observed in high yield, catalysis was blocked by the presence of the wire in the substrate binding pocket. This project did, however, reveal several interesting aspects of the nature in which cyt. P450s bind their substrates.⁵¹ The presence of a second heavy metal assisted in crystallization efforts and allowed researchers to observe significant conformational changes not before observed. The Gray group has also characterized both of these enzyme electrochemically, but again, without production of high-valent species.⁵²⁻⁵³ The goal of generating these species is ultimately to understand their catalytic cycles more completely, and in NOS in

particular there remain many questions about the exact mechanism by which NO is produced.

1.5 Tools of the Bioinorganic Chemist

The ultimate goal of the work presented herein is to further our understanding of the catalytic cycle of nitric oxide synthases in particular and heme-thiolates in general. There are many techniques for characterizing a metalloenzyme and its mechanism, even beyond those previously used by our group. One technique of great use to the Gray group is electronic absorption spectroscopy (UV-vis). This technique is particularly useful in the case of heme enzymes due to their characteristic absorption bands in the visible region of the electromagnetic spectrum. Both the Soret band and the Q bands are sensitive to oxidation state and ligation of the iron.¹⁸ Several examples of various common oxidation states with typical axial ligation (the sixth position, other than the four coordinating porphyrin nitrogens and the axial cysteine ligands) are shown in **Figure 1.5**. Shifts in Soret position (the intense band near 400 nm) are significant enough to allow a researcher to identify oxidation or ligation state often by simple UV-vis characterization.

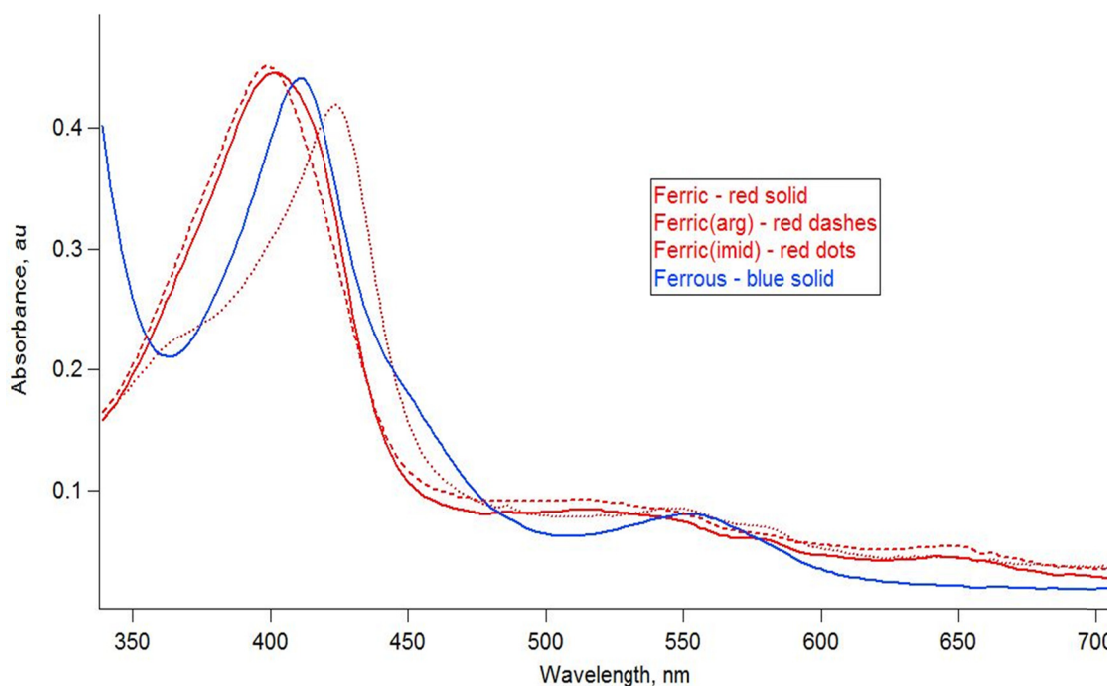


Figure 1.5. UV-visible absorption spectra of several oxidation and ligation states of wild type gsNOS. Note the shift in Soret band from 400 to 410 upon reduction of ferric (red solid) to ferrous (blue) and a shift to 426 nm upon introduction of the ligand imidazole (imid) to the ferric heme (red dots).

Several other techniques have been developed to allow chemists to gather extensive information about metalloenzymes. One such technique, electron paramagnetic spectroscopy (EPR), aids in assignment of spin state. This is incredibly important in these heme-thiolate systems where the energy difference between high-spin and low-spin iron complexes is small and thus both states are possible.²⁹ It has been demonstrated in other non-heme iron systems that spin state has a huge effect on the reactivity of the complex, altering reactivity by six orders of magnitude.⁵⁴ Definitive assignment of the spin state is often incredibly important. Another technique, electrochemistry (Echem), also yields valuable information on an enzyme under investigation. Echem informs about the reduction potential of a metal complex and often on its kinetics and further reactivity.⁵⁵ Several different electrochemical techniques can be employed, such as redox titrations to

determine an exact reduction potential and cyclic voltammetry to learn about the kinetics of such systems. These are just a few of the techniques available to a modern bioinorganic chemist, and such techniques will be introduced and explained further as they are used in the following work.

The final, but possibly most important, tool available to enzymologists (and chemists) today is site-directed mutagenesis. This process (awarded the Nobel Prize in Chemistry in 1993) allows researchers to select particular amino acids within a protein's sequence and change them into another amino acid, through creative use of primers and the polymerase chain reaction (PCR). Proteins can now be investigated and modified on the atomic level.

1.6 Conclusion

These techniques were used to investigate the nitric oxide synthase from *Geobacillus stearothermophilus* and its reactivity, with the goal of furthering our general understanding of NOS enzymes and their mechanism of NO production. This particular system provides stability not present in other NOSs and can be expressed in high yields in *Escherichia coli* in the lab (8 mg/L). Investigations were made into the nature of the heme active site and its reactivity.

This was done using two sets of mutant enzymes. The first set of mutants was designed to perturb the hydrogen bonding to the axial thiolate ligand. The native Trp was replaced in turn with His (which can still H-bond but cannot π -stack with the porphyrin), Phe (which can π -stack but not H-bond) and Tyr (again it can π -stack but not H-bond, but the hydroxylate group greatly alters its electronics). These mutants were analyzed using

various bioinorganic techniques, compared with the wild type, and used to learn about the tuning of the heme cofactor for the exact reactivity of NOSs.

The second set of mutants was made to investigate rates of NO release from the enzyme, once produced during catalysis. Different cellular functions of NO would require different rates of NO production and release.² It has been observed that two particular positions may be involved in gating NO release (positions 134 and 223 in gsNOS). Mutations were made to vary the bulk of side chains at these positions, and their rates of NO release and interactions with the diatomic mimic carbon monoxide (CO) were measured in detail. This thesis covers the work done investigating these two sets of mutants and the information gleaned from these experiments.

1.7 References

1. Moncada, S., Herman, A. G., and Vanhoutte, P. (1987) Endothelium-derived relaxing factor is identified as nitric-oxide, *Trends Pharmacol. Sci.* 8, 365.
2. Alderton, W. K., Cooper, C. E., and Knowles, R. G. (2001) Nitric oxide synthases: Structure, function and inhibition, *Biochem. J.* 357, 593.
3. Marletta, M. A. (1993) Nitric-oxide synthase structure and mechanism, *J. Biol. Chem.* 268, 12231.
4. Stuehr, D. J., Santolini, J., Wang, Z. Q., Wei, C. C., and Adak, S. (2004) Update on mechanism and catalytic regulation in the no synthases, *J. Biol. Chem.* 279, 36167.
5. Crane, B. R., Sudhamsu, J., and Patel, B. A. (2010) Bacterial nitric oxide synthases, In *Annual review of biochemistry*, vol 79, pp 445.
6. Sudhamsu, J., and Crane, B. R. (2009) Bacterial nitric oxide synthases: What are they good for?, *Trends Microbiol.* 17, 212.
7. Stuehr, D., Pou, S., and Rosen, G. M. (2001) Oxygen reduction by nitric-oxide synthases, *J. Biol. Chem.* 276, 14533.
8. Gorren, A. C. F., and Mayer, B. (2007) Nitric-oxide synthase: A cytochrome p450 family foster child, *Biochimica Et Biophysica Acta-General Subjects* 1770, 432.
9. Mowat, C. G., Gazur, B., Campbell, L. P., and Chapman, S. K. (2010) Flavin-containing heme enzymes, *Arch. Biochem. Biophys.* 493, 37.
10. Moncada, S., and Bolanos, J. P. (2006) Nitric oxide, cell bioenergetics and neurodegeneration, *J. Neurochem.* 97, 1676.
11. Zhou, L., and Zhu, D. Y. (2009) Neuronal nitric oxide synthase: Structure, subcellular localization, regulation, and clinical implications, *Nitric Oxide-Biol. Chem.* 20, 223.
12. Meunier, B., de Visser, S. P., and Shaik, S. (2004) Mechanism of oxidation reactions catalyzed by cytochrome p450 enzymes, *Chemical Reviews* 104, 3947.
13. Clague, M. J., Wishnok, J. S., and Marletta, M. A. (1997) Formation of n-delta-cyanoornithine from n-g-hydroxy-l-arginine and hydrogen peroxide by neuronal nitric oxide synthase: Implications for mechanism, *Biochemistry* 36, 14465.
14. Crane, B. R., Arvai, A. S., Gachhui, R., Wu, C. Q., Ghosh, D. K., Getzoff, E. D., Stuehr, D. J., and Tainer, J. A. (1997) The structure of nitric oxide synthase oxygenase domain and inhibitor complexes, *Science* 278, 425.
15. Crane, B. R., Arvai, A. S., Ghosh, D. K., Wu, C. Q., Getzoff, E. D., Stuehr, D. J., and Tainer, J. A. (1998) Structure of nitric oxide synthase oxygenase dimer with pterin and substrate, *Science* 279, 2121.
16. Woodward, J. J., Chang, M. M., Martin, N. I., and Marletta, M. A. (2009) The second step of the nitric oxide synthase reaction: Evidence for ferric-peroxo as the active oxidant, *J. Am. Chem. Soc.* 131, 297.
17. Dawson, J. H., and Sono, M. (1987) Cytochrome.P-450 and chloroperoxidase - thiolate-ligated heme enzymes - spectroscopic determination of their active-site structures and mechanistic implications of thiolate ligation, *Chem. Rev.* 87, 1255.
18. Sono, M., Roach, M. P., Coulter, E. D., and Dawson, J. H. (1996) Heme-containing oxygenases, *Chem. Rev.* 96, 2841.

19. Tejero, J. S., Biswas, A., Wang, Z. Q., Page, R. C., Haque, M. M., Hemann, C., Zweier, J. L., Misra, S., and Stuehr, D. J. (2008) Stabilization and characterization of a heme-oxy reaction intermediate in inducible nitric-oxide synthase, *J. Biol. Chem.* 283, 33498.
20. Wei, C. C., Wang, Z. Q., Meade, A. L., McDonald, J. F., and Stuehr, D. J. (2002) Why do nitric oxide synthases use tetrahydrobiopterin?, *J. Inorg. Biochem.* 91, 618.
21. Hurshman, A. R., Krebs, C., Edmondson, D. E., Huynh, B. H., and Marletta, M. A. (1999) Formation of a pterin radical in the reaction of the heme domain of inducible nitric oxide synthase with oxygen, *Biochemistry* 38, 15689.
22. Hurshman, A. R., Krebs, C., Edmondson, D. E., and Marletta, M. A. (2003) Ability of tetrahydrobiopterin analogues to support catalysis by inducible nitric oxide synthase: Formation of a pterin radical is required for enzyme activity, *Biochemistry* 42, 13287.
23. Stoll, S., NejatyJahromy, Y., Woodward, J. J., Ozarowski, A., Marletta, M. A., and Britt, R. D. (2010) Nitric oxide synthase stabilizes the tetrahydrobiopterin cofactor radical by controlling its protonation state, *J. Am. Chem. Soc.* 132, 11812.
24. Munro, A. W., Leys, D. G., McLean, K. J., Marshall, K. R., Ost, T. W. B., Daff, S., Miles, C. S., Chapman, S. K., Lysek, D. A., Moser, C. C., Page, C. C., and Dutton, P. L. (2002) P450bm3: The very model of a modern flavocytochrome, *Trends Biochem.Sci.* 27, 250.
25. Zhu, Y. Q., and Silverman, R. B. (2008) Revisiting heme mechanisms. A perspective on the mechanisms of nitric oxide synthase (nos), heme oxygenase (ho), and cytochrome p450s (cyp450s), *Biochemistry* 47, 2231.
26. Adak, S., and Stuehr, D. J. (2001) A proximal tryptophan in no synthase controls activity by a novel mechanism, *J. Inorg. Biochem.* 83, 301.
27. Wilson, D. J., and Rafferty, S. P. (2001) A structural role for tryptophan 188 of inducible nitric oxide synthase, *Biochemical and Biophysical Research Communications* 287, 126.
28. Adak, S., Crooks, C., Wang, Q., Crane, B. R., Tainer, J. A., Getzoff, E. D., and Stuehr, D. J. (1999) Tryptophan 409 controls the activity of neuronal nitric-oxide synthase by regulating nitric oxide feedback inhibition, *J. Biol. Chem.* 274, 26907.
29. Denisov, I. G., Makris, T. M., Sligar, S. G., and Schlichting, I. (2005) Structure and chemistry of cytochrome p450, *Chem. Rev.* 105, 2253.
30. Rittle, J., and Green, M. T. (2010) Cytochrome p450 compound i: Capture, characterization, and c-h bond activation kinetics, *Science* 330, 933.
31. Bird, L. E., Ren, J. S., Zhang, J. C., Foxwell, N., Hawkins, A. R., Charles, I. G., and Stammers, D. K. (2002) Crystal structure of sanos, a bacterial nitric oxide synthase oxygenase protein from staphylococcus aureus, *Structure* 10, 1687.
32. Pant, K., Bilwes, A. M., Adak, S., Stuehr, D. J., and Crane, B. R. (2002) Structure of a nitric oxide synthase heme protein from bacillus subtilis, *Biochemistry* 41, 11071.

33. Gusarov, I., Starodubtseva, M., Wang, Z. Q., McQuade, L., Lippard, S. J., Stuehr, D. J., and Nudler, E. (2008) Bacterial nitric-oxide synthases operate without a dedicated redox partner, *J. Biol. Chem.* 283, 13140.
34. Sudhamsu, J., and Crane, B. R. (2006) Structure and reactivity of a thermostable prokaryotic nitric-oxide synthase that forms a long-lived oxy-heme complex, *J. Biol. Chem.* 281, 9623.
35. Agapie, T., Suseno, S., Woodward, J. J., Stoll, S., Britt, R. D., and Marletta, M. A. (2009) No formation by a catalytically self-sufficient bacterial nitric oxide synthase from *sorangium cellulosum*, *Proc. Natl. Acad. Sci. U. S. A.* 106, 16221.
36. Stuehr, D. J., Tejero, J., and Haque, M. M. (2009) Structural and mechanistic aspects of flavoproteins: Electron transfer through the nitric oxide synthase flavoprotein domain, *Febs Journal* 276, 3959.
37. Ghosh, D. K., Crane, B. R., Ghosh, S., Wolan, D., Gachhui, R., Crooks, C., Presta, A., Tainer, J. A., Getzoff, E. D., and Stuehr, D. J. (1999) Inducible nitric oxide synthase: Role of the n-terminal [beta]-hairpin hook and pterin-binding segment in dimerization and tetrahydrobiopterin interaction, *EMBO J* 18, 6260.
38. Wang, Z. Q., Wei, C. C., Sharma, M., Pant, K., Crane, B. R., and Stuehr, D. J. (2004) A conserved val to ile switch near the heme pocket of animal and bacterial nitric-oxide synthases helps determine their distinct catalytic profiles, *J. Biol. Chem.* 279, 19018.
39. Beaumont, E., Lambry, J. C., Wang, Z. Q., Stuehr, D. J., Martin, J. L., and Slama-Schwok, A. (2007) Distal val134ile mutation in inducible no synthase promotes substrate-dependent no confinement, *Biochemistry* 46, 13533.
40. Cary, S. P. L., Winger, J. A., Derbyshire, E. R., and Marletta, M. A. (2006) Nitric oxide signaling: No longer simply on or off, *Trends Biochem.Sci.* 31, 231.
41. Weinert, E. E., Plate, L., Whited, C. A., Olea, C., and Marletta, M. A. (2010) Determinants of ligand affinity and heme reactivity in h-nox domains, *Angewandte Chemie-International Edition* 49, 720.
42. Boon, E. M., and Marletta, M. A. (2005) Ligand discrimination in soluble guanylate cyclase and the h-nox family of heme sensor proteins, *Curr. Opin. Chem. Biol.* 9, 441.
43. Johnson, E. G., Sparks, J. P., Dzikovski, B., Crane, B. R., Gibson, D. M., and Loria, R. (2008) Plant-pathogenic streptomyces species produce nitric oxide synthase-derived nitric oxide in response to host signals, *Chem. Biol.* 15, 43.
44. Gusarov, I., Shatalin, K., Starodubtseva, M., and Nudler, E. (2009) Endogenous nitric oxide protects bacteria against a wide spectrum of antibiotics, *Science* 325, 1380.
45. Chang, I. J., Gray, H. B., and Winkler, J. R. (1991) High-driving-force electron-transfer in metalloproteins - intramolecular oxidation of ferrocycytochrome-c by $\text{Ru}(2,2'\text{-bpy})_2(\text{im})(\text{his-33})_3^+$, *J. Am. Chem. Soc.* 113, 7056.
46. Huynh, M. H. V., Dattelbaum, D. M., and Meyer, T. J. (2005) Excited state electron and energy transfer in molecular assemblies, *Coord. Chem. Rev.* 249, 457.
47. Low, D. W., Winkler, J. R., and Gray, H. B. (1996) Photoinduced oxidation of microperoxidase-8: Generation of ferryl and cation-radical porphyrins, *J. Am. Chem. Soc.* 118, 117.

48. Berglund, J., Pascher, T., Winkler, J. R., and Gray, H. B. (1997) Photoinduced oxidation of horseradish peroxidase, *J. Am. Chem. Soc.* *119*, 2464.
49. Whited, C. A., Belliston-Bittner, W., Dunn, A. R., Winkler, J. R., and Gray, H. B. (2008) Probing the heme-thiolate oxygenase domain of inducible nitric oxide synthase with ru(ii) and re(i) electron tunneling wires, *Journal of Porphyrins and Phthalocyanines* *12*, 971.
50. Hartings, M. R., Kurnikov, I. V., Dunn, A. R., Winkler, J. R., Gray, H. B., and Ratner, M. A. (2010) Electron tunneling through sensitizer wires bound to proteins, *Coord. Chem. Rev.* *254*, 248.
51. Crane, B. R., Dunn, A. R., Dmochowski, I. J., Bilwes, A. M., Gray, H. B., and Waterman, M. R. (2002) Probing monooxygenase structure and reactivity with inorganic photosensitizers, *Drug Metabolism Reviews* *34*, 18.
52. Udit, A. K., Belliston-Bittner, W., Glazer, E. C., Nguyen, Y. H. L., Gillan, J. M., Hill, M. G., Marletta, M. A., Goodin, D. B., and Gray, H. B. (2005) Redox couples of inducible nitric oxide synthase, *J. Am. Chem. Soc.* *127*, 11212.
53. Udit, A. K., Hagen, K. D., Goldman, P. J., Star, A., Gillan, J. M., Gray, H. B., and Hill, M. G. (2006) Spectroscopy and electrochemistry of cytochrome p450bm3-surfactant film assemblies, *J. Am. Chem. Soc.* *128*, 10320.
54. Xue, G. Q., De Hont, R., Munck, E., and Que, L. (2010) Million-fold activation of the fe-2(μ -o)(2) diamond core for c-h bond cleavage, *Nat. Chem.* *2*, 400.
55. Leger, C., and Bertrand, P. (2008) Direct electrochemistry of redox enzymes as a tool for mechanistic studies, *Chem. Rev.* *108*, 2379.

Chapter 2

An Interest in Thiolate Coordination and Hydrogen Bonding

Parts reproduced with permission from Whited, C. A., W. Belliston-Bittner, A. R. Dunn, J. R. Winkler, H. B. Gray. Nanosecond photoreduction of inducible nitric oxide synthase by a Ru-diimine electron tunneling wire bound distant from the active site. *J. Inorg. Biochem.* 2009; *103*: 906–911.

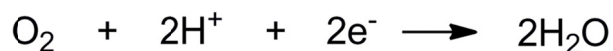
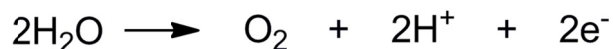
2.1 Abstract

The Gray group has been studying electron transfer in protein systems for the past three decades. During this time a vast amount of information has been collected concerning the nature of the protein matrix and its ability to facilitate such charge transfer reactions. This led to the development of techniques for the covalent attachment of photosensitizers to metalloproteins, and later to the development of compounds consisting of sensitizers linked to substrates (dubbed “wires”) in order to promote interactions between the photosensitizer and the metal active site buried deep within the protein. A Ru-diimine wire, $[(4,4',5,5'\text{-tetramethylbipyridine})_2\text{Ru}(\text{F}_9\text{bp})]^{2+}$ (tmRu-F₉bp, where F₉bp is 4-methyl-4'-methylperfluorobiphenylbipyridine), binds tightly to the oxidase domain of inducible nitric oxide synthase (iNOSoxy). The binding of tmRu-F₉bp is independent of tetrahydrobiopterin, arginine, and imidazole, indicating that the wire resides on the surface of the enzyme, distant from the active-site heme. Photoreduction of an imidazole-bound active-site heme iron in the enzyme-wire conjugate ($k_{\text{ET}} = 2(1) \times 10^7 \text{ s}^{-1}$) is fully seven orders of magnitude faster than the *in vivo* process. Wires such as this surface-binding example are used to study the various electron transfer processes in metalloenzymes in an effort to generate and characterize reactive intermediate species that are otherwise unobservable.

2.2 Introduction

Electron Transfer in Metalloproteins

All life on our planet must carefully balance both electrons and protons as well as defend itself against oxidative damage caused by our highly oxidizing atmosphere. Processes necessary for human life, such as respiration, require a complex system of proteins and enzymes in order to harness the energy in oxygen in a useful way without causing damage to an organism through Fenton chemistry and the like.¹ The two following reactions (**Scheme 2.1**) have been called the most important reactions on the planet (Harry Gray, countless presentations and informal conversations). These are photosynthesis (in part) and aerobic respiration.



Scheme 2.1. The two most important reactions on our planet: photosynthesis (top) and aerobic respiration (bottom).

In plants and photosynthetic bacteria, photosynthesis is the process of harnessing energy from sunlight to convert carbon monoxide into higher, more complex C_n -containing molecules necessary for the health of the organism.² Along the way water is oxidized, which produces dioxygen as a high-energy by-product. It is this oxygen that most higher life forms on this planet breathe in for the process of respiration, releasing the energy of dioxygen and producing water.

Protons and electrons must be finely controlled and delivered just when necessary in order to achieve the desired reactivity in each of these two processes and sustain life.

Electron transfers occur from one redox active compound to another. In biological systems these are commonly flavins, quinones, porphyrins, and metal centers. Nature developed protein scaffolds in order to insulate these redox sites from one another, preventing deleterious side reactions and promoting only the specific reaction of choice. The very nature of these protein scaffolds is designed to inhibit the random transfer of charge, making electron transfer difficult. The physical presence of the scaffold separates the two species participating in electron transfer. Without these scaffolds, species would simply move toward the thermodynamically favored state and cells would stop functioning. Particular reactions are desired, however, and therefore the protein must somehow also facilitate these vital charge transfers over large distances (sometimes greater than 20 Å). The Gray group has long been interested in understanding how proteins mediate these long-range electron transfer reactions.

A very powerful theory for studying and understanding electron transfer (ET) reactions has been developed by the Caltech professor Rudy Marcus. While, originally developed with simpler systems in mind, this theoretical formalism has proven applicable in protein systems and provides a context within which ET in metalloproteins can be studied.

Semi-Classical Marcus Theory

Marcus Theory is a formalism through which electron transfer reactions can be understood.³⁻⁴ It relies on the Franck-Condon Principal which states that when a molecule absorbs a photon the rearrangement of electrons is nearly instantaneous (occurs over the femtosecond timescale).⁴ However, the nuclei of the constituent atoms are much heavier than the electrons and, therefore, nuclear movement is incredibly slow on the timescale of

moving electrons. This nearly always results in positioning the molecule in a vibrational excited state within the new electronic state. Nonradiative decay allows the molecule to relax to the lowest vibrational state within the excited electronic state before releasing the energy as a photon (the lifetime of vibrational excited states are nearly always shorter than the lifetimes of electronic excited states). Finally, the molecule luminesces to return to its ground state, but the photon released is of lower energy than the originally absorbed photon (the difference being the energy of the vibrational states).

In Marcus Theory, the Franck-Condon Principle is applied to electronic states of both the donor molecule (D) and the acceptor (A). Each state can be represented by a parabola (**Figure 2.1**). In the case of much of the Gray group's work, the donor and acceptor are linked by a bridging moiety, B, through which the electron is transferred.

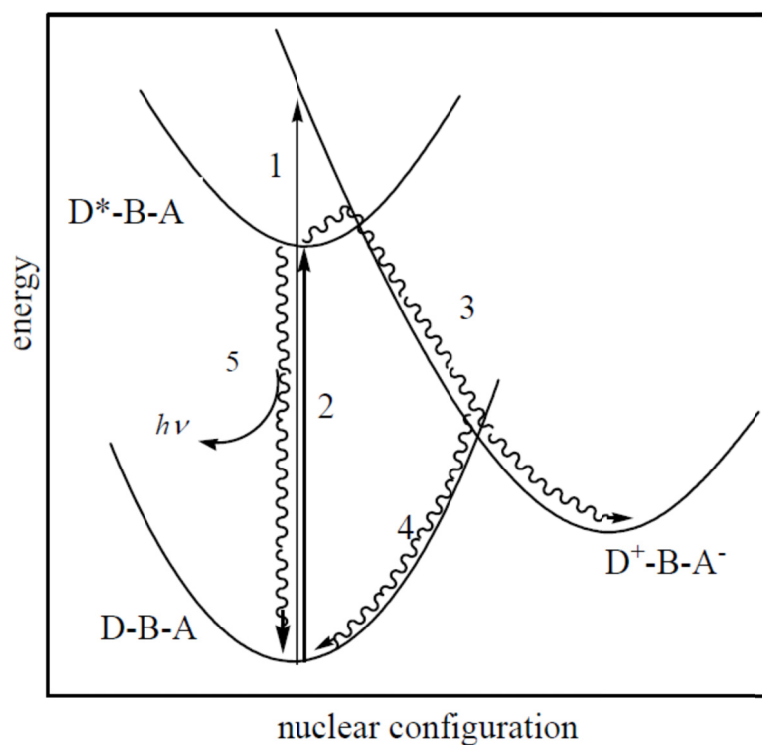


Figure 2.1. Electronic states of a representative D-B-A molecule.

First, a photon is absorbed, promoting the donor to its excited state. From this state it can either relax to the ground state through both radiative and non-radiative decay, or its excited electron can be transferred to the acceptor molecule. The Franck-Condon Principle requires that the nuclei, which remain fixed on the timescale of electronic movement, be in a configuration corresponding to the product complex, in other words the transition state lies at a point where the reactants and products have the same nuclear configuration (the point where two parabolas cross in **Figure 2.1**). From this requirement, a relationship between the rate of such a reaction and its driving force can be extrapolated.

In proteins in particular, electronic coupling between the donor and acceptor can often be quite weak. Metal centers are buried within insulating protein scaffolds and separated by tens of Ångstroms. The probability of transferring an electron is therefore quite low each time the nuclei form the transition state, meaning it must be formed and reformed many times before the desired reaction occurs. This places such reactions in the nonadiabatic limit. Semiclassical Marcus Theory predicts the following Equation 2.1 relating the rate of electron transfer to the driving force for the reaction (ΔG°), the electronic coupling between donor and acceptor (H_{AB}), and the reorganizational parameter (λ).

$$k_{ET} = \left(\frac{4\pi^3}{h^2 \lambda k_b T} \right)^{1/2} H_{AB}^2 \exp \left[\frac{-(\Delta G^\circ + \lambda)^2}{4\lambda k_b T} \right] \quad (2.1)$$

The coupling constant, H_{AB} , is a function of the distance between donor and acceptor (as defined by the edge-to-edge distance) and another factor β , Equation 2.2. This second

term, β , describes how well the intervening medium facilitates electron transfer, vacuum being the poorest at promoting ET. The abilities of various media to promote electron transfer has been studied extensively by the Gray group over the past few decades, enabling the generation of Tunneling Timetables (Figure 2.2). For each medium the smaller the slope and the higher the line lies on the plot, the greater the rate of ET over a particular distance, meaning that particular medium transfer electrons better than other media with greater slopes. (Intuitively, conjugated bonds facilitate ET far better than vacuum.)

$$H_{AB} = H_{AB}^o \exp\left[-\beta(r_{AB} - r_{AB}^o)/2\right] \quad (2.2)$$

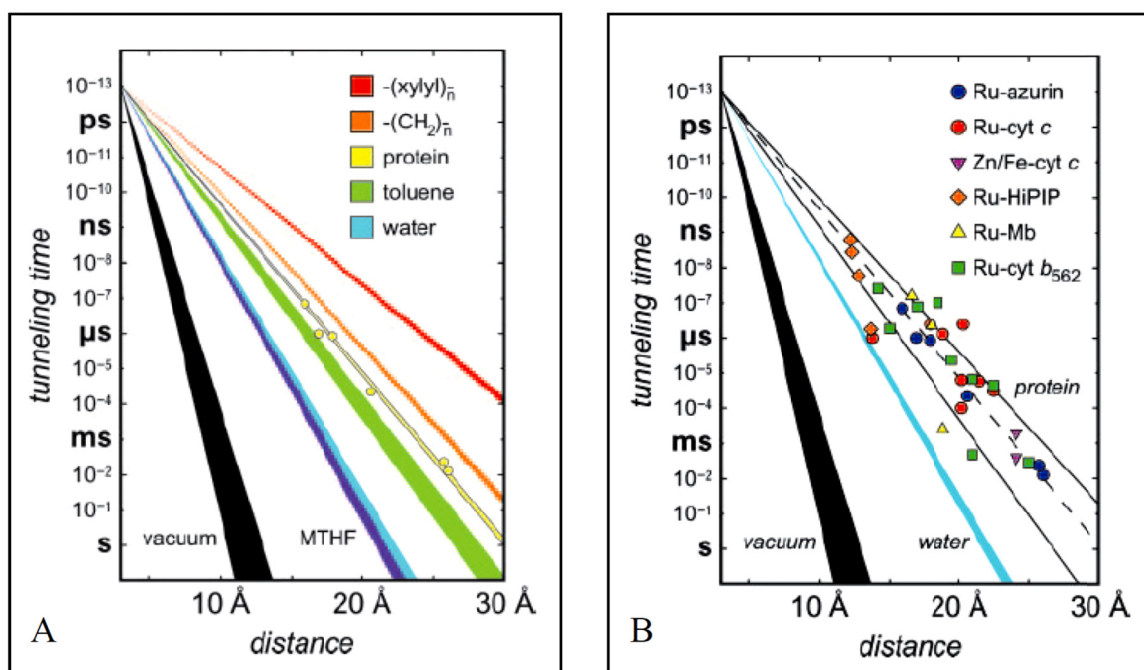


Figure 2.2. (A) Activationless electron Tunneling Timetable for various media: vacuum (black, $\beta = 2.9\text{--}4.0 \text{ \AA}^{-1}$), methyl-THF (violet, $\beta = 1.57\text{--}1.65 \text{ \AA}^{-1}$), toluene in glass form (green, $\beta = 1.18\text{--}1.28 \text{ \AA}^{-1}$), xylol bridge (red, $\beta = 0.76 \text{ \AA}^{-1}$), alkane bridges (orange, $\beta = 1.0 \text{ \AA}^{-1}$), and β -strand bridges in ruthenium modified azurin (yellow, $\beta = 1.1 \text{ \AA}^{-1}$). (B) Tunneling Timetable for intraprotein ET in ruthenium-modified azurin (blue circles), cytochrome c (red circles), myoglobin (yellow triangles), cytochrome b_{562} (green squares), high-potential iron protein (orange diamonds), and for interprotein ET in Fe:Zn cytochrome c crystals (fuchsia triangles). Solid lines illustrate the tunneling pathway predictions for coupling along β -strands ($\beta = 1.0 \text{ \AA}^{-1}$), and α -helices ($\beta = 1.3 \text{ \AA}^{-1}$); dashed line illustrates a 1.1 \AA^{-1} distance decay for reference. Distance decay through water is shown as a cyan wedge, vacuum in black.

One interesting consequence of Marcus Theory is the prediction of the so-called inverted region.⁵ Marcus Theory predicts that the rate of ET first increases with increasing driving force, as is intuitive. However, the rate constant reaches a maximum where the driving force is equal to the reorganization energy of the system. Beyond this point, the rate then actually decreases. The origin of this effect is shown in **Figure 2.3**.

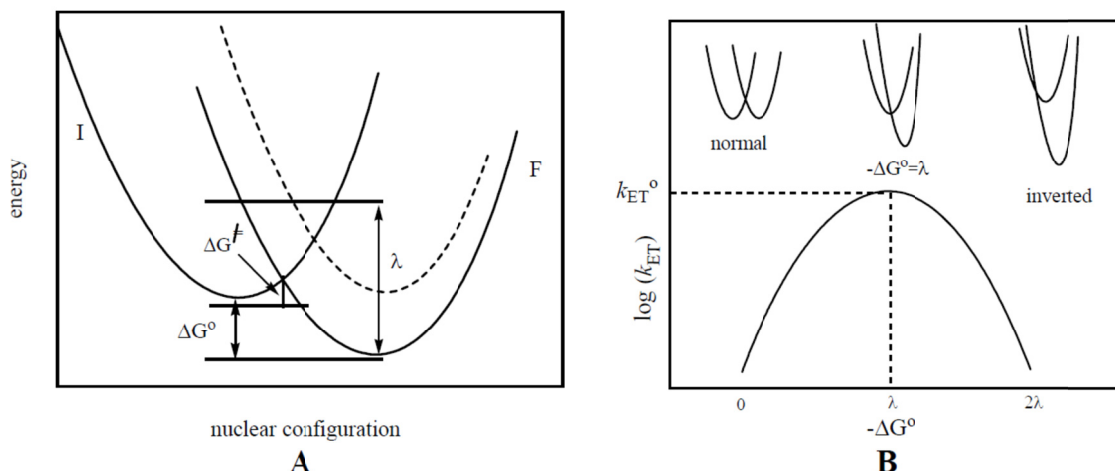
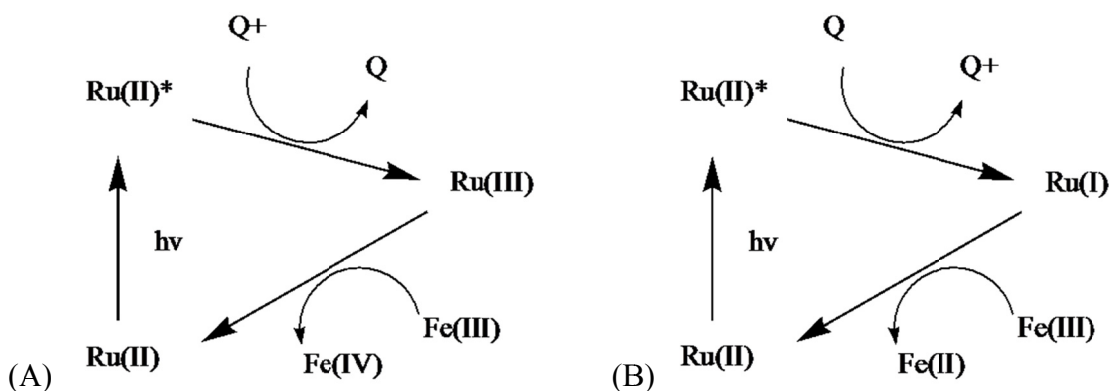


Figure 2.3. (A) Potential energy curves for an initial (I) and final (F) state, before and after ET, respectively. The dashed line represents that curve of the final state in a self-exchange reaction, where reactants and products are the same (isoergonic). (B) Rate of electron transfer as a function of increasing driving force showing the normal and inverted regions.

Flash/Quench Methodology

Excited states that have long lifetimes must be employed in order to study ET over the long distances often found in protein systems. The excited state of a Ru(II) tris-diimine complex is typically less than 1 μ s. To increase this lifetime and thus increase the possibility of productive electron transfer, a flash/quench methodology was developed.⁶ In this scheme another reactant is introduced, called a quencher (Q), which reacts with the excited state of the photosensitizer (Ru complex). A large excess of a small molecule quencher in solution can react quickly with the excited state of Ru(II), in effect quenching its excited state. Given the unique properties of Ru complexes, either oxidative or reductive quenchers can be used which will either oxidize or reduce the Ru to Ru(III) or Ru(I) (**Scheme 2.2**). This provides intermolecular charge separation and, in the absence of cage-trapped systems, greatly increases the length of time over which ET can occur. The new Ru species now lives on the order of milli- to microseconds, allowing for

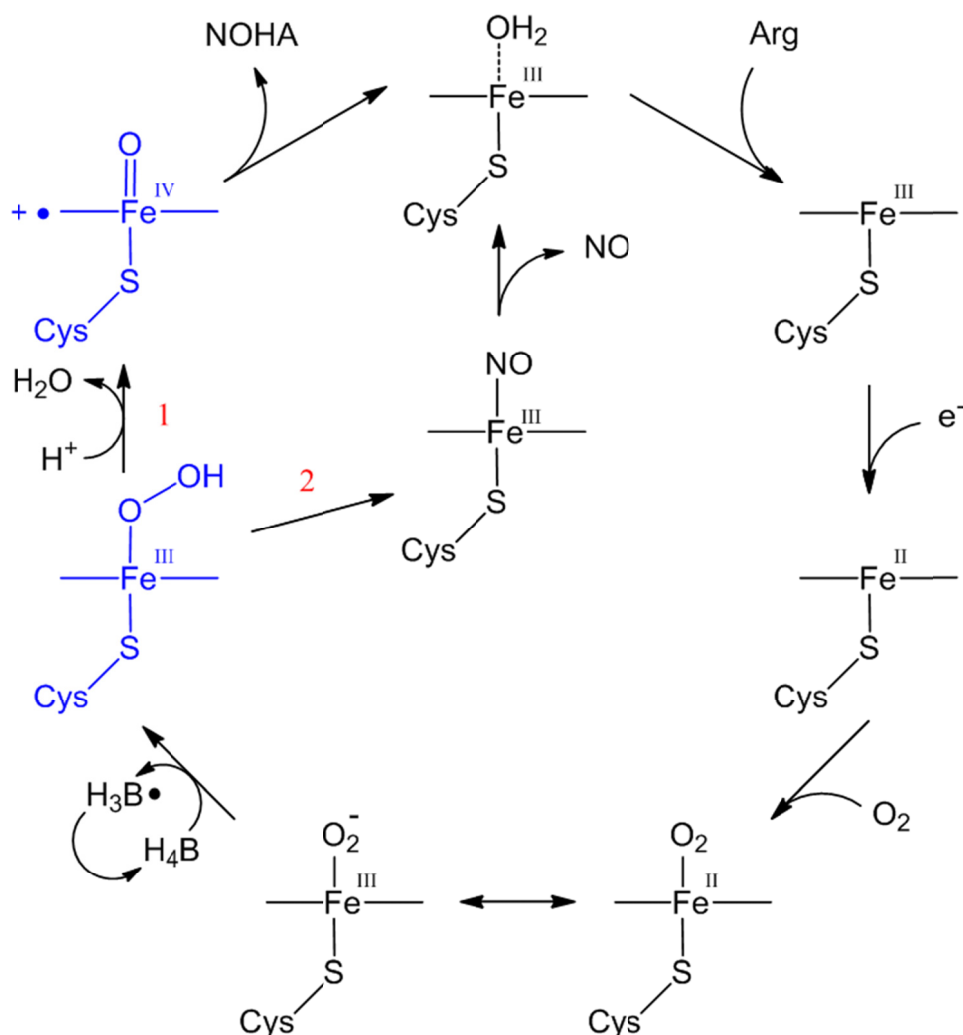
the observation of much slower ET processes. This technique has been successfully used to study ET in many protein and enzyme systems.⁷⁻⁹



Scheme 2.2. Oxidative (A) and reductive (B) flash/quench schemes showing the production of highly reactive Ru complexes for ET reactions with a distant, buried protein active site (Fe as in a heme protein).

The Wires Project

A long-standing goal in our group is the development of methods to generate and observe high-valent iron-oxo complexes which are believed to play key roles as intermediates in the catalytic cycles of heme enzymes.¹⁰⁻¹¹ Direct observation during turnover would allow definitive identification of the active oxidant. Drawing on studies of similar enzymes and using techniques such as electron paramagnetic resonance spectroscopy under cryogenic conditions and X-ray crystallography, investigators have amassed a large body of evidence that strongly indicates that Compound I (**Scheme 2.3**, the ferryl P-IX racial cation shown in blue) is the active species.¹²⁻¹⁴ The steps leading to formation of this highly reactive species are slow in comparison to the rate at which it reacts, making its observation problematic, as at best it is present in very low concentrations during catalysis.



Scheme 2.3. Catalytic cycle of nitric oxide synthases, with putative intermediates highlighted in blue (as predicted by the cytochrome P450 mechanism). These putative intermediates are also the compounds of greatest interest. The numbers 1 and 2 (red) represent the path taken in the first and second turnovers.

We have investigated the redox photochemistry of two heme enzymes, microperoxidase-8 (MP-8, a heme octapeptide fragment of cytochrome *c*) and horseradish peroxidase (HRP).^{7, 15} Visible excitation of $\text{Ru}(\text{bpy})_3^{2+}$ (bpy is 2,2'-bipyridine) in the presence of oxidative quenchers in solution generates a powerful Ru(III)-diimine oxidant, which reacts rapidly with the heme to form the protoporphyrin-IX radical cation, which then oxidizes Fe(III) to give high-valent iron-oxo complexes of MP-8 and HRP. Attempts to generate high-valent hemes in P450s in reactions with

uncomplexed photogenerated oxidants were not successful so we changed course, as discussed in the following paragraphs.

Since 1999, we have developed sensitizer-linked electron tunneling wires that are able to deliver electrons and holes rapidly to and from deeply buried active sites of heme enzymes.¹⁶ Attachment of the photosensitizer to the substrate promotes a close interaction between the two and increases the probability of electron transfer by increasing coupling (H_{AB}) (**Figure 2.4**). This technique proved very useful with cytochromes P450 and enabled the characterization of the enzyme in two states, open and closed as well as transient generation of a reduced state. These heavy-metal containing wires can actually promote crystallization of protein samples and provide a second transition metal besides the heme iron to aid in solving crystal structures. A selection of such molecules developed for the oxygenase domain of iNOS (iNOSoxy) is shown in **Table 2.1**.

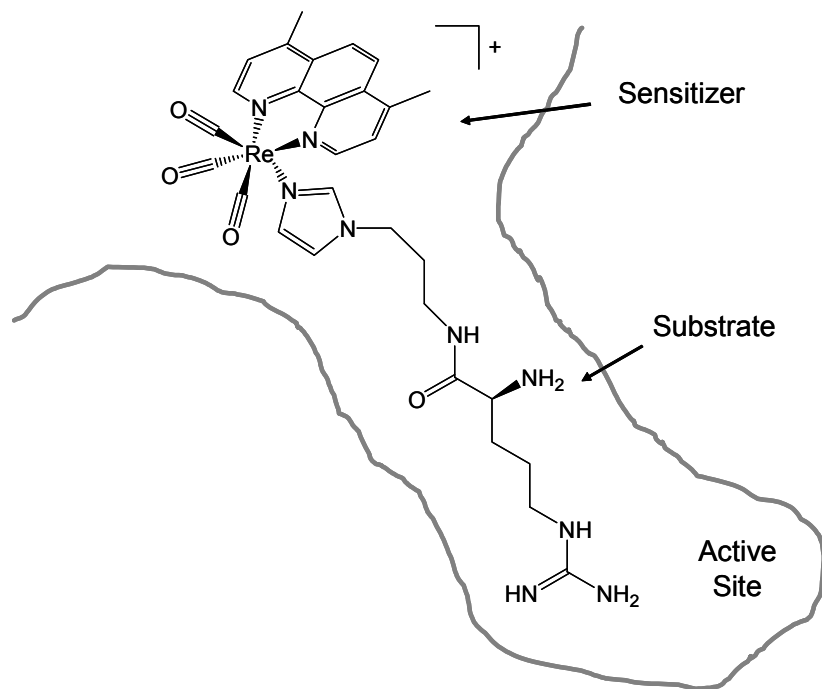
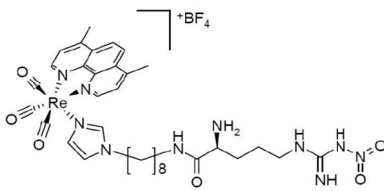
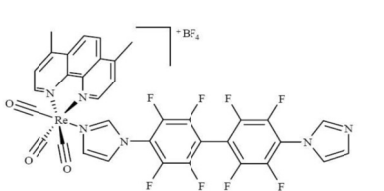
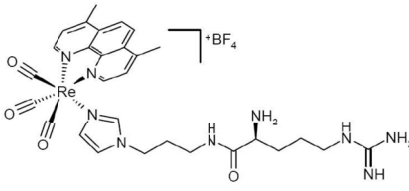
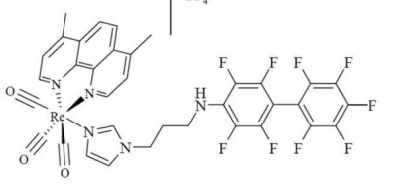
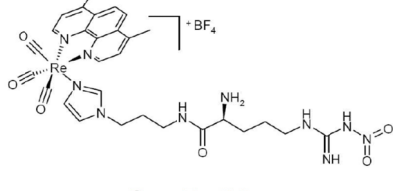
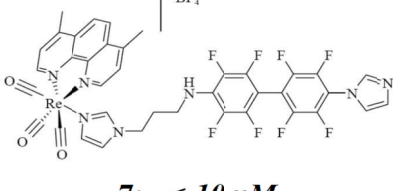
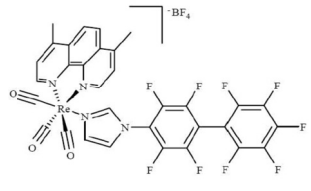
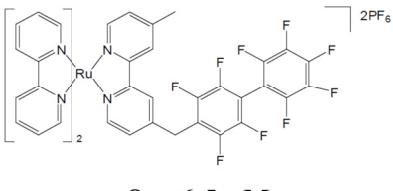


Figure 2.4: Substrates linked to sensitizers target active-site channels of enzymes.

Table 2.1: Ru(II) and Re(I) electron tunneling wires bind to iNOSoxy.

<i>Channel-Binding Wires</i>	
 <p>1: 3 μM</p>	 <p>5: 0.13 μM</p>
 <p>2: 2 μM</p>	 <p>6: < 10 μM</p>
 <p>3: 7 μM</p>	 <p>7: < 10 μM</p>
 <p>4: 1.4 μM</p>	 <p>8: 6.5 μM</p>

The dissociation constants of complexes that contain wires in the substrate channels of enzymes can be determined from analysis of shifts in Soret absorptions.¹⁷ Examples of these shifts in the case of iNOSoxy are shown in **Figure 2.5**. The wires luminesce upon 355 nm (Re(I)) or 480 nm (Ru(II)) excitation. The emission overlap with heme absorptions triggers Förster energy transfer (FET), which accounts for the steady-state emission quenching observed upon binding of wires to iNOSoxy (**Figure 2.6**).

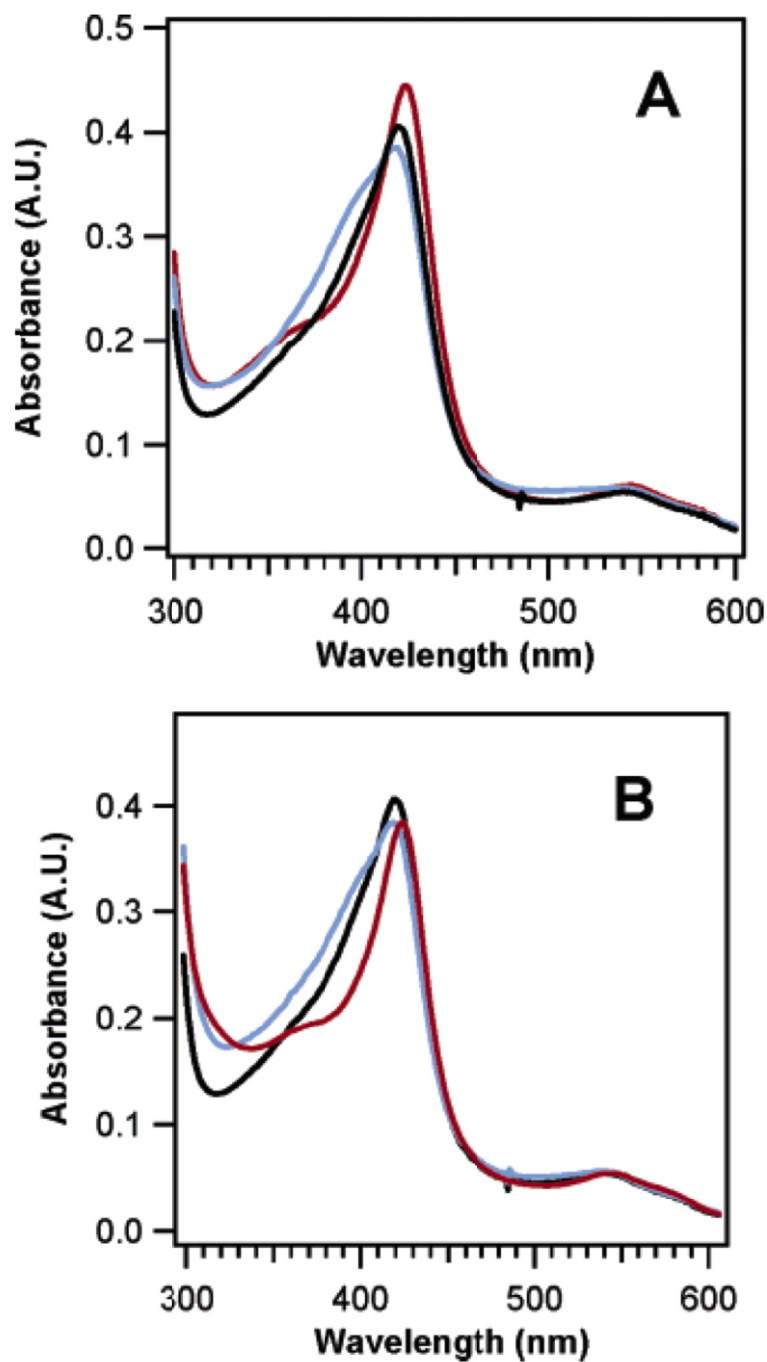


Figure 2.5: UV-visible absorption spectra of iNOSoxy: wire complexes. (A) iNOSoxy alone (5 μ M; black) and bound to 1 equivalent each of **5** (red) and **4** (blue). (B) iNOSoxy alone (5 μ M; black) and bound to 1 equivalent each of **7** (red) and **6** (blue).

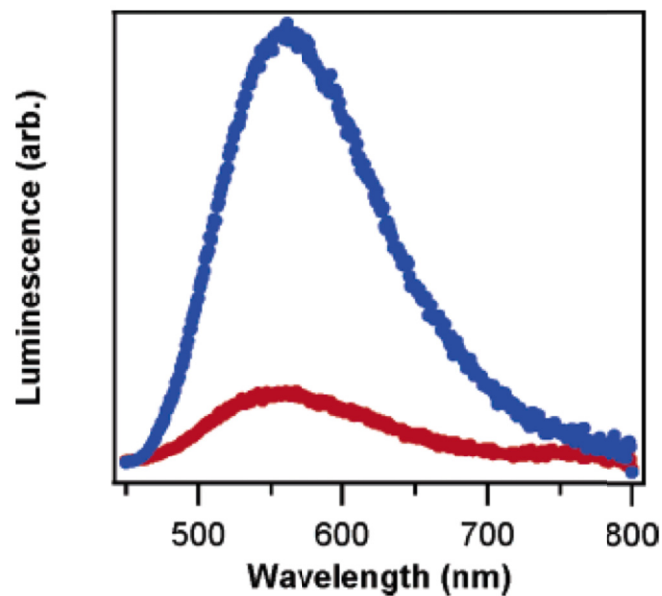


Figure 2.6: Steady-state luminescence spectra of **5** (2 μ M; blue) and a 1:1 mixture of **5** and iNOSoxy (2 μ M; red) with $\lambda_{\text{ex}} = 355$ nm.

Transient absorption measurements demonstrate that these wires reduce iNOSoxy upon 355 or 480 nm excitation. Reduction is indicated by a bleach near 420 nm, corresponding to the disappearance of the six-coordinate Fe(III) resting state and the formation of a new species (with absorption near 445 nm) assigned to six-coordinate Fe(II). Difference spectra were constructed from single-wavelength transient absorption traces 80 ns after excitation of the protein-bound wire **7** (**Figure 2.7**, blue) and 3 μ s after excitation of protein-bound wire **5** (**Figure 2.7**, red).

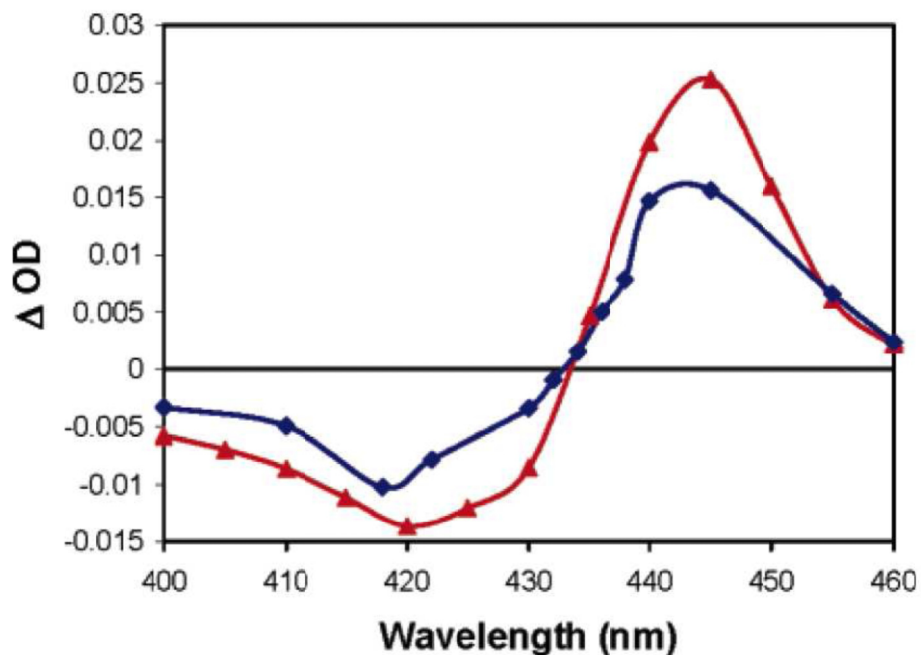


Figure 2.7. Difference spectra of a 1:1 mixture of **7** and iNOSoxy (5 μ M, 80 ns after 355 nm excitation, blue squares) and a 1:1 mixture of **5** and iNOSoxy (11 μ M, 3 μ s after 355 nm excitation, red triangles) showing a bleach of a six-coordinate Fe(III) Soret (420 nm) and the appearance of a six-coordinate Fe(II) Soret (445 nm). Individual points were taken from single-wavelength transient absorption traces.

Picosecond transient absorption measurements demonstrate rapid formation of Fe(II) in the presence of wires **5** and **7**. By pumping with 70 ps, 355 nm pulses and probing with 442 nm radiation from a continuous wave He:Cd laser, we obtained transient absorbance traces that document the formation of a ferrous heme on very short timescales (**Figure 2.8**). The traces were fit to a single exponential to give $k_f = 7(3) \times 10^9$ s⁻¹ for formation of Fe(II).

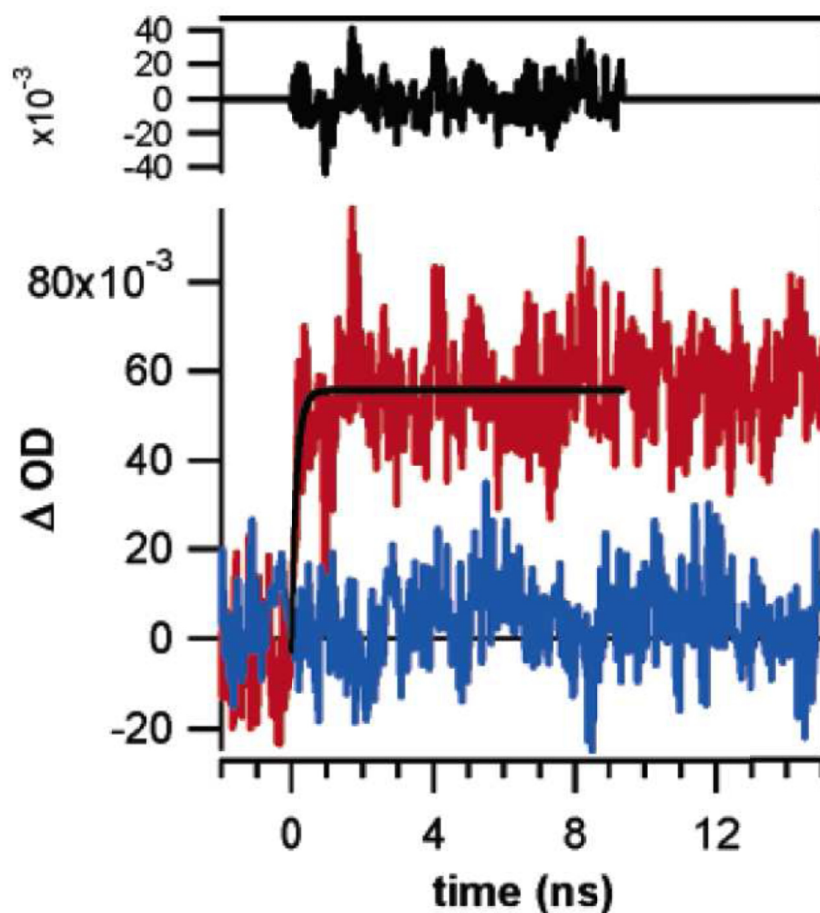


Figure 2.8. Transient absorbance at 442 nm of iNOSoxy alone (8 μ M, blue) and in the presence of excess **5** (red) with $\lambda_{\text{ex}} = 355$ nm. The red trace shows the rapid formation of the ferrous heme, fit to one exponential ($k_f = 7(3) \times 10^9 \text{ s}^{-1}$, black) with the residual shown above.

Although the demonstration of very rapid electron transfer to a heme active site represents a step toward the goal of observing high-valent intermediates, our electron delivering wires block access to substrate channels. We have exploited this property of channel binders in the construction of highly selective amine oxidase inhibitors by manipulation of the linker elements of wire structures.¹¹

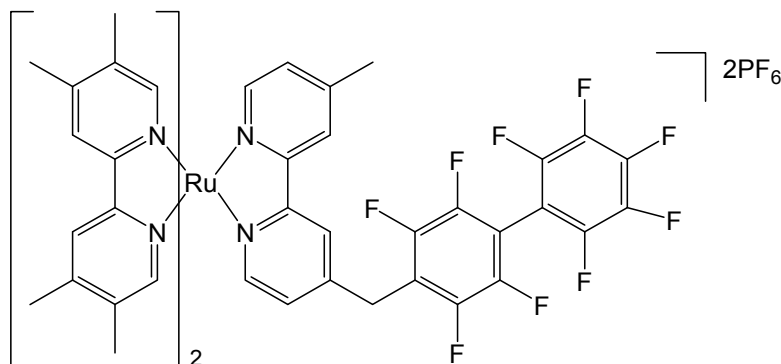
A Novel Surface-Binding Wire

Nitric oxide synthase (NOS) is a heme monooxygenase that catalyzes the five-electron oxidation of L-arginine and O_2 to citrulline and nitric oxide (NO). NOS effects

this transformation in two turnovers, producing N^G -hydroxy-L-arginine (NHA) as an enzyme-bound intermediate, requiring three electrons from its reductase domain. Each turnover is expected to proceed through a mechanism similar to that of cytochrome P450 (although the two turnovers may utilize a different species for substrate oxidation), central to which are two slow electron transfer (ET) events.^{12, 18-22} The first ET event reduces the resting, substrate-bound heme to the ferrous state, which then binds oxygen to create the last observable intermediate (ferric-superoxo).^{20, 23} It is thought that the second ET event, where the electron is supplied by the cofactor tetrahydrobiopterin (BH_4), produces one or more high-valent heme species, with substrate oxidation possibly occurring from a ferryl-porphyrin⁺⁺ intermediate (Compound I).^{20, 24} The sluggishness of the second ET step, however, has so far prevented the characterization of high-valent intermediates in the catalytic cycle in solution.^{12, 20, 25} Cryoreduction of the heme domain of ferric-superoxo endothelial NOS at 77 K leads to the formation of a ferric-peroxo species.¹² Annealing at 165 K results in conversion to the product state without the appearance of intermediates. These data suggest that O-O bond cleavage is slower than reaction with substrate.

By employing laser-induced ET to reduce the active-site heme very rapidly, it should be possible to observe high-valent intermediates that follow in the catalytic cycle. Toward this end, we and others have developed photoactive electron tunneling wires to deliver electrons and holes to and from the deeply buried heme active sites in P450cam^{8, 26-27} and NOS.^{16, 28-30} Importantly, one of the NOS wires, tmRu-F₉bp (**Scheme 2.4**), can potentially probe the catalytic cycle, since it binds tightly and specifically to the oxidase domain of the inducible form of the enzyme (iNOSoxy) in a region that is *distant* from

the active site.¹⁷ Here we demonstrate that an imidazole-ligated heme in tmRu-F₉bp:iNOSoxy can be photoreduced several million times faster ($k_{\text{ET}} = 2(1) \times 10^7 \text{ s}^{-1}$) than the physiological ET reaction.



Scheme 2.4. tmRu-F₉bp.

2.3 Materials and Methods

General

The tmRu-F₉bp complex was synthesized as described previously.^{8-9, 31} Tetramethylphenylenediamine (TMPD) was obtained from Aldrich and vacuum-sublimed before use. Tetrahydrobiopterin (BH₄, Aldrich) was stored under argon at -20 °C. All other chemicals were used as received from Sigma, JT Baker, Fischer, EM Sciences, and Mallinckrodt. UV-visible absorption spectra were acquired on an Agilent 8453 UV-visible spectrophotometer. Gel electrophoresis was run on a Phast System (Pharmacia) with 8–25 percent gradient precast agarose gels and SDS buffer strips. Samples were loaded in 4x SDS buffer and stained with Coomassie blue. Samples were run against Precision Plus All-Blue standards (BioRad).

iNOSoxy Expression and Purification

The heme domain of iNOS with a C-terminal His₆ tag was overexpressed in *E. coli* and purified as described previously³² with several exceptions. Briefly, expression cells were subjected to two rounds of chemical lysis by pelleting and resuspension in 40 mL of B-PER lysis buffer (protein extraction reagent B, Pierce). The lysis buffer included a cocktail of protease inhibitors (10 µg/mL benzamidine, 5 µg/mL leupeptin, 1 µg/mL each pepstatin, antipain, and chymostatin, and ~ 500 µM Pefabloc (Roche)) as well as 100 µg/mL DNase, 100 µg/mL RNase, ~ 500 µg/mL lysozyme, and 20 mM imidazole per liter of cells. The suspension was centrifuged and the supernatant was loaded directly onto a His₆ immobilized metal-ion affinity chromatography column (5 mL Ni²⁺:HisTrap, Amersham). Once the protein was completely loaded, it was washed with 20 column volumes of 20 mM imidazole in 50 mM NaP_i/300 mM NaCl/pH 8. The protein was eluted with 150 mM imidazole and concentrated to ~ 3 mL in an Amicon Ultra centrifugation device (10,000 MWCO, Millipore). The concentrated sample was then further purified over a size-exclusion column, as described previously.³² The anion exchange column was omitted when ≥ 95 percent purity was confirmed by UV-visible spectroscopy and gel electrophoresis. The purified protein was concentrated to ~ 200 µM, divided into 100 µL aliquots, and stored in 50% glycerol at -80 °C.

Sample Preparation

Small aliquots of iNOSoxy were thawed and exchanged into phosphate buffer (50 mM KP_i, 50 mM KCl, pH 7.4) using a PD-10 desalting column (BioRad) immediately before use. The position of the heme Soret maximum (422 nm) confirmed the presence of low-spin, water-bound heme.^{17, 32} The heme protein concentration was determined using

$\epsilon_{422} = 75 \text{ mM}^{-1}\text{cm}^{-1}$ per unit heme.¹⁷ For the inhibitor-bound samples, imidazole (400-500 μM) was added, and binding was confirmed by a Soret shift to 428 nm.^{17, 32} For substrate-bound, pterin-free samples, 1 mM arginine was added to dilute ($\sim 2\text{--}20 \mu\text{M}$) iNOSoxy and allowed to incubate at 4 °C for approximately 30 min. In the absence of pterin (BH_4), only partial conversion to a high-spin heme ($\lambda_{\text{max}} = 398 \text{ nm}$ ³²⁻³³) was observed. For substrate- and pterin-bound samples, fresh BH_4 solutions were prepared daily. Phosphate buffer was thoroughly deoxygenated by bubbling with argon for ≥ 10 min. Solid BH_4 was added to the degassed buffer under a counter-flow of argon. Dilute iNOSoxy ($\sim 2\text{--}20 \mu\text{M}$) was deoxygenated by at least 30 evacuation-Ar backfill cycles, taking care to avoid bubbling of the solution. Aliquots of concentrated, deoxygenated pterin and arginine stocks were then added to the protein solution, giving final concentrations of 100 μM BH_4 and 1 mM arginine. The solution was incubated for 2 h at 4 °C; binding of BH_4 and arginine was confirmed by a Soret shift to 396 nm.³⁴⁻³⁵

For quenching experiments, 1 M ascorbate stock solutions were prepared daily by dissolving ascorbate in thoroughly deoxygenated 1 M KOH. Ascorbate (1 M) and solid TMPD were added to deoxygenated protein solutions under a counter-flow of argon.

Transient Spectroscopy

Luminescence decay and transient absorption measurements were made as described previously.^{7, 36-37} The $\sim 8 \text{ ns}$, 480 nm excitation pulses were produced by a Nd:YAG pumped optical parametric oscillator. Data were collected at 1×10^9 samples s^{-1} using a LeCroy digital oscilloscope. Transient absorbance data were converted from intensity to absorbance using the following expression (Eq. 2.3):

$$\Delta Abs = -\log\left(\frac{I}{I_0}\right) \quad (2.3)$$

where I is the intensity of light transmitted through the sample excitation volume, and I_0 is the average transmitted light intensity during the 200 ns prior to the laser shot. Luminescence decay curves and transient absorbance traces were fit to one, two, or three exponentials using a nonlinear least-squares algorithm (Eq. 2.4, Igor Pro):

$$I(t) = c_0 + \sum_n c_n e^{-k_n t} \quad (2.4)$$

Each experiment was repeated at least three times unless indicated otherwise.

Determination of $Ru^I \rightarrow Fe^{III}$ ET Rate Constants

At a given time after excitation, the absorbance observed at a given wavelength (λ) between 400 and 450 nm is (Eq. 2.5):

$$\Delta Abs = (\epsilon_{Fe^{II}} - \epsilon_{Fe^{III}}) [Fe^{II}] + (\epsilon_{*Ru^{II}} - \epsilon_{Ru^{II}}) [*Ru^{II}] + (\epsilon_{Ru^I} - \epsilon_{Ru^{II}}) [Ru^I] \quad (2.5)$$

Since ascorbate, TMPD, and TMPD⁺⁺ do not absorb strongly in this region (under the conditions of these experiments, **Figure 2.9**), the contributions of these species were neglected. Owing to substantial populations of unbound Ru-complex, the absorbance changes at these wavelengths due to depopulation of Ru^{II} and formation of $*Ru^{II}$ are large compared to those for Fe^{II} formation because $[*Ru^{II}] \gg [Fe^{II}]$. Moreover, the presence of both free and iNOSoxy-bound wire complicates the transient absorbance kinetics. In fitting these data, we were unable to identify a phase that was distinct from those corresponding to $*Ru^{II}$ decay in bound and free wires, and that reliably could be attributed to intraprotein ET from Ru^I to Fe^{III} (k_{ET}).

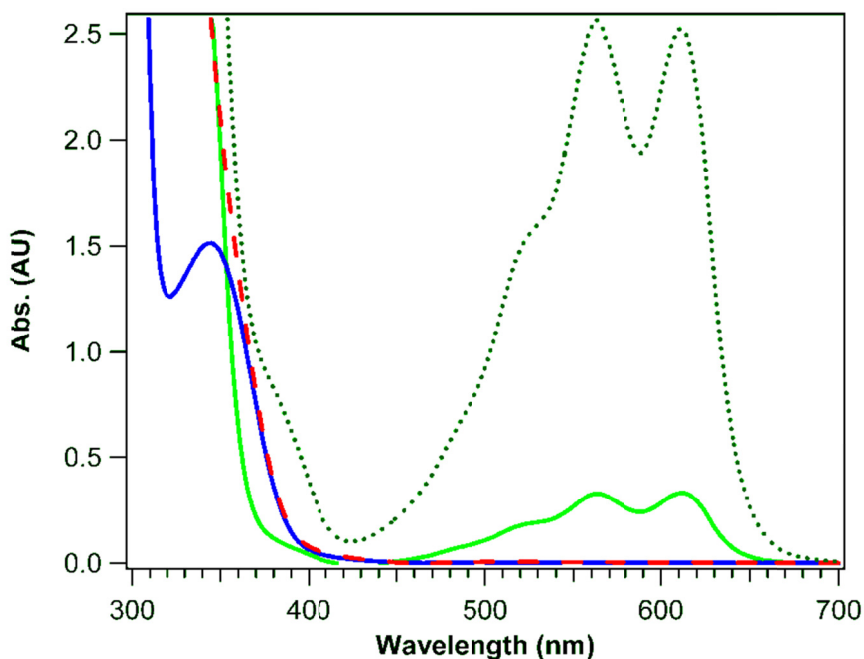


Figure 2.9. UV/visible absorption spectra of ascorbate and TMPD. Spectra were taken in the presence of tmRu-F₉bp (14 μ M) before (blue and light green traces) and after (red dashed and green dotted traces) photolysis at 480 nm and then corrected for absorbance due to tmRu-F₉bp. For the TMPD radical cation, $\epsilon_{565} = 12.5 \text{ mM}^{-1} \text{ cm}^{-1}$ and $\epsilon_{612} = 12.0 \text{ mM}^{-1} \text{ cm}^{-1}$.

In order to characterize the Ru^I to Fe^{III} ET kinetics, we developed a procedure to remove the *Ru^{II} contribution from the transient absorbance kinetics. The isosbestic point for low-spin, imidazole-bound Fe^{III} iNOSoxy and the product Fe^{II} species occurs at 438 nm. In each experiment, therefore, transient absorbance of the Im-iNOSoxy/wire/quencher system at 438 nm reflects the *Ru^{II} bleach and recovery, but contains no contribution from iNOSoxy. Using an experimentally validated *Ru^{II}-Ru^{II} difference spectrum, we determined scaling factors by which we could multiply the 438 nm transient signals to produce estimates of the *Ru^{II} contributions to the observed kinetics at several other wavelengths ([*Ru^{II}-Ru^{II}]: $\Delta\epsilon_{452}/\Delta\epsilon_{438} = 1.12$, $\Delta\epsilon_{425}/\Delta\epsilon_{438} = 0.66$). The calculated *Ru^{II} signals were subtracted from the observed transient kinetics to produce signals corresponding to the time dependence of [Fe^{II}]. Transient Ru^I absorbance

was neglected because its $\Delta\epsilon$ values are < 10 percent of those for $[\text{Fe}^{\text{II}}\text{-Fe}^{\text{III}}]$ (**Figure 2.10**). The resulting corrected traces were then fit to single exponential functions according to Eq. 2.4.

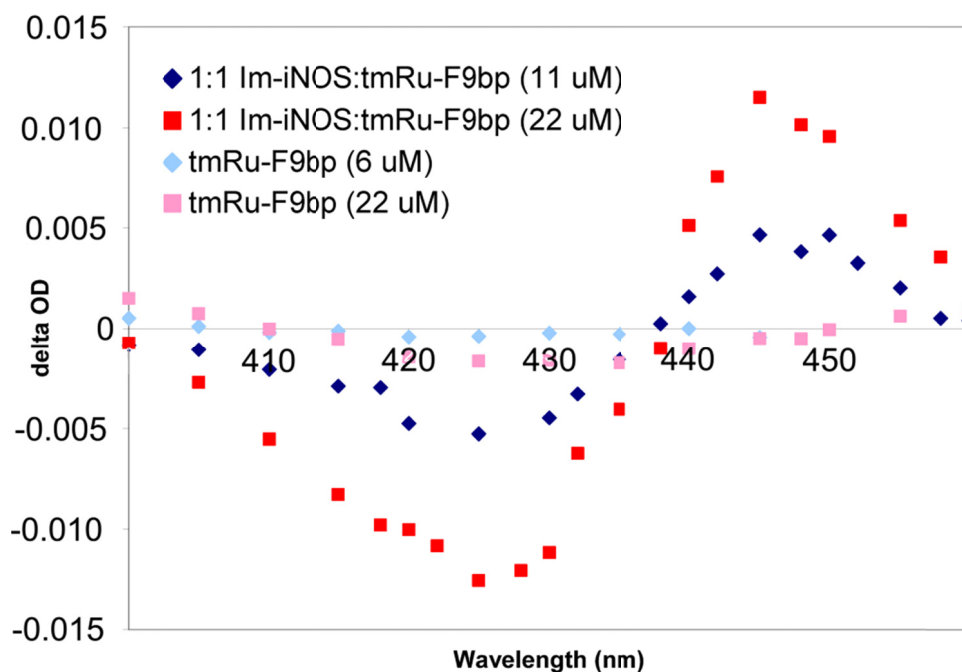


Figure 2.10. Transient absorbance at $2\ \mu\text{s}$ of quenched tmRu-F₉bp in the presence and absence of one equivalent of Im-iNOSoxy, demonstrating the negligible contribution of Ru(I) absorbance to the overall kinetics. Samples contain 10 mM ascorbate and saturated tmpd. $\lambda_{\text{ex}} = 480\ \text{nm}$.

2.4 Results and Discussion

Binding of tmRu-F₉bp to iNOSoxy

We have previously shown that tmRu-F₉bp (Chart 1) binds to iNOSoxy independently of substrate and BH₄ with a dissociation constant of $\sim 1\ \mu\text{M}$.¹⁷ Remarkably, this wire binds at a site distant from the active-site channel, as demonstrated by the finding that a known channel-binding wire does not displace tmRu-F₉bp from the enzyme.¹⁷ While the precise binding site has not been definitively established, Förster

energy transfer measurements indicate that it may be in the hydrophobic pocket thought to be the docking site for the iNOS reductase domain.^{17, 38} Experiments with $\text{Ru}(\text{bpy})_3^{2+}$ show that the photosensitizer alone does not bind to the enzyme (**Figure 2.11**), suggesting that the perfluorobiphenyl unit is largely responsible for the strong association of the wire with a hydrophobic iNOSoxy surface region.

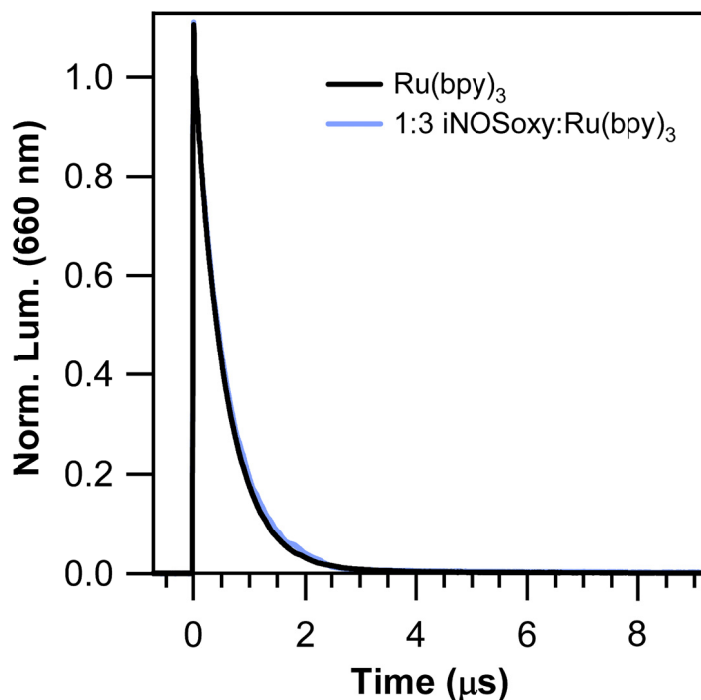
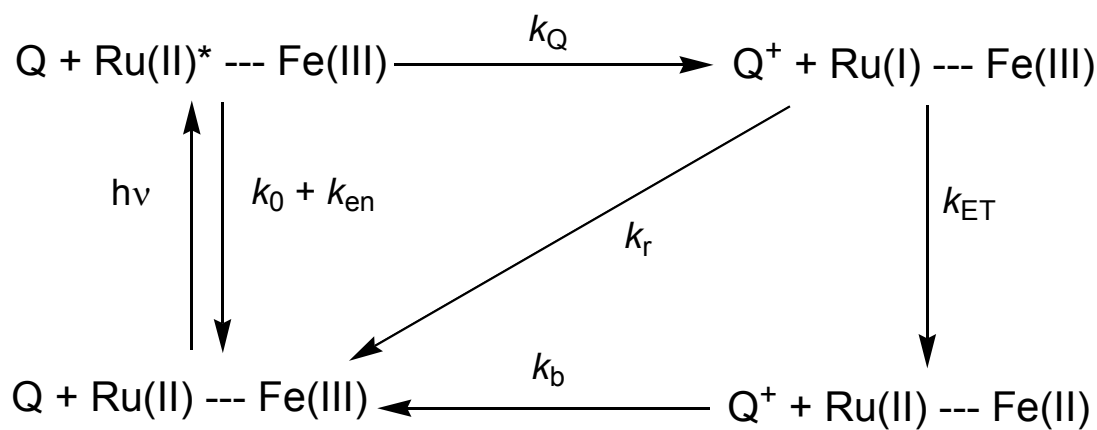


Figure 2.11. Transient luminescence of $\text{Ru}(\text{bpy})_3^{2+}$ in the presence and absence of iNOSoxy. These data demonstrate that $\text{Ru}(\text{bpy})_3^{2+}$ itself does not bind to iNOSoxy, even when present in threefold excess. $\lambda_{\text{ex}} = 480 \text{ nm}$.

Quenching of the Bound Ru-Wire

In previous work, we described Ru-diimine wires that reduce the heme of cytochrome P450 directly upon photoexcitation.⁸ In these experiments the wire termini ligated the iron center, providing an efficient through-bond coupling pathway between the sensitizer and the heme. In contrast, the Ru-wire described here does not directly photoreduce the heme, so we employed a flash/quench method with exogenous

reductants to produce Fe^{II} .⁶ In this experiment, a quencher (Q) reduces the photoexcited sensitizer to create a strongly reducing species (Ru^{I} in **Scheme 2.5**). In the absence of other electron acceptors, the lifetime of Ru^{I} is dependent on the rate of recombination with the oxidized quencher (k_r in **Scheme 2.5**). Because Q^+ and Ru^{I} are present at low and equal concentrations, recombination is slow (ms timescale) and heme reduction competes effectively.



Scheme 2.5. Representation of the reversible flash/quench experiment employed in this work. For simplicity, TMPD and ascorbate are represented together as Q. In a successful flash/quench experiment, quenching must compete with intrinsic relaxation (k_0) and energy transfer (k_{en}) for depletion of the Ru^{II} excited state ($k_{\text{Q}}[\text{Q}] \geq k_0 + k_{\text{en}}$); and electron transfer (k_{ET}) must be faster than recombination between oxidized quencher and reduced sensitizer ($t_{1/2} = 1/k_r[\text{Ru}^{\text{I}}]_0$).

Owing to its high solubility in water and lack of spectral interference with heme Soret changes, ascorbate (Asc) is an attractive choice as a quencher for this system. Even at high concentrations (10 mM), however, Asc quenching produces only small yields of Fe^{II} (**Figures 2.12 and 2.13**). TMPD (**Scheme 2.6**) is a better quencher than Asc, but has limited solubility in water.³⁹⁻⁴⁰ Further, TMPD autoxidizes to create a soluble bright blue cation radical in aqueous media.⁴¹ Under conditions necessary for efficient excited-state quenching, the production of the radical rapidly turns the solution dark blue, obscuring small transient changes in the heme spectrum.

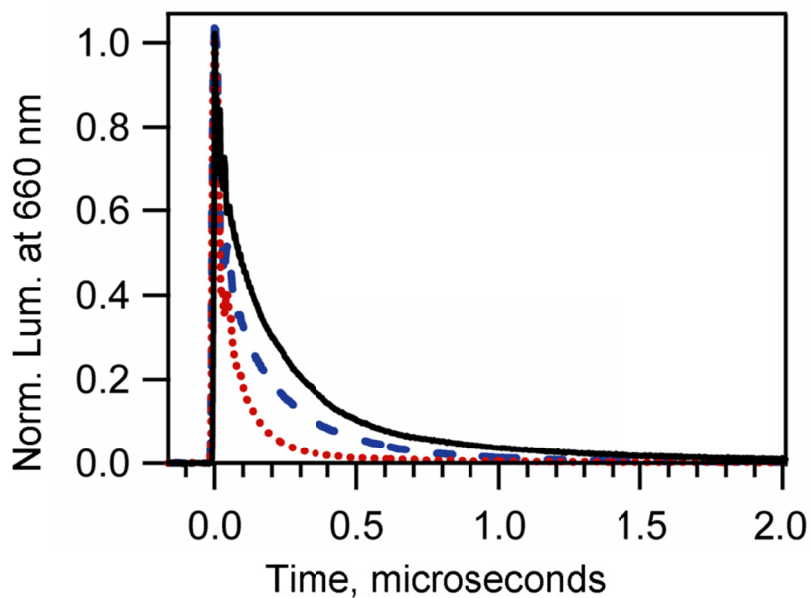
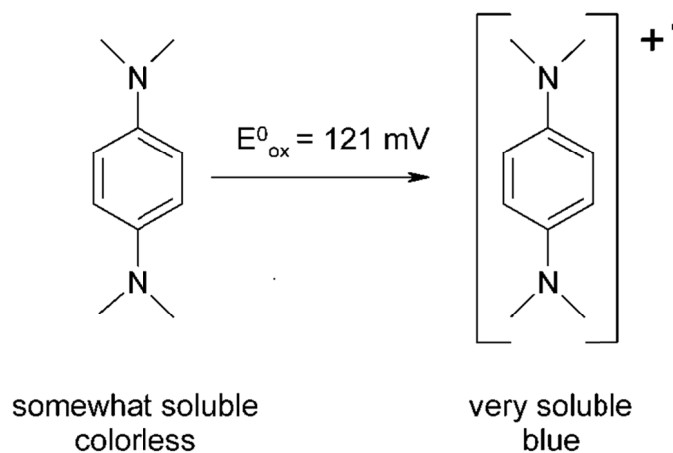


Figure 2.12. Luminescence decay of 6.2 μM tmRu-F₉bp bound to equimolar Im-iNOSoxy in the absence of quenchers (black line) and in the presence of 10 mM Asc (blue dashes) or 10 mM Asc and saturated TMPD (red dots). $\lambda_{\text{ex}} = 480$ nm and $\lambda_{\text{obs}} = 660$ nm.



Scheme 2.6. TMPD, a water-soluble reductive quencher, in its reduced and oxidized forms.

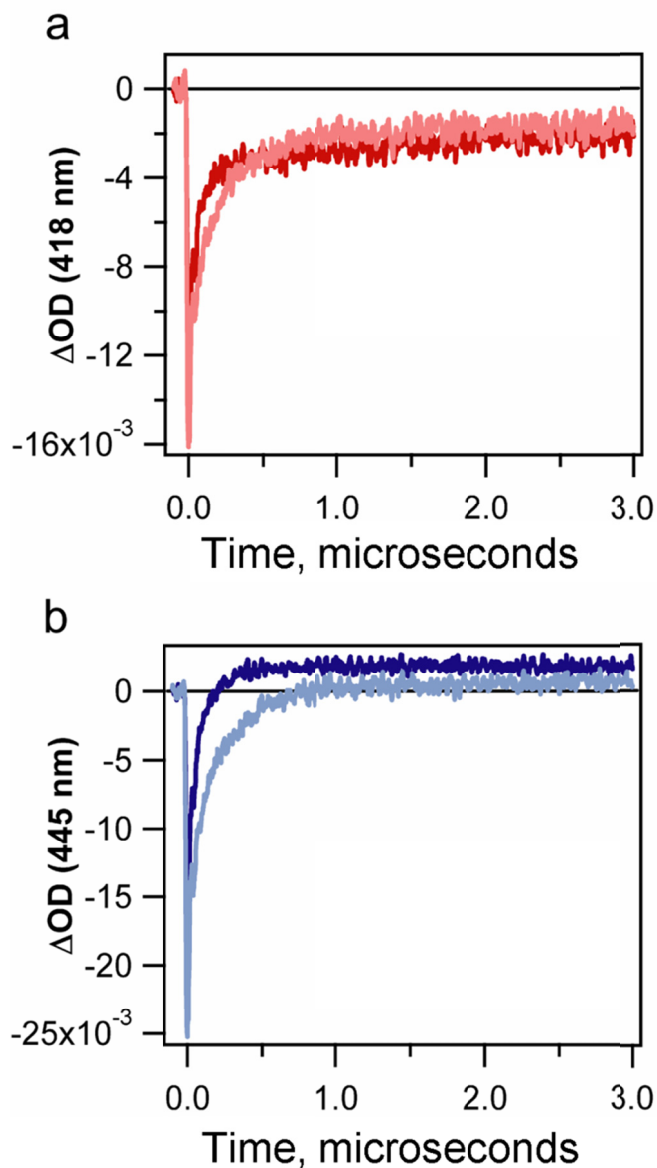


Figure 2.13. Transient absorbance of 1:1 mixtures of tmRu-F₉bp and Im-iNOSoxy (6.2 μM) in the presence of 10 mM Asc with (darker traces) and without (lighter traces) saturated TMPD. $\lambda_{ex} = 480$ nm. a) $\lambda_{obs} = 418$ nm. b) $\lambda_{obs} = 445$ nm. The addition of TMPD increases the yield of reduced heme.

These problems were overcome by employing both quenchers.⁴²⁻⁴³ In a sample containing 10 mM Asc with saturated TMPD, the superior quenching capability of TMPD can be exploited (Figure 2.10, red dotted trace) while Asc serves to keep the

TMPD reduced. With Asc present, TMPD^{++} does not accumulate, even after 60 min. of photoexcitation in the presence of tmRu-F₉bp.

Rapid Production of Reduced iNOSoxy

Single wavelength transient absorbance measurements with imidazole-bound iNOSoxy in the presence of one equivalent of tmRu-F₉bp, 10 mM Asc, and saturated TMPD reveal that photochemically generated Ru^{I} disappears with concomitant formation of a new Fe species within 50 ns of excitation at 480 nm (**Figure 2.14**).

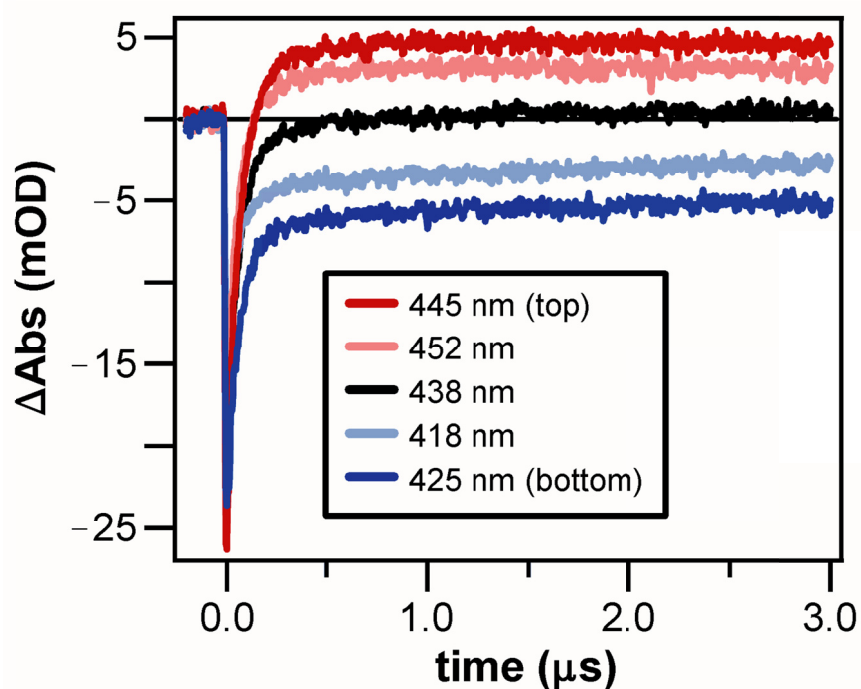


Figure 2.14. Transient absorbance of quenched Im-iNOSoxy bound to 1 equivalent of tmRu-F₉bp (11 μM with 10 mM Asc and saturated TMPD). $\lambda_{\text{ex}} = 480$ nm.

A difference spectrum constructed from the single-wavelength data at 2 μs (**Figure 2.15**) shows the bleach of the Im-Fe^{III} Soret absorption at 428 nm and increased absorbance to the red with a difference-spectrum maximum at 445 nm. The rate of decay of Ru^{I} and reappearance of Ru^{II} is approximately equal to the rate of changes in the Soret region. Given that Ru^{II} is reformed, the most likely explanation for spectral changes

between 400 and 450 nm is Ru^{I} to Fe^{III} ET, which produces a new Fe^{II} heme species. Control experiments with $\text{Ru}(\text{bpy})_3^{2+}$ indicate that the tmRu-F₉bp perfluorobiphenyl moiety is required for heme reduction (**Figure 2.16**). In the presence of $\text{Ru}(\text{bpy})_3^{2+}$ and quenchers, transient absorbance traces show only the production of Ru^{I} .

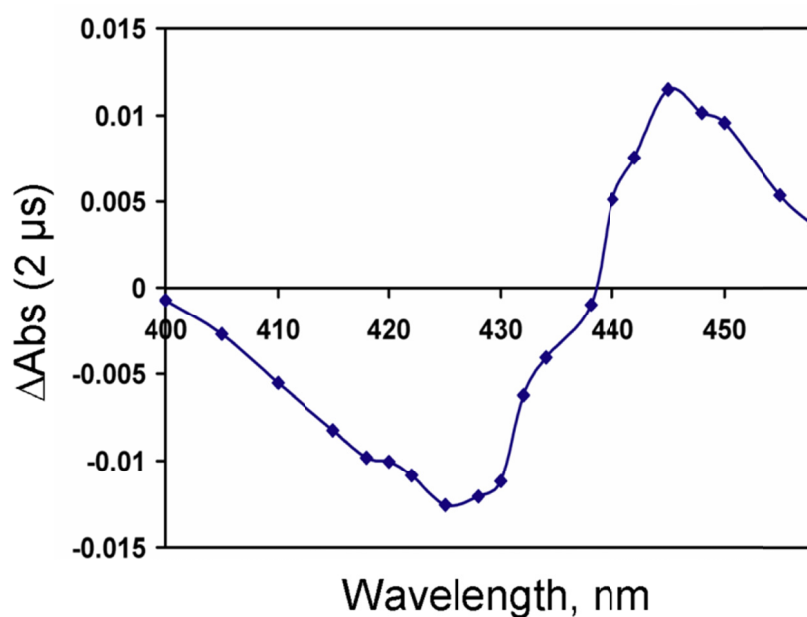


Figure 2.15. Transient absorbance of a 1:1 mixture of Im-iNOSoxy and tmRu-F₉bp (22 μM with 10 mM Asc and saturated TMPD) showing a characteristic Fe(III/II) difference spectrum. Individual points were taken from single wavelength transient absorbance traces at 2 μs after excitation at 480 nm.

In order to estimate the specific rate of Fe^{II} formation, $^*\text{Ru}^{\text{II}}$ contributions were subtracted from the transient absorbance data as described in Materials and Methods (representative single-wavelength traces are shown in **Figure 2.17**). The traces (a minimum of four wavelengths from each of four different experiments completed on different days) were fit to a single exponential function: $k_{\text{ET}} = 2(1) \times 10^7 \text{ s}^{-1}$.

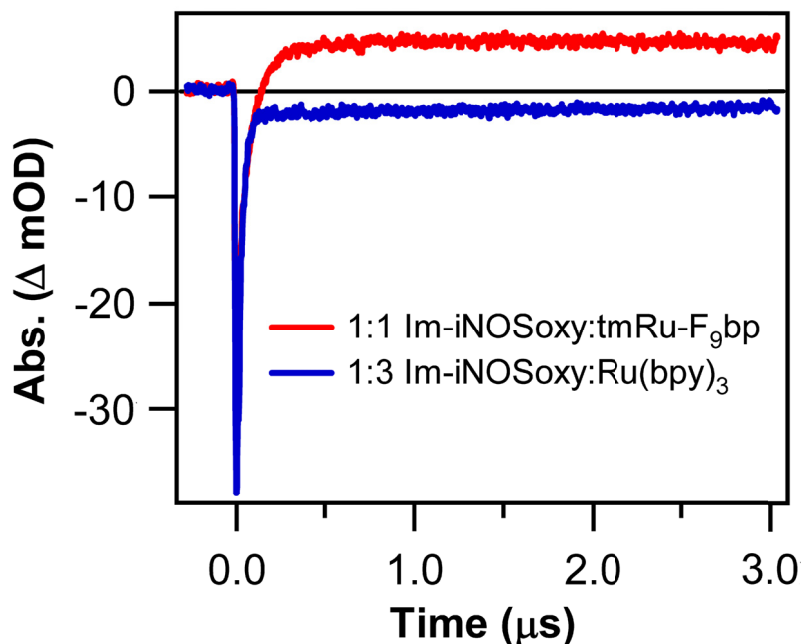


Figure 2.16. Transient absorbance of imidazole-bound iNOSoxy in the presence of tmRu-F₉bp or Ru(bpy)₃²⁺ and quenchers (10 mM ascorbate + saturated TMPD). $\lambda_{\text{ex}} = 480$ nm, $\lambda_{\text{obs}} = 445$ nm. In the absence of the perfluorobiphenyl wire, quenched Ru(bpy)₃²⁺ does not produce Fe^{II}. The long-lived bleach is due to Ru^I.

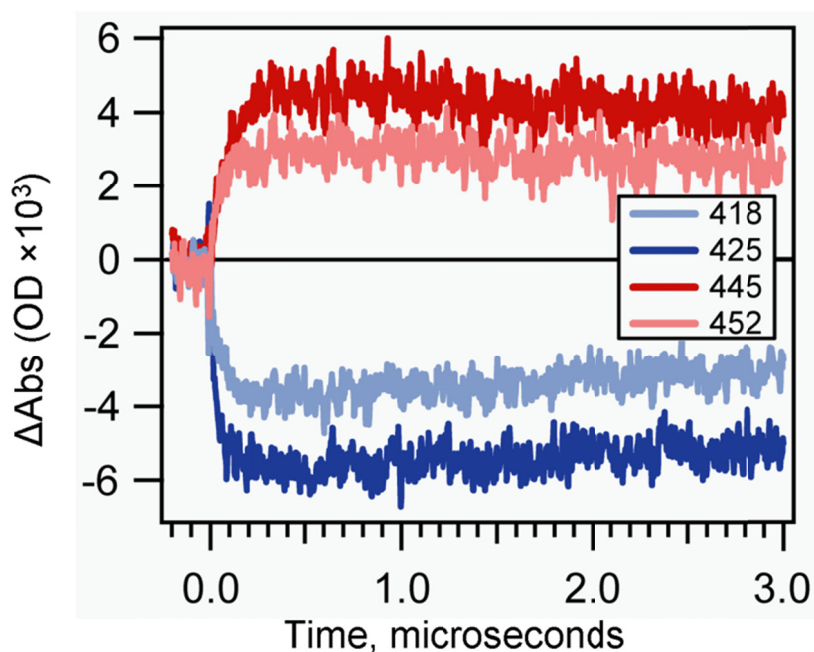


Figure 2.17. Transient absorbance of Im-iNOSoxy bound to 1 equivalent of tmRu-F₉bp (11 μ M with 10 mM Asc and saturated TMPD) corrected for absorbance due to *Ru^{II}: $k_{\text{ET}} = 2(1) \times 10^7$ s⁻¹; $\lambda_{\text{ex}} = 480$ nm.

This is a remarkably rapid reduction given the estimated Ru-heme distance of 20.2 Å¹⁷ and the absence of a through-bond pathway to the heme. Given its slim profile, hydrophobicity, and potential to π -stack with aromatic residues, the perfluorobiphenyl moiety of tmRu-F₉bp may intercalate into the protein interior, leaving open the possibility of a through-wire hopping mechanism.²⁸

Identity of the Reduced Species

In order to determine the nature of the product of electron transfer to the heme, the six-coordinate Fe^{III}-Im species was reduced under equilibrium conditions for comparison with the transient data. Reaction of Fe^{III}-Im with sodium dithionite in a glove box under an inert atmosphere, followed by removal of excess dithionite on a size-exclusion (PD-10) column equilibrated with 10 mM imidazole, produced a species with the absorption spectrum shown in **Figure 2.18**.

Reduction of NOS has been extensively studied.^{25, 35, 44-47} Six-coordinate ferrous-NO and -CO species have been characterized by several investigators,^{35, 46-47} and, in the absence of arginine and BH₄, it has been shown that these six-coordinate species are unstable. Addition of CO (or NO) to five-coordinate Fe^{II} causes a red-shift in the Soret band to 444 nm (or 440 nm).³⁵ The 444 nm band blue-shifts over time to 421 nm, which suggests that a species analogous to the inactive P420 form of cytochrome P450 is produced. It has been proposed that the axial thiolate is not bound to the heme iron in the 421 nm species^{35, 47} or that the thiolate is protonated.⁴⁸

The blue-shift of the iNOSoxy Soret peak upon dithionite reduction (**Figure 2.18**, inset) demonstrates that the red-shifted transient Fe^{II} species produced by photochemical heme reduction likely has different axial coordination. The steady-state Fe^{II} absorption

spectrum is in good agreement with that reported for *Drosophila melanogaster* DHR51, a heme protein believed to possess axial Cys and His ligands.⁴⁹ Similar spectra have been reported for Fe^{II} forms of mutant cytochrome *c* and myoglobin engineered to have axial Cys and His ligands.⁵⁰⁻⁵¹ In each of these Fe^{II} proteins, the Soret maximum is slightly blue-shifted relative to its position in the Fe^{III} form, indicating the presence of a low-spin Fe^{II} heme in which imidazole remains bound but the thiolate ligand has been displaced. Further, five-coordinate ferrous iNOSoxy has been generated, showing a blue-shift of the Soret from the ferric species similar to the spectrum in **Figure 2.18**.³⁵

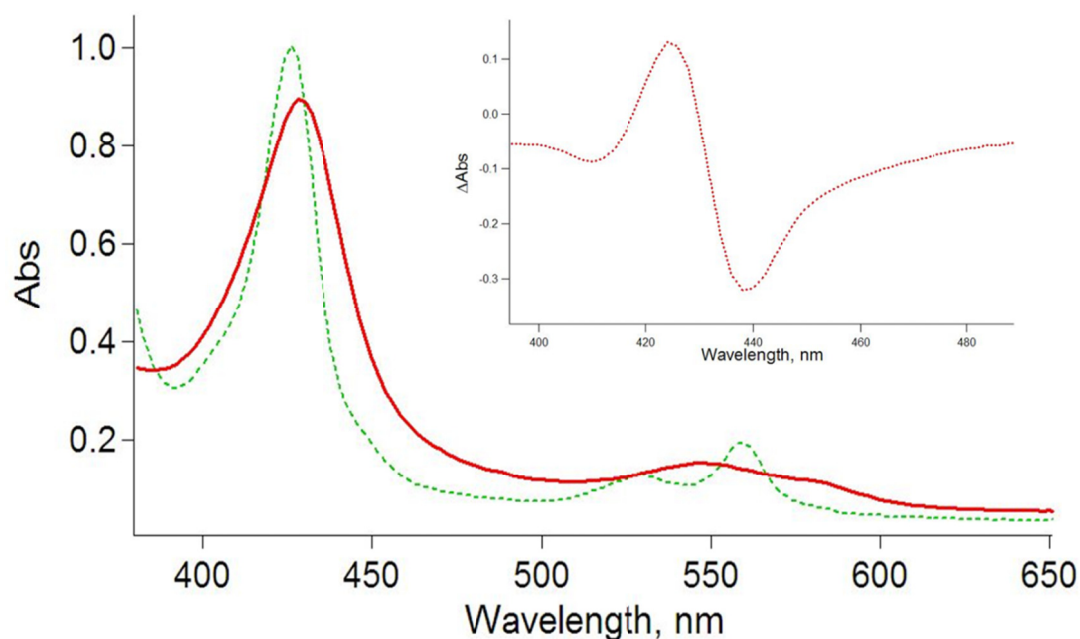


Figure 2.18. Steady-state spectra of ferric-imidazole (red solid line) and the reduced species (green dashed line). Inset: The difference spectrum generated upon reduction (red dotted line).

In contrast, the red-shifted Soret band found for photochemically reduced iNOS is analogous to that resulting from cryoreduction of ferric cytochrome P450. Irradiation of six-coordinate low-spin Fe^{III} P450 in a frozen matrix produces a low-spin, presumably six-coordinate Fe^{II} product.¹³ Annealing at higher temperatures leads to the high-spin Fe^{II}

product that is observed under equilibrium conditions. We suggest that the transient Fe^{II} iNOS species formed by photochemical reduction contains a low-spin Fe^{II} heme with axial Cys and imidazole ligands. In our experiment, this species is likely reoxidized by TMPD^{+} before loss of axial ligation, which would generate the species observed under equilibrium conditions.

2.5 Concluding Remarks and Discussion

We have developed a system in which the heme of inducible nitric oxide synthase can be photoreduced rapidly without interfering with substrate/cofactor binding. Employing flash/quench experiments with a surface-binding Ru-diimine wire in combination with reductive quenchers, we observed ET to the imidazole-bound heme of iNOSoxy fully seven orders of magnitude faster than the natural reduction. This finding represents an important step toward our goal of identifying reactive intermediates in the catalytic cycles of heme monooxygenases.

Interestingly, however, the product of this ET reaction is a six-coordinate heme. In contrast, the product of steady-state reduction of the heme is consistent with either a five-coordinate species with imidazole ligation or a complex where the negative axial thiolate ligand becomes protonated forming a neutral thiol ligand. On the millisecond timescale this six-coordinate species is stable, however, over the long term it will decay to the more thermodynamically favored five-coordinate or neutral thiol complex. This decay highlights the inherent instability of the thiolate-ligated heme complex.

Upon closer inspection of the environment around the thiolate ligand, one finds a collection of three hydrogen bond (H-bond) donors all directed toward the thiolate.

Comparison of iNOSoxy with other NOS enzymes reveals that these three hydrogen bond donors are universally conserved, with not a single exception. This high level of conservation underscores their potential importance. Not only are they conserved in nitric oxide synthases, but the crystal structures of other heme thiolate enzymes reveal similarly conserved hydrogen bond donors in all. Cytochrome P450s (cyt. P450) all contain three H-bond donors; chloroperoxidase (CPO) contains only two such donors.

When analyzing these polypeptide chains, one finds that in cyt. P450 and CPO all three donors in the proximal heme environment come not from amino acid side-chains but from amide protons in the backbone of the polypeptide chain. In NOS alone one and only one of the H-bond donors comes not from an amide but from the N-H of a tryptophan's indole ring, **Figure 2.19**. The universality of these H-bond donors pointing right at the axial thiolate ligand provokes questions of their function in the reactivity or stability or electronic tuning of these enzymes.

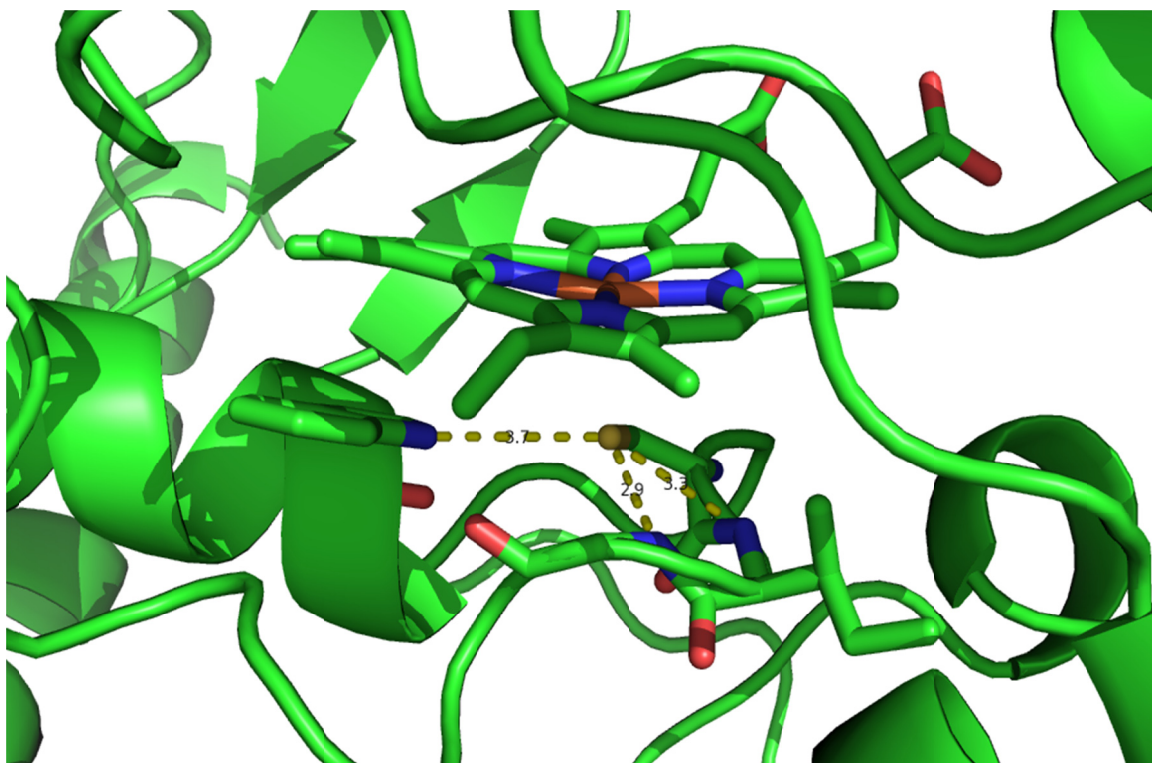


Figure 2.19. Close-up view of the heme center in a nitric oxide synthase showing the three hydrogen bond donors. The middle and the right are from amide groups on the protein backbone (2.9 and 3.3 Å) while the long H-bond on the left comes from a tryptophan (very long at 3.7 Å) (PDB file 2FLQ).

Others have attempted to investigate the possible roles of these H-bond donors in cyt. P450.⁵²⁻⁵⁴ The replacement of a glutamine that provides one amide group with a proline forces a kink in the loop below the heme and obviously replaces the N-H bond in the glutamine backbone with a N-C bond, incapable of participating in H-bonding. This also removes a hydrogen bond from the side chain of the Gln to the carbonyl moiety of the cysteine residue. The combination of these two effects as well as the shift in the backbone resulting from introduction of a proline makes results difficult to deconvolute. The work suggests, however, that this H-bond donor (not even a legitimate hydrogen bond) shifts the reduction potential of the heme by about +40 mV (removing it makes the potential more negative by about 40 mV). Resonance Raman suggests that this H-bond

donor decreases the σ -donating ability of the thiolate significantly; its removal strengthens the iron-sulfur bond. They “conclude that the functions of the proximal hydrogen bonding network in P450_{cam} are to stabilize the heme-thiolate coordination, and to regulate the redox potential of the heme iron.”⁵⁴ While these conclusions seem reasonable, it is difficult to say the effect of a particular H-bond when several things are affected at once.

We wish to determine the role of these H-bond donors and support or refute the previous findings, but particularly to study their effects in NOS. This family of enzymes provides a unique opportunity, given that one of the H-bond donors comes not from the backbone but from a side chain, allowing for facile and systematic variation using site-directed mutagenesis. Several such mutations have previously been made in NOS and characterized by resonance Raman.⁵⁵⁻⁵⁶ No further characterization has been reported.

One other mutant of interest replaced the tryptophan with a histidine, preserving and possibly increasing the H-bond donor ability of the group. In this mutant, researchers actually saw a slower kinetics profile and possibly a new intermediate by stopped-flow spectroscopy.²⁵ No further characterization was done and the new intermediate, based solely upon the position of the Soret band, was suggested to be Compound I (**Scheme 2.3**, the ferryl complex in blue). The lifetime of this new intermediate is on the order of a couple of seconds before decaying to product. Compound I is formally a Fe(V) complex, with a ferryl and another radical cation sometimes found on the porphyrin ring. The likelihood of such a species living for that length of time is incredibly low as it will be very reactive, making its assignment as Compound I doubtful.¹⁴ No other investigations into the role of this H-bond donor have been made.

We propose to investigate the role of these H-bond donors by systematically varying the functional groups on this side chain in question through the use of site-directed mutagenesis. The native tryptophan will be replaced with histidine, phenylalanine, or tyrosine. Histidine can also participate in hydrogen bonding, but lacks the ability to π -stack with the porphyrin ring. Phenylalanine complements the histidine mutation in that it can π -stack but cannot hydrogen bond. The tyrosine can also π -stack, but the electronics should be significantly altered due to the presence of the hydroxyl group on the aryl ring, which is at an angle that should prohibit hydrogen bonding with the thiolate. These three mutants will be expressed and thoroughly characterized using the tools of modern bioinorganic chemistry to investigate the thermodynamics of the resulting active site and its reactivity (EPR, electrochemistry, single turnover experiments, etc.). These studies should provide valuable insight into the specific role of these hydrogen bond donors and their purpose in NOS and other heme thiolate enzymes, and this work will be the focus of the bulk of this thesis.

2.6 References

1. Finkel, T., and Holbrook, N. J. (2000) Oxidants, oxidative stress and the biology of ageing, *Nature* 408, 239.
2. Arnon, D. I. (1959) Conversion of light into chemical energy in photosynthesis, *Nature* 184, 10.
3. Marcus, R. A., and Sutin, N. (1985) Electron transfers in chemistry and biology, *Biochimica Et Biophysica Acta* 811, 265.
4. Gray, H. B., and Winkler, J. R. (1996) Electron transfer in proteins, *Annu. Rev. Biochem.* 65, 537.
5. Marcus, R. A. (1956) On the theory of oxidation-reduction reactions involving electron transfer .1, *J. Chem. Phys.* 24, 966.
6. Chang, I.-J., Gray, H. B., and Winkler, J. R. (1991) High-driving-force electron transfer in metalloproteins: Intramolecular oxidation of ferrocycytochrome *c* by $\text{ru}(2,2'\text{-bipyridine})_2(\text{imidazole})(\text{histidine-33})^{3+}$, *J. Am. Chem. Soc.* 113, 7056.
7. Low, D. W., Winkler, J. R., and Gray, H. B. (1996) Photoinduced oxidation of microperoxidase-8 - generation of ferryl and cation-radical porphyrins, *J. Am. Chem. Soc.* 118, 117.
8. Dunn, A. R., Dmochowski, I. J., Winkler, J. R., and Gray, H. B. (2003) Nanosecond photoreduction of cytochrome p450cam by channel-specific rudiimine electron tunneling wires, *J. Am. Chem. Soc.* 125, 12450.
9. Dunn, A. R. (2003) Sensitizer-linked substrates as probes of heme enzyme structure and catalysis, In *Chemistry*, p 216, California Institute of Technology, Pasadena.
10. Hartings, M. R., Kurnikov, I. V., Dunn, A. R., Winkler, J. R., Gray, H. B., and Ratner, M. A. (2010) Electron tunneling through sensitizer wires bound to proteins, *Coord. Chem. Rev.* 254, 248.
11. Contakes, S. M., Nguyen, Y. H. L., Gray, H. B., Glazer, E. C., Hays, A. M., and Goodin, D. B. (2007) Conjugates of heme-thiolate enzymes with photoactive metal-diimine wires, In *Photofunctional transition metals complexes*, pp 177, Springer-Verlag Berlin, Berlin.
12. Davydov, R., Ledbetter-Rogers, A., Martásek, P., Larukhin, M., Sono, M., Dawson, J. H., Masters, B. S. S., and Hoffman, B. M. (2002) Epr and endor characterization of intermediates in the cryoreduced oxy-nitric oxide synthase heme domain with bound l-arginine or n^g-hydroxyarginine, *Biochemistry* 41, 10375.
13. Denisov, I. G., Makris, T. M., and Sligar, S. G. (2002) Cryoradiolysis for the study of p450 reaction intermediates, *Methods in Enzymology* 357, 103.
14. Rittle, J., and Green, M. T. (2010) Cytochrome p450 compound i: Capture, characterization, and c-h bond activation kinetics, *Science* 330, 933.
15. Berglund, J., Pascher, T., Winkler, J. R., and Gray, H. B. (1997) Photoinduced oxidation of horseradish peroxidase, *J. Am. Chem. Soc.* 119, 2464.
16. Whited, C. A., Belliston-Bittner, W., Dunn, A. R., Winkler, J. R., and Gray, H. B. (2008) Probing the heme-thiolate oxygenase domain of inducible nitric oxide synthase with ru(ii) and re(i) electron tunneling wires, *Journal of Porphyrins and Phthalocyanines* 12, 971.

17. Dunn, A. R., Belliston-Bittner, W., Winkler, J. R., Getzoff, E. D., Stuehr, D. J., and Gray, H. B. (2005) Luminescent ruthenium(ii)- and rhenium(i)- diimine wires bind nitric oxide synthase, *J. Am. Chem. Soc.* *127*, 5169.
18. Griffith, O. W., and Stuehr, D. J. (1995) Nitric oxide synthases: Properties and catalytic mechanism, *Annu. Rev. Physiol.* *57*, 707.
19. Groves, J. T., and Wang, C. C.-Y. (2000) Nitric oxide synthase: Models and mechanisms, *Curr. Opin. Chem. Biol.* *4*, 687.
20. Zhu, Y., and Silverman, R. B. (2008) Revisiting heme mechanisms. A perspective on the mechanisms of nitric oxide synthase (nos), heme oxygenase (ho), and cytochrome p450s (cyp450s), *Biochemistry* *47*, 2231.
21. Hurshman, A. R., Krebs, C., Edmondson, D. E., Huynh, B. H., and Marletta, M. A. (1999) Formation of a pterin radical in the reaction of the heme domain of inducible nitric oxide synthase with oxygen, *Biochemistry* *38*, 15689.
22. Wei, C.-C., Wang, Z.-Q., Tejero, J., Yang, Y.-P., Hemann, C., Hille, R., and Stuehr, D. J. (2008) Catalytic reduction of a tetrahydrobiopterin radical within nitric-oxide synthase, *J. Biol. Chem.* *283*, 11734.
23. Robinet, J. J., Cho, K.-B., and Gaudl, J. W. (2008) A density functional theory investigation on the mechanism of the second half-reaction of nitric oxide synthase, *J. Am. Chem. Soc.* *130*, 3328.
24. Stuehr, D. J., Santolini, J., Wang, Z.-Q., Wei, C.-C., and Adak, S. (2004) Update on mechanism and catalytic regulation in the no synthases, *J. Biol. Chem.* *279*, 36167.
25. Tejero, J., Biswas, A., Wang, Z.-Q., Page, R. C., Haque, M. M., Hemann, C., Zweier, J. L., Misra, S., and Stuehr, D. J. (2008) Stabilization and characterization of a heme-oxy reaction intermediate in inducible nitric-oxide synthase, *J. Biol. Chem.* *283*, 33498.
26. Wilker, J. J., Dmochowski, I. J., Dawson, J. H., Winkler, J. R., and Gray, H. B. (1999) Substrates for rapid delivery of electrons and holes to buried active sites in proteins, *Angew. Chem. Int. Edit.* *38*, 89.
27. Dmochowski, I. J., Dunn, A. R., Wilker, J. J., Crane, B. R., Green, M. T., Dawson, J. H., Sligar, S. G., Winkler, J. R., and Gray, H. B. (2002) Sensitizer-linked substrates and ligands: Ruthenium probes of cytochrome p450 structure and mechanism, *Method. Enzymol.* *357*, 120.
28. Belliston-Bittner, W., Dunn, A. R., Nguyen, Y. H. L., Stuehr, D. J., Winkler, J. R., and Gray, H. B. (2005) Picosecond photoreduction of inducible nitric oxide synthase by rhenium(i)-diimine wires, *J. Am. Chem. Soc.* *127*, 15907.
29. Nguyen, Y. H. L., Winkler, J. R., and Gray, H. B. (2007) Probing heme coordination states of inducible nitric oxide synthase with a re(i)(imidazole-alkyl-nitroarginine) sensitizer-wire, *J. Phys. Chem. B* *111*, 6628.
30. Beaumont, E., Lambry, J. C., Gautier, C., Robin, A. C., Gmouh, S., Berka, V., Tsai, A. L., Blanchard-Desce, M., and Slama-Schwok, A. (2007) Synchronous photoinitiation of endothelial no synthase activity by a nanotrigger targeted at its nadph site, *J. Am. Chem. Soc.* *129*, 2178.
31. Dmochowski, I. J. (2000) Probing cytochrome p450 with sensitizer-linked substrates, In *Chemistry*, p 305, California Institute of Technology, Pasadena.

32. Hurshman, A. R., and Marletta, M. A. (2002) Reactions catalyzed by the heme domain of inducible nitric oxide synthase: Evidence for the involvement of tetrahydrobiopterin in electron transfer, *Biochemistry* 41, 3439.
33. Wang, J. L., Rousseau, D. L., Abusoud, H. M., and Stuehr, D. J. (1994) Heme coordination of no in no synthase, *P. Natl. Acad. Sci. USA* 91, 10512.
34. Hurshman, A. R., and Marletta, M. A. (1995) Spectral characterization and effect on catalytic activity of nitric oxide complexes of inducible nitric oxide synthase, *Biochemistry* 34, 5627.
35. Abu-Soud, H. M., Wu, C., Ghosh, D. K., and Stuehr, D. J. (1998) Stopped-flow analysis of co and no binding to inducible nitric oxide synthase, *Biochemistry* 37, 3777.
36. Kuciasukas, D., Freund, M. S., Gray, H. B., Winkler, J. R., and Lewis, N. S. (2001) Electron transfer dynamics in nanocrystalline titanium dioxide solar cells sensitized with ruthenium or osmium polypyridyl complexes, *J. Phys. Chem. B* 105, 392.
37. Dmochowski, I. J., Winkler, J. R., and Gray, H. B. (2000) Enantiomeric discrimination of ru-substrates by cytochrome p450_{cam}, *J. Inorg. Biochem.* 81, 221.
38. Garcin, E. D., Bruns, C. M., Lloyd, S. J., Hosfield, D. J., Tiso, M., Gachhui, R., Stuehr, D. J., Tainer, J. A., and Getzoff, E. D. (2004) Structural basis for isozyme-specific regulation of electron transfer in nitric-oxide synthase, *J. Biol. Chem.* 279, 37918.
39. Rao, P. S., and Hayon, E. (1975) Oxidation of aromatic-amines and diamines by oh radicals - formation and ionization-constants of amine cation radicals in water, *J. Phys. Chem.* 79, 1063.
40. Fujita, S., and Steenken, S. (1981) Pattern of oh radical-addition to uracil and methyl-substituted and carboxyl-substituted uracils - electron-transfer of oh adducts with n,n,n',n'-tetramethyl-para-phenylenediamine and tetranitromethane, *J. Am. Chem. Soc.* 103, 2540.
41. Hobel, B., and von Sonntag, C. (1998) Oh-radical induced degradation of ethylenediaminetetraacetic acid (edta) in aqueous solution: A pulse radiolysis study, *J. Chem. Soc. Perk. T. 2*, 509.
42. Schweizer, M., and Richter, C. (1994) Nitric-oxide potently and reversibly deenergizes mitochondria at low-oxygen tension, *Biochem. Biophys. Res. Commun.* 204, 169.
43. Devoe, I. W., and Gilchrist, J. E. (1976) Localization of tetramethylphenylenediamine-oxidase in outer cell-wall layer of neisseria-meningitidis, *J. Bacteriol.* 128, 144.
44. Marchal, S., Gorren, A. C. F., Sorlie, M., Andersson, K. K., Mayer, B., and Lange, R. (2004) Evidence of two distinct oxygen complexes of reduced endothelial nitric oxide synthase, *J. Biol. Chem.* 279, 19824.
45. Roman, L. J., and Masters, B. S. S. (2006) Electron transfer by neuronal nitric-oxide synthase is regulated by concerted interaction of calmodulin and two intrinsic regulatory elements, *J. Biol. Chem.* 281, 23111.
46. Migita, C. T., Salerno, J. C., Masters, B. S. S., Martasek, P., McMillan, K., and Ikeda-Saito, M. (1997) Substrate binding-induced changes in the epr spectra of

- the ferrous nitric oxide complexes of neuronal nitric oxide synthase, *Biochemistry* 36, 10987.
47. Huang, L., Abu-Soud, H. M., Hille, R., and Stuehr, D. J. (1999) Nitric oxide-generated p420 nitric oxide synthase: characterization and roles for tetrahydrobiopterin and substrate in protecting against or reversing the p420 conversion, *Biochemistry* 38, 1912.
 48. Sabat, J., Stuehr, D. J., Yeh, S. R., and Rousseau, D. L. (2009) Characterization of the proximal ligand in the p420 form of inducible nitric oxide synthase, *J. Am. Chem. Soc.* 131, 12186.
 49. de Rosny, E., de Groot, A., Jullian-Binard, C., Borel, F., Suarez, C., Le Pape, L., Fontecilla-Camps, J. C., and Jouve, H. I. n. M. (2008) Dhr51, the drosophila melanogaster homologue of the human photoreceptor cell-specific nuclear receptor, is a thiolate heme-binding protein, *Biochemistry* 47, 13252.
 50. Raphael, A. L., and Gray, H. B. (1991) Semisynthesis of axial-ligand (position 80) mutants of cytochrome c, *J. Am. Chem. Soc.* 113, 1038.
 51. Matsui, T., Nagano, S., Ishimori, K., Watanabe, Y., and Morishima, I. (1996) Preparation and reactions of myoglobin mutants bearing both proximal cysteine ligand and hydrophobic distal cavity: protein models for the active site of p-450, *Biochemistry* 35, 13118.
 52. Galinato, M. G. I., Spolitak, T., Ballou, D. P., and Lehnert, N. (2011) Elucidating the role of the proximal cysteine hydrogen-bonding network in ferric cytochrome p450cam and corresponding mutants using magnetic circular dichroism spectroscopy, *Biochemistry* 50, 1053.
 53. Ueyama, N., Nishikawa, N., Yamada, Y., Okamura, T., and Nakamura, A. (1996) Cytochrome p-450 model (porphinato)(thiolato)iron(iii) complexes with single and double nh center dot center dot center dot s hydrogen bonds at the thiolate site, *J. Am. Chem. Soc.* 118, 12826.
 54. Yoshioka, S., Tosha, T., Takahashi, S., Ishimori, K., Hori, H., and Morishima, I. (2002) Roles of the proximal hydrogen bonding network in cytochrome p450(cam)-catalyzed oxygenation, *J. Am. Chem. Soc.* 124, 14571.
 55. Couture, M., Adak, S., Stuehr, D. J., and Rousseau, D. L. (2001) Regulation of the properties of the heme-no complexes in nitric-oxide synthase by hydrogen bonding to the proximal cysteine, *J. Biol. Chem.* 276, 38280.
 56. Lang, J., Driscoll, D., Gelinas, S., Rafferty, S. P., and Couture, M. (2009) Trp180 of endothelial nos and trp56 of bacterial sanos modulate sigma bonding of the axial cysteine to the heme, *J. Inorg. Biochem.* 103, 1102.

Chapter 3

Thiolate Hydrogen Bonding Mutants: Thermodynamics

3.1 Abstract

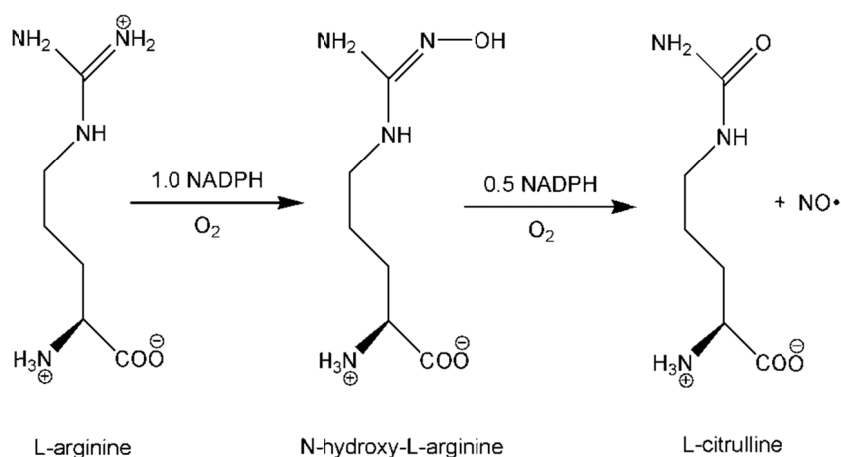
All heme thiolate enzymes have conserved hydrogen bonding networks surrounding the axial thiolate ligand. In order to understand the role of this proximal hydrogen bonding network in nitric oxide synthases, three mutants of the NOS enzyme from *Geobacillus stearothermophilus* were expressed and characterized. The wild type enzyme has a tryptophan residue at position 70 that π -stacks with the porphyrin ring and donates a long hydrogen-bonding interaction to the thiolate ligand of the heme iron. The native Trp was replaced with His, Phe, and Tyr. These three residues were selected to investigate the two effects of the Trp, H-bonding and π -stacking. Several different spectroscopic techniques were used to investigate the stability and properties of these mutant enzymes. The identity of each mutant was confirmed by mass spectrometry. Both UV-visible absorption and circular dichroism spectroscopies were used to assess the stability of the new proteins. It was shown using binding assays, generation of the ferrous-CO species, and redox titrations that the σ -donating abilities of the thiolate are increased after removal of the hydrogen bonding group in the Trp. Finally, electron paramagnetic resonance spectroscopy and Evans method nuclear magnetic resonance spectroscopy were used to characterize the spin state of the iron center in each mutant, reflecting the increased σ -donating capabilities of the thiolate upon removal of the hydrogen bonding group. The reduction potential of wild type and W70H were determined by chemical titration to be -362 and -339 mV vs. NHE, respectively. This is the first report of the reduction potential of any bacterial nitric oxide synthase.

3.2 Introduction

Heme-thiolate enzymes play important roles in human physiology such as drug metabolism and in the production of signaling molecules involved in processes such as neurotransmission.¹⁻² Cytochromes P450 (cyt. P450) are a super-family of these interesting heme enzymes and many different forms are found in mammals.³ They carry out a broad array of biological transformations from epoxidation of alkenes to isomerizations and many different oxidation and reduction reactions. They are most famous for their ability to hydroxylate unactivated carbon-hydrogen bonds. It would take a unique and highly reactive complex to afford such difficult and varied reactions.

There are only a small number of heme-thiolate enzymes (counting cyt. P450 as a single entity).³ Joining cyt. P450 are the nitric oxide synthases (NOS) and chloroperoxidase (CPO). CPO carries out the typical peroxidase and catalase activities of any standard peroxidase enzyme.⁴ It is unique among peroxidases, however, in its ability to use hydrogen peroxide to oxidize the halogens iodide, bromide, and chloride, and use them to form carbon-halogen bonds on substrates.

The family of enzymes called nitric oxide synthases (NOSs) is responsible for biological production of NO.⁵ This family includes three isoforms named for the tissues in which they are found: endothelial NOS (eNOS), neuronal (nNOS), and an inducible form found in macrophages (iNOS). The function of eNOS and nNOS is regulated by calcium ions and a calmodulin linker, while the inducible isoform is calcium ion independent.⁶ NOSs catalyze the oxidation of L-arginine (Arg) to L-citrulline in two turnovers, with N^ω-hydroxy-L-arginine (NOHA) as an intermediate (the product of the first turnover).⁷ The overall reaction is shown in **Scheme 3.1**.



Scheme 3.1: The five-electron oxidation of arginine to form NO and citrulline.

All three isoforms are found as homodimers, each monomer consisting of an oxygenase domain and a reductase domain.⁸ The reductase domain binds flavin adenine dinucleotide (FAD) and flavin mononucleotide (FMN) which shuttle electrons from nicotinamide adenine dinucleotide phosphate (NADPH),⁹ the ultimate source of electrons for the reaction, to the oxygenase domain where substrate oxidation occurs. The oxygenase domain contains a thiolate-ligated heme group (protoporphyrin IX) like that in cytochromes P450 and the cofactor (6R)-5,6,7,8-tetrahydrobiopterin (pterin, H₄B).⁸ This domain successfully forms NO when supplied with a source of electrons (e.g., NADPH),¹⁰ but the pterin cofactor is needed for catalysis.¹¹⁻¹² No crystal structure for a full-length NOS has been reported, but several structures of each domain of many isoforms have been published separately.¹³⁻¹⁴

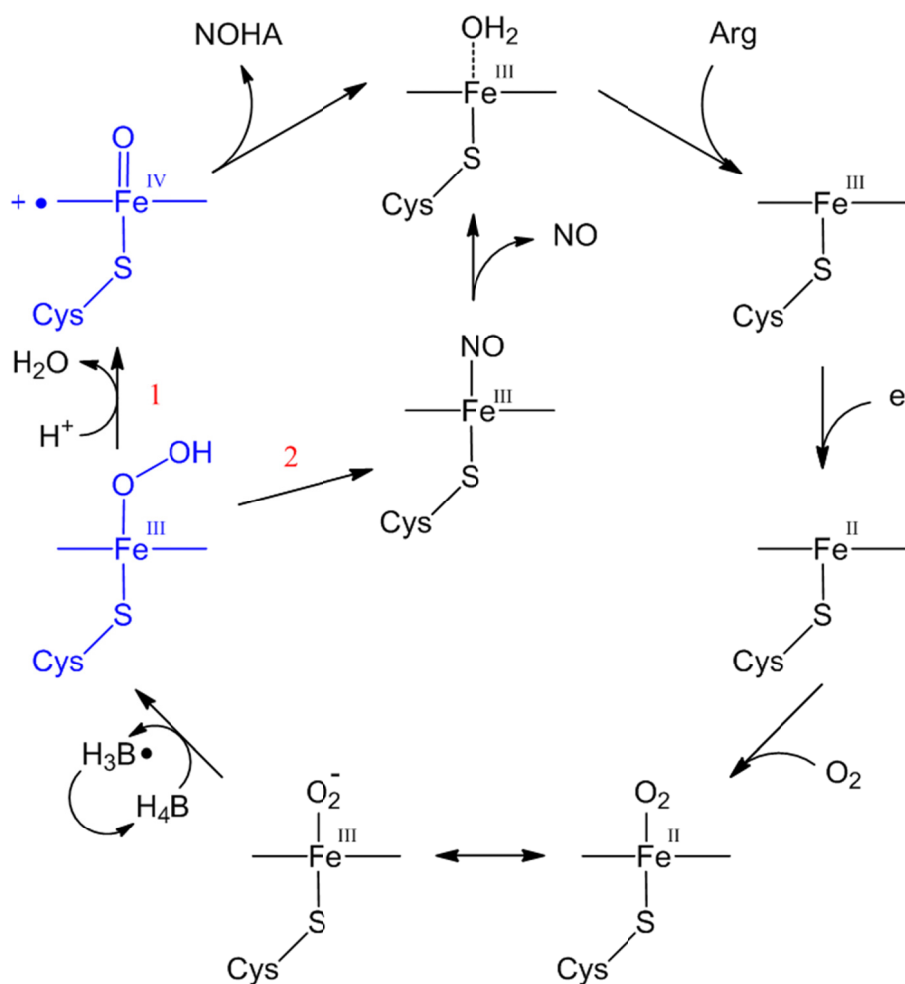
The mechanism of NOS is not fully understood.¹⁵ The resting state of the enzyme is ferric heme with a water molecule occupying the sixth ligand position (four positions are occupied by the porphyrin, one by an axial cysteine, Cys194).¹⁶ Catalysis begins with the binding of the substrate in both turnovers. This displaces the water molecule, but neither Arg nor NOHA ligates the heme. Binding events shift the Soret band

(characteristic absorbance of metalloporphyrins, 421 nm for substrate- and pterin-free iNOS)¹⁷ as well as the spin-state (from low- to high-spin ferric).¹⁸ The Soret of pterin- and arginine-loaded iNOS occurs at 390 nm. This is followed by a one-electron reduction of the iron to ferrous. Ferrous heme readily binds oxygen, forming a ferrous-oxy species (equivalent to ferric-superoxide),⁸ the last observed intermediate in the catalytic cycle.^{8, 19}

The role pterin has been extensively investigated.^{11, 16, 20} This molecule binds in a pocket alongside the heme, forming hydrogen bonds with a carboxylate group on the heme directly coupling it to the iron active site.¹³ It is known that a pterin-based radical forms and is reduced during the cycle (**Scheme 3.2**), as determined by rapid-freeze electron paramagnetic resonance experiments.^{12, 21} The current hypothesis is that proton-coupled electron transfer from pterin aids in formation of the hydroxylating species.^{10, 20} No turnover has ever been observed without the pterin cofactor bound.²² The pterin cofactor is thought to be essential for producing the active hydroxylating species through proton-coupled electron transfer. The efforts of this study focus on characterizing the iron active site.

The known mechanistic data and overall reaction bear many similarities to cytochrome P450s (CYP450). The CYP450s contain cysteine-ligated hemes and hydroxylate their substrates via a two-electron oxidation.²³⁻²⁴ Their mechanism also begins with substrate binding and is followed by reduction, dioxygen binding, and another reduction step leading to the formation of high-valent iron-oxo species which are very reactive and hydroxylate the nearby substrate.²⁴ Separate enzymes serve as reductases for CYP450s, but they too can hydroxylate substrate when supplied with an

external source of electrons.²⁵ Due to the similarities, the mechanism of NOS is postulated to be the same as CYP450s, at least for the first turnover.²⁶ The second turnover is unique in biology; there is no precedent for a three-electron oxidation of this sort.²⁷ It has been hypothesized that a protonated ferric-hydroperoxide may act as the nucleophile in the second turnover¹⁹ rather than the ferryl-porphyrin radical cation known as Compound I.⁸



Scheme 3.2. The proposed catalytic cycle of nitric oxide synthase. Blue denotes species that have been proposed, but not observed. The numbers 1 and 2 in red show the pathway taken in each turnover.

Stopped-flow mixing coupled to UV-visible absorption spectroscopy is commonly used to observe catalytic intermediates. Unfortunately, the reactivity of nitric

oxide synthases is too fast to catch all of the intermediate steps. Using this technique, the final observable species before product formation is the ferrous-oxy (or ferric-superoxo depending on formal placement of the electron).⁶ In the first turnover, the next species observed is the resting ferric state and in the second turnover it is the ferric-NO complex, which slowly releases NO to finish the cycle. No other intermediates can be seen by stopped-flow, presumably due to the speed with which they react.

Evidence supporting that the hydroperoxo species (in blue) is the active oxidant in the second turnover comes mainly from the ENDOR (electron-nuclear double resonance spectroscopy) studies conducted on the NOS from *Geobacillus stearothermophilus* (gsNOS) by Brian Hoffman and Roman Davydov.²⁸⁻²⁹ These experiments show cleavage of the O-O bond prior to reaction with substrate in the first turnover, supporting the formation of Compound I or a similar species. In the second turnover, however, no cleavage of the O-O bond is observed prior to attack on substrate. They hypothesize that the presence of the hydroxyl group in NOHA makes the substrate easier to oxidize. The hydroperoxo heme complex might have enough oxidizing power to react with NOHA but not the arginine, requiring Compound I in the first turnover.

It is the O-O bond cleavage event that is vital to the reactivity of NOS and cyt. P450. Without this, Compound I cannot form and the active site will fail to produce a species with sufficient oxidizing power to react with substrates such as unactivated alkanes. It has been hypothesized that the role of the thiolate ligand is to promote this cleavage.³⁰ The strong σ -donating ability of the anionic ligand pushes more electron density into the iron and therefore also into the iron-oxygen bond and weakening the O-O bond. This has been dubbed the “thiolate push”.³¹

Upon closer inspection of the environment around the thiolate ligand, one finds a collection of three hydrogen bond (H-bond) donors all directed toward the thiolate. Comparison of gsNOS with other NOS enzymes reveals that these three hydrogen bond donors are universally conserved, with not a single exception.³² This high level of conservation underscores their potential importance. Not only are they conserved in nitric oxide synthases, but the crystal structures of other heme thiolate enzymes reveal similarly conserved hydrogen bond donors in all. Cytochrome P450s (cyt. P450) all contain three H-bond donors; chloroperoxidase (CPO) contains only two such donors.³

When analyzing these polypeptide chains, one finds that in cyt. P450 and CPO all three donors in the proximal heme environment come not from amino acid side-chains but from amide protons in the backbone of the polypeptide chain. In NOS alone one and only one of the H-bond donors comes not from an amide but from the N-H of a tryptophan's indole ring, **Figure 3.1**. The universality of these H-bond donors pointing right at the axial thiolate ligand provokes questions of their function in the reactivity or stability or electronic tuning of these enzymes.

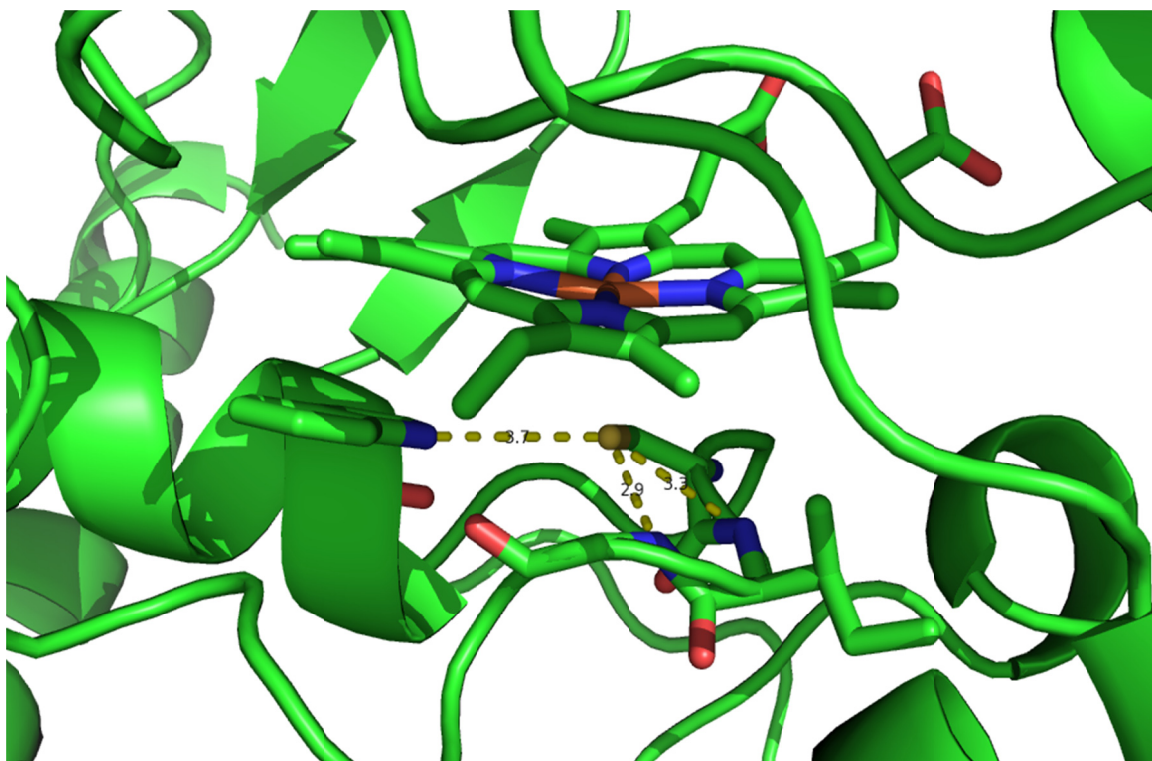


Figure 3.1. Close-up view of the heme center in a nitric oxide synthase showing the three hydrogen bond donors. The middle and the right are from amide groups on the protein backbone (2.9 and 3.3 Å) while the long H-bond on the left comes from a tryptophan residue at position 70 (very long at 3.7 Å) (PDB file 2FLQ).

Others have attempted to investigate the possible roles of these H-bond donors in cyt. P450.³³⁻³⁵ The replacement of a glutamine that provides one amide group with a proline forces a kink in the loop below the heme and obviously replaces the N-H bond in the glutamine backbone with a N-C bond, incapable of participating in H-bonding. This also removes a hydrogen bond from the side chain of the Gln to the carbonyl moiety of the cysteine residue. The combination of these two effects as well as the shift in the backbone resulting from introduction of a proline makes results difficult to deconvolute. The work suggests, however, that this H-bond donor (not even a legitimate hydrogen bond) shifts the reduction potential of the heme by about +40 mV (removing it makes the potential more negative by about 40 mV).³⁴ Resonance Raman suggests that this H-bond

donor decreases the σ -donating ability of the thiolate significantly; its removal strengthens the iron-sulfur bond.³³ They “conclude that the functions of the proximal hydrogen bonding network in P450_{cam} are to stabilize the heme-thiolate coordination, and to regulate the redox potential of the heme iron”.³⁵ While these conclusions seem reasonable, it is difficult to say the effect of a particular H-bond when several things are affected at once.

We wish to determine the role of these H-bond donors and support or refute the previous findings,³⁶ but particularly to study their effects in NOS. This family of enzymes provides a unique opportunity, given that one of the H-bond donors comes not from the backbone but from a side chain, allowing for facile and systematic variation using site-directed mutagenesis. Several such mutations have previously been made in NOS and characterized by resonance Raman.³⁷⁻³⁸ These studies show that removal of this H-bond donor strengthens the Fe-S bond. No further characterization has been reported.

One other mutant of interest replaced the tryptophan with a histidine, preserving and possibly increasing the H-bond donating ability of the group. In this mutant, researchers actually saw a slower kinetics profile and possibly a new intermediate by stopped-flow spectroscopy.³⁹ No further characterization was reported, and this new intermediate was suggested to be Compound I, based solely upon the position of the Soret band (**Scheme 3.2**, the ferryl complex in blue). The lifetime of this new intermediate is on the order of a couple seconds before decaying to product. Compound I is formally a Fe(V) complex, with a ferryl and another radical cation sometimes found on the porphyrin ring. The likelihood of such a species living for that length of time is

incredibly low as it will be very reactive, making its assignment as Compound I doubtful.⁴⁰ No other investigations into the role of this H-bond donor have been made.

We investigated the role of these H-bond donors by systematically varying the functional groups on this side chain in question through the use of site-directed mutagenesis. The native tryptophan was replaced with histidine, phenylalanine, or tyrosine. Histidine can also participate in hydrogen bonding, but lacks the ability to π -stack with the porphyrin ring. Phenylalanine complements the histidine mutation in that it can π -stack but cannot hydrogen bond. The tyrosine can also π -stack, but the electronics should be significantly altered due to the presence of the hydroxyl group on the aryl ring, which is at an angle that should prohibit hydrogen bonding with the thiolate. These three mutants have been expressed and thoroughly characterized using the tools of modern bioinorganic chemistry to investigate the thermodynamics of the resulting active site (EPR, electrochemistry, etc.). These studies provide valuable insight into the specific role of these hydrogen bond donors and their purpose in NOS and other heme thiolate enzymes.

All studies were conducted using the nitric oxide synthase from the thermophilic bacterium *Geobacillus stearothermophilus*. This particular organism spends its entire existence at elevated temperatures, forcing the optimization of the function of its enzymes to this elevated temperature range (a thermal melting curve for the wild type enzyme gsNOS is shown in **Figure 3.2**). Due to this, the NOS from *G. bacillus* (gsNOS) functions optimally at temperatures well above other NOSs and shows a remarkably slowed kinetics profile at standard laboratory temperatures (such as 4 and 10 °C). Researchers conducted single turnover experiments with this enzyme and found it to form

a ferrous-oxy complex stable on the order of 60 seconds at 4 °C, which is remarkable. Thermophilic enzymes tend to be more stable under standard conditions in a research lab, unlike their mammalian counterparts which, in the case of NOS, often degrade in a matter of just a few hours at room temperature. This thermophilic enzyme provides a much more stable subject for the necessary detailed investigations and increases the likelihood of expressing appreciable yields of mutant forms in *E. coli*.

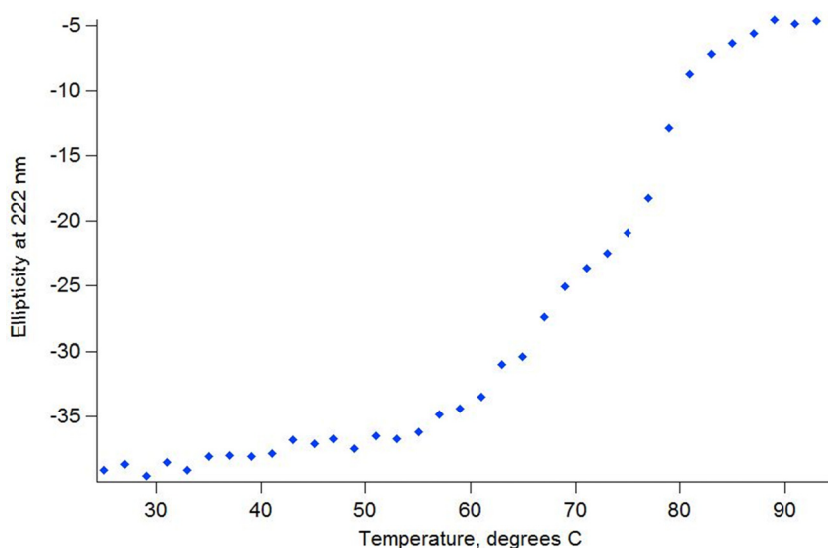


Figure 3.2. Thermal denaturation curve of wild type gsNOS as measured by circular dichroism spectroscopy. The midpoint of the melting curve is 74 °C.

This enzyme was first expressed and characterized in the lab of Brian Crane.⁴¹⁻⁴²

Researchers were able to crystallize the enzyme and found the overall fold to be quite similar to that of other NOSs. Like bacterial enzymes, it lacks the zinc-binding domain which caps the pterin binding site. However, all other key structural features are preserved, including residues surrounding the substrate and cofactor binding sites and the dimer interface. The fold of the enzyme is slightly more compact than other NOSs (Figure 3.3), which may contribute to its thermal stability.

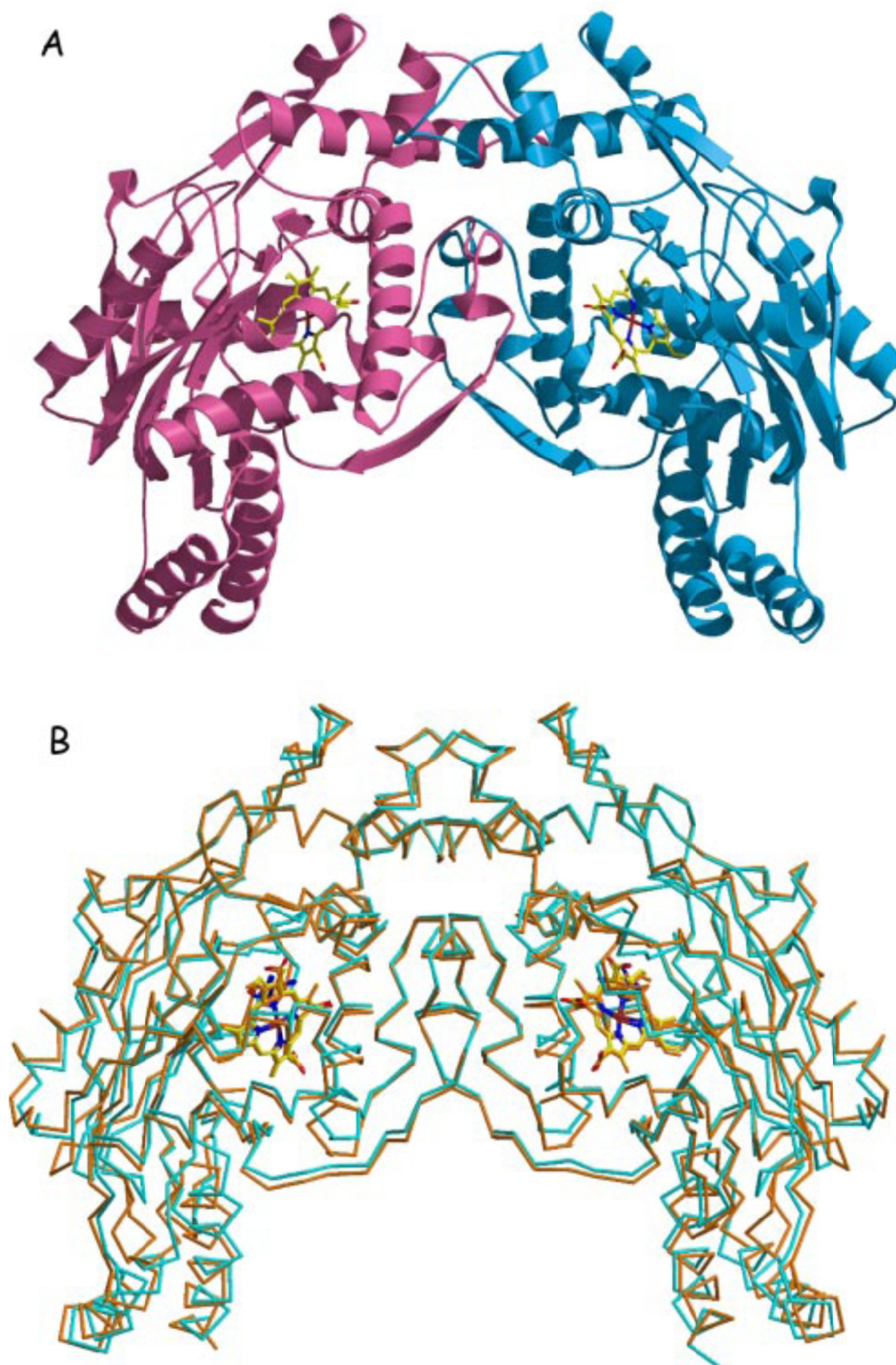


Figure 3.3. (A) The crystal structure of gsNOS showing the heme center. gsNOS crystallizes as a tight dimer, as is the case with all NOS enzymes. (B) Overlay of the backbones of gsNOS and NOS from *Bacillus subtilis* showing the increased packing and constriction in gsNOS.⁴¹

The wild type enzyme has a tryptophan residue at position 70 which hydrogen bonds with the thiolate ligand and π -stacks with the porphyrin ring of the heme. This Trp was replaced systematically by His, Tyr, and Phe. The wild type and these three mutant enzymes were studied by several techniques to characterize the thermodynamics of the active site. It was found that while these mutations do not greatly alter the stability of the protein or its overall fold, they do tune the electronics of the active site, shifting the spin state and altering the potential of the site.

3.3 Materials and Methods

General

The plasmid for the nitric oxide synthase from *Geobacillus stearothermophilus* was a gift from the lab of Brian Crane. This enzyme was expressed as previously described by Sudhamsu and Crane with no significant deviations in procedure.⁴¹ The enzyme was overexpressed in *Escherichia coli* BL21 (DE3) cells. Cells were grown to an optical density of approximately 1.0–1.4 and induced by adding a solution containing iron(III) chloride, IPTG, and δ -aminolevulinic acid (Aldrich) to final concentrations of 125 mg/L, 100 μ M, and 50 mg/L, respectively, in milliQ water. The pETDuet vector (Novagen) coded for a C-terminal cleavable His₆-tag so samples were purified using metal affinity chromatography. (This vector also confers chloramphenicol resistance to the cells, so 34 μ g/mL of this antibiotic were added to all cultures in Luria broth.) The His₆-tag was then cleaved using bovine thrombin (Calbiochem). Both thrombin and the His-tag were removed using size exclusion chromatography. Sample purity and Soret band epsilon values were determined through use of the Hemochromagen Assay.

A QuikChange site-directed mutagenesis kit from Stratagene was used to make the desired mutations in the amino acid chain. Primers were designed according to the guidelines outlined by the QuikChange kit manual. Unless otherwise noted, protein solutions were made in the following buffer: 50 mM Tris (2-amino-2-hydroxymethylpropane-1,3-diol), 150 mM NaCl, pH 7.5 (the same buffer used for size exclusion chromatography).

Circular Dichroism Spectroscopy

Circular dichroism spectroscopy was used to determine the stability of each protein sample. Chiral objects interact with circularly polarized light in such a way as to turn or distort the polarization of the light.⁴³ This is measured as ellipticity. Chiral features in macromolecules such as alpha helices or beta sheets are associated with particular signals by circular dichroism. Due to the size of the protein samples in question (gsNOS contains 375 residues with significant contributions from both alpha helices and beta sheets) the concentration of NOS in each cuvette was kept below 2 μ M. Samples with greater concentrations gave signals too large for the spectrometer to resolve. Alpha helices give characteristic ellipticity at 222 nm, to the red of the part of the spectrum where buffer would begin to affect the signal. For this reason, the standard Tris buffer was still used for these measurements. Spectra were collected scanning from 210 nm to 260 nm, stepping every one nm, to record the elliptical properties of the enzyme sample. In all cases the maximum signal was observed between 220 and 225 nm. To record the effects of temperature on each sample, the detector was fixed at 222 nm and the temperature was increased slowly, by steps of 2 °C, from 25 to 95 °C.

UV-Visible Absorption Spectroscopy

UV-visible absorption spectroscopy is a particularly useful technique for characterizing heme proteins, as the position and shape of the Soret absorption band of the heme center is extremely sensitive to both the oxidation state of the iron and the coordination sphere around that iron. The maximum absorption of the Soret band can shift tens of Ångströms due to simple additions of coordinating molecules such as imidazole or carbon monoxide.⁴⁴ UV-visible absorption spectra were acquired on an Agilent 8453 UV-visible spectrophotometer with a 2 nm resolution.

A common method for characterizing heme-thiolate enzymes and assessing their stability is by forming the ferrous-CO complex.³⁷ It is the strong, sharp absorption of this band at 450 nm that gives cytochrome P450 its name. The Soret band of ferrous-CO NOS typically lies to the blue of cyt. P450 at 446 nm. Samples were brought into an anaerobic glove box and reduced using dithionite. Excess dithionite was then removed using a PD-10 desalting column (although removal is not necessary in all situations). The samples are then sealed by Kōntes valve in a quartz cuvette and brought out of the box. The headspace of this special cuvette was then connected to a tank of carbon monoxide and this gas was bubbled over the headspace, replacing the atmosphere. As CO diffuses into solution, the ferrous-CO complex is rapidly formed. The cuvette was then re-sealed and UV-vis spectra collected.

Hemochromagen Assay

The heme center with its Soret absorption band provides a particularly useful handle for determining protein concentration as well. The Hemochromagen Assay allows researchers to characterize the molar absorptivities of heme centers in protein samples to

a degree that is far more accurate than the standard Bradford Assay.⁴⁵ In this method, the protein is denatured using strong base to liberate the heme center and pyridine is added in large excess to force coordination of the heme. This five-coordinate pyridine-heme is then reduced with dithionite to yield a ferrous complex (called a hemochrome) with a known and distinct absorption in the Q-band region. This new complex has two sharp Q-bands, the lower energy of which has a larger molar absorptivity of $34,640 \text{ M}^{-1}\text{cm}^{-1}$.⁴⁵ As long as the original spectrum of the fully-oxidized resting state of the enzyme is recorded first, the hemochrome can then be generated and the concentration of the sample can be calculated based on heme concentration using the known epsilon value of the hemochrome.

Samples of wild type gsNOS and all three mutants were made with absorbances between 0.3 and 1.0 (to keep the % transmittance within the best working range of the spectrophotometer). Each sample was prepared in a specialized cuvette (**Figure 3.4**), allowing the sealing of the sample from atmosphere, or its connection to a Schlenk line, all while in a quartz cuvette allowing for measurement of the UV-visible absorption spectrum. A spectrum of each protein sample was collected initially, before any additions or degassing; each sample was exactly 1 mL of approximately 4–10 μM enzyme. Then 125 μL of each pyridine and 1 M NaOH were added to the sample. The spectrum was again recorded to verify denaturation of the protein. Samples then had to be very thoroughly degassed through at least 30 rounds of gentle pump/purge to remove oxygen from the atmosphere and allow equilibration of the argon atmosphere with solution. Several crystals of solid dithionite were placed in the bulb, while the sample was kept anaerobic, and then the atmosphere above the dithionite was exchanged for argon again

on a Schlenk line. The spectrum of the degassed sample was recorded to determine any concentration changes due to the time spent under vacuum, and then the valve connecting the sample to the bulb containing dithionite was opened and the crystals of dithionite were added to reduce the system. This final spectrum was collected (quickly) and showed clearly the spectrum common to all hemochromes from systems with *b*-type hemes, two Q-bands, the redder of which has a larger epsilon and a maximum absorbance at 556 nm. This was used to determine the molar absorptivity of the heme center in each of the four protein samples studied.



Figure 3.4. Special cuvette used for Hemochromagen Assay, showing the bulb on the left and the quartz cuvette on the right.

Binding Assays

The interaction of substrates with the active site can be characterized spectroscopically using UV-visible absorption spectroscopy. With heme proteins, the introduction of substrates or inhibitors to the binding pocket often shifts the position and shape of the Soret band in a characteristic manner.⁴⁶ Here, the substrate is arginine and the inhibitor is imidazole. The relationship between the concentration of substrate/inhibitor added and the resulting spectral shift has been calculated as follows in Equation 3.1,

$$\frac{1}{\Delta OD} = m \frac{1}{[imid]} - \frac{1}{K_S} \quad (3.1)$$

where ΔOD is the change in absorbance due to the presence of the substrate or inhibitor and m is the slope of the resulting line, $[imid]$ is the concentration of analyte added (in this case, imidazole).⁴⁷ This simple linear relationship allows for the calculation of a dissociation constant, K_S , through facile spectroscopic characterization by UV-vis (the symbol K_S is used to distinguish this term as a spectral dissociation constant rather than a traditional dissociation constant, K_D). This technique requires a large shift in absorbance to give reliable results. In some cases, a competition assay was required in order to see significant shifts in the Soret band (the protein was pre-loaded with imidazole of a known concentration and then arginine was added to that sample to displace the imidazole).

Electron Paramagnetic Resonance Spectroscopy (EPR)

One unique feature of heme-thiolate systems is related to the spin state of the iron. The electronics of these systems is poised just so that the pairing energy (the energetic cost of placing two electrons in the same orbital due to their mutual repulsion) and $\Delta_{Octahedral}$ (the splitting between the E_g and T_{2g} states of the metal center) are nearly

identical. Under different conditions both high spin and low spin states can be observed, and often a mixture of the two states is seen. With Fe(III), high spin complexes have a spin of $S = 5/2$ and low spin complexes have a spin of $S = 1/2$.

EPR requires the glassing of frozen samples and the random alignment of all paramagnetic species. In order to ensure glass formation, high glycerol concentrations are used. Samples were prepared with the following conditions: 20 μM NOS, 20% by volume glycerol, 50 mM NaCl, 50 mM Tris at pH 7.5. Samples containing arginine had an Arg concentration of 300 μM in order to ensure full formation of the arginine-bound complex, and all were pre-frozen by rapid immersion in liquid nitrogen. Spectra were collected using a Bruker EMX Biospin instrument with a Gunn diode microwave source. Liquid helium was used to cool the instrument and sample and spectra were collected at 20 K. EPR parameters were simulated using the software package SPINCOUNT.⁴⁸

Evans Method NMR

To determine the spin state of samples at room temperature, Evans method nuclear magnetic resonance spectroscopy (NMR) was applied. With this method, one can determine the spin state of a sample by the paramagnet's affect on the surrounding solvent.⁴⁹ Samples were prepared with 1 mM protein sample inside of a capillary-like insert (Wilmad, part number WGS-5BL). These inserts are designed to fit inside of a standard NMR tube, with buffer in the surrounding space. This allowed the use of less than 100 μL of protein sample, reducing the total amount of protein required. The presence of the paramagnetic iron center in the protein shifts the NMR peak of the water in the buffer. The magnitude of this shift is directly related to the concentration of the paramagnet and the number of unpaired electrons in that species (Equations 3.2, 3.3, and

3.4, specifically for a 600 MHz NMR spectrometer, from the manual for Chemistry 3b at Caltech). Samples were prepared with the standard buffer (50 mM Tris, 150 mM NaCl, pH 7.5) but with 20% D₂O and 80% H₂O rather than 100% H₂O as an internal standard to allow for proper tuning of the magnet.

$$X_g = \left(\frac{3}{4\pi}\right) \left(\frac{\Delta\nu}{\nu}\right) \left(\frac{1}{m}\right) + X_0 \quad (3.2)$$

In the above equation, X_g is the gram susceptibility of the sample, ν is the measured frequency of the NMR signal, m is the mass of the paramagnetic material in 1 mL of solution, and X_0 is the gram susceptibility of the pure solvent (water being $-7.203 \times 10^{-7} \text{ cm}^3 \text{ g}^{-1}$). This gram susceptibility is then used in Equation 3.3 to determine the number of unpaired electrons in the paramagnetic sample.

$$X_M = X_g M \quad (3.3)$$

$$\mu = 2.84 \sqrt{X_M T} = \sqrt{n(n+2)} \quad (3.4)$$

X_M is the molar susceptibility of the sample in question, M is its molecular weight, and T is the temperature in Kelvin. These equations allow one to calculate the number of unpaired electrons in a given system as long as the two solvent peaks (with and without the paramagnetic species) can be resolved.

Redox Titrations

In order to measure the reduction potential of each protein sample, redox titrations were carried out. In this technique, a chemical oxidant or reductant is added to the protein sample. This chemical reactant should have a reduction potential close to that of the protein being studied ($\pm 100 \text{ mV}$) in order to observe equilibrium between oxidized and reduced forms from sub-stoichiometric reaction with the protein sample. The reduction

potential of other NOSs has been measured previously and found to typically lie in the range of -250 to -300 mV vs. NHE.^{16, 39} $\text{Ru}^{3+}(\text{acac})_3$ was chosen as a chemical oxidant because it has a reversible reduction potential at -275 mV. The protein was reduced under inert atmosphere in a glove bag (experiments were carried out in the lab of Michael Marletta at UC Berkeley) and sealed in a cuvette along with the $\text{Ru}(\text{acac})_3$ sample (in the syringe) of a specialized apparatus for this reaction shown in **Figure 3.5**. Small aliquots of ruthenium complex were added at a time, the sample was mixed and the resulting spectrum collected. This technique relies on the absorption of the oxidized and reduced species of one of the two reactants to be well resolved. From the UV-vis spectrum, the concentrations of the oxidized and reduced form of each of the two reactants can be calculated given the molar absorptivities and the Nernst Equation applied to give the reduction potential of the protein.

$$\Delta G = -nFE = -RT \ln K_{eq} \quad (3.5)$$

$$E = E^0 - \frac{RT}{nF} \ln K_{eq} \quad (3.6)$$



Figure 3.5. Apparatus for chemical redox titration. The protein sample is held in the quartz cuvette at the bottom, the oxidant/reductant is held in the gas-tight syringe above the cuvette. Samples can be degassed and assembled in an anaerobic chamber or degassed on a Schlenk line using the side arm (left).

3.4 Results and Discussion

Enzyme Stability

Circular dichroism spectroscopy was used to assess the stability of each of the protein samples studied. While only a single mutation was made, one residue can have a large effect on the overall fold of a macromolecule.⁵⁰ The tryptophan naturally occurring at this position in gsNOS is universally conserved in all nitric oxide synthases and it has been shown in cytochromes P450 that a phenylalanine residue at a similar location, which also π -stacks with the porphyrin ring is necessary for proper expression and folding of the enzyme.⁵¹ This Trp not only π -stacks, but interacts with the axial thiolate through a long hydrogen bond. Removal of one or both of these functions could greatly affect the stability of the enzyme.

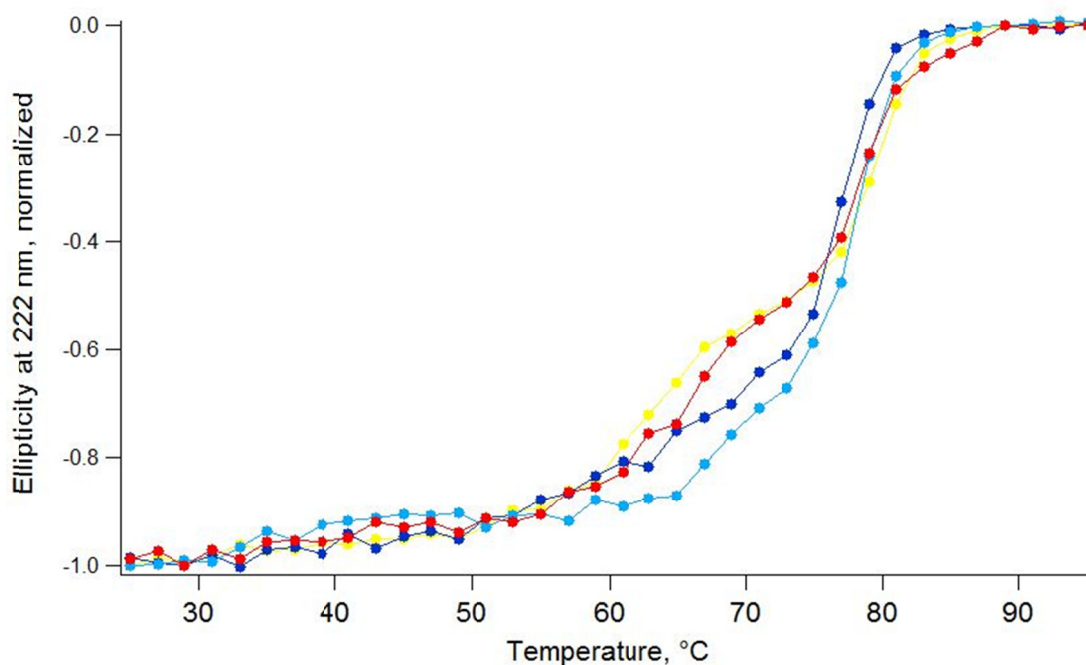


Figure 3.6. Thermal denaturation curves for each of the four protein samples studied herein, wild type (red), W70H (yellow), W70Y (light blue), and W70F (dark blue).

The thermal denaturation data collected show a somewhat remarkable result: none of the mutant enzymes shows a marked decrease in stability toward temperature. Given the two roles of this residue at position 70, it was hypothesized that these roles were vital to the fold of the protein. The fact that all four enzymes are stable to 60 °C and show similar behavior to the wild type above that temperature proves this hypothesis to be false. The His mutant (shown in yellow in **Figure 3.6**) may begin to unfold at slightly lower temperatures than wild type, consistent with the π -stacking of the Trp being important for positioning the heme in the enzyme. However, this effect is very small. The Tyr and Phe mutants, if anything, show increased stability over the wild type. Again, this is consistent with the hypothesis, as these two residues preserve the π -stacking function. They cannot provide a hydrogen bond to the thiolate (the hydroxyl group of the tyrosine side chain is pointed at an unfavorable angle, away from the thiolate), but the data show that this does not destabilize the enzyme.

Another common method for determining the stability of heme-thiolate enzymes involves the generation of the ferrous-CO complex. It is this form of the enzyme that absorbs strongly near 450 nm, giving cytochromes P450 their name. This tests specifically the stability of the heme center and the iron-thiolate bond. Cyt. P450s and NOSs are known to form an inactive form called P420 under some conditions.⁵² This has been proposed to be either loss of axial thiolate coordination or protonation of the axial thiolate to make a neutral thiol ligand. In the case of NOS, it has even been shown to be reversible inactivation of the enzyme, but without the proper thiolate ligation the enzyme cannot produce NO.^{35, 52}

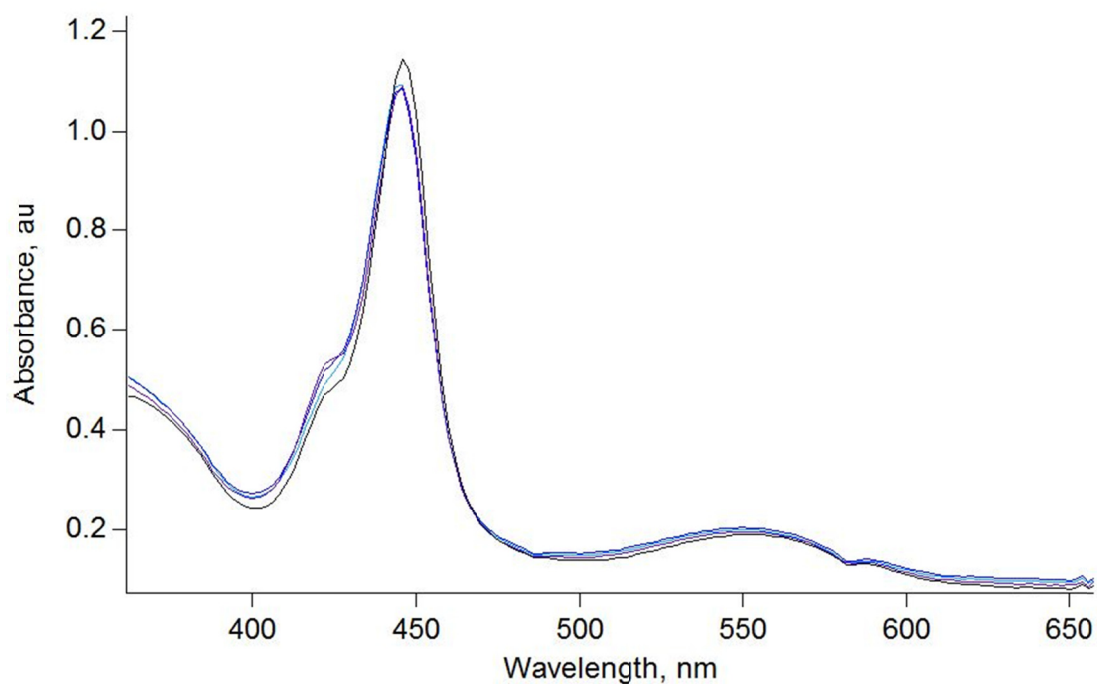


Figure 3.7. Ferrous-CO complex of wild type gsNOS, spectra collected over the course of 24 hours with no significant absorbance change. $\lambda_{\text{max}} = 446$ nm.

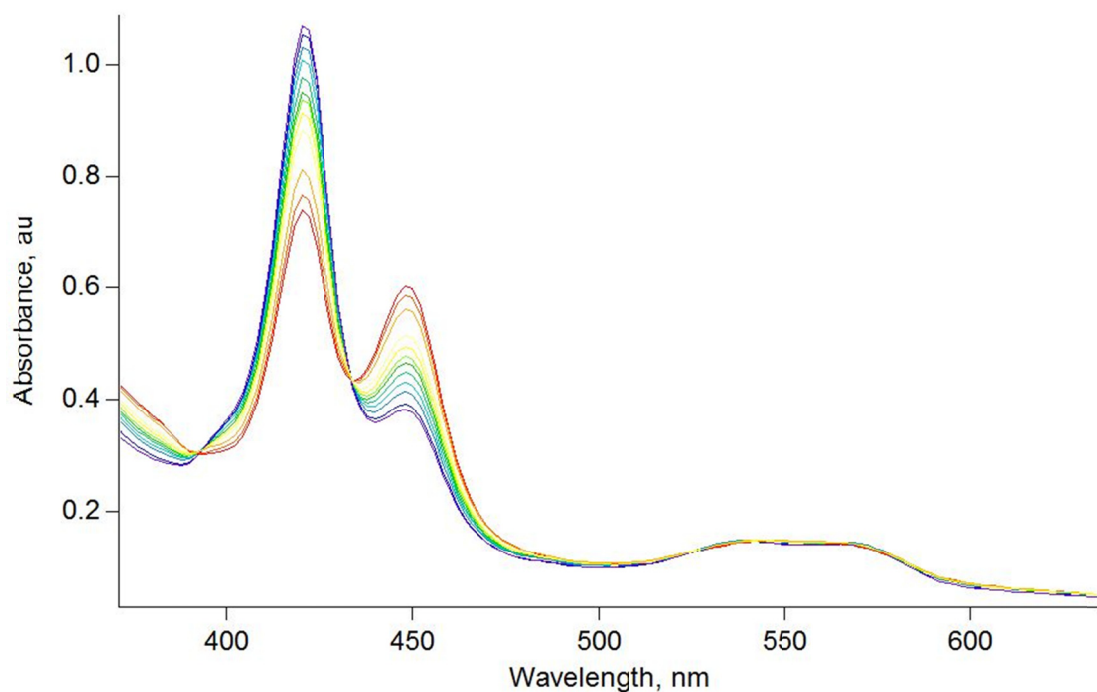


Figure 3.8. Ferrous-CO complex of W70F gsNOS, spectra collected over the course of 24 hours showing P420 formation, the first spectrum (red) was collected within 5 minutes of generating the complex. $\lambda_{\text{max}} = 446$ nm decreasing, 420 nm increasing.

Upon formation of the ferrous-CO complex, the wild type gsNOS shows stable formation of the six-coordinate complex with maximum absorption at 446 nm as expected (**Figure 3.7**). The W70H mutant also shows stable formation of this complex, however with a blue-shifted Soret band at 440 nm. The reason for this blue shift is unknown, but may arise from altered tuning of the porphyrin ring. The two remaining mutant enzymes, W70Y and W70F, both remove hydrogen bonding capabilities. Over the course of 24 hours, both mutants show near complete formation of the P420 species (**Figure 3.8**). Removal of this one H-bond donor may increase interactions with the other two donors and increase the σ -donating ability of the thiolate ligand to the iron center. The data suggest that this third, distant (3.7 Å) H-bond donor stabilizes the enzyme in the active form by either decreasing the thiolate ligand's σ -donating ability or by preventing any one H-bond from being too strong in order to reduce the risk of protonation of the thiolate, or some combination thereof.

In the catalytic cycle of NOS, a similar ferrous-O₂ complex must form and remain stable on the timescale of catalysis in order for the enzyme to productively form NO. The electron density on the iron must be tuned in order to stabilize that six-coordinate species, yet still allow for ligand dissociation from the ferric-NO species formed in the last step of catalysis (**Scheme 3.2**). This unique requirement, the release of NO, may be the reason for the differences between the NOS and cyt. P450 proximal H-bonding network. In cyt. P450 all three H-bonds come from the amide backbone, while only two come from the backbone in NOS, the third coming from this Trp residue. Cyt. P450 has a separate phenylalanine residue for π -stacking with the porphyrin ring, rather than combining these two functions in a single Trp residue.³⁸

Binding Assays

Large changes in the UV-visible absorption of the heme center provide a clear handle for the study of ligand interactions with the active site. In nitric oxide synthases, the Soret band of the five-coordinate ferric complex (resting state of the enzyme) has a maximum absorbance at 396 nm. The six-coordinate complex, however, formed upon introduction of the inhibitor imidazole, has a sharp Soret band at 426 nm (**Figure 3.9**). These spectral changes can be used to calculate dissociation constants for inhibitors and substrates, as described in the Methods section using Equation 3.1.

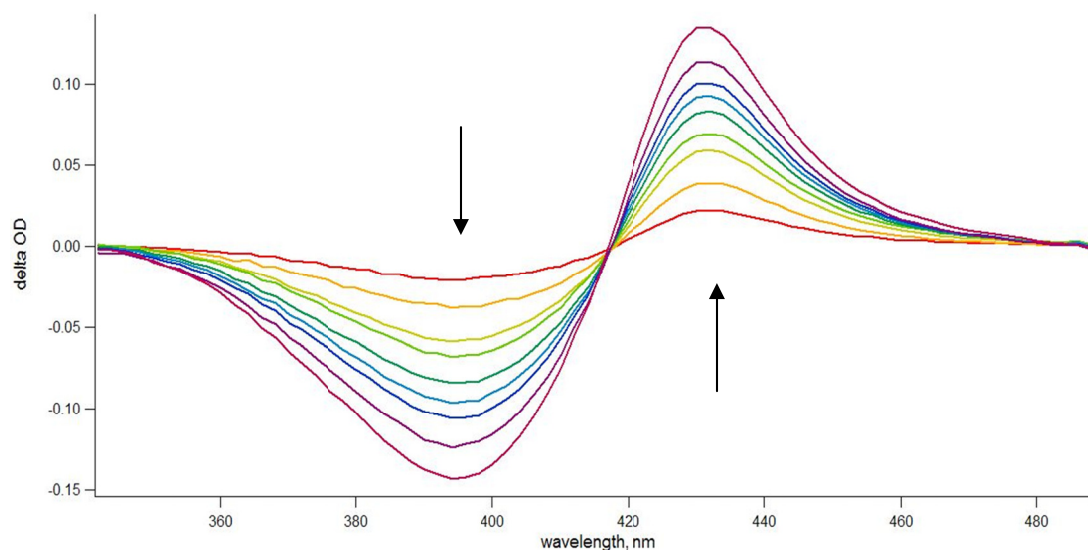


Figure 3.9. Spectral changes induced upon introduction of increasing concentrations of imidazole to wild type gsNOS.

According to Equation 3.1, plotting $1/[\text{imidazole}]$ vs. $1/\text{deltaOD}$ (x vs. y, the maximum absorbance change) should result in a linear relationship where m (the slope) depends on the concentration of protein in each sample, and the negative reciprocal of the y-intercept gives the spectral dissociation constant (**Figure 3.10**). The same can be done for the

substrate arginine, and each dissociation constant for arginine and imidazole from each of the four mutant enzymes is shown in **Table 3.1**.

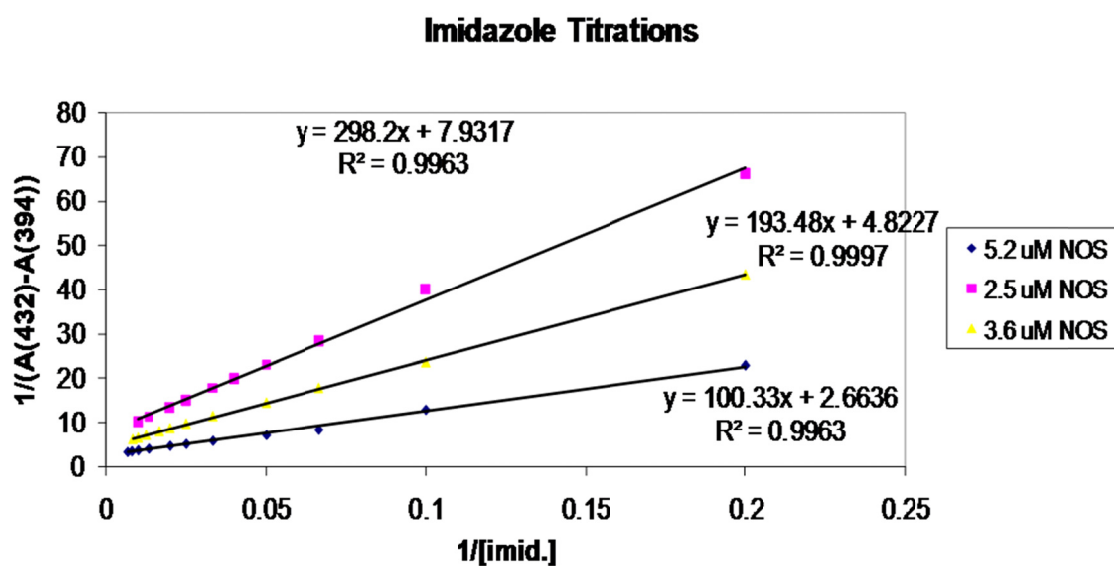


Figure 3.10. Calculation of the dissociation constant of imidazole from gsNOS.

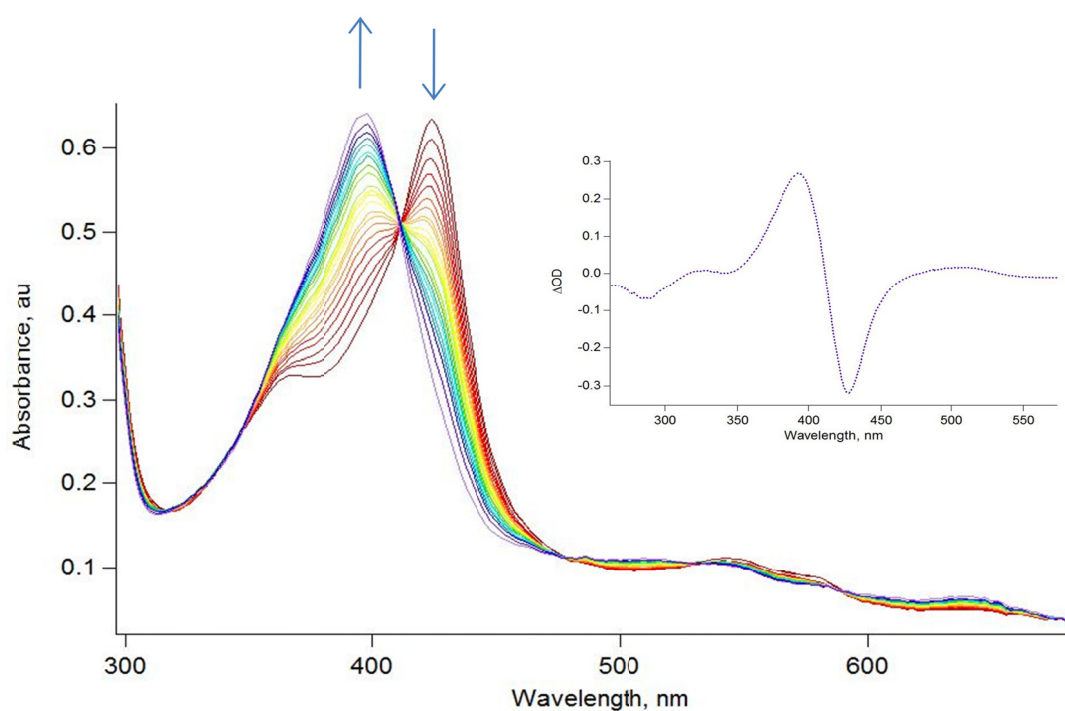


Figure 3.11. UV-visible absorbance changes upon introduction of arginine to a solution of wild type gsNOS with a known concentration of imidazole (20 mM) for a competitive binding assay.

Table 3.1. Spectral dissociation constants of imidazole and arginine.

(μ M)	K_s (arg)	K_s (imid)
WT	4.0	38
W70H	4.5	88
W70F	3.2	130
W70Y	4.3	210

It is clear from the values in **Table 3.1** that while the interaction of imidazole with the heme is greatly affected by mutations at position 70, the dissociation constant of arginine remains unaffected. This can be explained by the manner in which each substance binds. Arginine is positioned in the binding pocket above the heme, without directly ligating the iron. It is held in place by hydrogen bonds and hydrophobic contacts within the substrate channel.^{13, 53} A high spin five-coordinate complex is formed; arginine merely kicks out the water molecule that weakly coordinates the iron. Imidazole, on the other hand, directly coordinates the iron, forming a bond between the iron and nitrogen of the ring. As the hydrogen bond donating group is removed, the thiolate becomes a better donor to the iron. This increases the electron density on the iron. The direct ligation of the imidazole forces even more electron density into the iron, which is disfavored, so as the thiolate becomes a better donor, the imidazole binds less tightly.

UV-Visible Characterization of the Resting State

As stated previously, electronic absorption spectroscopy is a useful tool for characterizing heme enzymes. The Hemochromagen Assay is used to determine protein concentration based on heme concentration. This assumes the presence of one heme unit per polypeptide chain. All measurements made herein depend on signal changes in the

spectra of the heme center (UV-vis, EPR, NMR due to the presence of paramagnetic iron center, etc.), thus any polypeptide chains of NOS that do not contain a heme unit will be invisible to all other measurements as well, making the Hemochromagen Assay the most appropriate measure of concentration for these purposes. The Bradford Assay is also commonly used to determine protein concentrations, but is less sensitive than the Hemochromagen Assay and detects all polypeptides including those without heme. Within the error of the experiment, all four proteins studied herein have similar Soret band molar absorptivities of about $80,000 \text{ M}^{-1}\text{cm}^{-1}$. The mutations appear not to greatly affect this value.

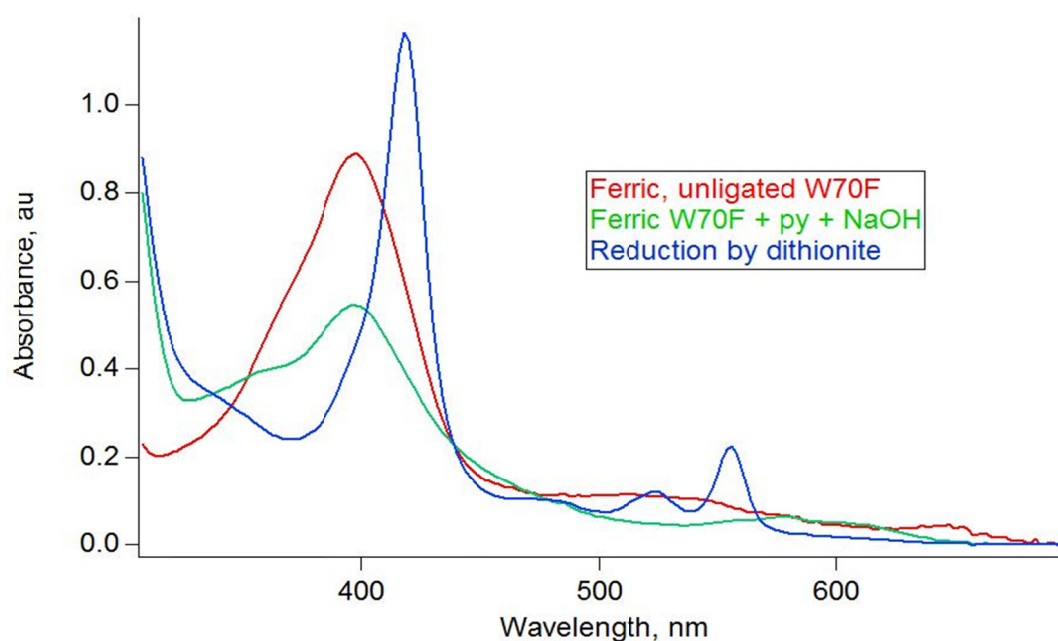


Figure 3.12. Formation of the five-coordinate Fe(II)(pyridine)(porphyrin) “hemochrome” complex with characteristic absorption bands in the Q-band region.

Table 3.2. Molar absorptivities of the four NOS mutants studied.

	Wild Type	W70H	W70F	W70Y
$\epsilon(\text{Soret}), \text{M}^{-1}\text{cm}^{-1}$	79,000	73,000	84,000	78,000

It was observed, however, that mutations at position 70 affect the shape of the Soret band. As seen in **Figure 3.13**, removal of the hydrogen-bond donating group by introduction of a Phe or a Tyr leads to sharpening of the Soret band, while the His mutant preserves both the H-bond and the broader shape of the peak. It is known that displacing the loosely coordinated water molecule in the distal axial position converts the iron center from a mixture of spin states to the high-spin five-coordinate complex.⁵⁴ Other cyt. P450s has Soret bands further to the red in the resting state without substrate (P450cam has a maximum at 417 and P450-BM3 at 418 nm)⁵⁵ that shift to approximately 400 nm upon introduction of substrate (camphor or a long chain fatty acid). This observed shift in Soret band location and shape in **Figure 3.13** may arise from the shifting of the iron center further towards high spin. The UV-vis spectra suggest that the two mutants without an H-bond donor at position 70 have almost no water coordination (the equilibrium lies far to the five-coordinate state) due to the increased donating abilities of the thiolate ligand.

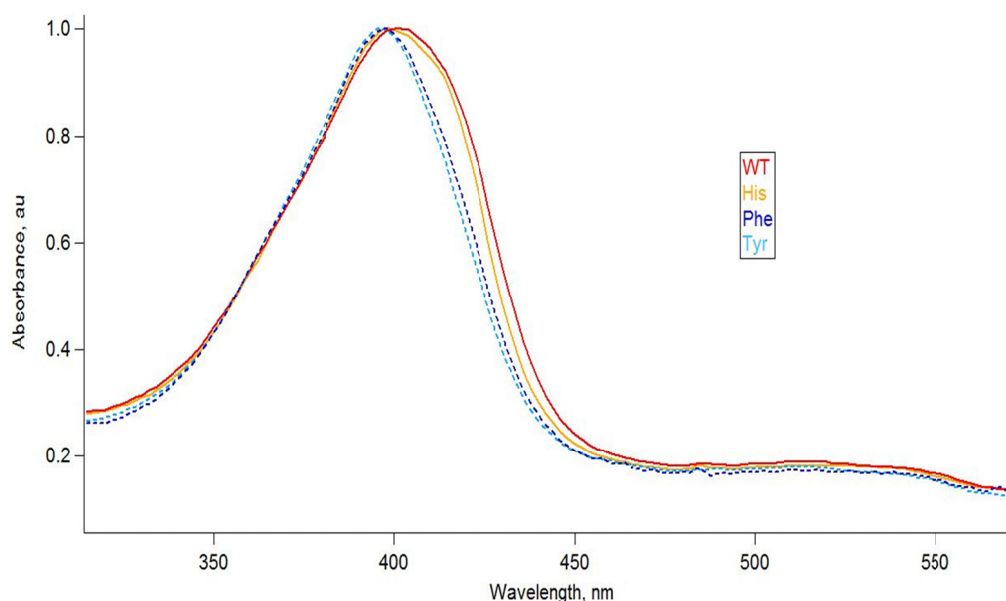
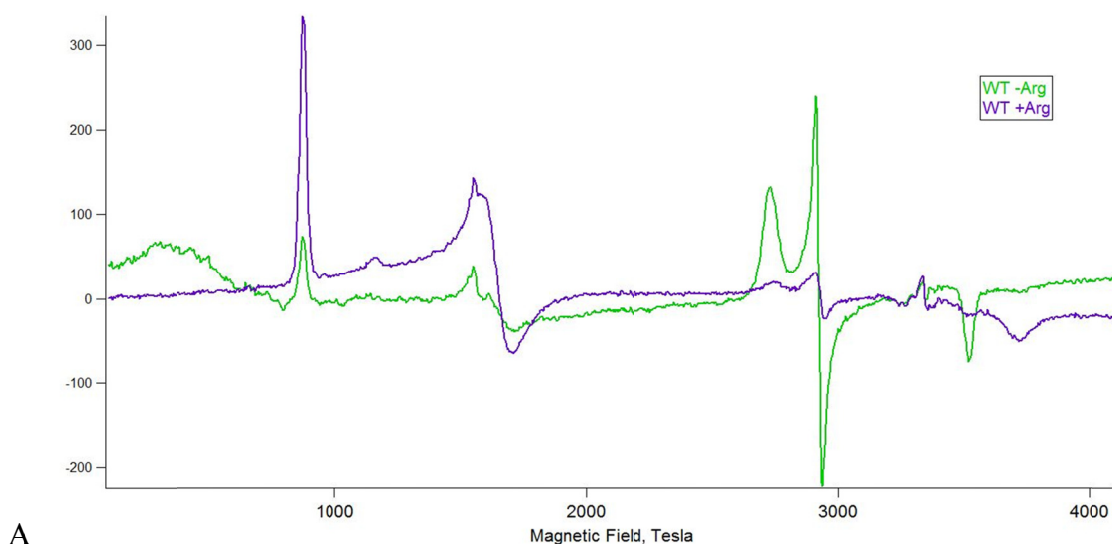


Figure 3.13. Absorption spectra in the visible region of all four protein samples under investigation. Wild type (red), W70H (yellow), W70F (dark blue), W70Y (light blue).

Characterization of the Resting Spin State

In order to investigate the spin state of each of these samples, electron paramagnetic resonance spectroscopy was employed. Experiments were carried out at 20 K with and without arginine, as this should force complete formation of the high spin complex. Unfortunately, in all cases signals could be observed for both the low and high spin complex, even after addition of the substrate. By EPR the samples appear predominantly low spin in the absence of substrate, arginine inducing a near complete shift to high spin (**Figure 3.14**). UV-visible spectroscopy suggests that all samples are composed of mostly the high spin complex, based on the position of the Soret band. All signals are similar to the reported values for mammalian NOSs (**Table 3.3**).⁵⁶⁻⁵⁷



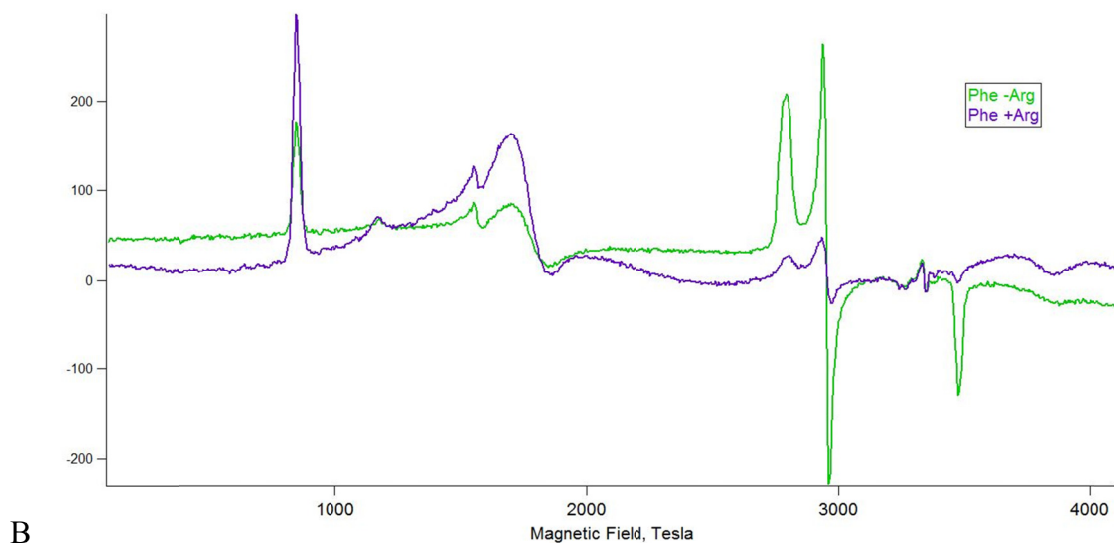


Figure 3.14. (A) EPR spectra of wild type gsNOS (representative of the His mutant as well) with (purple) and without (green) the substrate arginine. (B) EPR spectra of the W70F mutant of gsNOS (representative of the W70Y mutant as well) with (purple) and without (green) the substrate arginine.

Table 3.3. EPR parameters for both high and low spin states of the heme center.

	Spin State	g(x)	g(y)	g(z)
w.t.	high	7.69	4.10	1.80
His	high	7.69	4.12	1.81
Phe	high	7.95	3.78	1.73
Tyr	high	7.88	3.89	1.76
w.t.	low	1.90	2.29	2.46
His	low	1.90	2.29	2.47
Phe	low	1.93	2.27	2.40
Tyr	low	1.92	2.28	2.41

It was hypothesized that the large temperature difference could be the cause of this discrepancy. Evans method is an NMR-based technique for the determination of

paramagnetic spin state. NMR experiments can be carried out at room temperature, allowing for a more direct comparison with UV-vis. The presence of paramagnetic compounds in high concentrations shifts the resonance of the solvent peak. This shift is related to the number of unpaired electrons in the complex by the Equations 3.2, 3.3, and 3.4. **Table 3.4** shows results of these measurements. Strengthening the H-bonding capabilities of the residue at position 70 decreases the number of unpaired electrons relative to wild type, while removing that H-bond increases the number of unpaired electrons and shifts the sample further towards high spin. These results agree with those from UV-vis and together confirm that the enzyme is predominantly high spin in character at room temperature (low spin would have one unpaired electron, high spin would have five).

Table 3.4. Unpaired electrons for each mutant as determined by Evans method.

Sample	delta, ppm	[NOS], mM	n (unpaired e)
WT	0.041	1.00	3.9
His	0.040	1.26	3.3
Phe	0.057	1.16	4.4
Tyr	0.062	1.38	4.1

Redox Titrations

In order to fully characterize the electronics of the ground state of each enzyme's active site, a measurement of the heme ($\text{Fe}^{3+/2+}$) reduction potential is necessary. Determination of the reduction potential of a redox active center is not always straightforward, particularly when the complex of interest is buried within a protein

scaffold. The backbone of a protein is made mostly from insulating C-C and C-N bonds and is designed to discourage random electron transfer reactions in favor of one particular function of the enzyme. Nature must find the balance between discouraging deleterious redox reactions and promoting productive reactions. The presence of the protein scaffold buries the active site and in most cases prevents communication with electrodes, rendering standard electrochemical techniques useless. Small molecules, however, which can freely diffuse through solution, can still react with most metal sites within proteins. For this reason, chemical redox titrations are the method of choice for measuring reduction potentials.

For chemical redox titrations no electrodes or potentiostats are required; however, spectroscopic handles are necessary to indicate that a redox process has occurred. Many metalloproteins have absorption bands in the visible region, making them amenable to characterization by UV-visible spectroscopy. Provided there are wavelengths where the two redox forms show characteristic absorption bands, relative protein concentration can be measured. A chemical oxidant/reductant is employed with a known reduction potential near (within ± 100 mV) the expected potential of the protein under analysis, in this case Ru(acac)₃ with a Ru^{3+/2+} reduction potential of -275 mV vs. NHE. This feature is required for the measurement of a precise equilibrium constant in Equation 3.6 as sub-stoichiometric reactions will be observed. A small molecule chemical titrant must be designed to have desirable UV-visible absorption properties so as not to obscure the changes taking place with the enzyme as well as a potential close to that of the sample in order to observe equilibrium between the two. However, if the titrant has clear optical changes upon change in oxidation state, it too can be used to calculate the concentration

of each species in solution. Equation 3.6 is employed, where E is the difference between the reduction potential of the titrant and the protein, and E^0 is the reduction potential of the titrant itself.

First, the optical spectra of Ru(acac)₃ were recorded at various potentials using a standard spectroelectrochemical cell (CH Instruments) (**Figure 3.15**). A solution of 95 μ M Ru(acac)₃ in 150 mM NaCl, 50 mM Tris, pH 7.5 was made and degassed to remove oxygen from solution. The potential was held at -400 mV vs. the Ag/AgCl reference electrode (about -200 vs. NHE) for a few minutes to allow full equilibration and the first spectrum (in red) was recorded. The potential was then stepped in 20 mV increments (10 mV when nearing the reduction potential of the compound) to the negative, each time several minutes were allowed for full equilibration of the solution before a UV-vis spectrum was recorded. This was continued until no further optical changes were detected (the final spectrum is shown in purple). These data confirm the reported reduction potential of -275mV and identify isosbestic points at 290 and 398 nm.

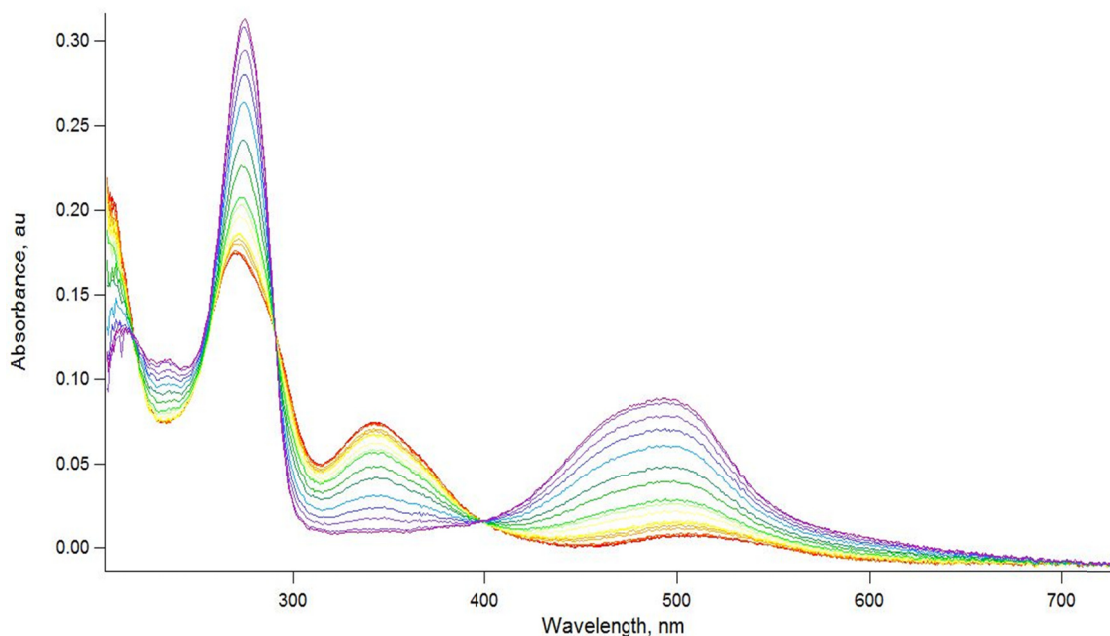


Figure 3.15. Spectroelectrochemical characterization of $\text{Ru}(\text{acac})_3$, 95 μM in Tris buffer. Oxidized, $\text{Ru}(\text{III})$, red. Reduced, $\text{Ru}(\text{II})$, purple.

This ruthenium complex was then used to oxidize the reduced form of each enzyme. Samples of five-coordinate ferrous enzyme were made in an anaerobic chamber and excess reductant was removed using desalting columns. The sample was then sealed in a specialized cuvette (**Figure 3.5**) with $\text{Ru}(\text{III})(\text{acac})_3$ in the syringe. This ruthenium complex was then added in a stepwise manner and UV-vis spectra were recorded along the way (**Figures 3.16 and 3.17**). These measurements are extremely sensitive to the presence of any oxygen, as it reacts rapidly and stoichiometrically with the reduced iron center. Any leak would cause large deviations in observed spectra.

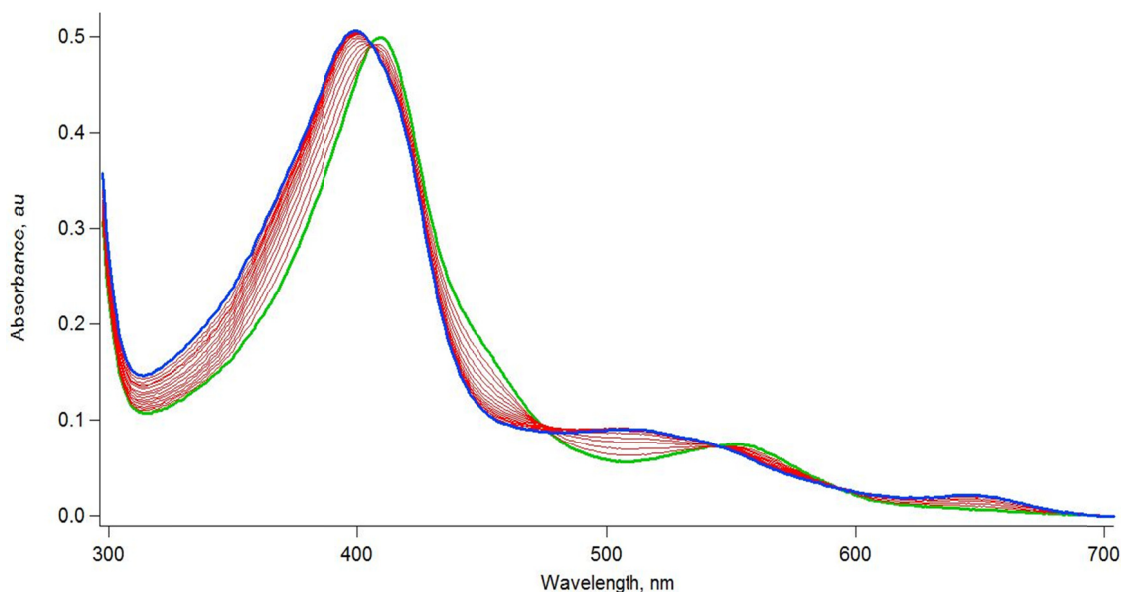


Figure 3.16. Redox titration using $\text{Ru}(\text{acac})_3$ to oxidize wild type ferrous gsNOS, showing a shift from reduced NOS (green) to oxidized protein plus excess Ru complex (blue).

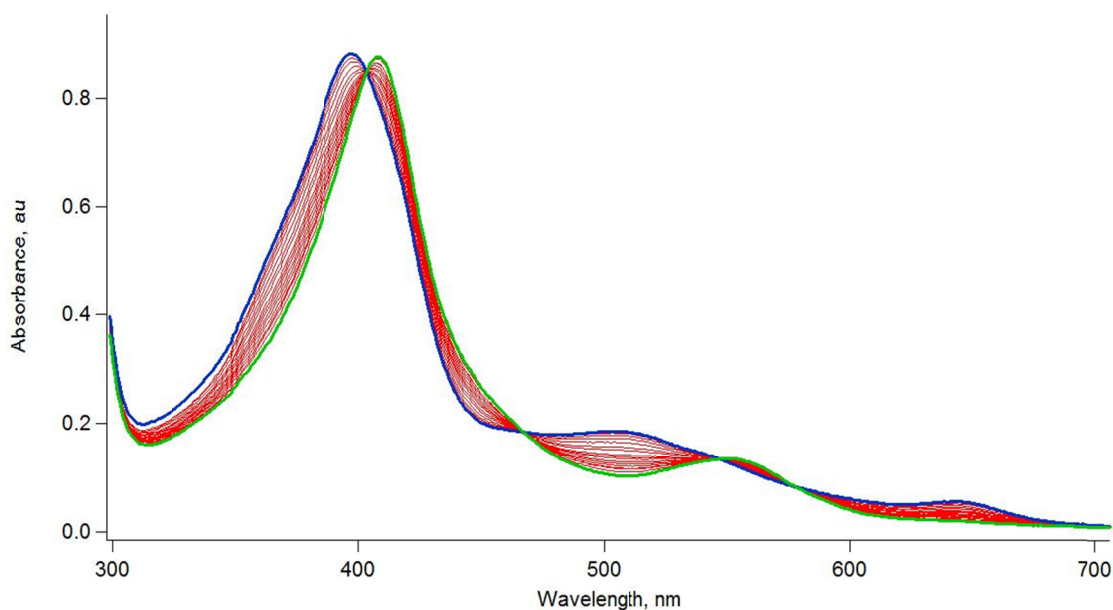


Figure 3.17. Titration using $\text{Ru}(\text{acac})_3$ to oxidize W70F ferrous gsNOS, showing a shift from reduced NOS (green) to oxidized protein plus excess Ru complex (blue).

Accurate measurement of reduction potentials is particularly difficult when the potentials in question are very negative of 0 vs. NHE and reactions are slow, as is the

case here. Reliable potentials were determined for wild type (-362 ± 5 mV) and W70H (-339 ± 5 mV). These numbers are both within 100 mV of the potential of the chemical titrant, $\text{Ru}(\text{acac})_3$. The other two mutant enzymes, however, should have significantly lower potentials as the thiolate ligand becomes a better donor to the iron as literature suggests.³⁸ This would lead to stoichiometric reaction with the Ru complex. If equilibrium cannot be observed, the potential of the iron site cannot be determined. This was in fact the case, as only stoichiometric oxidation of the iron was observed and no measure of the K_{eq} could be obtained for W70F and W70Y. It is sufficient to conclude that removal of this strategic hydrogen bond donor substantially decreases the reduction potential of the center, consistent with the lack of stability in the ferrous-CO complexes of these two mutants.

It is also of note that the potentials measured for wild type and W70H are not as expected from previous work.⁵⁸ The potential of most NOS enzymes falls between -240 and -270 mV vs. NHE. One exception to this is mammalian inducible NOS which has a potential near -350 mV without substrate present.¹⁶ This is too negative to be reduced by the flavins in the NOS reductase domain. Upon introduction of the substrate, the potential shifts up toward -250 mV and the iron center can now be reduced by the flavins. In other mammalian forms, the presence of calcium ions regulates electron transfer between the two domains. In its absence, the oxygenase domain and reductase domain are too far separated for electron transfer to occur. In inducible NOS, the activity of which is independent of calcium ion concentration, it is this redox switch that most likely prevents deleterious side reactions. (If the heme center is reduced without substrate present, reactive oxygen species are formed which can damage the cell. However, if the heme is

only reduced when the substrate is present, this unproductive reduction event is avoided.) This is the first measurement of the reduction potential of any bacterial NOS. These enzymes may be regulated in a manner similar to inducible NOS, which is fitting in light of their lack of dedicated reductase domain.

The potential of the histidine-containing mutant lies positive of the wild type enzyme. This same effect was seen in inducible NOS, where the corresponding mutation (W188H) shifts the potential positive by 88 mV (as opposed to only 20 mV as seen here). It may be that the tighter fold of gsNOS alters this interaction relative to inducible NOS. The histidine may not come into as close contact as the tryptophan, or the electronics of the porphyrin ring may be affected in a unique way. A crystal structure of these mutant enzymes would aid in this discussion. Samples have been sent to the lab of Brian Crane at Cornell, however crystals of NOS are notoriously difficult and slow-growing. Efforts to determine the structure of these three new mutants are ongoing.

3.5 Conclusions

The thermodynamics of wild type and three mutants of gsNOS were characterized by various methods. Data from circular dichroism spectroscopy show that mutations at position 70 do not decrease the overall stability of the protein fold. The evidence from multiple techniques is clear, however, that these mutations significantly affect the electronics of the heme center. It was shown using binding assays, generation of the ferrous-CO species, and redox titrations that the σ -donating abilities of the thiolate are increased after removal of the hydrogen bonding group in the Trp. Both chemical redox titrations and instability of ferrous-CO complexes of the two mutants lacking this key

hydrogen bond (W70F and W70Y) suggest that they have more negative reduction potentials than the two mutants with this hydrogen bond (wild type and W70H). Evans methods NMR was used to confirm the results of UV-visible spectroscopy which suggest that removal of this hydrogen bond shifts the heme center toward the high-spin state due to strengthening of the Fe-S bond, as seen in the binding assays.

It can be concluded that this universally-conserved tryptophan residue serves several roles, but positioning of the heme within the protein (as has been suggested for cyt. P450s) is not one of them. In order to produce NO the electronics of the heme center must be tuned in such a way as to stabilize high-valent iron species for the oxidation of substrate. During catalysis, the site must also be tuned not only to support six-coordinate ferrous-oxy complex, but promote release of NO \cdot from the heme in the end. If the $3/2+$ reduction potential of the site is too negative, the ferrous-oxy may be unstable or the high-valent iron species too stable to perform the desired reactivity. If too negative, release of NO will be disfavored and decrease the rate of release to undesirable levels. The reactivity of these mutants will shed further light on the role of this key hydrogen-bond donating group.

3.6 References

1. Denisov, I. G., Makris, T. M., Sligar, S. G., and Schlichting, I. (2005) Structure and chemistry of cytochrome p450, *Chem. Rev.* 105, 2253.
2. Alderton, W. K., Cooper, C. E., and Knowles, R. G. (2001) Nitric oxide synthases: Structure, function and inhibition, *Biochem. J.* 357, 593.
3. Sono, M., Roach, M. P., Coulter, E. D., and Dawson, J. H. (1996) Heme-containing oxygenases, *Chem. Rev.* 96, 2841.
4. Dawson, J. H., and Sono, M. (1987) Cytochrome.P-450 and chloroperoxidase - thiolate-ligated heme enzymes - spectroscopic determination of their active-site structures and mechanistic implications of thiolate ligation, *Chem. Rev.* 87, 1255.
5. Li, H. Y., Igarashi, J., Jamal, J., Yang, W. P., and Poulos, T. L. (2006) Structural studies of constitutive nitric oxide synthases with diatomic ligands bound, *J. Biol. Inorg. Chem.* 11, 753.
6. Stuehr, D. J., Santolini, J., Wang, Z. Q., Wei, C. C., and Adak, S. (2004) Update on mechanism and catalytic regulation in the no synthases, *J. Biol. Chem.* 279, 36167.
7. Marletta, M. A. (1993) Nitric oxide synthase structure and mechanism, *J. Biol. Chem.* 268, 12231.
8. Alderton, W. K., Cooper, C. E., and Knowles, R. G. (2001) Nitric oxide synthases: Structure, function and inhibition, *Biochem. J.* 357, 593.
9. Stuehr, D. J., Cho, H. J., Kwon, N. S., Weise, M. F., and Nathan, C. F. (1991) Purification and characterization of the cytokine-induced macrophage nitric-oxide synthase - an fad-containing and fmn-containing flavoprotein, *Proc. Nat. Acad. Sci. USA* 88, 7773.
10. Hurshman, A. R., and Marletta, M. A. (2002) Reactions catalyzed by the heme domain of inducible nitric oxide synthase: Evidence for the involvement of tetrahydrobiopterin in electron transfer, *Biochemistry* 41, 3439.
11. Hevel, J. M., and Marletta, M. A. (1992) Macrophage nitric-oxide synthase - relationship between enzyme-bound tetrahydrobiopterin and synthase activity, *Biochemistry* 31, 7160.
12. Hurshman, A. R., Krebs, C., Edmondson, D. E., Huynh, B. H., and Marletta, M. A. (1999) Formation of a pterin radical in the reaction of the heme domain of inducible nitric oxide synthase with oxygen, *Biochemistry* 38, 15689.
13. Crane, B. R., Arvai, A. S., Ghosh, D. K., Wu, C. Q., Getzoff, E. D., Stuehr, D. J., and Tainer, J. A. (1998) Structure of nitric oxide synthase oxygenase dimer with pterin and substrate, *Science* 279, 2121.
14. Garcin, E. D., Bruns, C. M., Lloyd, S. J., Hosfield, D., Tiso, M., Stuehr, D. J., Tainer, J. A., and Getzoff, E. D. (2004) Structural basis for isozyme specific regulation of electron transfer in nitric oxide synthase, *J. Biol. Chem.* 279, 37918.
15. Zhu, Y., and Silverman, R. B. (2008) Revisiting heme mechanisms. A perspective on the mechanisms of nitric oxide synthase (nos), heme oxygenase (ho), and cytochrome p450s (cyp450s), *Biochemistry*.
16. Presta, A., Weber-Main, A. M., Stankovich, M. T., and Stuehr, D. J. (1998) Comparative effects of substrates and pterin cofactor on the heme midpoint

- potential in inducible and neuronal nitric oxide synthases, *J. Am. Chem. Soc.* **120**, 9460.
17. Lippard, S. J., Berg, J. M. (1994) *Principles of bioinorganic chemistry*, University Science Books, Mill Valley, CA.
 18. Hurshman, A. R., and Marletta, M. A. (1995) Nitric oxide complexes of inducible nitric oxide synthase: Spectral characterization and effect on catalytic activity, *Biochemistry* **34**, 5627.
 19. Belliston-Bittner, W., Dunn, A. R., Nguyen, Y. H. L., Stuehr, D. J., Winkler, J. R., and Gray, H. B. (2005) Picosecond photoreduction of inducible nitric oxide synthase by rhenium(i)-diimine wires, *J. Am. Chem. Soc.* **127**, 15907.
 20. Wang, Z. Q., Wei, C. C., Santolini, J., Panda, K., Wang, Q., and Stuehr, D. J. (2005) A tryptophan that modulates tetrahydrobiopterin-dependent electron transfer in nitric oxide synthase regulates enzyme catalysis by additional mechanisms, *Biochemistry* **44**, 4676.
 21. Wei, C. C., Wang, Z. Q., Hemann, C., Hille, R., and Stuehr, D. J. (2003) A tetrahydrobiopterin radical forms and then becomes reduced during n-omega-hydroxyarginine oxidation by nitric-oxide synthase, *J. Biol. Chem.* **278**, 46668.
 22. Ghosh, D. K., Wu, C. Q., Pitters, E., Moloney, M., Werner, E. R., Mayer, B., and Stuehr, D. J. (1997) Characterization of the inducible nitric oxide synthase oxygenase domain identifies a 49 amino acid segment required for subunit dimerization and tetrahydrobiopterin interaction, *Biochemistry* **36**, 10609.
 23. Denisov, I. G., Makris, T. M., Sligar, S. G., and Schlichting, I. (2005) Structure and chemistry of cytochrome p450, *Chem. Rev.* **105**, 2253.
 24. Meunier, B., de Visser, S. P., and Shaik, S. (2004) Mechanism of oxidation reactions catalyzed by cytochrome p450 enzymes, *Chem. Rev.* **104**, 3947.
 25. Udit, A. K., Hill, M. G., and Gray, H. B. (2006) Electrochemistry of cytochrome p450 bm3 in sodium dodecyl sulfate films, *Langmuir* **22**, 10854.
 26. Udit, A. K., Belliston-Bittner, W., Glazer, E. C., Le Nguyen, Y. H., Gillan, J. M., Hill, M. G., Marletta, M. A., Goodin, D. B., and Gray, H. B. (2005) Redox couples of inducible nitric oxide synthase, *J. Am. Chem. Soc.* **127**, 11212.
 27. Martin, N. I., Woodward, J. J., Winter, M. B., Beeson, W. T., and Marletta, M. A. (2007) Design and synthesis of c5 methylated l-arginine analogues as active site probes for nitric oxide synthase, *J. Am. Chem. Soc.* **129**, 12563.
 28. Davydov, R., Sudhamsu, J., Lees, N. S., Crane, B. R., and Hoffman, B. M. (2009) Epr and endor characterization of the reactive intermediates in the generation of no by cryoreduced oxy-nitric oxide synthase from geobacillus stearothermophilus, *J. Am. Chem. Soc.* **131**, 14493.
 29. Davydov, R., Ledbetter-Rogers, A., Martásek, P., Larukhin, M., Sono, M., Dawson, J. H., Masters, B. S. S., and Hoffman, B. M. (2002) Epr and endor characterization of intermediates in the cryoreduced oxy-nitric oxide synthase heme domain with bound l-arginine or n^g-hydroxyarginine, *Biochemistry* **41**, 10375.
 30. Ogliaro, F., de Visser, S. P., and Shaik, S. (2002) The 'push' effect of the thiolate ligand in cytochrome p450: A theoretical gauging, *J. Inorg. Biochem.* **91**, 554.

31. Wang, R., and de Visser, S. P. (2007) How does the push/pull effect of the axial ligand influence the catalytic properties of compound i of catalase and cytochrome p450?, *J. Inorg. Biochem.* *101*, 1464.
32. Meunier, B., de Visser, S. P., and Shaik, S. (2004) Mechanism of oxidation reactions catalyzed by cytochrome p450 enzymes, *Chem. Rev.* *104*, 3947.
33. Galinato, M. G. I., Spolidakis, T., Ballou, D. P., and Lehnert, N. (2011) Elucidating the role of the proximal cysteine hydrogen-bonding network in ferric cytochrome p450cam and corresponding mutants using magnetic circular dichroism spectroscopy, *Biochemistry* *50*, 1053.
34. Ueyama, N., Nishikawa, N., Yamada, Y., Okamura, T., and Nakamura, A. (1996) Cytochrome p-450 model (porphinato)(thiolato)iron(iii) complexes with single and double nh center dot center dot center dot s hydrogen bonds at the thiolate site, *J. Am. Chem. Soc.* *118*, 12826.
35. Yoshioka, S., Tosha, T., Takahashi, S., Ishimori, K., Hori, H., and Morishima, I. (2002) Roles of the proximal hydrogen bonding network in cytochrome p450(cam)-catalyzed oxygenation, *J. Am. Chem. Soc.* *124*, 14571.
36. Voegtli, H. L., Sono, M., Adak, S., Pond, A. E., Tomita, T., Perera, R., Goodin, D. B., Ikeda-Saito, M., Stuehr, D. J., and Dawson, J. H. (2003) Spectroscopic characterization of five- and six-coordinate ferrous-heme complexes. Evidence for heme Fe-proximal cysteinate bond cleavage in the ferrous-heme adducts of the trp-409tyr/phe proximal environment mutants of neuronal nitric oxide synthase, *Biochemistry* *42*, 2475.
37. Couture, M., Adak, S., Stuehr, D. J., and Rousseau, D. L. (2001) Regulation of the properties of the heme-heme complexes in nitric-oxide synthase by hydrogen bonding to the proximal cysteine, *J. Biol. Chem.* *276*, 38280.
38. Lang, J., Driscoll, D., Gelinas, S., Rafferty, S. P., and Couture, M. (2009) Trp180 of endothelial nos and trp56 of bacterial nos modulate sigma bonding of the axial cysteine to the heme, *J. Inorg. Biochem.* *103*, 1102.
39. Tejero, J., Biswas, A., Wang, Z.-Q., Page, R. C., Haque, M. M., Hemann, C., Zweier, J. L., Misra, S., and Stuehr, D. J. (2008) Stabilization and characterization of a heme-oxy reaction intermediate in inducible nitric-oxide synthase, *Journal of Biological Chemistry* *283*, 33498.
40. Rittle, J., and Green, M. T. (2010) Cytochrome p450 compound i: Capture, characterization, and C-H bond activation kinetics, *Science* *330*, 933.
41. Sudhamsu, J., and Crane, B. R. (2006) Structure and reactivity of a thermostable prokaryotic nitric-oxide synthase that forms a long-lived oxy-heme complex, *J. Biol. Chem.* *281*, 9623.
42. Kabir, M., Sudhamsu, J., Crane, B. R., Yeh, S. R., and Rousseau, D. L. (2008) Substrate-ligand interactions in *Geobacillus stearothermophilus* nitric oxide synthase, *Biochemistry* *47*, 12389.
43. Sreerama, N., Venyaminov, S. Y. U., and Woody, R. W. (1999) Estimation of the number of α -helical and β -strand segments in proteins using circular dichroism spectroscopy, *Protein Science* *8*, 370.
44. Wang, J. L., Rousseau, D. L., Abusoud, H. M., and Stuehr, D. J. (1994) Heme coordination of NO in NO synthase, *P. Natl. Acad. Sci. USA* *91*, 10512.

45. Berry, E. A., and Trumpower, B. L. (1987) Simultaneous determination of hemes-a, hemes-b, and hemes-c from pyridine hemochrome spectra, *Anal. Biochem.* *161*, 1.
46. Dmochowski, I. J., Dunn, A. R., Wilker, J. J., Crane, B. R., Green, M. T., Dawson, J. H., Sligar, S. G., Winkler, J. R., and Gray, H. B. (2002) Sensitizer-linked substrates and ligands: Ruthenium probes of cytochrome p450 structure and mechanism, *Method. Enzymol.* *357*, 120.
47. Schenkma.Jb, Remmer, H., and Estabroo.Rw. (1967) Spectral studies of drug interaction with hepatic microsomal cytochrome, *Mol. Pharmacol.* *3*, 113.
48. Lancaster, K. M., Sproules, S., Palmer, J. H., Richards, J. H., and Gray, H. B. (2010) Outer-sphere effects on reduction potentials of copper sites in proteins: The curious case of high potential type 2 c112d/m121e pseudomonas aeruginosa azurin, *J. Am. Chem. Soc.* *132*, 14590.
49. Schubert, E. M. (1992) Utilizing the evans method with a superconducting nmr spectrometer in the undergraduate laboratory, *Journal of Chemical Education* *69*, 62.
50. Hartings, M. R., Gray, H. B., and Winkler, J. R. (2008) Probing melittin helix-coil equilibria in solutions and vesicles, *J. Phys. Chem. B* *112*, 3202.
51. Porter, T. D. (1994) Mutagenesis at a highly conserved phenylalanine in cytochrome p450 2e1 affects heme incorporation and catalytic activity, *Biochemistry* *33*, 5942.
52. Sabat, J., Stuehr, D. J., Yeh, S. R., and Rousseau, D. L. (2009) Characterization of the proximal ligand in the p420 form of inducible nitric oxide synthase, *J. Am. Chem. Soc.* *131*, 12186.
53. Crane, B. R., Arvai, A. S., Gachhui, R., Wu, C. Q., Ghosh, D. K., Getzoff, E. D., Stuehr, D. J., and Tainer, J. A. (1997) The structure of nitric oxide synthase oxygenase domain and inhibitor complexes, *Science* *278*, 425.
54. Jovanovic, T., Farid, R., Friesner, R. A., and McDermott, A. E. (2005) Thermal equilibrium of high- and low-spin forms of cytochrome p450bm-3: Repositioning of the substrate?, *J. Am. Chem. Soc.* *127*, 13548.
55. Sono, M., Ledbetter, A. P., McMillan, K., Roman, L. J., Shea, T. M., Masters, B. S. S., and Dawson, J. H. (1999) Essential thiol requirement to restore pterin- or substrate-binding capability and to regenerate native enzyme-type high-spin heme spectra in the escherichia coli-expressed tetrahydrobiopterin-free oxygenase domain of neuronal nitric oxide synthase†, *Biochemistry* *38*, 15853.
56. Migita, C. T., Salerno, J. C., Masters, B. S. S., Martasek, P., McMillan, K., and Ikeda-Saito, M. (1997) Substrate binding-induced changes in the epr spectra of the ferrous nitric oxide complexes of neuronal nitric oxide synthase†, *Biochemistry* *36*, 10987.
57. Salerno, J. C., McMillan, K., and Masters, B. S. S. (1996) Binding of intermediate, product, and substrate analogs to neuronal nitric oxide synthase: Ferriheme is sensitive to ligand-specific effects in the l-arginine binding site†, *Biochemistry* *35*, 11839.
58. Tejero, J. S., Biswas, A., Wang, Z. Q., Page, R. C., Haque, M. M., Hemann, C., Zweier, J. L., Misra, S., and Stuehr, D. J. (2008) Stabilization and characterization

of a heme-oxy reaction intermediate in inducible nitric-oxide synthase, *J. Biol. Chem.* 283, 33498.

Chapter 4

Thiolate Hydrogen Bonding Mutants: Kinetics

4.1 Abstract

The heme-thiolate enzymes cytochromes P450, chloroperoxidase, and nitric oxide synthase all activate dioxygen to oxidize substrates. In each of these enzymes, there is a conserved hydrogen bonding network around the proximal thiolate ligand. These hydrogen bond donors come predominantly from backbone amide groups and help to tune the electronics of the heme center. However, in nitric oxide synthase one of these three hydrogen-bond donating groups comes from the side chain of a tryptophan residue, making nitric oxide synthases unique. Three mutant forms of the nitric oxide synthase from *Geobacillus stearothermophilus* were expressed in *E. coli*. These mutants each have a single point mutation, converting this native tryptophan residue to a histidine, phenylalanine, or tyrosine. The reactivity of each the wild type enzyme and the three new mutants were tested using stopped-flow mixing coupled with UV-visible absorption spectroscopy and the Griess Assay. Autoxidation rates measured by stopped-flow suggest that the Tyr and Phe mutants do indeed have significantly more negative reduction potentials, but that the His mutant is particularly slow to oxidize. The Griess Assays showed that all four enzymes produce nitrite in solution, when provided with substrate, cofactor, and hydrogen peroxide (as a source of reducing equivalents). In single turnover experiments, however, only three of the four enzymes showed evidence of ferric-NO production. The His mutant showed no intermediate absorbance near 440 nm (which would be indicative of ferric-NO formation), suggesting that it releases NO^- rather than the radical species NO^\cdot .

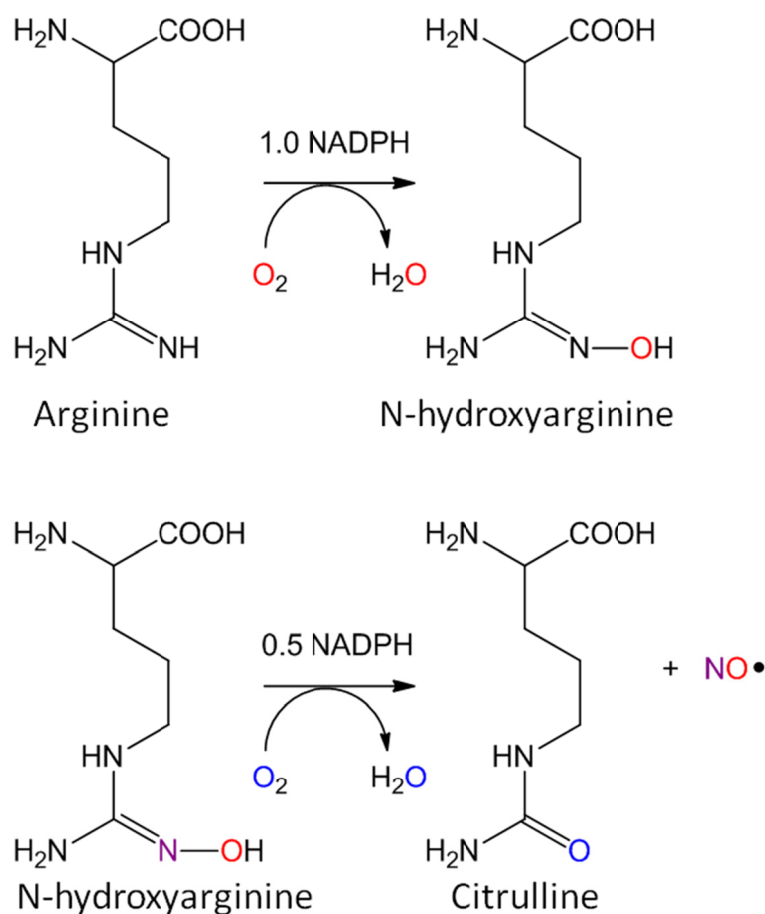
4.2 Introduction

As stated previously, nitric oxide synthases are the family of enzymes responsible for production of the signaling molecule NO.¹⁻² It was shown by Moncado³ that the active biological signaling molecule is in fact NO \cdot and not any other NO_x species. It is this molecule that induces relaxation of the cells lining the walls of blood vessels, thus regulating blood flow in mammals. Since that time, the field of NO signaling has grown rapidly and it is now known that nitric oxide is also involved in neurotransmission, the immune response, and apoptosis.^{1-2, 4}

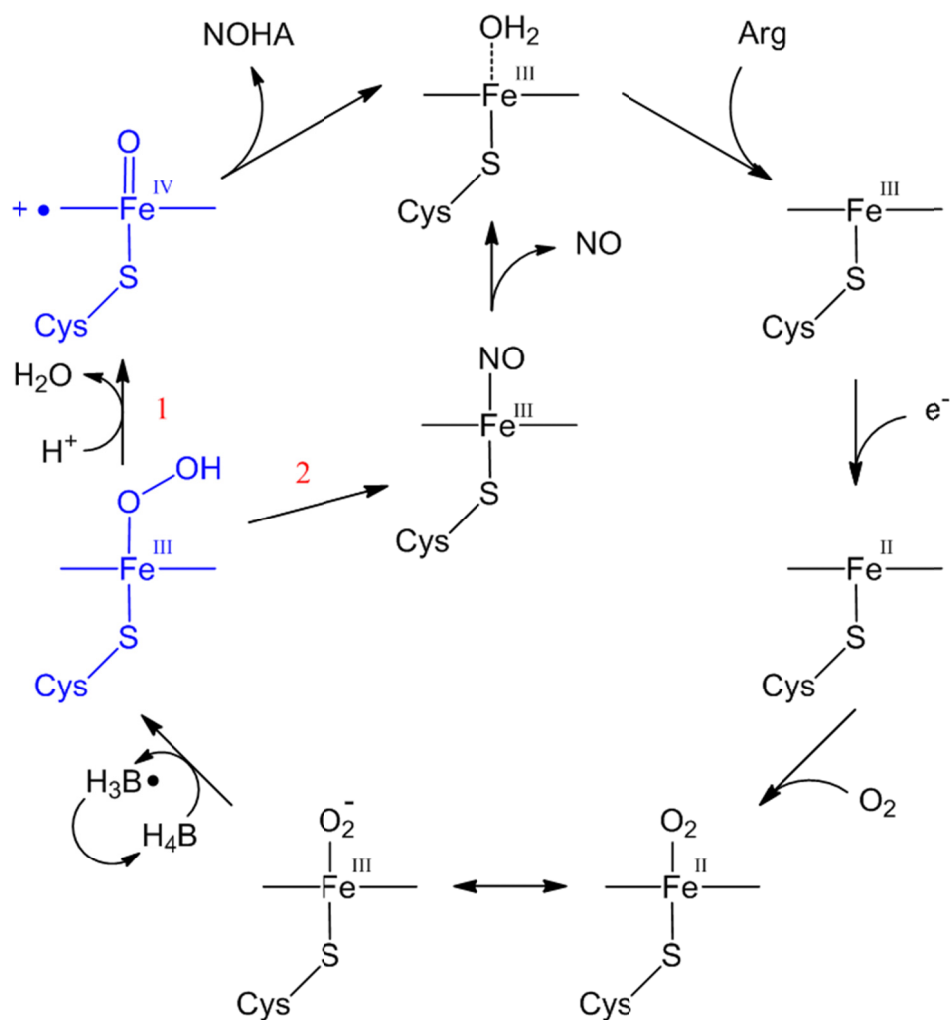
This family of enzymes makes NO from arginine (Arg) in two turnovers, through the enzyme-bound intermediate N-hydroxyarginine (NOHA) (**Scheme 4.1**).⁵⁻⁶ Much of what is known about its catalytic cycle is similar to the well-studied cytochrome P450.⁷⁻⁸ The observed intermediates (as well as probable intermediates in blue) are shown in the cycle in **Scheme. 4.2**.

The resting state of the enzyme is a ferric heme with a loosely coordinated water molecule.⁹ This is displaced sterically when substrate binds within the enzyme, forcing a five-coordinate complex and shifting the iron to the high spin state. The heme is then reduced (in mammalian systems, reducing equivalents come from a dedicated reductase domain fused into the same polypeptide chain) to form a ferrous-heme complex. Reduced iron species readily bind dioxygen in biological systems. The ferric-oxy species (or ferric-superoxo depending on assignment of electrons, as shown by the equilibrium at the bottom of the cycle in **Scheme 4.2**) in cytochrome P450 is reduced by another electron from the reductase domain. NOS is unique in that this electron comes from a redox active cofactor called tetrahydrobiopterin (pterin) (**Scheme 4.3**). After this event, the next

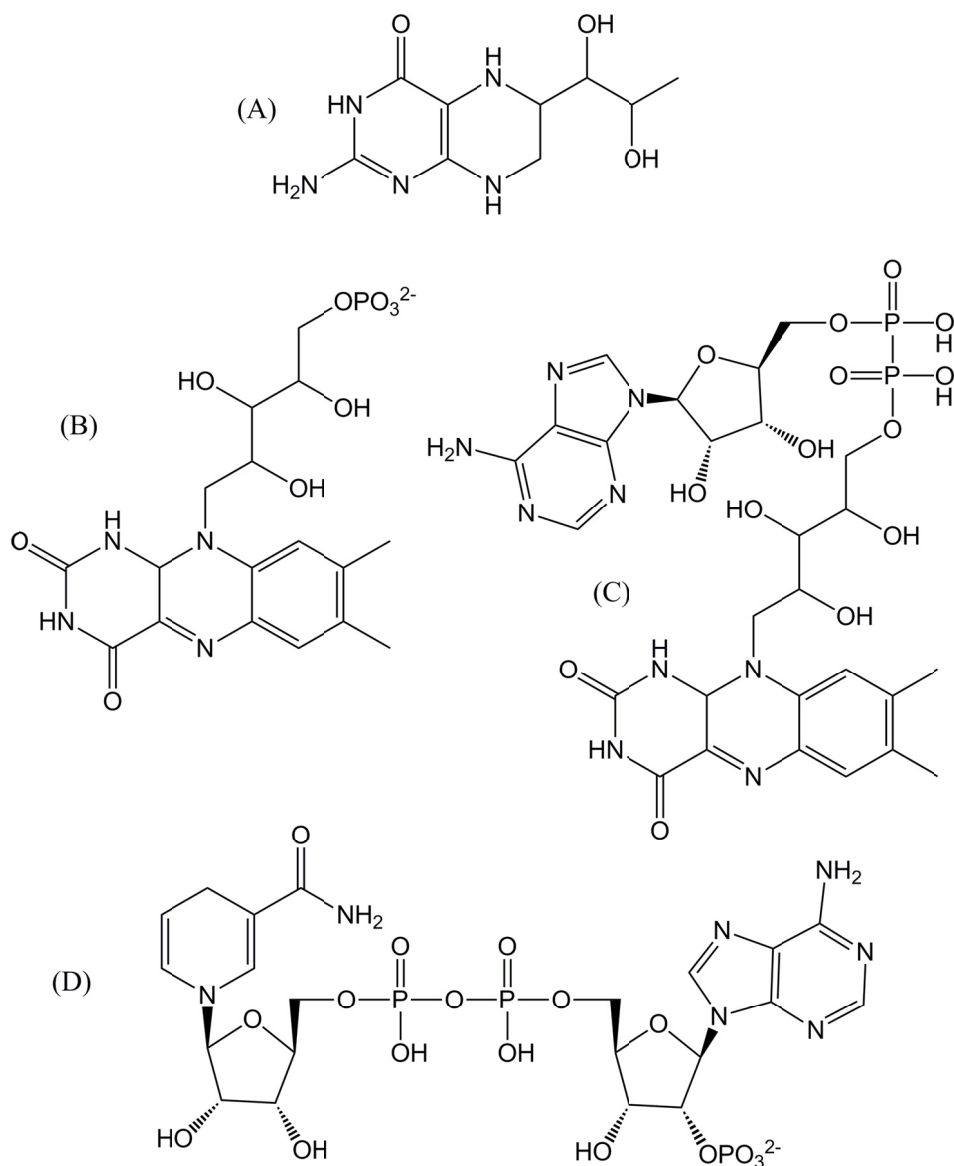
observed species is either the resting state of the enzyme (in the first turnover) or the ferric-NO complex (second turnover). The ferric-NO complex slowly releases NO to regenerate the resting state. The species responsible for actively oxidizing the substrate has not been definitively identified.¹⁰



Scheme 4.1. Production of NO and citrulline by nitric oxide synthases from the starting material arginine through the enzyme-bound intermediate N-hydroxyarginine.



Scheme 4.2. The putative reaction mechanism of nitric oxide synthases: (1) first turnover, Arg hydroxylation, (2) second turnover, NO production.

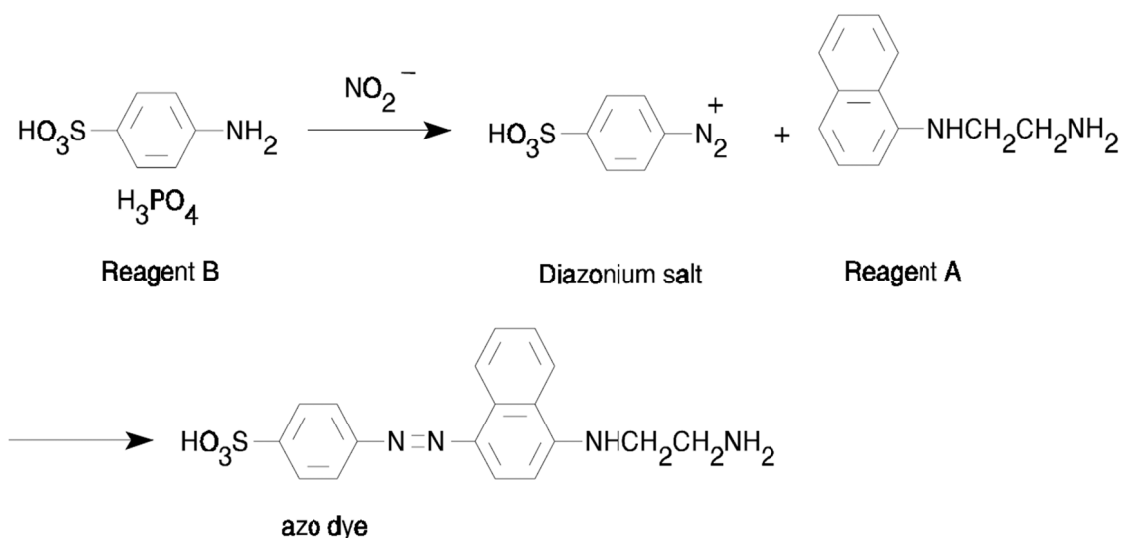


Scheme 4.3. Cofactors involved in electron transfer in NOS: (A) tetrahydrobiopterin, (B) FMN, (C) FAD, and (D) NADPH.¹¹ B–D all bind in the reductase domain of mammalian enzymes rather than in the oxygenase domain common to all species.

The mechanism of NOS has been studied extensively in order to elucidate the details of NO production.¹²⁻¹³ The most useful technique to date has been stopped-flow mixing coupled with UV-visible absorption spectroscopy. With UV-vis, one can follow the ligation and oxidation state of the heme center. Coupling this with a rapid mixing

setup allows researchers to follow the heme spectroscopically as it turns over and produces nitric oxide.¹⁴

In stopped-flow experiments, catalysis is initiated through careful mixing of the enzyme with a reactant. In the case of NOS, a degassed solution of the reduced form of the enzyme, with tetrahydrobiopterin and the enzyme-bound intermediate NOHA fully loaded, is mixed with aerated buffer to introduce oxygen. Oxygen is the last ingredient needed to initiate turnover. However, because no extra reductant is present to re-reduce the heme and pterin after the cycle, only a single turnover can occur. When monitored by UV-vis, these stopped-flow mixing experiments allow researchers to watch NOS at work as it produces NO. Using this technique, researchers have characterized the ferrous-oxy and ferric-NO complexes of the enzyme, but other intermediates react too quickly to be detected.² Observation of the ferric-NO complex during turnover is used as a spectroscopic handle in order to show that an enzyme does in fact produce NO.



Scheme 4.4. Reaction scheme for the Griess Assay.

Another common method used to characterize NO production is called a Griess Assay. In aqueous solution, nitric oxide rapidly reacts to form nitrite and other NO_x species.⁶ Reagents were developed to react specifically with nitrite, again in aqueous solution, in order to spectroscopically characterize *in vivo* NO production (**Scheme 4.4**).¹⁵ Reagent B reacts with NO₂⁻ (nitrite) to form a diazonium salt, which then reacts with Reagent A to form an azo dye with an intense visible absorption band at 540 nm. The molar absorptivity of this band is known so it can be used to determine the amount of nitrite in solution.

Both stopped-flow UV-vis spectroscopy and the Griess Assay were used to investigate the kinetics and reactivity of a series of mutant enzymes of nitric oxide synthase. The NOS used in these studies is that from *Geobacillus stearothermophilus* (gsNOS).¹⁶⁻¹⁷ This particular organism is a bacterial thermophile, and therefore its enzymes have been optimized to function at elevated temperatures. This adds to the stability of their fold,¹⁵ a notorious problem for the mammalian nitric oxide synthases. This enzyme, gsNOS, has a particularly stable ferrous-oxy intermediate. In the absence of substrate, rate constant for its decay is less than 0.1 s⁻¹. This has led to its use in other studies, such as the experiments conducted by Davydov and Hoffman which give the only evidence for both of the blue intermediates shown in **Scheme 4.2**.¹²⁻¹³

The mutants investigated in the studies presented here have been introduced previously (see Chapters 1 and 3, **Figure 4.1**). The role(s) of the proximal hydrogen bonding network involving the axial thiolate ligand were investigated. Three mutant enzymes, W70H, W70F, and W70Y, were expressed and their reactivity (along with the wild type enzyme) was investigated by stopped-flow UV-visible absorption spectroscopy

as well as through use of the Griess Assay. It was found that their autoxidation rates support the data from redox titrations (Chapter 3) and together suggest that the potential of W70H is slightly higher than wild type, while the potentials of W70F and W70Y are much more negative. The Griess Assay confirmed nitrite production in all four of the mutants, however with either significant de-coupling or a decreased rate in the W70F and W70Y mutants. The presence of a ferric-NO intermediate was confirmed using single turnover experiments in three of the four enzymes. Surprisingly, no evidence for this species was observed in the W70H mutant, suggesting production of NO^- rather than the radical NO.

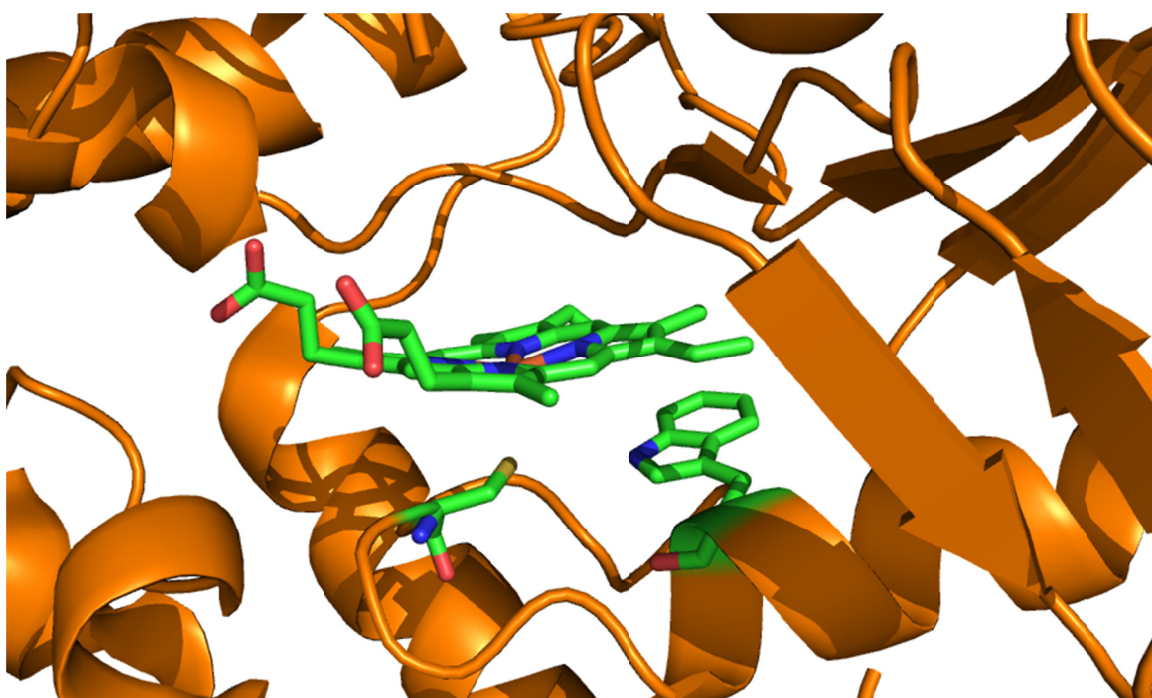


Figure 4.1. Close up of the heme center of gsNOS, with the axial thiolate and Trp70 highlighted in green (PDB file 2FLQ).

4.3 Materials and Methods

Sample Preparation

The plasmid for the nitric oxide synthase from *Geobacillus stearothermophilus* was a gift from the lab of Brian Crane. This enzyme was expressed as previously described by Sudhamsu and Crane with no significant deviations in procedure.¹⁵ The enzyme was overexpressed in *Escherichia coli* BL21 (DE3) cells. Cells were grown to an optical density of approximately 1.0–1.4 and induced by adding a solution containing iron(III) chloride, IPTG, and δ -aminolevulinic acid (Aldrich) to final concentrations of 125 mg/L, 100 μ M, and 50 mg/L, respectively, in milliQ water. The pETDuet vector (Novagen) coded for a C-terminal cleavable His₆-tag so samples were purified using metal affinity chromatography. (This vector also confers chloramphenicol resistance to the cells, so 34 μ g/mL of this antibiotic were added to all cultures in Luria broth.) The His₆-tag was then cleaved using bovine thrombin (Calbiochem). Both thrombin and the His-tag were removed using size exclusion chromatography. Sample purity and Soret band epsilon values were determined through use of the hemochromagen assay.

A QuikChange site-directed mutagenesis kit from Stratagene was used to make the desired mutations in the amino acid backbone. Primers were designed according to the guidelines outlined by the QuikChange kit manual. Unless otherwise noted, protein solutions were made in the following buffer: 50 mM Tris (2-amino-2-hydroxymethylpropane-1,3-diol), 150 mM NaCl, pH 7.5 (the same buffer used for size exclusion chromatography). Steady-state UV-visible spectra were collected on an Agilent HP 8452 diode array spectrophotometer.

Stopped Flow UV-Visible Spectroscopy

Samples were prepared anaerobically and transferred to an anaerobic tonometer with 1.5 equivalents of dithionite to scavenge any residual oxygen. Dithionite was used to scavenge oxygen from the stopped flow spectrophotometer (HiTech Scientific) syringes and excess dithionite was removed by repeated washing with anaerobic buffer. For autoxidation rates, samples of reduced protein (4–6 μM gsNOS) free of substrate and pterin cofactor were mixed with aerated buffer. Autoxidation rates were also measured in the presence of 2.5 mM Arg and 15 μM pterin. Protein samples for single turnover experiments (4–6 μM gsNOS loaded with, 60 μM H4B and 200 μM N-hydroxy-L-arginine) were rapidly mixed with air-saturated buffer. All experiments were conducted at 4 °C. The formation and release of NO in the single turnover experiments was monitored using a diode array detector and the rates fit globally using SpecFit32 (HiTech Scientific). Measured rates were independent of protein concentration under experimental conditions and all measurements were repeated at least six times before averaging.

Griess Assay

In order to quantify turnover in each of the enzymes, NO production was monitored using the Griess Assay. Reagents A and B were purchased from Cayman Chemicals. Solutions were made containing of 100 μL of 30 μM NOS and 1 mM arginine in 150 mM NaCl, 50 mM Tris buffer at pH 7.5. To these solutions, 2 μL of 1M H_2O_2 was added to a final concentration of 20 mM. The solution was allowed to react for three minutes before addition of Reagent B, which stops the reaction and denatures the protein. The sample must be allowed to sit for ten minutes before addition of Reagent A in order to allow formation of nitrite from aqueous nitric oxide. The UV-visible

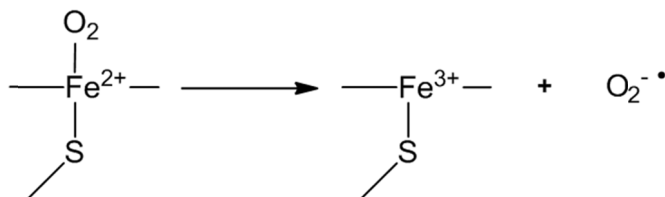
absorption spectrum is then recorded. Absorbance at 540 nm is related to the concentration of nitrite by the following equation (from Cayman Chemicals). All measurements were made in triplicate.

$$\text{Absorbance} = 0.030 + 0.029[\text{nitrite}] \quad (4.1)$$

4.4 Results and Discussion

Autoxidation Rates

The reactivity of each wild type gsNOS and three mutants (W70H, W70F, and W70Y) was studied by stopped-flow UV-visible spectroscopy. The reduced form of all heme-thiolate enzymes reacts quickly with dioxygen. Samples of approximately 5 μM NOS in Tris buffer were mixed in a 1:1 ratio with oxygenated buffer (air-saturated) and the regeneration of the ferric state was monitored. Given that this particular enzyme has such a long-lived ferrous-oxy species, the kinetics of each mutant's reactivity with dioxygen was investigated. It is unclear how this enzyme is tuned to produce such a stable complex and what purpose that may serve. Upon mixing with dioxygen, samples quickly form a ferrous-oxy species which then dissociates into the ferric form of the enzyme and a reduced superoxide species (**Scheme 4.5**). In the absence of substrate and pterin cofactor, clean formation of the ferrous-oxy species is not observed, only the transformation from ferrous enzyme to ferric enzyme.



Scheme 4.5. Reaction of oxygen with reduced gsNOS forms a ferrous-oxy complex, and then releases superoxide from the oxidized heme.

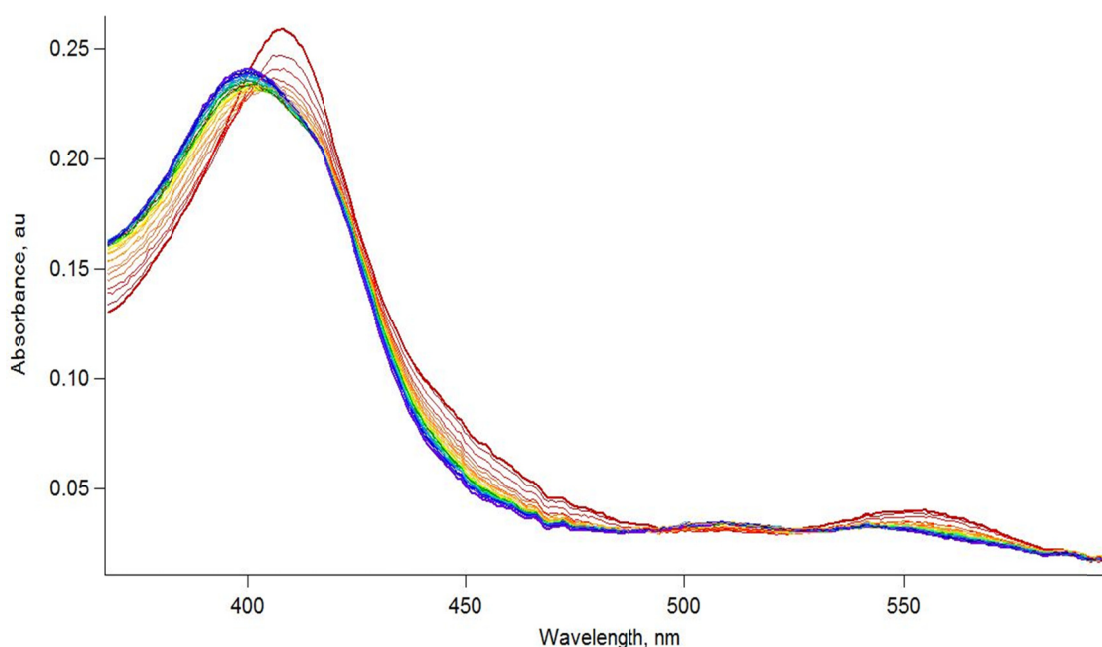


Figure 4.2. Oxidation of W70F upon rapid mixing of reduced enzyme with oxygenated buffer. Ferrous gsNOS (red trace) partially converts to the ferric heme over the course of 22.5 seconds. For full kinetics analysis, scans were collected out to 45 seconds to allow for full formation of the ferric species.

These three single point mutations at position 70 were found to have a large effect on autoxidation rates. For the wild type enzyme, scans of 225 seconds were required in order to catch the full transformation to the oxidized resting state. The ferrous state of the Tyr mutant reacts much more quickly, taking only 9 seconds to completely oxidize. The Phe and Tyr mutants have higher rate constants than wild type for autoxidation by factors of 2.5 and 6, respectively. Interestingly, the His mutant has a rate constant that is one full order of magnitude lower. This is certainly caused by altered electronics of the heme center, but the exact reason for this is unknown. While the reduction potential of this enzyme was reported to be significantly higher than the wild type in mammalian inducible NOS by another group,¹⁸ our data suggest that the potential of this enzyme is

not as elevated relative to wild type (Chapter 3). Another factor may be the π -stacking of the tryptophan residue with the porphyrin ring, of which histidine is incapable.

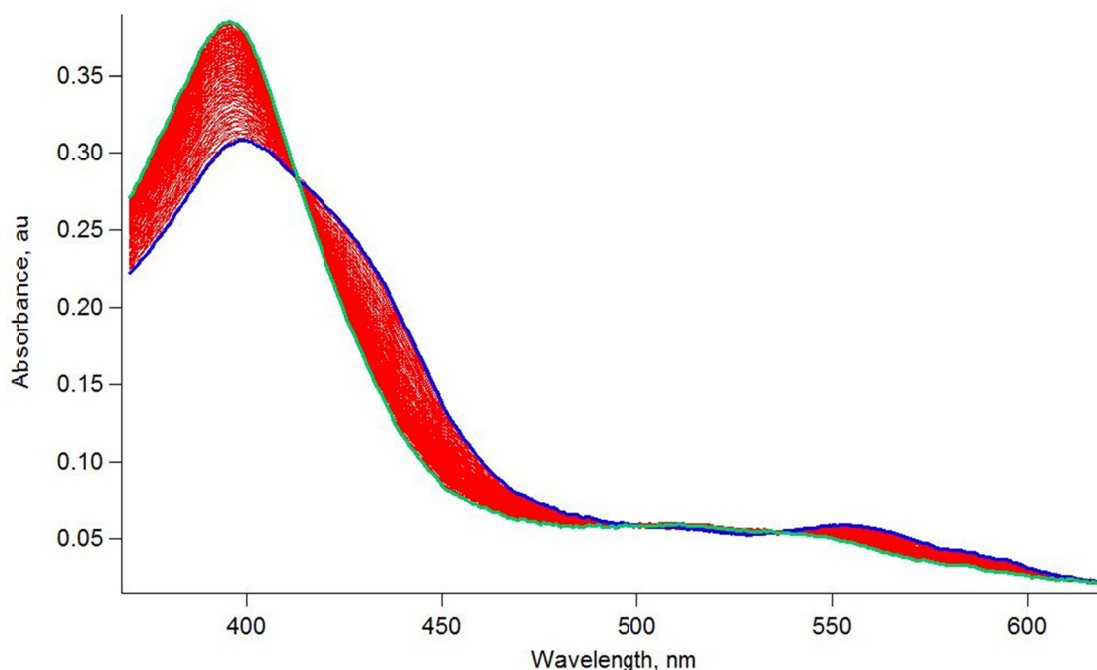


Figure 4.3. Oxidation of W70H in the presence of arginine and tetrahydrobiopterin. Initial scan upon mixing (blue trace) before formation of the ferric state (green).

It has been shown previously that both substrate and tetrahydrobiopterin cofactor contribute to the decay of the ferrous-oxy species and speed formation of the resting state. This is presumably due to the ability of the enzyme to now undergo catalysis, as all necessary ingredients are present. Faster scans show clean formation of the ferrous-oxy species, rather than catching only a shoulder (blue trace, **Figure 4.3**) before conversion to the ferric state. However, longer scanning times are required to observe full formation of the ferric state. The rate constant of interest is that of the oxidation to ferric, so longer scans were used for kinetics analysis. All data were fit to a three-state model, where the ferrous-oxy is formed very rapidly, followed by conversion to the ferric enzyme.

Calculated rate constants for conversion of the ferrous-oxy intermediate to the ferric resting state (from SpecFit software) are shown in **Table 4.1**.

Table 4.1. Rate constants for oxidation of each mutant enzyme, with and without substrate/cofactor.

Sample	Oxidation rate, s^{-1}	With substrate, s^{-1}
WT	0.096	0.51
His	0.0098	0.19
Phe	0.23	2.6
Tyr	0.62	4.3

The effect of the presence of arginine and the pterin cofactor is apparent from **Table 4.1**. The rate constant for oxidation of the wild type enzyme is increased by the smallest amount among the four enzymes, a factor of approximately 5, while the W70H mutant oxidizes faster in the presence of these two additional substances by a factor of nearly 20. This is a remarkable increase. The data show that the ferrous-oxy species of the W70H mutant is much more stable than the others, by an order of magnitude or more, but this effect is lessened under catalytic conditions where reactivity of the enzyme toward substrate dominates the kinetics rather than simple oxidation of the iron center.

Assuming that all four samples interact with dioxygen in the same manner, the rates of autoxidation of the heme should correlate with the reduction potentials. This is consistent with results from Chapter 3 showing that the reduction potential of the Phe and Tyr mutants are significantly more negative than wild type and W70H. The presence of this single, long hydrogen bonding interaction brings the reduction potential more

positive. The potential of the W70F and W70Y mutants is most likely too negative to allow reduction by a reductase enzyme *in vivo*.

Griess Assay

The function of nitric oxide synthases is to produce nitric oxide. This radical species reacts rapidly in aqueous solution, making it difficult to quantify NO production. One of the compounds that NO forms in buffered solutions is NO_2^- , nitrite. A colorimetric assay for this species has been developed and patented, allowing for the facile determination of nitrite concentrations in solution. This should be proportional to the amount of NO originally formed by the enzyme.

Table 4.2. Nitrite production rates by gsNOS mutants.

Sample	NO_2^- production, $\text{heme}^{-1} \text{ min}^{-1} \times 100$
WT	10.7 ± 0.6
His	13.9 ± 0.7
Phe	4.3 ± 0.1
Tyr	3.4 ± 0.1

With wild type as a benchmark, W70H shows increased nitrite production while W70F and W70Y show a marked decrease in production. This decrease could be caused by any of several things. First, if a mutant produces NO at a decreased rate, this would lead to decreased consumption of reducing equivalents from the hydrogen peroxide and less nitrite in the solution. Alternatively, if the electronics of the system have been unbalanced, a decrease in quantity of nitrite could mean similar or even increased consumption of reducing equivalents, but with uncoupling of this from NO production. The enzyme would instead release superoxide or other compounds, or even oxidize parts

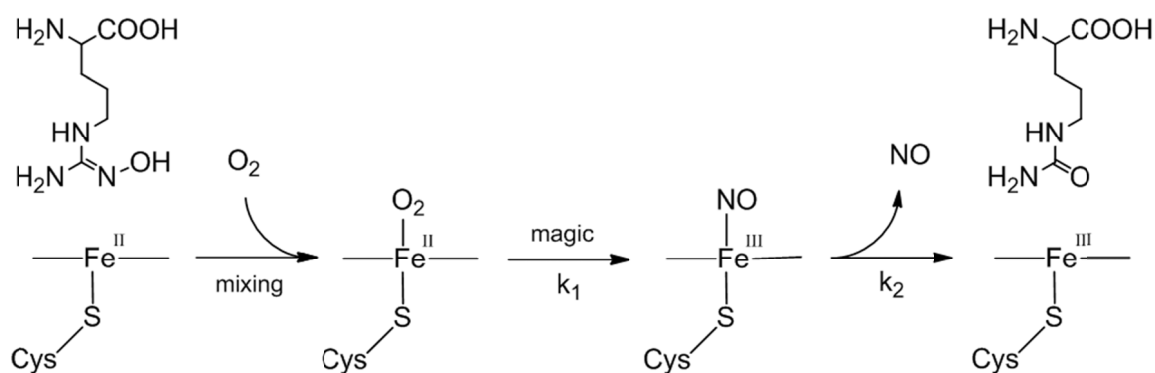
of the protein itself leading to degradation. Unfortunately, the Griess Assay can tell us only the amount of nitrite in any given aqueous solution.

Hydrogen peroxide has sufficient driving force to reduce all four of these protein samples (-680 mV). Upon mixture with the enzyme, a ferric-hydroperoxo species is formed (the first complex in blue in **Scheme 4.2**). Due to their more negative reduction potentials, the Tyr and Phe mutant enzymes autoxidize very rapidly. This means that their rate of consumption of reducing equivalents should be equal or even increased compared with wild type regardless of catalytic activity. Without this conserved hydrogen bond, the hydroperoxo complex may react too quickly to release reactive oxygen species and the ferric enzyme without reacting with the substrate. Alternatively, with a better donating thiolate ligand, O-O bond cleavage may occur incredibly rapidly. This would form Compound I (second species in blue in **Scheme 4.2**) and facilitate the first turnover, but perhaps not provide enough time for the ferric-hydroperoxo to react with NOHA in the second turnover, preventing NO formation. Catalysis using hydrogen peroxide as reductant and the source of dioxygen has been shown to produce cyano-ornithine in mammalian inducible NOS rather than citrulline (and NO).¹⁹

Single Turnover Experiments

To observe turnover of the enzyme, stopped-flow mixing was employed coupled with UV-visible absorption spectroscopy for detection of intermediates. The resting state of the enzyme, with substrate and cofactor bound, has a Soret band with a maximum absorption at 396 nm. The position of this band is very consistent across isoforms, while the substrate and cofactor-free forms can vary from 400 (gsNOS)¹⁵ to 421 nm (mammalian iNOS).¹⁹⁻²⁰ The ferrous-oxy complex, formed immediately after mixing the

enzyme with aerated buffer, has a maximum absorption around 428–430 nm, depending on isoform.¹⁴ This is the last intermediate observed before the formation of the NO-bound ferric heme complex, with a maximum absorption near 440 nm.²¹ This releases NO to regenerate the resting state of the enzyme. Each of these species can be observed by stopped-flow and resolved by UV-vis, allowing researchers to literally watch NOS as it functions. This reaction scheme is shown in **Scheme 4.6**, detailing the steps from the ferrous enzyme introduced in one syringe, to the production of citrulline and NO. Unfortunately, the active oxidant (Compound I or the hydroperoxo-heme complex) reacts much too quickly to build up to any appreciable level and be observable by this technique, thus k_1 is ultimately a mixture of several elementary steps leading to ferric-NO formation.²² Compound I has only been cleanly generated and characterized recently by stopped-flow in a thermophilic cytochrome P450.²³



Scheme 4.6. Reaction of reduced NOS with oxygenated buffer, provided that tetrahydrobiopterin is present, showing the release of NO.

For fitting purposes, a three-state model is used, beginning with the ferrous-oxy species and finishing with formation of the resting state through another intermediate (which correlates with the ferric-NO complex). These correspond to the second, third, and fourth complex shown in **Scheme 4.6**, with the software fitting two rate constants, k_1

and k_2 . Despite k_1 incorporating many elementary steps, this model for fitting the kinetics data fits all spectra well using the SpecFit software.

In all cases the first trace shows the five-coordinate ferrous species, prior to formation of the ferrous-oxy. This arises due to the use of excess reductant, which is necessary to ensure that the enzyme remains fully reduced in the syringe. The reductant, sodium dithionite, reacts several orders of magnitude more rapidly with oxygen than the enzyme.²⁴ Thus, the small excess of dithionite (less than 1 equivalent of the enzyme so as not to greatly alter the initial concentration of oxygen in solution) will react completely before the other chemical reactions occur. Typical traces for the wild type enzyme are shown in **Figure 4.4** below. The ferrous complex can be seen in the first (and only the first) trace, red. The second trace, in green, corresponds well with formation of the ferrous-oxy complex. This formation is complete before the second trace can be collected, thus the rate is too fast to be calculated accurately from these data. For all kinetics analyses the first spectrum is discarded, as this is the only spectrum where the ferrous-unligated complex is visible. In every case the spectra first red-shift (relative to the five-coordinate ferrous starting material) before blue shifting to the ferric species.

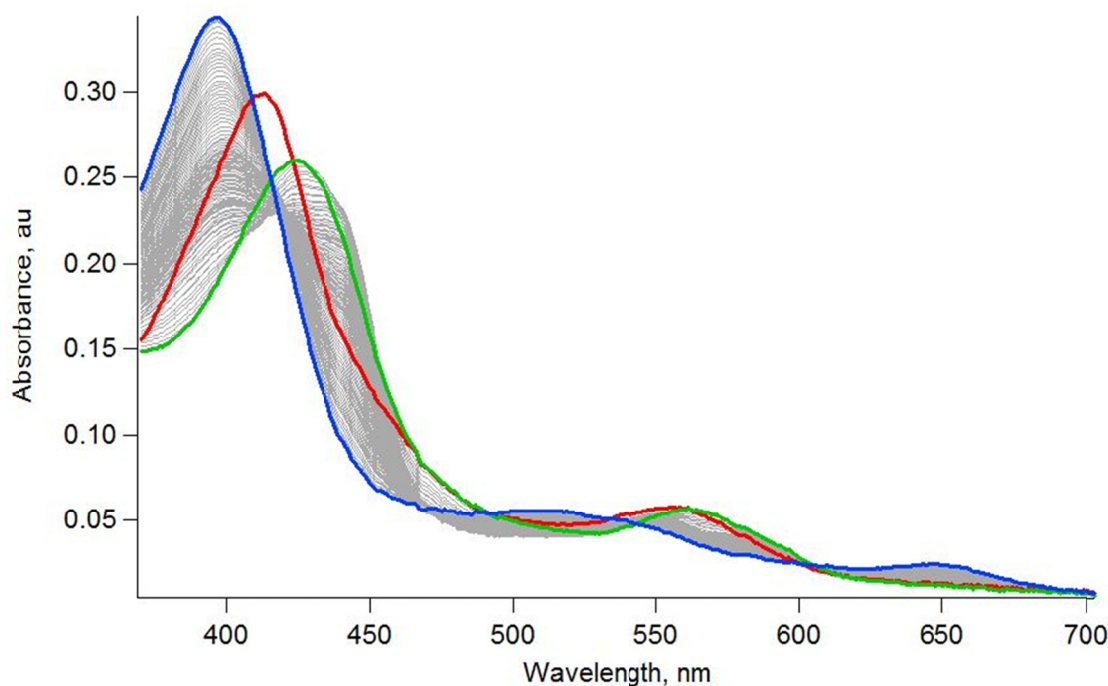


Figure 4.4 Single turnover reaction of wild type gsNOS. Five-coordinate ferrous (red), ferrous-oxy (green), and the resting ferric state (blue).

The spectra shown above are consistent with stopped-flow data collected on other nitric oxide synthases, such as for the NOSs from mammalian macrophages (iNOS) and *Bacillus subtilis*.^{14, 25} One key feature is the further red-shift of the Soret band beyond the ferrous-oxy complex (seen in gray just to the right of the maximum absorbance for the green trace). The Soret band for the pure ferric-NO complex has a maximum absorbance at 440–442 nm, depending on isoform.¹⁴ The formation of this complex can be seen more clearly for the W70Y mutant, shown in **Figure 4.5**.

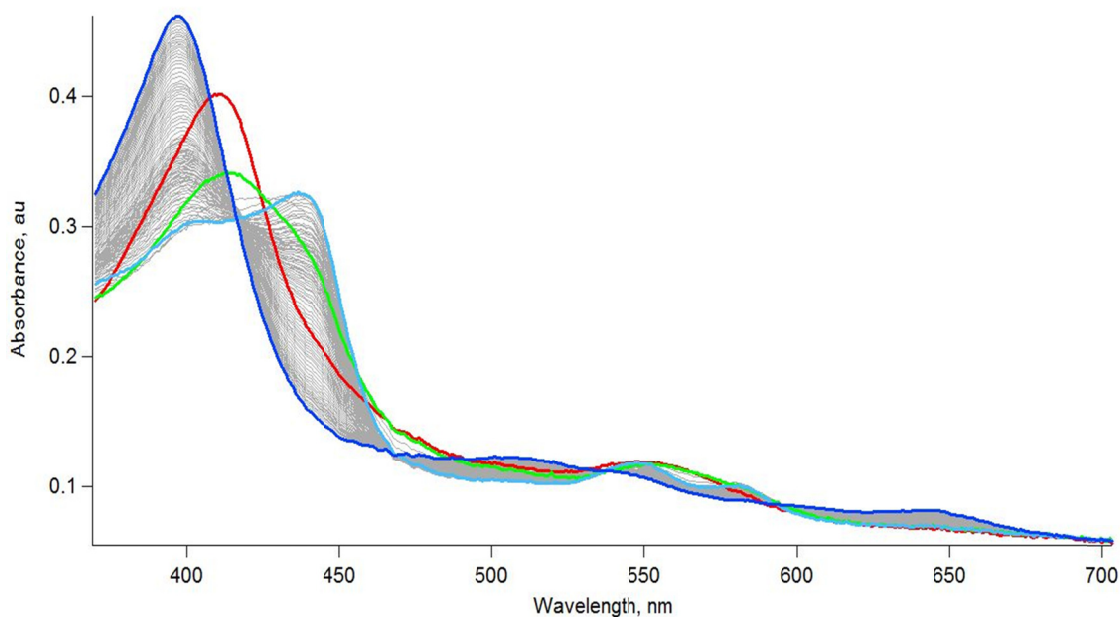


Figure 4.5. Single turnover reactions of W70Y gsNOS. In these traces, the formation of the ferric-NO complex can be seen most clearly in this mutant. These are also representative of the W70F mutant.

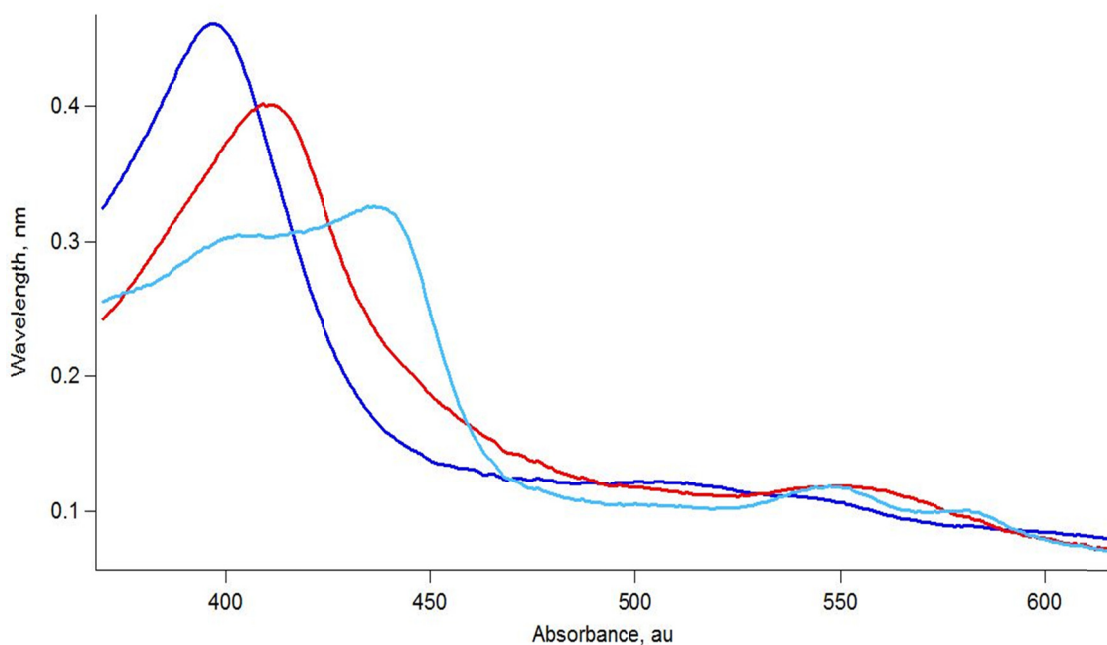


Figure 4.6. The spectrum generated for intermediate B (light blue) with the ferrous (red) and ferric (dark blue) spectra for reference. The light blue trace clearly shows a mixture of two species by Soret bands, the ferric-NO complex, with a maximum absorbance at 438 nm in this spectrum, and the ferric resting state of the enzyme, with a maximum absorbance of 398 nm.

While clear evidence is seen for the formation of the ferric-NO complex for the wild type enzyme and the W70F and W70Y mutants, this is absent in the W70H mutant. Traces collected for the histidine mutant are shown in **Figure 4.7**. The spectrum with the Soret band farthest to the red is that of the second trace, with a peak at 430 nm and broad Q-bands corresponding to the ferrous-oxy complex. At no point do any of the traces shift further to the red and the fitting software is unable to extract any intermediate with a spectrum with even a shoulder near 440 nm. No evidence could be found to support the formation of a ferric-NO species in this particular mutant NOS.

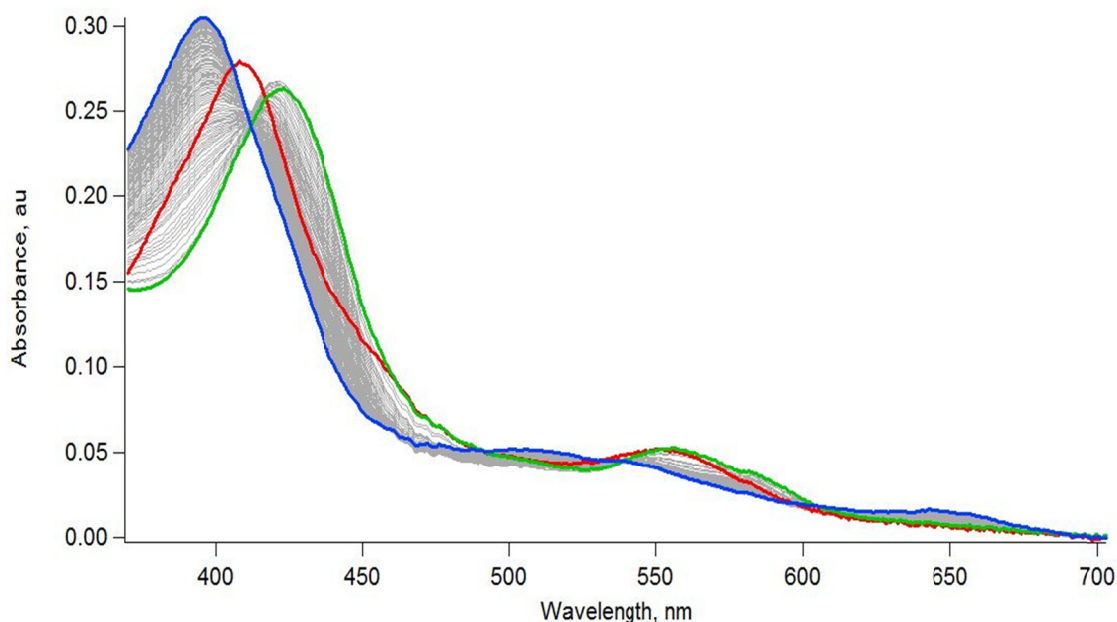


Figure 4.7. Single turnover reactions of W70H gsNOS. The second trace, green, shows clear formation of the ferrous-oxy complex, but no further red-shift of the spectra is seen.

It can be concluded from stopped-flow UV-vis data that the W70H mutant does not form a ferric-NO complex. Spectra look nearly identical to those collected with Arg and pterin, probing the oxidation rate in the first turnover but with an oxidation rate of 0.07 rather than 0.2. (This complex is observed by stopped-flow/UV-vis in all other NOS enzymes reported to date.) From the Griess Assay, it was shown that this enzyme releases

some NO_x at a rate actually increased relative to wild type. These data together suggest that the W70H mutant enzyme does not release $\text{NO}\cdot$ but rather NO^- from the heme center. The other three enzymes, however, clearly form ferric-NO complexes, as observed by stopped-flow.

4.5 Conclusions

Stopped-flow coupled with UV-visible spectroscopy was employed to characterize wild type gsNOS and these three new mutant enzymes. It was shown that their autoxidation rates correlate with reduction potential data discussed in Chapter 3. The histidine mutant has an elevated reduction potential and the slowest autoxidation rate relative to the other three. The wild type is more negative by approximately 20 mV with a potential of -362 mV vs. NHE. This reduction potential is similar to that of mammalian inducible NOS, but these two are then more negative than other NOS enzymes by 100 mV.²⁶ The reason for this behavior in gsNOS is unknown, but in iNOS the presence of the substrate sterically excludes a water molecule that coordinates the heme and this binding event shifts the reduction potential into the normal range for NOSs. The two mutants lacking this conserved hydrogen bond, W70F and W70Y, have significantly more negative potentials and were found to have very fast rate constants for autoxidation, consistent with more negative potentials.

The production of NO_x species of all four enzymes was characterized by the Griess Assay. The wild type produces nitrogen oxide species at a rate similar to other NOSs. The W70H mutant has an elevated rate of NO_x release/formation. The two mutants without this hydrogen bond have significantly decreased rates of NO_x

production. Clearly this hydrogen bond plays a role in the rate of NO release from the enzyme or the speed with which it is formed (as all four should react sufficiently rapidly with hydrogen peroxide for reduction not to be a factor).

Finally, stopped-flow was once again employed in order to determine if the Griess Assay was indeed detecting NO^\bullet or rather NO^- which are indistinguishable by that method. The ferric-NO complex, the immediate precursor to the nitric oxide product, was observed for three of the four enzymes. Interestingly, this could not be observed for the W70H mutant. This mutant most likely releases NO^- .

The conserved proximal hydrogen bond donating group found near the axial thiolate ligand in all nitric oxide synthases plays a key role in tuning the electronics of the active site. This is a uniquely long hydrogen bonding interaction between this tryptophan and the thiolate, at just 3.7 Å. Without this interaction, the enzyme is still capable of producing NO, as found for both the W70F and W70Y mutants by single turnover experiments. Their reduction potentials, however, are incredibly negative and most likely fall far below the biologically relevant window. The replacement of this tryptophan with a histidine results in an enzyme with a more elevated potential, however it cannot release NO radical. The histidine residue, lacking the aryl ring, most likely cannot π -stack with the porphyrin ring, giving it more flexibility. This may allow it to move closer to the thiolate to improve this hydrogen bonding interaction. If this interaction is too strong, NO^- is released.

In the second turnover of the catalytic cycle, an electron from the heme center must be shuttled back into the tetrahydrobiopterin cofactor to re-reduce it. The potentials of both the heme and the pterin must be tuned perfectly to allow forward electron transfer

into the ferrous-oxy complex followed by back electron transfer into the pterin. This back electron transfer allows release of $\text{NO}\cdot$ and not NO^- .²⁷ If the potential of the heme center is too high, this back electron transfer cannot occur, preventing $\text{NO}\cdot$ release. Thus, the hydrogen bonding interaction is necessary for tuning the reduction potential high enough for the reduction of the heme by a reductase domain/enzyme. However, when too strong, the potential is tuned too high to send an electron back into the pterin after catalysis, which is necessary for formation of the product NO .

4.6 References

1. Marletta, M. A. (1993) Nitric-oxide synthase structure and mechanism, *J. Biol. Chem.* 268, 12231.
2. Stuehr, D. J., Santolini, J., Wang, Z. Q., Wei, C. C., and Adak, S. (2004) Update on mechanism and catalytic regulation in the no synthases, *J. Biol. Chem.* 279, 36167.
3. Palmer, R. M. J., Ferrige, A. G., and Moncada, S. (1987) Nitric-oxide release accounts for the biological-activity of endothelium-derived relaxing factor, *Nature* 327, 524.
4. Alderton, W. K., Cooper, C. E., and Knowles, R. G. (2001) Nitric oxide synthases: Structure, function and inhibition, *Biochem. J.* 357, 593.
5. Griffith, O. W., and Stuehr, D. J. (1995) Nitric oxide synthases: Properties and catalytic mechanism, *Annu. Rev. Physiol.* 57, 707.
6. Groves, J. T., and Wang, C. C.-Y. (2000) Nitric oxide synthase: Models and mechanisms, *Curr. Opin. Chem. Biol.* 4, 687.
7. Sono, M., Stuehr, D. J., Ikedaisaito, M., and Dawson, J. H. (1995) Identification of nitric-oxide synthase as a thiolate-ligated heme protein using magnetic circular-dichroism spectroscopy - comparison with cytochrome p-450-cam and chloroperoxidase, *J. Biol. Chem.* 270, 19943.
8. Sono, M., Roach, M. P., Coulter, E. D., and Dawson, J. H. (1996) Heme-containing oxygenases, *Chem. Rev.* 96, 2841.
9. Dawson, J. H., and Sono, M. (1987) Cytochrome.P-450 and chloroperoxidase - thiolate-ligated heme enzymes - spectroscopic determination of their active-site structures and mechanistic implications of thiolate ligation, *Chem. Rev.* 87, 1255.
10. Martin, N. I., Woodward, J. J., Winter, M. B., Beeson, W. T., and Marletta, M. A. (2007) Design and synthesis of c5 methylated l-arginine analogues as active site probes for nitric oxide synthase, *J. Am. Chem. Soc.* 129, 12563.
11. Mowat, C. G., Gazur, B., Campbell, L. P., and Chapman, S. K. (2010) Flavin-containing heme enzymes, *Arch. Biochem. Biophys.* 493, 37.
12. Davydov, R., Ledbetter-Rogers, A., Martásek, P., Larukhin, M., Sono, M., Dawson, J. H., Masters, B. S. S., and Hoffman, B. M. (2002) Epr and endor characterization of intermediates in the cryoreduced oxy-nitric oxide synthase heme domain with bound l-arginine or n^g-hydroxyarginine, *Biochemistry* 41, 10375.
13. Davydov, R., Sudhamsu, J., Lees, N. S., Crane, B. R., and Hoffman, B. M. (2009) Epr and endor characterization of the reactive intermediates in the generation of no by cryoreduced oxy-nitric oxide synthase from geobacillus stearothermophilus, *J. Am. Chem. Soc.* 131, 14493.
14. Wei, C. C., Wang, Z. Q., and Stuehr, D. J. (2002) Nitric oxide synthase: Use of stopped-flow spectroscopy and rapid-quench methods in single-turnover conditions to examine formation and reactions of heme-o-2 intermediate in early catalysis, In *Enzyme kinetics and mechanism, pt f: Detection and characterization of enzyme reaction intermediates*, pp 320, Academic Press Inc, San Diego.

15. Sudhamsu, J., and Crane, B. R. (2006) Structure and reactivity of a thermostable prokaryotic nitric-oxide synthase that forms a long-lived oxy-heme complex, *J. Biol. Chem.* 281, 9623.
16. Kabir, M., Sudhamsu, J., Crane, B. R., Yeh, S. R., and Rousseau, D. L. (2008) Substrate-ligand interactions in geobacillus stearothermophilus nitric oxide synthase, *Biochemistry* 47, 12389.
17. Kinloch, R. D., Sono, M., Sudhamsu, J., Crane, B. R., and Dawson, J. H. (2010) Magnetic circular dichroism spectroscopic characterization of the nos-like protein from geobacillus stearothermophilus (gsnos), *J. Inorg. Biochem.* 104, 357.
18. Tejero, J. S., Biswas, A., Wang, Z. Q., Page, R. C., Haque, M. M., Hemann, C., Zweier, J. L., Misra, S., and Stuehr, D. J. (2008) Stabilization and characterization of a heme-oxy reaction intermediate in inducible nitric-oxide synthase, *J. Biol. Chem.* 283, 33498.
19. Hurshman, A. R., and Marletta, M. A. (1995) Nitric-oxide complexes of inducible nitric-oxide synthase - spectral characterization and effect on catalytic activity, *Biochemistry* 34, 5627.
20. Nguyen, Y. H. L., Winkler, J. R., and Gray, H. B. (2007) Probing heme coordination states of inducible nitric oxide synthase with a re(i)(imidazole-alkyl-nitroarginine) sensitizer-wire, *J. Phys. Chem. B* 111, 6628.
21. Agapie, T., Suseno, S., Woodward, J. J., Stoll, S., Britt, R. D., and Marletta, M. A. (2009) No formation by a catalytically self-sufficient bacterial nitric oxide synthase from sorangium cellulosum, *P. Natl. Acad. Sci. USA* 106, 16221.
22. Zhu, Y. Q., and Silverman, R. B. (2008) Revisiting heme mechanisms. A perspective on the mechanisms of nitric oxide synthase (nos), heme oxygenase (ho), and cytochrome p450s (cyp450s), *Biochemistry* 47, 2231.
23. Rittle, J., and Green, M. T. (2010) Cytochrome p450 compound i: Capture, characterization, and c-h bond activation kinetics, *Science* 330, 933.
24. Tao, Z., Goodisman, J., and Souid, A.-K. (2008) Oxygen measurement via phosphorescence: Reaction of sodium dithionite with dissolved oxygen, *The Journal of Physical Chemistry A* 112, 1511.
25. Wang, Z. Q., Wei, C. C., Sharma, M., Pant, K., Crane, B. R., and Stuehr, D. J. (2004) A conserved val to ile switch near the heme pocket of animal and bacterial nitric-oxide synthases helps determine their distinct catalytic profiles, *J. Biol. Chem.* 279, 19018.
26. Presta, A., Weber-Main, A. M., Stankovich, M. T., and Stuehr, D. J. (1998) Comparative effects of substrates and pterin cofactor on the heme midpoint potential in inducible and neuronal nitric oxide synthases, *J. Am. Chem. Soc.* 120, 9460.
27. Wei, C. C., Wang, Z. Q., Hemann, C., Hille, R., and Stuehr, D. J. (2003) A tetrahydrobiopterin radical forms and then becomes reduced during n-omega-hydroxyarginine oxidation by nitric-oxide synthase, *J. Biol. Chem.* 278, 46668.

Chapter 5

Influences of Pathway Mutations on the Kinetics of CO Rebinding and NO Release in a Nitric Oxide Synthase

Reproduced with permission from Whited, C. A., Lavoie, K. D., Weinert, E. E., Agapie, T., Winkler, J. R., and Gray, H. B. Pathways of NO Release in Nitric Oxide Synthase. *submitted*. 2011.

5.1 Abstract

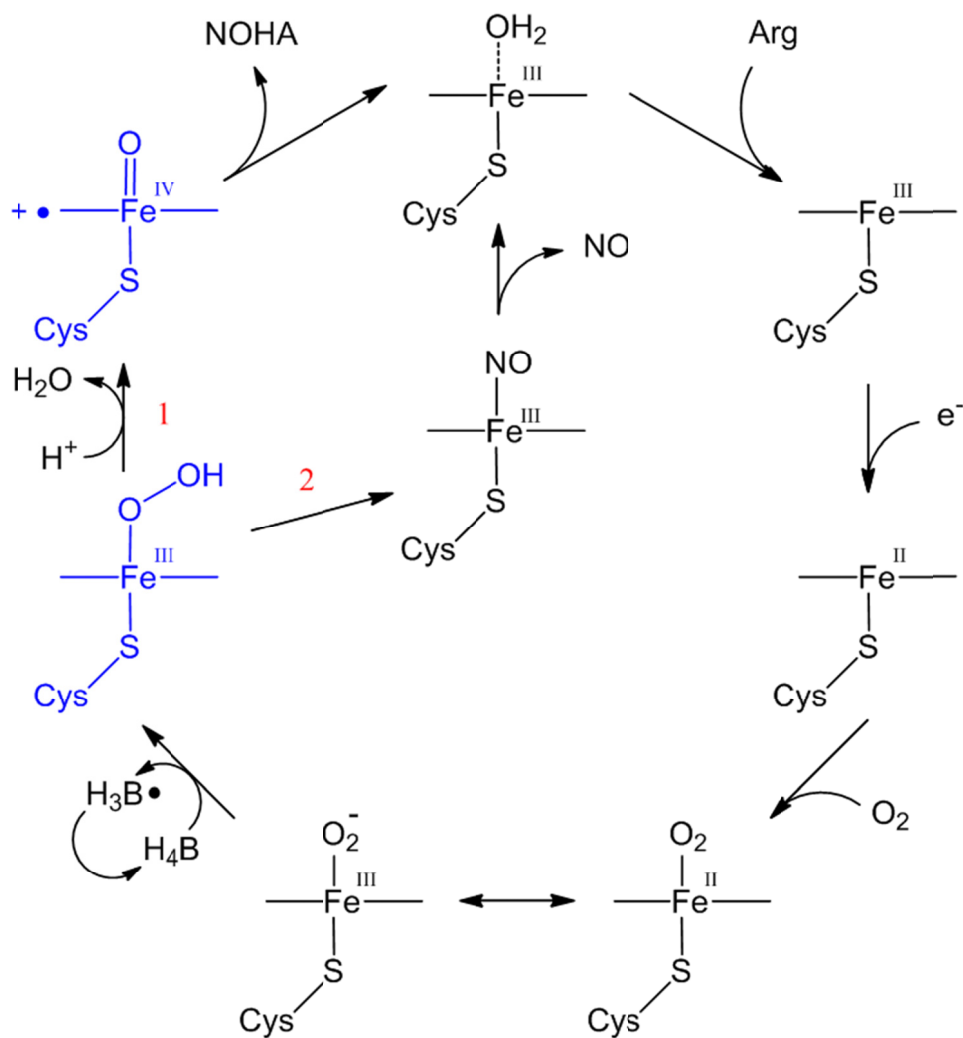
Nitric oxide synthases (NOS) are a family of enzymes responsible for the production of the signaling molecule nitric oxide (NO). The rate at which NO is released by each enzyme varies greatly among isoforms and species, over nearly two orders of magnitude. One residue (an isoleucine located above the heme in bacterial enzymes) involved in the gating of NO release has been previously identified by Stuehr. However, this single residue does not account for the entirety of the differences among the forms of NOS. Another residue, a histidine at position 134 in NOS from *Geobacillus stearothermophilus* (gsNOS), was hypothesized to also participate in gating NO release based on an observed correlation between rates of NO release and the bulk of side chains at this position. Each single point mutation, H134S and I223V, and the double mutant were expressed in gsNOS and their reactivity toward the diatomic molecules CO and NO were studied. CO rebinding was investigated using laser flash photolysis and NO release using stopped flow UV-visible spectroscopy. The presence of both monomer and dimer was observed in solution and position 134 was shown to be another key residue in gating NO release. Wild type gsNOS contains both the bulkier Ile223 and His134 and has the slowest measured NO release (0.039 s^{-1}) of all NOS enzymes. Each single mutation increased NO release substantially, while the double mutant has a rate constant of 1.0 s^{-1} , nearly as fast as mammalian iNOS at 2.3 s^{-1} , identifying position 134 as another important factor determining rate constants for NO release.

5.2 Introduction

Nitric oxide synthases (NOS) are found in all eukaryotes, as well as a selection of prokaryotes, and are responsible for biological production of nitric oxide (NO).¹⁻² In mammals, various isoforms of NOS are involved in processes such as neurotransmission and vasodilation.³ Interestingly, the immune system uses high levels of NO to kill invading bacterial cells. Given this function of NO, the discovery of NOS-like enzymes in bacteria was unexpected. The role of NO in these bacteria is still under debate, although it has been proposed to be a method to combat host immune responses.⁴⁻⁶ Different functions most likely require different rates of NO release in cells. This can be controlled through several methods such as regulation of protein expression within a cell (as is the case for mammalian inducible NOS found in macrophages) or on the molecular level within the enzyme. These studies focus on the latter, namely the manner in which the enzyme itself regulates NO release.

Nitric oxide synthases contain a thiolate-ligated heme active site, very similar to that found in cytochromes P450.⁷⁻⁸ This superfamily of enzymes carries out a vast array of biological oxidations, using the heme cofactor to activate dioxygen.⁹ NOS, on the other hand, catalyzes only the oxidation of arginine to produce NO in two turnovers (through the enzyme-bound intermediate N-hydroxy-L-arginine). The first turnover involves a two-electron oxidation of substrate like cytochromes P450, while the second is formally a three-electron oxidation and is unique in biology.¹⁰⁻¹¹ What is known of the catalytic cycle is shown in **Scheme 5.1** colored black. The two species in blue are intermediates from the cycle of cytochromes P450 used to fill in gaps in our knowledge

of the NOS cycle. The numbers in red represent the pathways taken in each turnover and highlight the differences.



Scheme 5.1. A proposed catalytic cycle for both turnovers of NOS producing NO.

The last step of catalysis involves formation of a ferric-NO species which slowly releases the radical species NO. The ferrous-oxy and ferric-NO species are the only two intermediates observed during turnover and it is solely on the basis of the demonstrated cytochrome P450 cycle that the two compounds in blue are included. (There is some recent evidence for these from EPR and ENDOR studies, but they have not been

corroborated.¹²⁾ However, multiple groups have demonstrated ferric-NO formation and its decay to release the radical species. In mammals, a series of complex steps has evolved in order to regulate enzyme function and keep tight control on each step, such as delivery of electrons and the tuning of redox potentials.¹³ It is not fully understood how the protein matrix controls NO release and what factors cause this rate to vary among forms of NOS enzymes, nor how NO production is controlled in bacterial systems.

In order to study NO release, stopped flow UV-visible spectroscopy has been employed. The unique spectroscopic features of heme enzymes allow for the differentiation of various species during catalysis. Single turnover experiments, where the fully-reduced, substrate-bound enzyme is held in de-oxygenated buffer and then mixed rapidly with buffer that is saturated in oxygen, have allowed the determination of rates of NO release in many NOS enzymes.¹⁴⁻¹⁷

It was observed in such stopped flow measurements that while the mammalian NOS isoforms release NO on the order of 2 to 5 s⁻¹, many bacterial enzymes release NO about one order of magnitude slower.¹⁶ Crystallographic studies reveal a valine residue in mammalian forms which is replaced with an isoleucine in many bacterial forms.¹⁸⁻²⁰ This isoleucine is within Van der Waals contact of any diatomic bound at the iron center. Stuehr and coworkers showed that installation of an isoleucine at this position in the mammalian inducible NOS slows the rate of NO release, while removal of this methyl group through mutation to a valine in the bacterial NOS from *Bacillus subtilis* increases its rate of NO release.¹⁶ While this is an important finding, the rate constants do not change by the full order of magnitude that separates them (in iNOS, 2.3 s⁻¹ slows to 0.77

and in bsNOS 0.23 increases to 0.82). Clearly additional factors modulate the rates of NO release.

Flash photolysis is another technique commonly used to study the interactions of diatomic molecules with proteins.²¹⁻²³ Most heme centers form stable complexes with carbon monoxide (CO) in the ferrous state.^{7, 24} While indefinitely stable in the dark, when exposed to visible (green) light the iron-carbon bond of the ferrous-CO species is broken, liberating CO and transiently generating a five coordinate ferrous heme. Under an atmosphere of CO, the six-coordinate species is reformed.²⁵ Due to large differences between the absorbance spectra of the five- and six-coordinate heme species, transient absorption spectroscopy is again an ideal technique for observing reactivity.²⁵⁻²⁶ CO is used preferentially over NO and O₂ because it alone is redox inactive. Exposure of reduced enzyme immediately leads to oxidation of the iron center. The lifetime of a ferrous-oxy species is incredibly short (milliseconds to seconds at best). Nature has been forced to take steps to prevent this reaction in order to prevent the release of superoxide into cells. If the protein is reduced when substrate and cofactor are not present, superoxide will certainly be released, leading to cellular damage. NO also undergoes redox chemistry with the ferrous iron to oxidize it. CO is the closest mimic that will not undergo the same chemical reactions. The interactions of CO with myoglobin,²⁷⁻³⁰ microperoxidase-8,³¹ human myeloperoxidase,³² and cytochrome P450³³⁻³⁵ have been previously studied extensively. It was found that CO is a good mimic for the study of oxygen binding to these biologically important proteins.^{24, 29}

Both flash photolysis and stopped flow coupled with transient UV-visible spectroscopy were used to study the interactions of diatomics with the nitric oxide

synthase from *Geobacillus stearothermophilus* (gsNOS).³⁶⁻³⁷ The wild type enzyme, with isoleucine in position 223 (gsNOS numbering) directly above the heme as is commonly found in bacterial enzymes, as well as three other mutant species were studied by both techniques. Site-directed mutagenesis was used to insert a valine at position 223, as previously demonstrated in bsNOS to increase the rate of NO release. Mutations were also made at position 134.

We have observed a correlation between reported rate constants of NO release in the literature with residues found at this position. We will call these two positions gates. bsNOS has a histidine residue at this alternate position and has a particularly small rate constant of 0.23 s^{-1} , while the NOS from *Deinococcus radiodurans*, also bacteria, has a larger release rate constant of 0.50 s^{-1} and a smaller alanine residue at this second gate.³⁸ Both bacterial enzymes have an isoleucine in the first gate, keeping the overall rate smaller than mammalian forms. The NOS from mammalian neurons,³⁹ however, has a larger release rate constant of 5 s^{-1} and both gating positions contain smaller residues, valine near the heme and a serine corresponding to position 134 in gsNOS. The enzyme with the fastest recorded release rate constant comes from the bacterium *Sorangium cellulosum*¹⁷ which has a valine above the heme and glycine at the second gate, and releases NO at a rate of $7\text{--}10 \text{ s}^{-1}$. Clearly, smaller residues at these two positions correlate with faster release of NO, while bulkier groups at 134 and 223 slow down NO release.

A series of four variants of gsNOS were expressed: wild type, I223V, H134S, and the double mutant H134S/I223V. The wild type enzyme with the bulkier side chains was found to have the slowest reported NO release rate of 0.039 s^{-1} by stopped flow spectroscopy. Each single mutant increased this rate constant substantially, I223V to 0.30

s^{-1} and H134S to 0.16 s^{-1} . The double mutant increased the rate of NO release to 1.0 s^{-1} , nearly the same as the mammalian isoforms. These data show that position 134 is in fact another residue key to enzymatic regulation of NO release, along with the known valine/isoleucine mutation. These results, together with CO flash photolysis studies provide a clear picture of the interactions of both NO and CO with this biologically important enzyme.

5.3 Experimental Methods

Sample Preparation

The plasmid for the nitric oxide synthase from *Geobacillus stearothermophilus* was a gift from the lab of Brian Crane. This enzyme was expressed as previously described by Sudhamsu and Crane with no significant deviations in procedure.³⁶ The enzyme was overexpressed in *Escherichia coli* BL21 (DE3) cells. Cells were grown to an optical density of approximately 1.0–1.4 and induced by adding a solution containing iron(III) chloride, IPTG, and δ -aminolevulinic acid (Aldrich) to final concentrations of 125 mg/L, 100 μM , and 50 mg/L, respectively, in milliQ water. The pETDuet vector (Novagen) coded for a C-terminal cleavable His₆-tag so samples were purified using metal affinity chromatography. (This vector also confers chloramphenicol resistance to the cells, so 34 $\mu\text{g/mL}$ of this antibiotic were added to all cultures in Luria broth.) The His₆-tag was then cleaved using bovine thrombin (Calbiochem). Both thrombin and the His-tag were removed using size exclusion chromatography. Sample purity and Soret band epsilon values were determined through use of the hemochromagen assay.

A QuikChange site-directed mutagenesis kit from Stratagene was used to make the desired mutations in the amino acid backbone. Primers were designed according to the guidelines outlined by the QuikChange kit manual. Unless otherwise noted, protein solutions were made in the following buffer: 50 mM Tris (2-amino-2-hydroxymethylpropane-1,3-diol), 150 mM NaCl, pH 7.5 (the same buffer used for size exclusion chromatography). Steady-state UV-visible spectra were collected on an Agilent HP 8452 diode array spectrophotometer.

For laser experiments, oxygen-free samples were pumped into an anaerobic chamber (with an atmosphere of 100% N₂) and reduced under excess dithionite. A small excess of dithionite was left in samples in order to ensure that the heme center remained in the reduced, ferrous state throughout the entirety of the experiment. Samples were then placed in a quartz cuvette (Starna Cells) with a graded seal connecting the cuvette to a Köntes valve, enabling the secure sealing of the cuvette from atmosphere. The cuvettes were then sealed and removed from the anaerobic chamber. The side arm of the cuvette was attached to a Schlenk line and evacuated and backfilled with carbon monoxide (100% or 20% with 80% N₂) three times. Once the side arm was under the desired atmosphere of CO, the Köntes valve was opened to the side arm. The headspace of the cuvette, above the protein solution, was evacuated and back-filled with CO from the Schlenk line three times and sealed under this new atmosphere. The sample was gently shaken over night, in the dark, at 4 °C to allow for full equilibration of the atmosphere with the solution. Inadequate equilibration time resulted in irreproducibility between samples.

Formation of the ferrous-CO complex was confirmed using its characteristic absorption band at 446 nm. The stability of the sample was monitored by UV-visible spectroscopy after its generation, and immediately before and after laser irradiation. No samples showed significant degradation after irradiation by the laser.

Nanosecond Transient Absorption Spectroscopy

All transient UV-visible spectroscopic measurements for CO flash-photolysis experiments were conducted at the Beckman Institute Laser Resource Center at Caltech. For time-resolved measurements, a 10 Hz Q-switched Nd:YAG pulsed laser was used to provide 8 ns pulses of irradiation (Spectra-Physics Quanta-Ray PRO-Series). This laser was used to pump an optical parametric oscillator, which allows tuning pulses from the laser (355 nm output) in the visible region, between 400 and 650 nm (Spectra-Physics Quanta-Ray MOPO-700). The details of this setup have been previously described.⁴⁰ All samples were excited with 560 nm laser pulses and exposed to less than 5 mJ/pulse of power. All traces are an average of 500 laser shots using 1 nm slits.

Stopped Flow UV-Visible Spectroscopy

Samples were prepared anaerobically and transferred to an anaerobic tonometer with 1.5 equivalents of dithionite to scavenge any residual oxygen. Dithionite was used to scavenge oxygen from the stopped flow spectrophotometer (HiTech Scientific) syringes and excess dithionite was removed by repeated washing with anaerobic buffer. Protein samples (4–6 μ M gsNOS, 60 μ M H4B, and 200 μ M N-hydroxy-L-arginine) were rapidly mixed with air saturated buffer at 4 °C. The formation and release of NO was monitored using a diode array detector and the rates fit globally using SpecFit32 (HiTech

Scientific). Measured rates were independent of protein concentration under these experimental conditions.

Data Analysis

Transient absorption traces were converted to optical density using Equation 5.1 and fit using Igor-Pro graphing software. All data were fit to a double exponential decay function, with residuals less than 1% of the signal.

5.4 Results

Steady-State Spectroscopy

UV-visible spectroscopy was used to characterize the resting state and to verify the formation of the ferrous-carbonyl species of each mutant sample. This technique is particularly useful given the sensitivity of heme absorption bands to their environment, ligation, and oxidation state. Each enzyme displayed a single Soret peak with an absorbance maximum at 446 nm as is typical for nitric oxide synthases and close to that of the related cytochromes P450, named for the sharp absorption of their ferrous-carbonyl species at 450 nm.⁷ The spectra of several such forms of the wild type enzyme are shown in **Figure 5.1**.

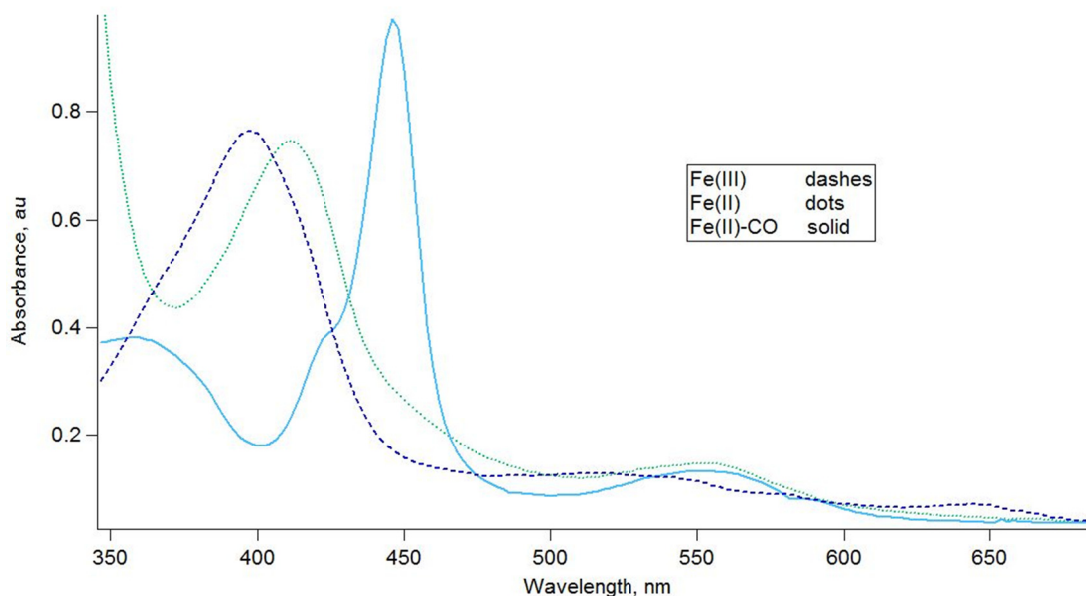


Figure 5.1. Absorption spectra of wild type gsNOS in three forms: ferric resting state (dashes), five-coordinate ferrous (dots), and the six-coordinate ferrous-CO complex (solid line). All samples are in the following buffer: 50 mM Tris, 150 mM NaCl, pH 7.5.

For flash photolysis experiments, 560 nm light was used to pump the sample, breaking the Fe-C bond of the ferrous-CO complex. This liberates CO and transiently generates a five-coordinate ferrous-heme complex. Both of these species can be generated and characterized under steady-state conditions (as shown above), allowing generation of the difference spectrum expected from transient studies. A trace of (Fe^{II})-(Fe^{II}-CO) difference spectrum for the wild type enzyme is shown in **Figure 5.2**.

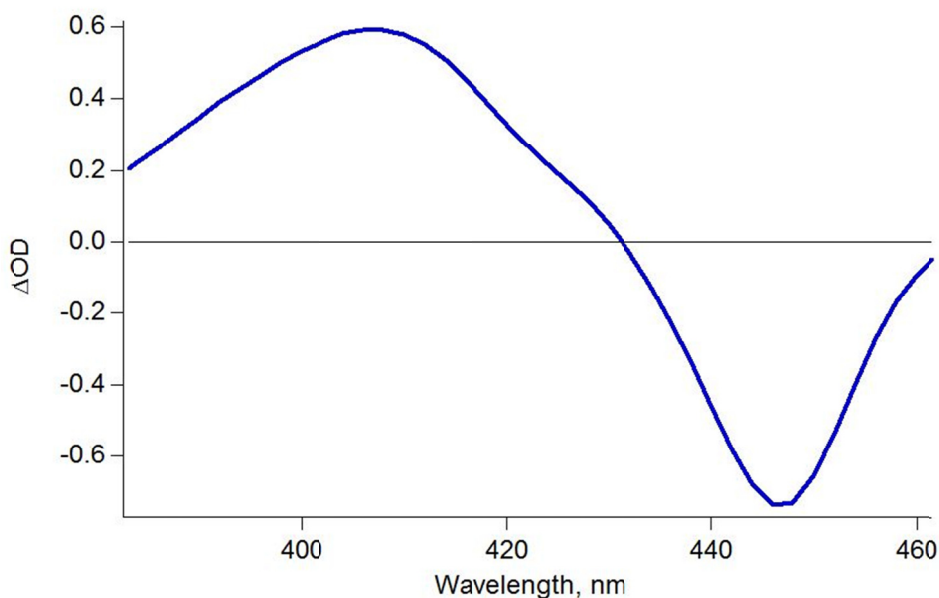


Figure 5.2. Steady-state difference spectrum produced by subtracting the spectrum of the wild type ferrous-CO complex from the five-coordinate ferrous species. This represents 100% conversion between species. Buffer: 50 mM Tris, 150 mM NaCl, pH 7.5.

CO Flash Photolysis

Upon irradiation with 560 nm light, CO is immediately liberated from the protein sample and the ferrous-CO complex reforms over the millisecond timescale. This rebinding process was monitored at 440 nm (near the maximum absorption of the six-coordinate species) and 410 nm (near the maximum absorption of the transiently-generated five-coordinate species). These two wavelengths give us separate handles on what should be the same kinetic process. Typical traces are shown in **Figure 5.3**. One can clearly see the signal bleach at 440 nm (B) upon loss of the CO complex and the signal from the transiently generated species at 410 nm (A), and that the two relax to ground state on roughly the same timescale.

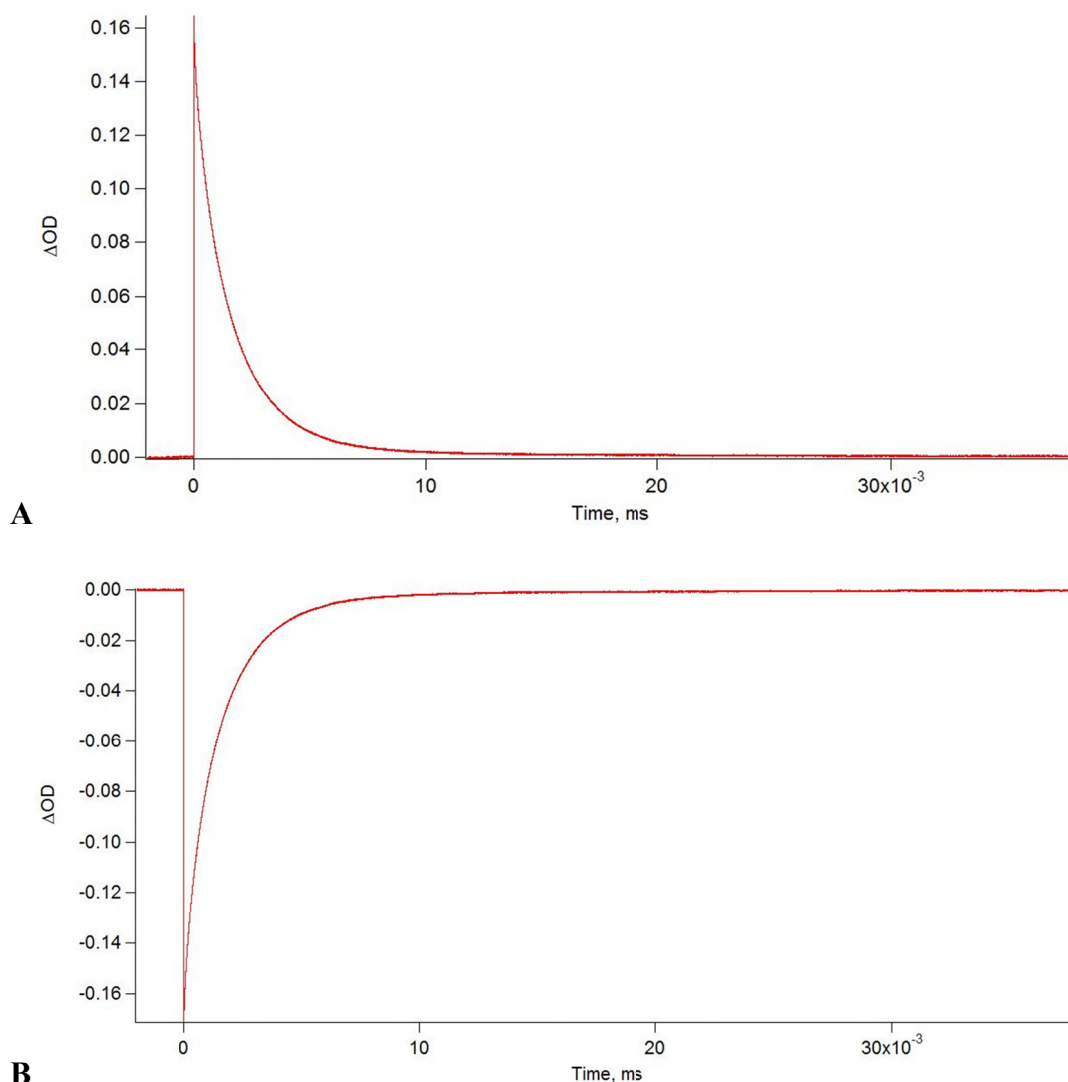


Figure 5.3. (A) Typical transient recorded at 410 nm, wild type enzyme, 40 ms timescale, 100% CO atmosphere. (B) Bleach upon loss of six-coordinate complex at 440 nm and its recovery. 6.1 μ M enzyme, and buffer: 50 mM Tris, 150 mM NaCl, pH 7.5.

The current output generated at the detector (a nine-stage photon multiplier tube) was converted to change in optical density (OD) through the following equation,

$$\Delta OD = -\log(I/I_0) \quad (5.1)$$

where I is the signal intensity and I_0 is the intensity before the laser pulse at $t = 0$. To confirm that the observed photochemical process is in fact dissociation of carbon monoxide and formation of the five-coordinate ferrous heme, a transient difference

spectrum was generated by collecting traces between 395 and 460 nm without alteration of the optics to maximize the signal. The signal at $t = 1$ ms was recorded for each wavelength (stepping every 5 nm), generating the following difference spectrum 1 ms after irradiation, **Figure 5.4** (note the similarity to the spectrum in **Figure 5.2**).

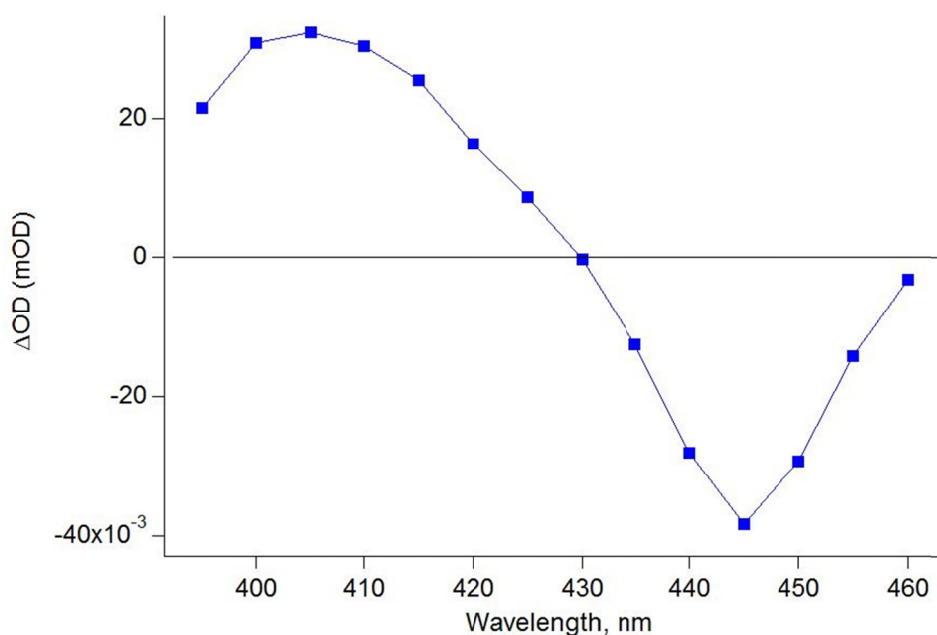


Figure 5.4. Transient difference spectrum generated 1 ms after laser pulse. 6.1 μ M enzyme, and buffer: 50 mM Tris, 150 mM NaCl, pH 7.5.

Kinetics traces were collected at both 410 and 440 nm for each protein sample; all measurements were made at least in duplicate. Traces were fit using Igor Pro to a double exponential decay. This equation (5.2) provided the best fit to the data, yielding residuals of less than 1% of the signal strength. Kinetics parameters for each protein sample are given in **Table 5.1A**. Typical traces collected at 440 nm are shown in **Figure 5.5**.

$$y = A_1 \cdot \exp(-t/\tau_1) + A_2 \cdot \exp(-t/\tau_2) \quad (5.2)$$

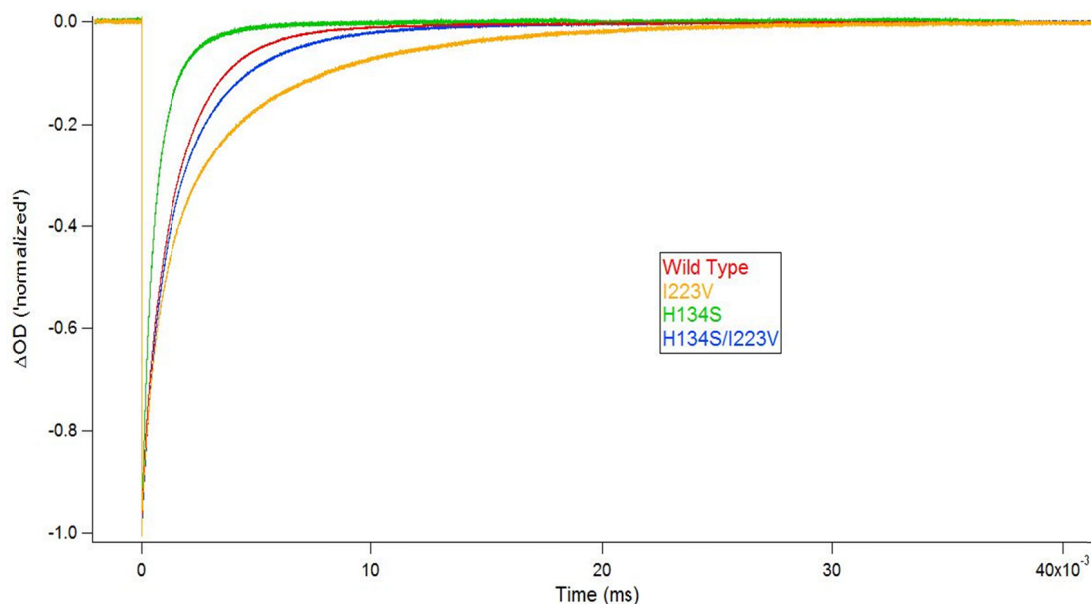


Figure 5.5. Typical kinetics traces for each of the four species studied (440 nm).

A double exponential decay was somewhat unexpected. In order to further characterize the kinetics, the dependence on CO concentration was analyzed. The concentration of CO in solution was altered by changing the content of CO in the gas filling the head space of each cuvette. The effects of CO concentration on the observed rate constants can be seen in **Table 5.1B**.

Table 5.1. CO recombination rates for both fast and slow second-order processes.

% CO, k_1 (s^{-1})	WT	I223V	H134S	H134S/I223V
(A)				
100 – t_1	510	190	750	310
100 – t_2	1500	1100	2400	1200
(B)				
20 – t_1	100	45	120	54
20 – t_2	390	240	370	240

We also analyzed the effect of these mutations on the pre-exponential factor of each rate from the double exponential fit. By introducing these small changes, we appear to be altering significantly the amount of the fast and slow phase, relative to one another. By introducing a single serine residue near the surface of the enzyme, the ratio of A1 to A2 is shifted from 2:1 to 1:2.

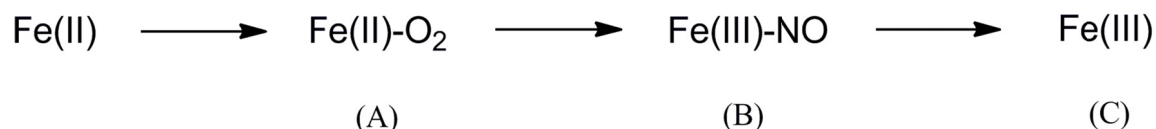
Table 5.2. Relative percentages of each rate constant by mutant.

100% CO	WT	I223V	H134S	H134S/I223V
A1 (t_1)	66%	46%	36%	43%
A2 (t_2)	34%	54%	64%	57%

Stopped-Flow UV-Visible Spectroscopy

NO release rates were measured for each protein sample using single turnover experiments. The enzyme was loaded with the redox active cofactor, tetrahydrobiopterin, and the substrate N-hydroxyarginine and then reduced using sodium dithionite. These samples were prepared anaerobically, sealed in a gas-tight syringe, and mixed with fully aerated buffer ($[O_2] \approx 258 \mu\text{M}$) to initiate turnover. Catalysis was monitored using UV-visible spectroscopy between 370 and 710 nm, with spectra taken at regular intervals over millisecond to second timescales. On faster timescales, the five-coordinate ferrous heme complex can be observed in the initial trace due to the excess dithionite present. Nearly immediately (within 5 ms, the dead time of the mixer), the ferrous-oxy species is formed; this formation is too rapid for stopped-flow spectroscopy to characterize the rate. (Note: dithionite reacts with oxygen several orders of magnitude faster than the enzymes under study and is therefore completely reacted before the second trace is collected.) The ferrous-oxy subsequently forms an intermediate complex, which finally decays to the resting ferric state of the enzyme (**Scheme 5.2**). In all cases, the first trace is discarded, as

the presence of a small amount of excess reductant (necessary to ensure the protein remains fully reduced) confuses the kinetics. All other traces are used in global fitting analysis using the SpecFit32 software package to extract spectra of all intermediates and rates of each species formation and/or decay. All spectral data were initially fit to a three-state kinetics model, with two rates to be extracted.^{14, 16} This model was used in order to be consistent with all previously published analyses of NOS stopped-flow data. The traces of the first and last states, A and C, can be generated independently, A from mixing reduced enzyme with oxygenated buffer in the absence of substrate and cofactor. The ferrous-oxy species, A, decays over a period of approximately 90 s in the wild type enzyme at 4 °C, allowing for reliable characterization.¹⁷ Species C is simply the resting, ferric, state of the enzyme. Thus, fitting software need only generate a single transient spectrum and two rates.



Scheme 5.2. Model for the conversion of the ferrous state of the enzyme to the resting ferric state (C), in the presence of oxygen, cofactor, and substrate through two intermediates: (A) a ferrous-oxy complex and (B) a ferric-NO complex.

From these experiments, several species can be characterized for each mutant enzyme, the ferrous-oxy and the putative ferric-NO, as well as the rate that the oxy complex reacts to form the NO complex and the rate that NO is subsequently released to form the resting five-coordinate ferric state. Typical traces collected are shown in **Figure 5.6** for the wild type enzyme. This work will focus only on the NO release rates, as formation rates of all samples were typical for NO synthases. Rate constants of NO release are listed in **Table 5.3**, along with the rates of NO release of other NOS enzymes.

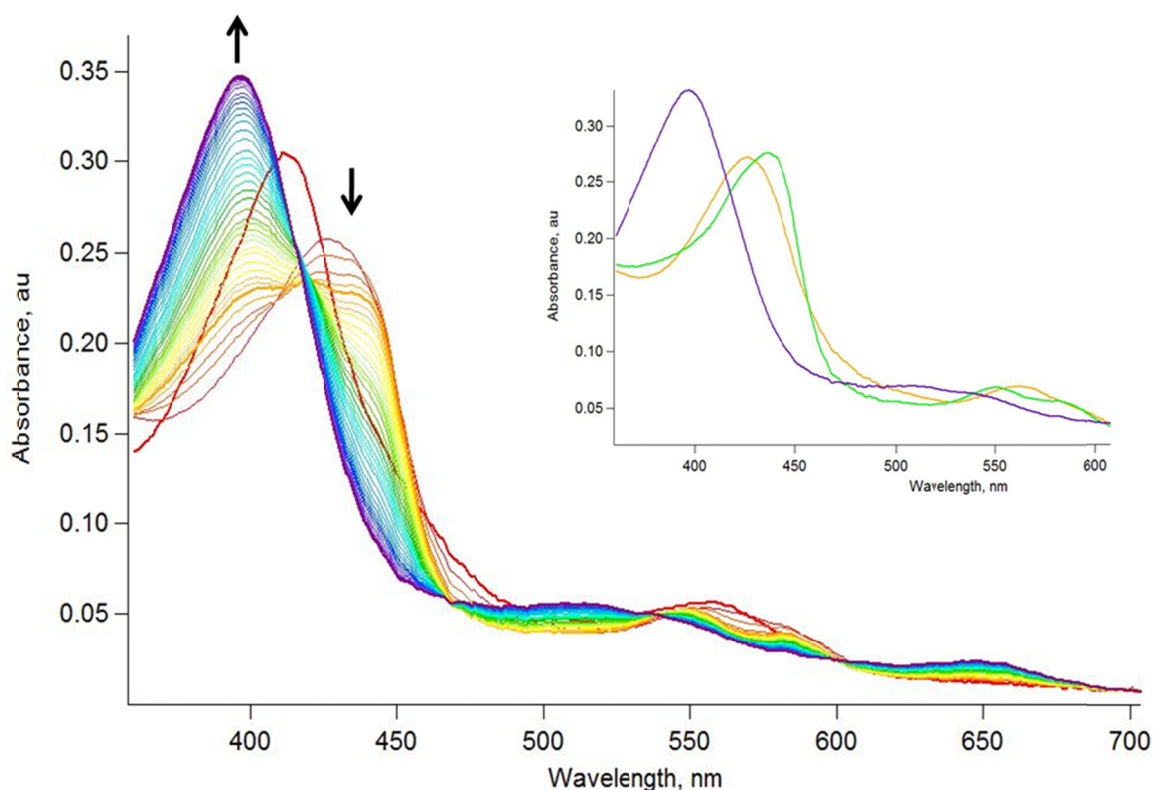


Figure 5.6. Transient spectra collected upon reaction of 4.5 μM reduced gsNOS (60 μM H4B and 200 μM N-hydroxy-L-arginine) with air-saturated buffer at 4 $^{\circ}\text{C}$. Inset: spectra of intermediate species as generated by SpecFit32 using a three-state model.

Table 5.3. NO release rate constants of the four mutants in this study as well as three other NOS rates for comparison.^a

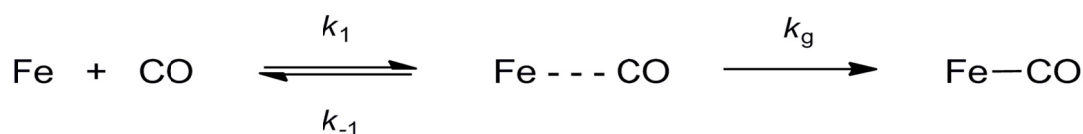
Mutations	Rate (s^{-1})	Gate 1	Gate 2	Temp. ($^{\circ}\text{C}$)	Source
wt	0.039	Ile	His	4	a
H134S	0.16	Ile	Ser	4	a
I223V	0.30	Val	His	4	a
H134S/I223V	1.0	Val	Ser	4	a
iNOS	2.3	Val	Ala	10	16
scNOS	7-10	Val	Gly	10	17
bsNOS	0.23	Ile	His	10	16

^aiNOS has a rate typical for mammalian enzymes. bsNOS has a rate typical for bacterial enzymes. scNOS and gsNOS represent the fastest and slowest (respectively) release rates among NOS enzymes.

5.5 Discussion

CO Flash Photolysis

The kinetics of CO rebinding to proteins such as myoglobin has been studied extensively and two common themes stand out. First, second-order recombination occurs typically with a rate constant on the order of 10^5 to $10^6 \text{ M}^{-1} \text{ s}^{-1}$, regardless of the size of the protein (wild type Mb: 6.5×10^5 and wild type P450_{nor}: 6.1×10^5).^{28, 33} Second, for nearly all systems studied, a simple three-state kinetics model is consistent with all observed data (**Scheme 5.3**). With such a scheme, one would expect to observe two processes: fast, first-order geminate recombination (k_g) where CO never escapes the protein's binding pocket and a slower, second-order bimolecular recombination step (k_1) that is pseudo-first order under experimental conditions given the large excess of CO in solution. It has been previously noted that at room temperature under similar conditions (1 atm. of 100% CO in the sample headspace) no geminate process can be observed as essentially all of the CO has sufficient energy to leave the protein's interior and escape to solvent.^{25, 41} In light of these results we initially expected the observed behavior to fit a single exponential decay, however in all samples such a model cannot provide a good fit for recorded traces; a double exponential decay must be invoked. (A comparison of the fits and residuals of both single and double exponential models is shown in **Figure 5.7**). Further, both processes occur on the millisecond timescale, ruling out the possibility of geminate recombination which occurs on much faster timescales.⁴²



Scheme 5.3. Standard kinetics model for the recombination of CO with heme centers.^{25, 27, 33} Fe represents the protein, k_g the geminate, and k_1 the second-order recombination.

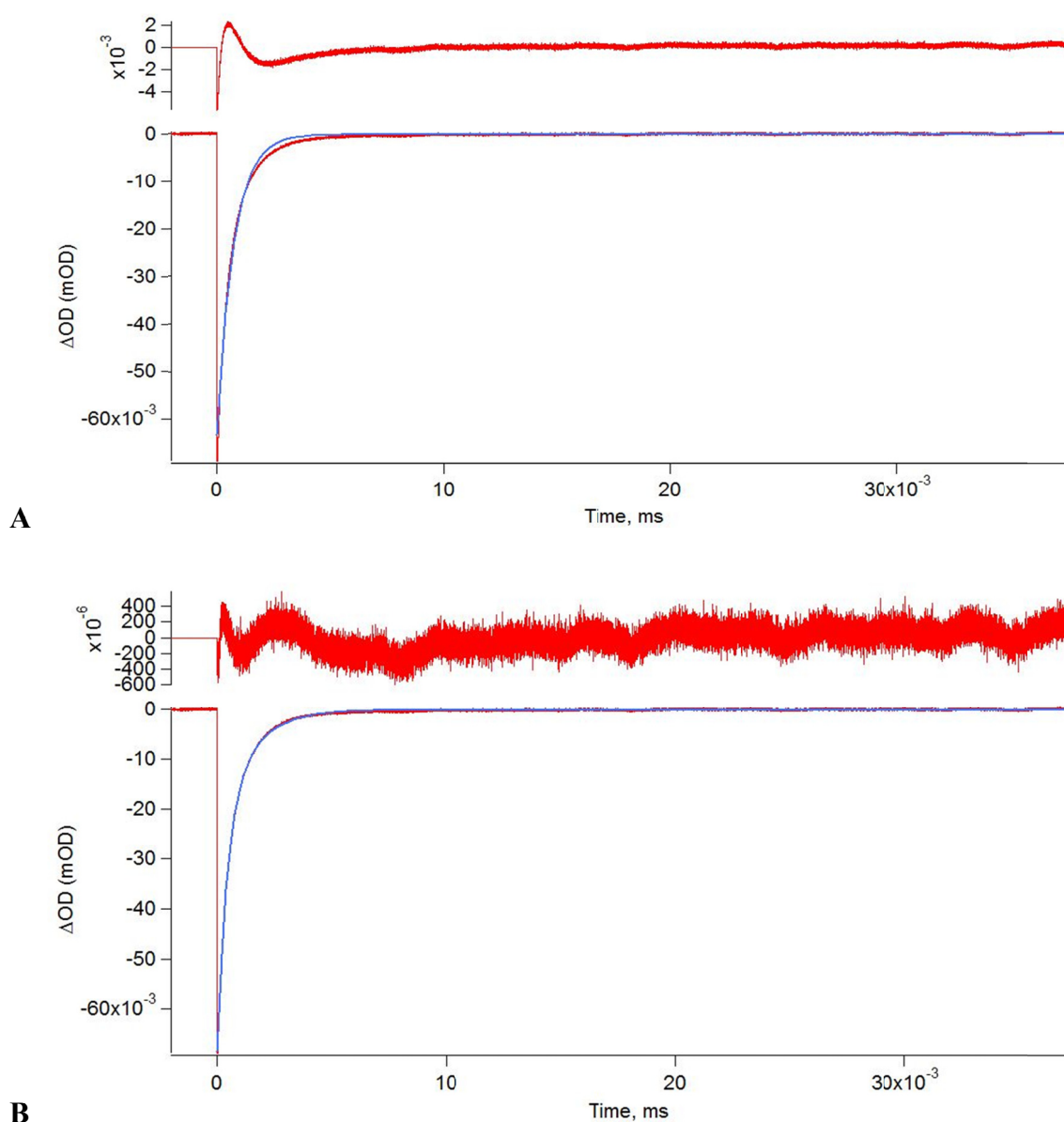


Figure 5.7. CO photolysis and rebinding under an atmosphere of 100% CO. Fits with residuals for both single exponential and double exponential decay models of transient data, typical of all four mutants. Fits are shown in blue above data (red). Residuals are shown in red on separate axes above the data. Note the scale of each y-axis.

To learn more about the two observed processes, we varied the percentage of CO in the headspace of samples. This reduction in CO concentration by one fifth lead to a decrease in CO rebinding rate constant for both processes in every sample, corresponding to about 1/4 to 1/6 of the previous rate. This indicates that both are first order in CO.

Further, the amplitudes of each exponential component of the fits are significant, with no one component accounting for less than 30% of the signal (**Table 5.2**). We hypothesized, given what is known about nitric oxide synthases and how they differ from other systems studied by this method, that we might be observing both the monomer and dimer in solution. It is known that NOS functions only as a dimer in mammals and disrupting dimerization shuts down catalysis.¹ During purification, bands for both monomer and dimer were observed on a size exclusion column in the same buffer with the same ionic strength. To test this hypothesis, samples were made with varying concentrations and we monitored the amplitude of both the faster and slower processes. **Table 5.4** shows the clear effect of concentration on the amplitudes of the faster and slower signals, consistent with the presence of monomer and dimer. Further, the two rate constants are similar in magnitude and both on the millisecond timescales, which agrees with both processes being second-order recombination with slightly different barriers. Introducing the presence of both monomer and dimer would account for the observed behavior of all samples.

Table 5.4. Effects of concentration on the relative proportion of the two processes. Concentration in μM .

[NOS]	A ₁	A ₂
6.1	64%	36%
9.9	58%	42%
27	35%	65%

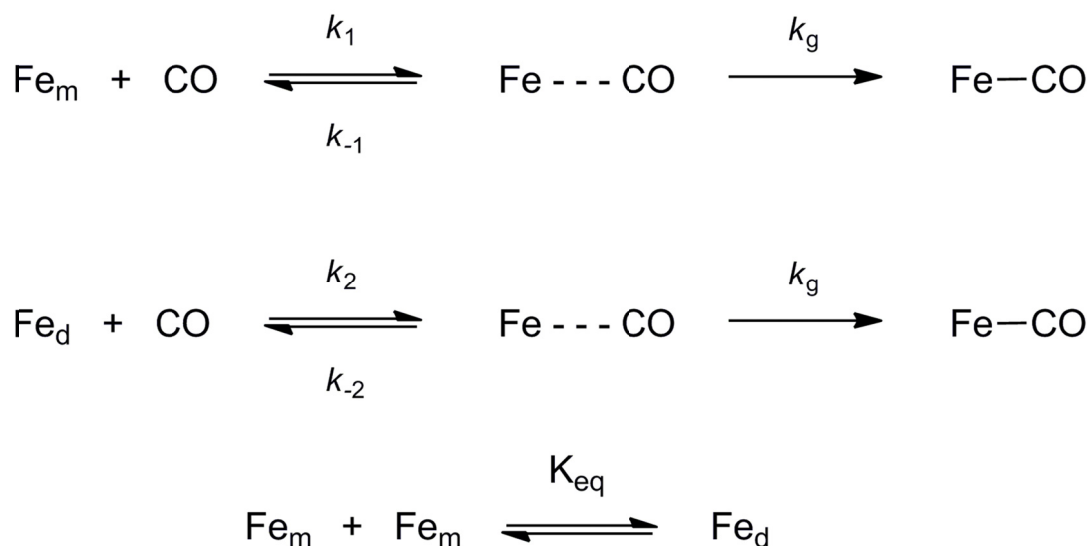
Another possibility exists, however, as explanation for two observed millisecond processes. In proteins such as hemoglobin, a phenomenon called cooperativity is

observed.⁴³⁻⁴⁴ When laser irradiation hits the sample, because of the large quantum yield for this photochemical process, a high percentage of photodissociation is observed. One can imagine a case where the protein exists completely as a dimer in solution and when irradiated either one or both bound CO molecules are liberated. If cooperativity (or anti-cooperativity) is a contributing factor, dimers with a single CO molecule still bound would have a higher recombination rate constant than those where both are dissociated due to changes in protein conformation. In such a situation, the proportion of CO that is released from the protein will vary with laser intensity according to a standard power dependence and the proportion of the faster rate should decrease. A tenfold increase in laser power did not alter the proportion of the two rates observed, it merely increased the overall signal strength (**Table 5.5**).

Table 5.5. Power dependence of the relative amplitudes of each signal.

Power at sample (mJ/pulse)	$\text{inv}\tau_1 \text{ (s}^{-1}\text{)}$	$\text{inv}\tau_2 \text{ (s}^{-1}\text{)}$	A1	A2
0.6	91	9.9×10^2	58%	42%
0.7	91	1.0×10^3	57%	43%
2.8	88	9.6×10^2	59%	41%
6.4	87	9.4×10^2	59%	41%
7.0	87	9.4×10^2	59%	41%

From all these results we conclude that we are in fact observing both the monomer and dimer forms of the enzyme under experimental conditions, that both react with CO to give a rebinding rate constant on the order of $10^5 \text{ M}^{-1} \text{ s}^{-1}$ as has been found in other proteins, and propose the following kinetics model, **Scheme 5.4**.



Scheme 5.4. A modified kinetics model for the recombination of CO with gsNOS, incorporating the presence of both monomer and dimer forms of the enzyme. Fe represents the protein, k_g the geminate recombination rate, k_1 the second-order recombination rate for the monomer (Fe_m), and k_2 the second-order recombination rate for the dimer (Fe_d). Monomer and dimer must equilibrate on a slower timescale than CO recombination occurs.

From here, we can begin determining the effects of the point mutations that were made. The wild type enzyme has the two bulkiest groups at positions 134 and 223, histidine and isoleucine. These groups should slow the rate of diatomics traveling into and out of the protein's heme pocket. Thus, we hypothesized that the wild type would be the slowest of all the samples. The data show that while one mutant is faster than wild type (H134S), I223V is slower and the double mutant lies between the two single mutants, close to the wild type (**Figure 5.5**). The amplitudes of the fast and slow rate constants make it clear that each mutation affects not only the kinetics of second-order recombination events, but also the relative proportion of monomer and dimer in solution. This is consistent with our kinetics model in **Scheme 5.3**, however the competition between the two processes makes the two effects difficult to deconvolute.

NO Formation and Release

In order to determine the effect of these mutations on the NO release rate constant, we conducted single turnover experiments in the lab of Prof. Michael Marletta at UC Berkeley with the assistance of Dr. Emily Weinert. This allows for the direct comparison of our mutations with previously published rates of NO release. The wild type enzyme was found to release NO with a rate constant of 0.039 s^{-1} , which closely matches the rate constant previously published by Crane and Sudhamsu of 0.04 s^{-1} , under the same experimental conditions.³⁶ This enzyme has the smallest reported rate constant of all NOS enzymes. Each single mutation (H134S and I223V) increases the rate significantly, while the double mutant brings the rate to 1.0 s^{-1} , close to the higher rates found in mammalian enzymes (which were measured at a slightly higher temperature). The ability of a mutation at position 134 to both increase the rate on its own and to further increase the rate beyond the single mutation already known at position 223 (**Table 5.3**) confirms that it is in fact another key residue gating NO release.

Transient Spectra Generated by Modeling

During the fitting procedure, it was observed that the spectrum generated for the intermediate ferric-NO complex is not always consistent. For the fastest mutant, H134S/I223V, the ferric-NO species is nearly cleanly resolved, showing a peak near 440 nm (**Figure 5.8**). The slower mutants and the wild type enzyme showed a mixture of Soret bands (**Figure 5.9**). The observation of multiple bands like this clearly indicates that the model is incomplete — what is being fitted as a single intermediate is actually a mixture of species. This has been observed before in both a bacterial NOS and a slower mutant of a mammalian enzyme.¹⁶ It has been proposed that the presence of the Ile near

the heme confines NO in the pocket.¹⁹ A new model was developed in order to better fit the data and fully resolve these spectra.

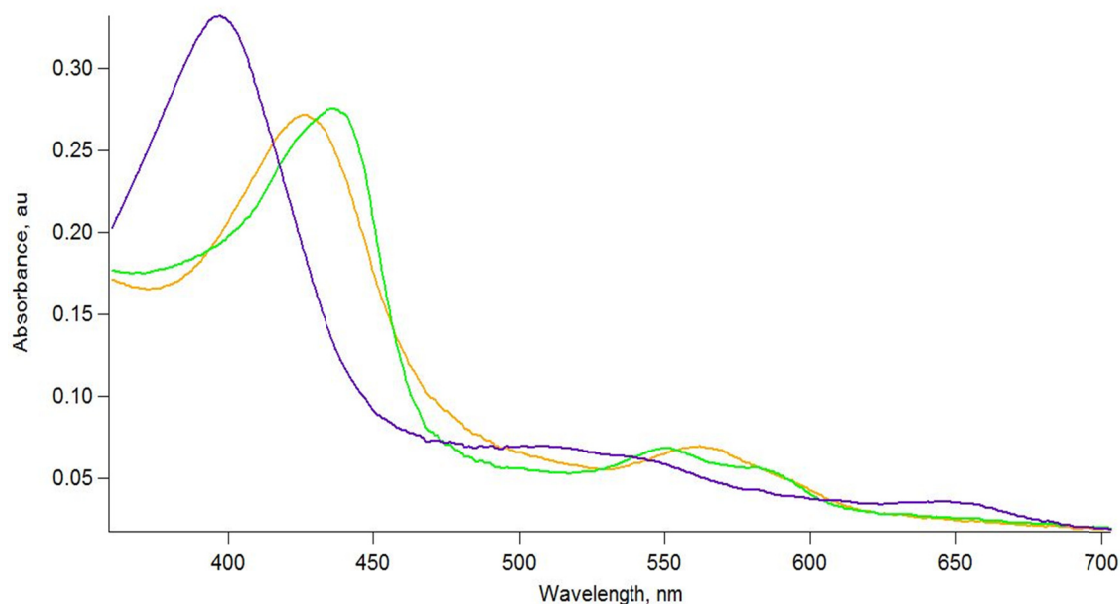


Figure 5.8 Spectra of intermediates generated by SpecFit software, for H134S/I223V gsNOS. Conditions: 50 mM Tris, 150 mM NaCl, pH 7.5, 4.4 μ M NOS, 60 μ M tetrahydrobiopterin, 200 μ M N-hydroxy-L-arginine, approximately 130 μ M oxygen. Green: ferric-NO, yellow: ferrous-oxy, purple: ferric resting state. Representative of single mutant I223V and the double mutant H134S/I223V.

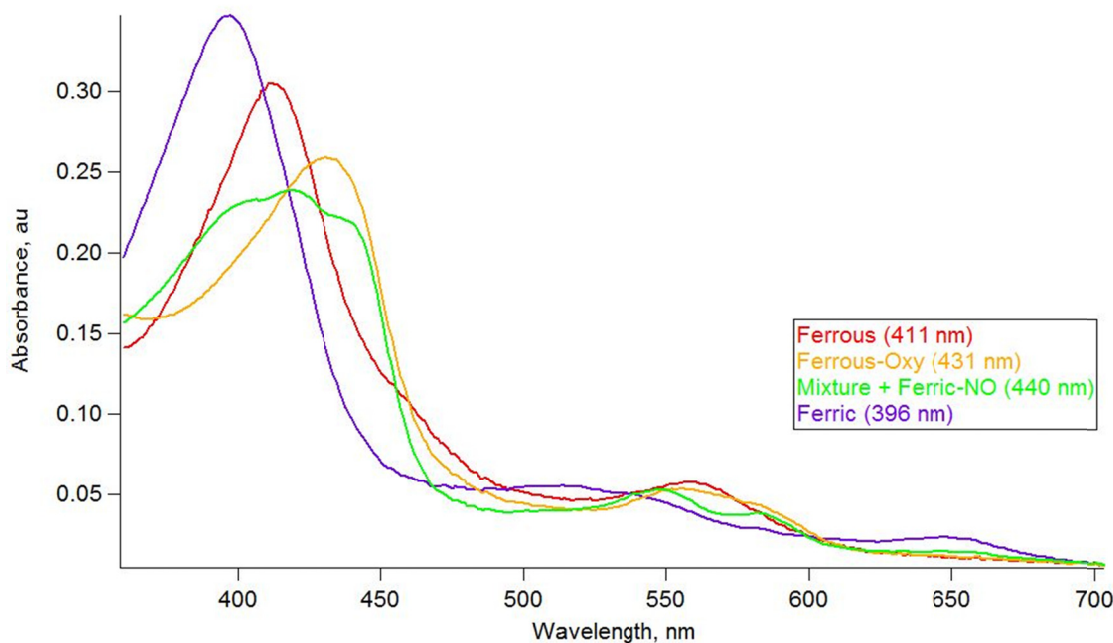
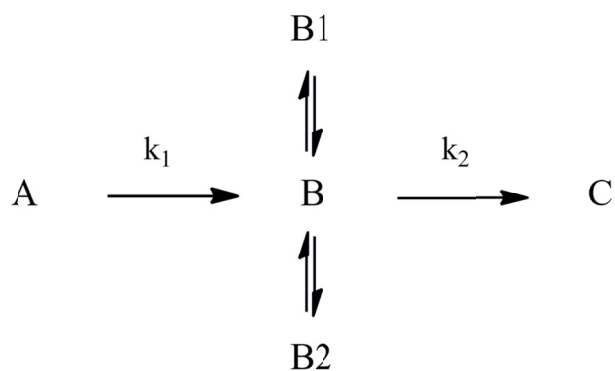


Figure 5.9. Spectra of intermediates generated by SpecFit software, for wild type gsNOS. Conditions: 50 mM Tris, 150 mM NaCl, pH 7.5, 4.4 μ M NOS, 60 μ M tetrahydrobiopterin, 200 μ M N-hydroxy-L-arginine, approximately 130 μ M oxygen. Yellow: ferric-oxy, green: ferric-NO, red: ferrous, purple: ferric resting state. Representative of both wild type and the single mutant H134S.

In order to fully resolve each individual species/intermediate, a five-state model was required. Any fewer species resulted in spectra with mixed Soret bands (as can be seen in green in **Figure 5.9**). It was also required that the three intermediate species be in rapid equilibrium with each other. This result fits well with the previously used three-state model. In the event that the equilibria favor the central species, the other two cannot be observed and the five-state model collapses to the three-state model. The final model used to fit all collected spectra is shown below (**Scheme 5.5**).



Scheme 5.5. The five-state model used to fit all transient stopped-flow data. B1 and B2 need not be off-pathway species, but all three B species must be in rapid equilibrium.

The above model fits all stopped-flow data well, resulting in reasonable rates and the generation of intermediate spectra with single Soret bands. Some extra information must be given to the fitting software, otherwise the system will be under-defined. When provided with the spectrum of B, in this case the ferric-NO species, and sufficiently large rates for each part of both equilibria, reasonable spectra and rates are calculated for A, B1, B2, C, k_1 , and k_2 . The values of k_2 for each enzyme as fitted by both models are shown in **Table 5.6**.

Table 5.6. Full kinetics details of fitting model for each of the four enzymes including a comparison of the NO release rate with the three-state model.

Enzyme	Process	Rate Constant	3-State Model's Fit
Wild Type	A > B	8.1×10^{-2}	
	B > B1	1.5×10^5	
	B1 > B	8.2×10^4	
	B > B2	1.5×10^3	
	B2 > B	2.9×10^3	
	B > C	0.10	0.04
H134S	A > B	1.7×10^{-2}	
	B > B1	1.1×10^6	
	B1 > B	1.4×10^6	
	B > B2	1.6×10^3	
	B2 > B	6.7×10^5	
	B > C	0.31	0.16
I223V	A > B	1.0×10^1	
	B > B1	4.9×10^4	
	B1 > B	8.9×10^4	
	B > B2	1.2×10^1	
	B2 > B	1.6×10^3	
	B > C	0.51	0.30
H134S/I223V	A > B	1.6×10^1	
	B > B1	1.8×10^4	
	B1 > B	4.1×10^0	
	B > B2	1.4×10^3	
	B2 > B	1.9×10^0	
	B > C	1.9	1.0

In this model, A is the ferrous-oxy complex as before. Again, the spectrum of this species is well known and can be used to verify the accuracy and chemical reasonableness of the model and fit. The spectrum of B is specified as the ferric-NO spectrum with a maximum absorbance at 441 nm (courtesy of Dr. Joshua Woodward from the Marletta group), which is known to form during turnover. The spectrum of C is the final resting state of the enzyme, the five-coordinate ferric species. The spectrum

generated for one of the two new intermediates is essentially identical to that of the ferric resting state. This is consistent with an equilibrium between rapid release and rebinding of NO trapped in the binding pocket, which would be very fast when compared with the other processes occurring. It is also consistent that this would be seen to the greatest extent in the two enzymes with the Ile residue present near the heme. The methyl group of this residue is right at Van der Waals contact distance from any diatomoids bound to the iron and clearly blocks any exit from the binding pocket (as is clear from the crystal structure, PDB file 2FLQ).

The identity of the other intermediate is less obvious, but at least one reasonable possibility exists. The species is clearly formed after the majority of catalysis, being in equilibrium with the ferric-NO species. Several other models were applied, but the only one that fits the collected data is one where this species is in rapid equilibrium with the ferric-NO complex. As seen in **Figure 5.10**, this species has a Soret maximum near 420 nm. A species with a similar absorbance has been previously observed under catalytic conditions for the first turnover (Arg rather than NOHA was used as substrate).¹⁵ This is also a slower enzyme, with a Trp to His mutation as discussed in Chapters 3 and 4, but made in the mammalian inducible NOS isoform. In this study, the authors proposed that this newly characterized species is Compound I.

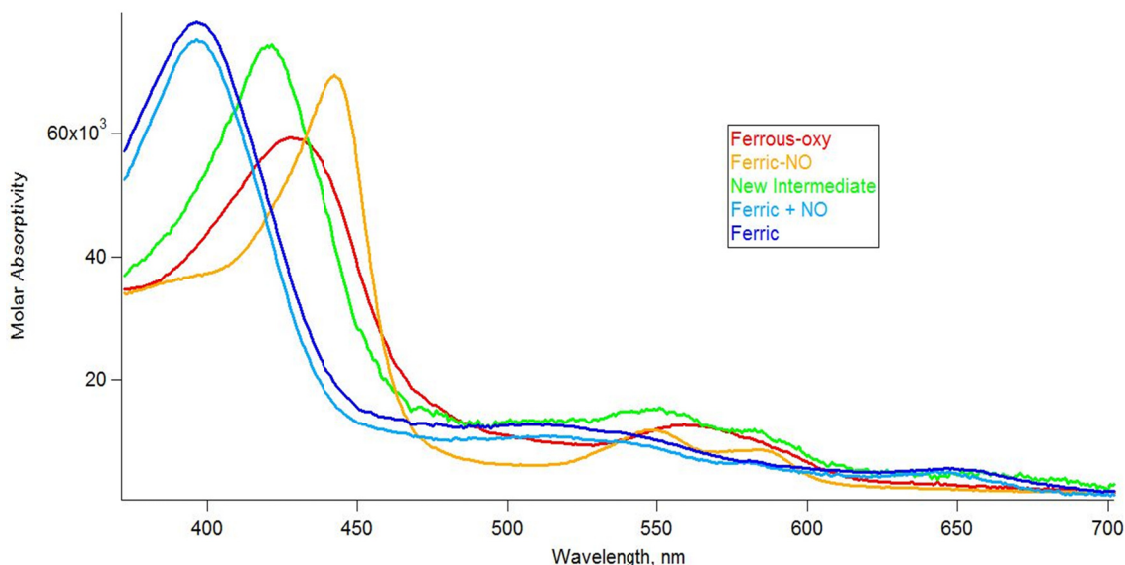


Figure 5.10. Spectra of all intermediate species in the five-state model of the wild type enzyme. All spectra match their reported literature values within ± 2 nm, as well as the shape of the Q-bands. The identity of the species in green remains unknown.

Compound I is a Fe(IV)=O with another radical cation typically found on the porphyrin ring or another amino acid close to the heme center. This is formally a Fe(V) complex and is incredibly reactive. This complex was recently isolated and characterized and shown to react completely with substrate in less than 1 second, even in a thermophilic enzyme at 4 °C. In this NOS mutant, the complex with Soret band at 422 nm lives approximately 10–15 seconds at 10 °C before fully decaying. It is doubtful that such a reactive oxidant would live for that amount of time with substrate present and ready to be oxidized by the complex and Compound I has been shown to have a maximum absorption near 365 nm. We have made the same Trp to His mutation and saw no evidence for this species at 422 nm (see Chapter 4).

We propose that this species in our system may be either an HNO complex with the enzyme or a P420 form of the iron center. It is known that one electron from the heme complex must be sent back to the pterin cofactor to re-reduce it and release NO in the

second turnover.⁴⁵ The observed species may be the product heme complex before electron transfer to the pterin. The spectrum is nearly identical (simply 4 nm blue-shifted) of the spectrum of HNO-myoglobin.⁴⁶ However, this cannot be the species observed in the study of mammalian NOS, as they were probing the first turnover. An alternative explanation is that this 420 nm species is analogous to the P420 species (Chapter 3) where the thiolate ligand is protonated and/or dissociates. We may be observing the equilibrium between two protonation states of this ligand. Identification of a species based solely on a single UV-visible spectrum is difficult at best, but further attempts are being made to understand the origin of this spectrum.

5.6 Conclusions

First, CO is a valuable diatomic mimic for the more reactive dioxygen and nitric oxide, however with a caveat. One must remember the conditions under which experiments are performed. For CO photolysis, systems are under saturating conditions with large excesses of carbon monoxide. This is a good system for comparison with oxygen binding to hemoglobin in the lungs. Nitric oxide formation, on the contrary, involves the production of a single molecule of NO per protein, far from saturating conditions. Further, NO reacts rapidly in aerated aqueous solution, further preventing its buildup and keeping the system from reaching equilibrium. Also, the driving force ultimately behind each of these processes involves formation or cleavage of two distinct bonds. CO is very similar to NO, but on a fundamental level an Fe-N bond is not an Fe-C bond. While experiments with CO provide a wealth of information about the overall

kinetics model for reactivity with diatomics, for an NO release rate one must perform the single turnover experiments.

With these experiments, we have confirmed that the isoleucine residue at position 223 does gate NO release in gsNOS, slowing the decay of the ferric-NO species. We have also demonstrated that position 134, occupied by a histidine in wild type gsNOS, also gates NO release, with smaller residues at this position corresponding to faster release rates. Together, these two positions can account for the majority of the differences in rate between any two NOS enzymes.

Further, we have used a new, more accurate model to fit our data, showing rapid equilibrium between the bound and unbound NO, and another unidentified species. This species has been previously observed. It was called Compound I. The Compound I in cytochromes P450 has a much more blue-shifted Soret band with a maximum near 365 nm and it reacts much more quickly. It is of note that this species with absorbance at 420 nm has now been observed in both turnovers. Unfortunately, its identity remains a mystery.

5.7 References

1. Marletta, M. A. (1993) Nitric-oxide synthase structure and mechanism, *J. Biol. Chem.* 268, 12231.
2. Wei, C. C., Wang, Z. Q., and Stuehr, D. J. (2002) Nitric oxide synthase: Use of stopped-flow spectroscopy and rapid-quench methods in single-turnover conditions to examine formation and reactions of heme-o-2 intermediate in early catalysis, In *Enzyme kinetics and mechanism, pt f: Detection and characterization of enzyme reaction intermediates*, pp 320, Academic Press Inc, San Diego.
3. Alderton, W. K., Cooper, C. E., and Knowles, R. G. (2001) Nitric oxide synthases: Structure, function and inhibition, *Biochem. J.* 357, 593.
4. Gusarov, I., Shatalin, K., Starodubtseva, M., and Nudler, E. (2009) Endogenous nitric oxide protects bacteria against a wide spectrum of antibiotics, *Science* 325, 1380.
5. Gusarov, I., Starodubtseva, M., Wang, Z. Q., McQuade, L., Lippard, S. J., Stuehr, D. J., and Nudler, E. (2008) Bacterial nitric-oxide synthases operate without a dedicated redox partner, *J. Biol. Chem.* 283, 13140.
6. Johnson, E. G., Sparks, J. P., Dzikovski, B., Crane, B. R., Gibson, D. M., and Loria, R. (2008) Plant-pathogenic streptomyces species produce nitric oxide synthase-derived nitric oxide in response to host signals, *Chem. Biol.* 15, 43.
7. Dawson, J. H., and Sono, M. (1987) Cytochrome.P-450 and chloroperoxidase - thiolate-ligated heme enzymes - spectroscopic determination of their active-site structures and mechanistic implications of thiolate ligation, *Chem. Rev.* 87, 1255.
8. Gorren, A. C. F., and Mayer, B. (2007) Nitric-oxide synthase: A cytochrome p450 family foster child, *Biochimica Et Biophysica Acta-General Subjects* 1770, 432.
9. Sono, M., Roach, M. P., Coulter, E. D., and Dawson, J. H. (1996) Heme-containing oxygenases, *Chem. Rev.* 96, 2841.
10. Stuehr, D., Pou, S., and Rosen, G. M. (2001) Oxygen reduction by nitric-oxide synthases, *J. Biol. Chem.* 276, 14533.
11. Stuehr, D. J., Santolini, J., Wang, Z. Q., Wei, C. C., and Adak, S. (2004) Update on mechanism and catalytic regulation in the no synthases, *J. Biol. Chem.* 279, 36167.
12. Davydov, R., Sudhamsu, J., Lees, N. S., Crane, B. R., and Hoffman, B. M. (2009) Epr and endor characterization of the reactive intermediates in the generation of no by cryoreduced oxy-nitric oxide synthase from geobacillus stearothermophilus, *J. Am. Chem. Soc.* 131, 14493.
13. Stuehr, D. J., Tejero, J., and Haque, M. M. (2009) Structural and mechanistic aspects of flavoproteins: Electron transfer through the nitric oxide synthase flavoprotein domain, *Febs Journal* 276, 3959.
14. Boggs, S., Huang, L. X., and Stuehr, D. J. (2000) Formation and reactions of the heme-dioxygen intermediate in the first and second steps of nitric oxide synthesis as studied by stopped-flow spectroscopy under single-turnover conditions, *Biochemistry* 39, 2332.
15. Tejero, J. S., Biswas, A., Wang, Z. Q., Page, R. C., Haque, M. M., Hemann, C., Zweier, J. L., Misra, S., and Stuehr, D. J. (2008) Stabilization and characterization

- of a heme-oxy reaction intermediate in inducible nitric-oxide synthase, *J. Biol. Chem.* **283**, 33498.
16. Wang, Z. Q., Wei, C. C., Sharma, M., Pant, K., Crane, B. R., and Stuehr, D. J. (2004) A conserved val to ile switch near the heme pocket of animal and bacterial nitric-oxide synthases helps determine their distinct catalytic profiles, *J. Biol. Chem.* **279**, 19018.
 17. Agapie, T., Suseno, S., Woodward, J. J., Stoll, S., Britt, R. D., and Marletta, M. A. (2009) No formation by a catalytically self-sufficient bacterial nitric oxide synthase from *sorangium cellulosum*, *Proc. Natl. Acad. Sci. U. S. A.* **106**, 16221.
 18. Sudhamsu, J., and Crane, B. R. (2009) Bacterial nitric oxide synthases: What are they good for?, *Trends Microbiol.* **17**, 212.
 19. Beaumont, E., Lambry, J. C., Wang, Z. Q., Stuehr, D. J., Martin, J. L., and Slama-Schwok, A. (2007) Distal val1346ile mutation in inducible no synthase promotes substrate-dependent no confinement, *Biochemistry* **46**, 13533.
 20. Salard, I., Mercey, E., Rekka, E., Boucher, J. L., Nioche, P., Mikula, I., Martasek, P., Raman, C. S., and Mansuy, D. (2006) Analogies and surprising differences between recombinant nitric oxide synthase-like proteins from *staphylococcus aureus* and *bacillus anthracis* in their interactions with l-arginine analogs and iron ligands, *J. Inorg. Biochem.* **100**, 2024.
 21. Gautier, C., Mikula, I., Nioche, P., Martasek, P., Raman, C. S., and Slama-Schwok, A. (2006) Dynamics of no rebinding to the heme domain of no synthase-like proteins from bacterial pathogens, *Nitric Oxide-Biol. Chem.* **15**, 312.
 22. Feng, C. J., Thomas, C., Holliday, M. A., Tollin, G., Salerno, J. C., Ghosh, D. K., and Enemark, J. H. (2006) Direct measurement by laser flash photolysis of intramolecular electron transfer in a two-domain construct of murine inducible nitric oxide synthase, *J. Am. Chem. Soc.* **128**, 3808.
 23. Scheele, J. S., Bruner, E., Kharitonov, V. G., Martasek, P., Roman, L. J., Masters, B. S. S., Sharma, V. S., and Magde, D. (1999) Kinetics of no ligation with nitric-oxide synthase by flash photolysis and stopped-flow spectrophotometry, *J. Biol. Chem.* **274**, 13105.
 24. Phillips, G. N., Teodoro, M. L., Li, T. S., Smith, B., and Olson, J. S. (1999) Bound co is a molecular probe of electrostatic potential in the distal pocket of myoglobin, *J. Phys. Chem. B* **103**, 8817.
 25. Austin, R. H., Beeson, K. W., Eisenstein, L., Frauenfelder, H., and Gunsalus, I. C. (1975) Dynamics of ligand-binding to myoglobin, *Biochemistry* **14**, 5355.
 26. Springer, B. A., Sligar, S. G., Olson, J. S., and Phillips, G. N. (1994) Mechanisms of ligand recognition in myoglobin, *Chem. Rev.* **94**, 699.
 27. Cao, W. X., Ye, X., Georgiev, G. Y., Berezhna, S., Sjodin, T., Demidov, A. A., Wang, W., Sage, J. T., and Champion, P. M. (2004) Proximal and distal influences on ligand binding kinetics in microperoxidase and heme model compounds, *Biochemistry* **43**, 7017.
 28. Cao, W. X., Ye, X., Sjodin, T., Christian, J. F., Demidov, A. A., Berezhna, S., Wang, W., Barrick, D., Sage, J. T., and Champion, P. M. (2004) Investigations of photolysis and rebinding kinetics in myoglobin using proximal ligand replacements, *Biochemistry* **43**, 11109.

29. Olson, J. S., Soman, J., and Phillips, G. N. (2007) Ligand pathways in myoglobin: A review of trp cavity mutations, *IUBMB Life* 59, 552.
30. Kleinert, T., Doster, W., Leyser, H., Petry, W., Schwarz, V., and Settles, M. (1998) Solvent composition and viscosity effects on the kinetics of co binding to horse myoglobin, *Biochemistry* 37, 717.
31. Park, J., Lee, T., and Lim, M. (2010) Viscosity-dependent dynamics of co rebinding to microperoxidase-8 in glycerol/water solution, *J. Phys. Chem. B* 114, 10897.
32. Murphy, E. J., Marechal, A., Segal, A. W., and Rich, P. R. (2010) Co binding and ligand discrimination in human myeloperoxidase, *Biochemistry* 49, 2150.
33. Shiro, Y., Kato, M., Iizuka, T., Nakahara, K., and Shoun, H. (1994) Kinetics and thermodynamics of co binding to cytochrome p450(nor), *Biochemistry* 33, 8673.
34. Ionascu, D., Gruia, F., Ye, X., Yu, A. C., Rosca, F., Beck, C., Demidov, A., Olson, J. S., and Champion, P. M. (2005) Temperature-dependent studies of no recombination to heme and heme proteins, *J. Am. Chem. Soc.* 127, 16921.
35. Campbell, B. N., Araiso, T., Reinisch, L., Yue, K. T., and Hager, L. P. (1982) A kinetic-study of the binding of carbon-monoxide to ferrous chloroperoxidase, *Biochemistry* 21, 4343.
36. Sudhamsu, J., and Crane, B. R. (2006) Structure and reactivity of a thermostable prokaryotic nitric-oxide synthase that forms a long-lived oxy-heme complex, *J. Biol. Chem.* 281, 9623.
37. Kabir, M., Sudhamsu, J., Crane, B. R., Yeh, S. R., and Rousseau, D. L. (2008) Substrate-ligand interactions in geobacillus stearothermophilus nitric oxide synthase, *Biochemistry* 47, 12389.
38. Reece, S. Y., Woodward, J. J., and Marletta, M. A. (2009) Synthesis of nitric oxide by the nos-like protein from deinococcus radiodurans: A direct role for tetrahydrofolate, *Biochemistry* 48, 5483.
39. Zhou, L., and Zhu, D. Y. (2009) Neuronal nitric oxide synthase: Structure, subcellular localization, regulation, and clinical implications, *Nitric Oxide-Biol. Chem.* 20, 223.
40. Dempsey, J. L., Winkler, J. R., and Gray, H. B. (2010) Kinetics of electron transfer reactions of h-2-evolving cobalt diglyoxime catalysts, *J. Am. Chem. Soc.* 132, 1060.
41. Doster, W., Beece, D., Bowne, S. F., Diiorio, E. E., Eisenstein, L., Frauenfelder, H., Reinisch, L., Shyamsunder, E., Winterhalter, K. H., and Yue, K. T. (1982) Control and ph-dependence of ligand-binding to heme-proteins, *Biochemistry* 21, 4831.
42. Gibson, Q. H., Regan, R., Elber, R., Olson, J. S., and Carver, T. E. (1992) Distal pocket residues affect picosecond ligand recombination in myoglobin - an experimental and molecular-dynamics study of position 29 mutants, *J. Biol. Chem.* 267, 22022.
43. Perrella, M. (1999) Understanding mechanisms in a cooperative protein: The co ligation intermediates of hemoglobin, *Biophys. Chem.* 81, 157.
44. Bellelli, A. (2010) Hemoglobin and cooperativity: Experiments and theories, *Curr. Protein Pept. Sc.* 11, 2.

45. Gorren, A. C. F., Sorlie, M., Andersson, K. K., Marchal, S., Lange, R., and Mayer, B. (2005) Tetrahydrobiopterin as combined electron/proton donor in nitric oxide biosynthesis: Cryogenic uv-vis and epr detection of reaction intermediates, In *Nitric oxide, pt e*, pp 456.
46. Farmer, P. J., and Sulc, F. (2005) Coordination chemistry of the hno ligand with hemes and synthetic coordination complexes, *J. Inorg. Biochem.* 99, 166.

Chapter 6

Electrochemical Properties of gsNOS by Protein Film Voltammetry

6.1 Abstract

The accurate measurement of a protein's electrochemical properties is an important part of understanding its function. Several methods have been developed to facilitate communication between deeply buried protein metal centers and electrodes. One such technique, protein film voltammetry (PFV), involves the immobilization of proteins on the surface of electrodes by various means. Such techniques can result in clear signals from proteins, allowing the measurement of not only reduction potentials but kinetics as well. Two types of PFV have been employed in the study of the nitric oxide synthase from *Geobacillus stearothermophilus*. First, a mutant of this NOS was covalently connected to a gold electrode. It was hypothesized that the use of a hydrophilic linker would maintain a normal aqueous environment around the enzyme and avoid the shifting of potentials (a common problem in PFV). When it was found that this technique still resulted in measuring responses with significantly shifted potentials (as compared with those measured by redox titration in solution), a more traditional film was employed. The kinetics of gsNOS was studied in DDAB films and compared with the mammalian inducible isoform. It was found to show similar behavior, and experiments are still underway to further characterize the kinetics of wild type and three mutants of gsNOS (W70H, W70F, and W70Y, introduced in Chapter 3).

6.2 Introduction and Background

Key to the function of most metalloenzymes is the redox activity of transition metals. These metals have the unique ability, as distinct from most organic molecules, to easily access multiple oxidation states. This electrochemical property of metal sites enables the catalysis of difficult but essential chemical reactions, e.g., the oxidation of unactivated C-H bonds, the reduction of dinitrogen to ammonia, and the generation of hydrogen from water. Clearly, the accurate measurement of a protein's electrochemical properties is an important part of understanding its function. The protein matrix often separates active sites from the surface of the protein by many Ångströms, rendering the standard electrochemical techniques used by inorganic chemists useless.¹⁻³ In many cases, no electrochemical response can be observed.

Several methods have been developed to facilitate communication between deeply buried protein metal centers and electrodes. One such technique, protein film voltammetry (PFV), involves the immobilization of proteins on the surface of electrodes by various means.⁴ Such techniques can result in clear signals from proteins, allowing the measurement of not only reduction potentials but kinetics as well.⁵⁻⁷ However, such methods have recorded potentials vastly different from those measured by other methods, as shown in **Table 6.1** for the case of a heme protein called cytochrome P450 (cyt. P450).

Table 6.1. The $\text{Fe}^{\text{III/II}}$ reduction potential of a cytochrome P450-BM3 as measured by different methods.⁸⁻¹⁰

Method	Potential	Reference
PFV – DDAPSS	+4 mV vs. NHE	Blair 2004
PFV – SDS	-133 mV vs. NHE	Udit 2006
Redox titration	-303 mV vs. NHE	Sligar 1979

Discrepancies in measured reduction potentials are not limited to cyt. P450s or even iron enzymes in general. A chemically modified electrode, cysteamine on Au(111), was used to measure the $\text{Cu}^{\text{II/I}}$ potential of the enzyme copper nitrite reductase. The authors neglect to specifically mention the measured potential in the report; however, the included cyclic voltammograms show a quasi-reversible wave slightly negative of 0 mV vs. SCE.¹¹ The same group published later voltammetric studies of the same copper-containing nitrite reductase, this time using gold electrodes modified not with cysteamine but with self-assembled monolayers of alkane thiols.¹² They again fail to mention the $E_{1/2}$ they measured, but the couple clearly lies at nearly +100 mV vs. SCE. Two different monolayers on the same electrode resulted in two different reduction potentials. Curiously, these differing potentials go undiscussed but for one mention of differing dielectric constants between films and aqueous solution.⁴ The cause of these shifts remains unknown.

Interestingly, varied electrochemical approaches have produced consistent results in other cases. Film voltammetric methods have been used for several small electron transfer (ET) proteins, such as cytochromes *c* and cupredoxins, **Figure 6.1**. The reduction potential cupredoxin azurin, for example, falls near +300 mV vs. NHE regardless of electrochemic method.¹³⁻¹⁵ A trend seems apparent: technique-based discrepancies in reduction potential are endemic to larger metalloproteins, but measured values tend to converge as molecular size decreases.

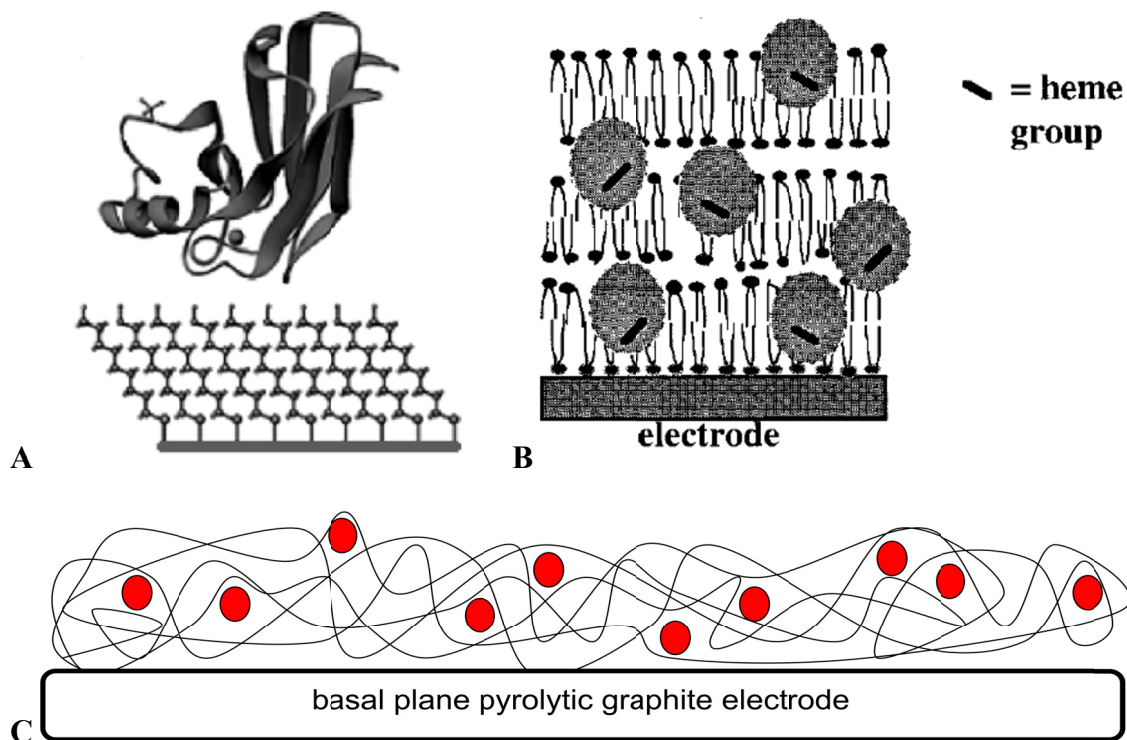
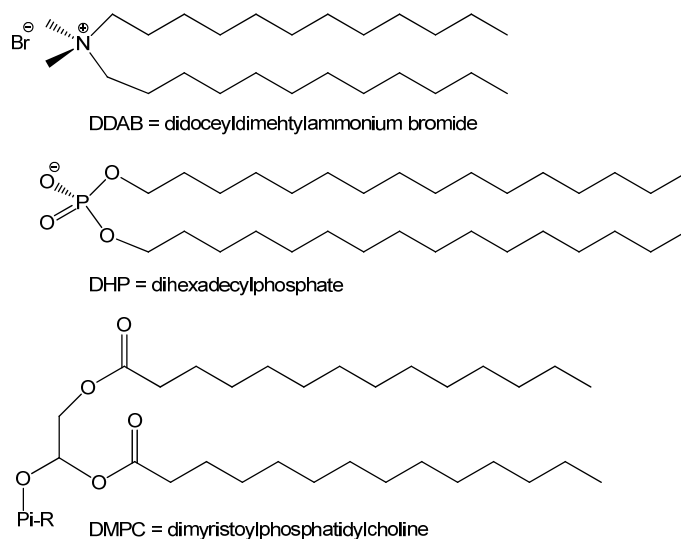


Figure 6.1. Depictions of proteins immobilized on electrodes (A) using SAMs (azurin),¹⁶ (B) using phospholipid-like films (cytochrome *c*),⁴ and (C) using a DDAB film and nitric oxide synthase.

When simple Coulombic interactions will not suffice, alternative methods of attachment have been employed in order to promote electronic coupling between protein active sites and electrodes. Self-assembled monolayers (SAMs) on gold surfaces have been studied in detail.¹⁷ SAMs have been used extensively by Gray and coworkers to characterize the electrochemical properties of azurin and cytochrome *c*, among other small ET proteins. Monolayers of mixed hydroxyl and alkyl-terminated thiols on gold are soaked in protein solutions, then rinsed, and used in voltammetric experiments. It is unclear, to date, what exactly the nature of this interaction is (surface characterization methods have provided sparse insights),¹¹ but clear signals can be recorded.

Another non-covalent method of attaching a protein sample to an electrode involves surfactant films. Characterization of a protein sample within this matrix is very

difficult; only when using a specially designed cell and extensive reflections can one take a UV-visible or IR spectrum of a protein within a film.¹⁸ Films have successfully been employed with a number of enzymes including cyt. P450, myoglobin, and nitric oxide synthase.¹⁹ A selection of some of the surfactants that have been used for film voltammetry is shown in **Scheme 6.1**.



Scheme 6.1. Surfactants commonly used for protein film voltammetry.

These surfactants typically contain a polar head group and a long alkyl chain, making them similar to lipids and, presumably, cell membranes. Solutions of these surfactants in organic solvents are dropped onto polished electrode surfaces and the solvent is allowed to evaporate.²⁰ An interlocking network of the surfactant, or a film, is left behind. When soaked in an aqueous solution of protein sample, some protein is taken up into the film or otherwise interacts with it. This technique has demonstrated the largest deviation from solution reduction potentials amongst the many electrochemical techniques. The reason for this is hypothesized to be the lipid-like nature of the film. Perhaps lipid-like films provide a more accurate measure of the potential of membrane-bound proteins, although no concrete data support this hypothesis. Unfortunately,

detailed characterization of biological samples on solid surfaces is difficult as most characterization techniques are solution-based.

Covalent attachment of the samples of interest can be used to couple the active site to the electrode. Mutagenesis to install a single, solvent-exposed cysteine will allow for attachment of the protein to a gold electrode directly through the cysteine sulfur atom. Alternatively, this cysteine can be used to functionalize the protein with some other group for attachment to the surface, as demonstrated by Liu and coworkers.²¹ Investigators have proposed that these methods block movement of the protein and lock it out of potentially necessary conformations, particularly with respect to protein-electrode ET pathways.^{4, 7} This lack of motion is a concern with all methods that tether the sample to the electrode surface. Comparison of the results of voltammetry with both covalent and non-covalent attachment to gold electrodes using SAMs should provide insight into the issue of sample diffusion on the electrode surface.

Electrochemistry was carried out using covalent attachment of NOS to standard SAMs, but the potential measured was +195 mV vs. NHE, about 450 mV positive of other NOS enzymes.²² A hydrophilic SAM terminated in a maleimido functionality was then used to attach gsNOS to the surface in a covalent fashion rather than the traditional hydrophobic SAMs. It was hypothesized that the hydrophilic SAMs on a gold electrode would promote a normal hydration sphere around the protein and prevent the shift in potential previously observed in PFV of mammalian iNOS. Cyclic voltammograms were collected on gsNOS. This bacterial enzyme displayed similar properties as iNOS, with the observable dissociation of water upon reduction of the iron center. Unfortunately, the measured potential was again shifted very positive of the potential measured in solution.

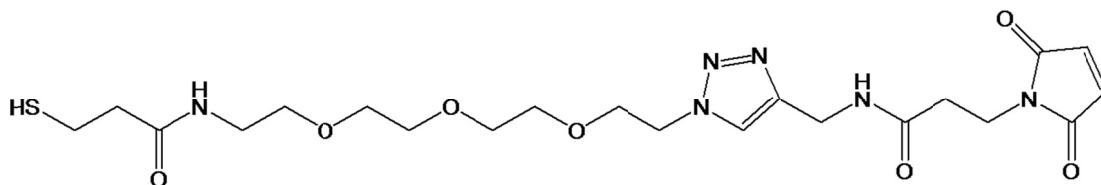
Given that this technique using covalent attachment still showed altered reduction potentials for the iron site, the complicated synthesis and electrode prep were deemed unnecessary and further investigations were made using traditional films. Films of DDAB and wild type gsNOS were co-deposited onto the surface of basal plane pyrolytic graphite electrodes and their electrochemical properties were investigated.

6.3 Materials and Methods

Electrodes were purchased from Pine Instruments. Chemicals, such as arginine and TrisHCl buffer, were purchased from Sigma-Aldrich. The enzymes used in this study were expressed and mutated as described previously in Chapter 3.

A mutant form of gsNOS was expressed, containing a single, solvent-exposed cysteine residue for use in covalent attachment. The native enzyme has four cysteine residues at positions 76, 161, 227, and 269. Cys76 ligates the iron center and is necessary for activity and for heme incorporation. Position 161 is completely buried within the protein interior and hidden from solvent. These residues were left un-mutated as they should not interfere in any way with the protein labeling process. Positions 227 and 269, however, are exposed to solvent at the surface of the protein, so these two residues were mutated to serines so as not to interfere with covalent labeling reactions which rely on a nucleophilic thiolate. A cysteine was installed near the heme (in order to facilitate communication with the electrode) at position 115, where a lysine residue is found in the wild type and is fully solvent exposed. SAMs were made with polyethylene glycolated (PEG-ylated) thiols in order to produce a hydrophilic surface. This PEG-ylated thiol was terminated in an azide to facilitate “click” chemistry. A small molecule containing an

alkyne and a maleimide was “clicked” to the surface using a Cu(bathophenanthroline) catalyst. The complete molecule used for the film is shown in **Scheme 6.2**.



Scheme 6.2. The maleimide-terminated thiol used to attach gsNOS to the surface of a gold electrode for voltammetry.

For DDAB films, a solution containing DDAB in DMSO was co-spotted onto BPG electrodes with aqueous solutions of NOS. Not only was the wild type studied, but the mutant enzymes described in Chapter 3, W70H, W70F, and W70Y were as well, to investigate the effect of the proximal hydrogen bonding network on the electronics of the heme site. The buffer used for these studies was 150 mM NaCl, 50 mM Tris, pH 7.5.

6.4 Results

First, “click” chemistry was used to attach gsNOS covalently to standard SAMs (alkane thiols) on gold electrodes, as shown in **Figure 6.2**. When the electrochemical response of NOS was measured using cyclic voltammetry, strong signals were observed. The potentials that were measured, however, were far positive of those found in Chapter 3 by redox titration (**Figure 6.3**).

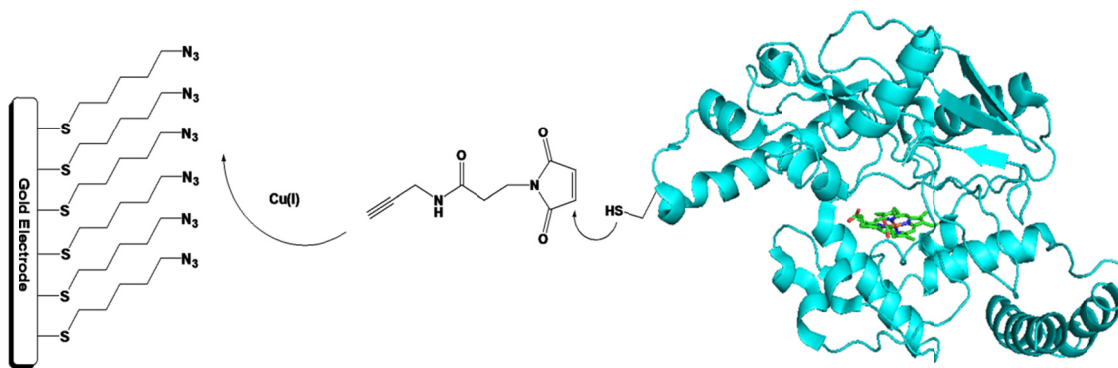


Figure 6.2. Method of attachment of gsNOS to gold electrodes.

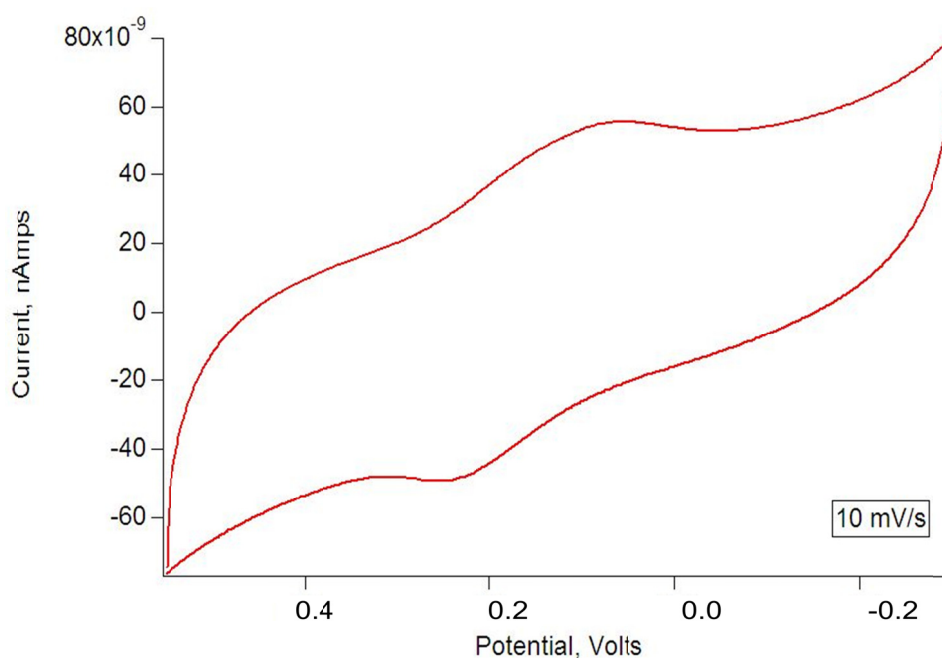


Figure 6.3. Cyclic voltammogram of K115C/C227S/C269S gsNOS when covalently attached to a gold electrode by the molecule shown in **Figure 6.2**, 10 mV/s scan rate. The surface coverage was determined to be 3 pmol/cm² (50% coverage) as determined by integrating the area of each peak.

These samples, while giving very elevated potentials, did give good electrochemical responses. To verify that the protein was in fact bound to the surface, the scan rate dependence of the signals were studied. The electrochemistry of surface-bound species varies with scan rate in a predictable manner.²³⁻²⁴ The scan rate dependence can be fit to Equation 6.1 if the samples are indeed sequestered on the surface and not

diffusing through solution. **Figure 6.4** shows the broadening of the voltammetric signal in response to an increased rate of scanning the potential. **Figure 6.5** shows the fit of the observed scan rate dependence to Equation 6.1. Voltammograms were simulated using CH Instruments software assuming $\alpha = 0.5$, allowing the calculation/approximation of the electron transfer rate between the iron center and the electrode as well as the reorganization energy: average $k^o \sim 10^{-1} \text{ s}^{-1}$ and $\lambda \sim 1 \text{ eV}$.

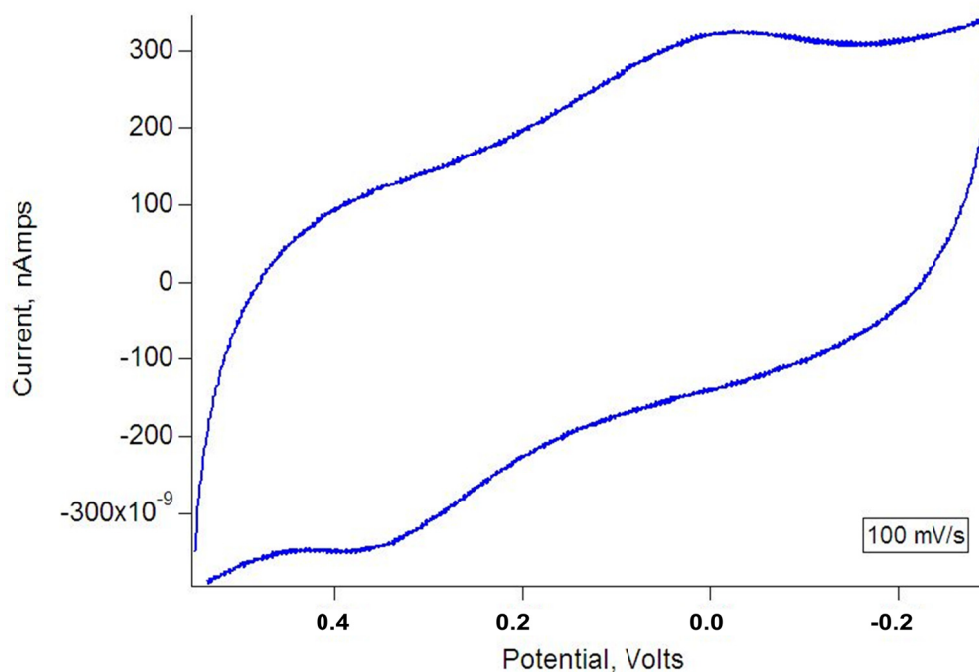


Figure 6.4. Voltammetric response at an increased scan rate, 100 mV/s.

$$k_{red,ox} = \mu \rho k_B T \int \frac{\exp[-(x-(\lambda \pm \eta))/(k_B T))^2 * k_B T/(4\lambda)] dx}{[1+\exp(x)]} \quad (6.1)$$

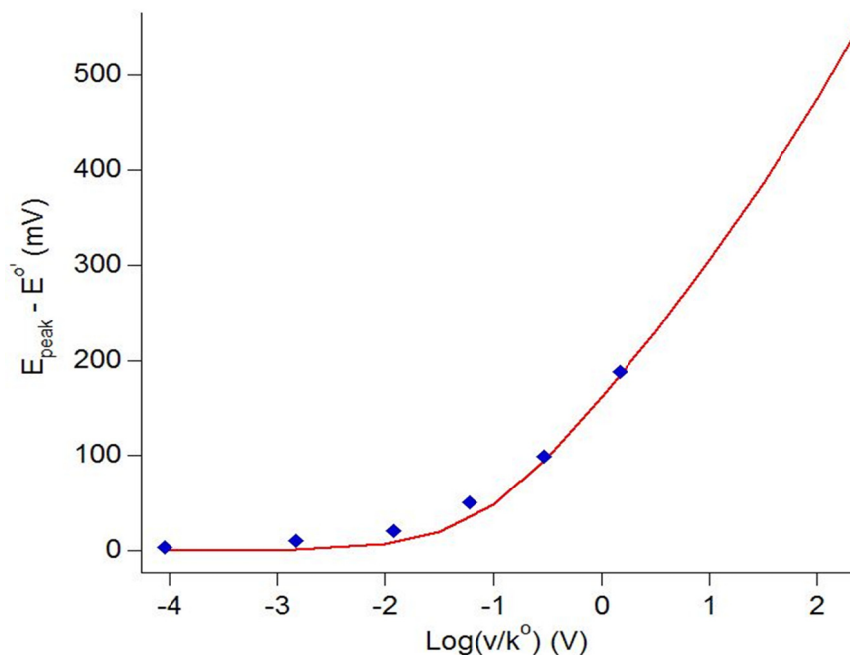


Figure 6.5. The red line in the theoretical fit for scan rate dependence for surface-bound species, Equation 6.1. The blue diamonds are the actual peak separations measured in gsNOS samples on gold-thiols as the scan rate is varied.²³

The potentials measured with this method are shifted nearly half a volt positive of the known value of the redox couple under investigation. In order to observe a more reasonable potential for this couple, SAMs were made using the hydrophilic molecule shown in **Scheme 6.1**. It was hypothesized that the presence of water around the PEG groups and near the surface of the protein would shift the potential closer to that measured in aqueous solution. The voltammetric response using the molecule from **Scheme 6.2** to form the SAM and connect NOS to the electrode can be seen in **Figures 6.6** and **6.7**.

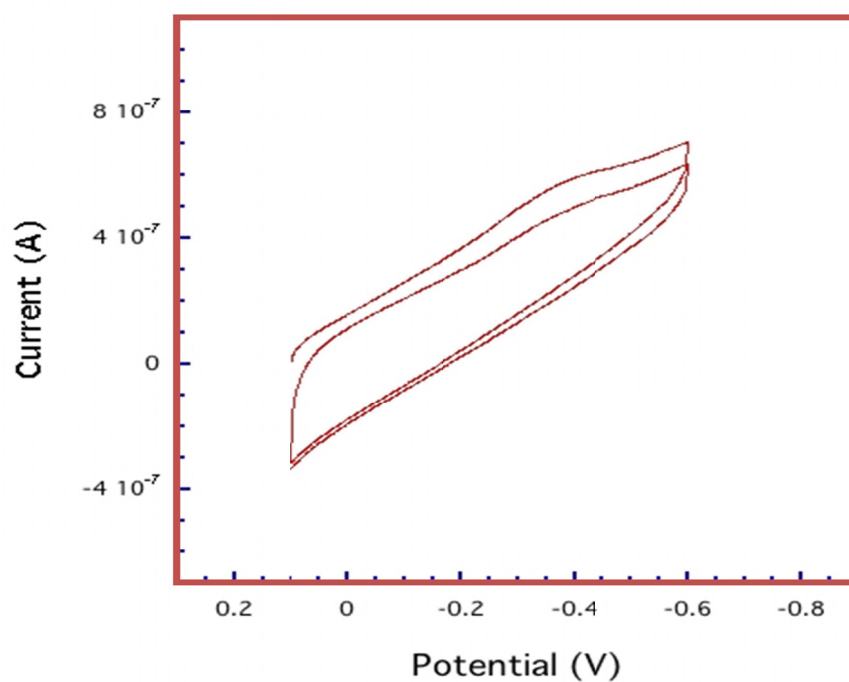


Figure 6.6. Cyclic voltammogram of K115C/C227S/C269S gsNOS on PEG-ylated SAMs on a gold electrode.

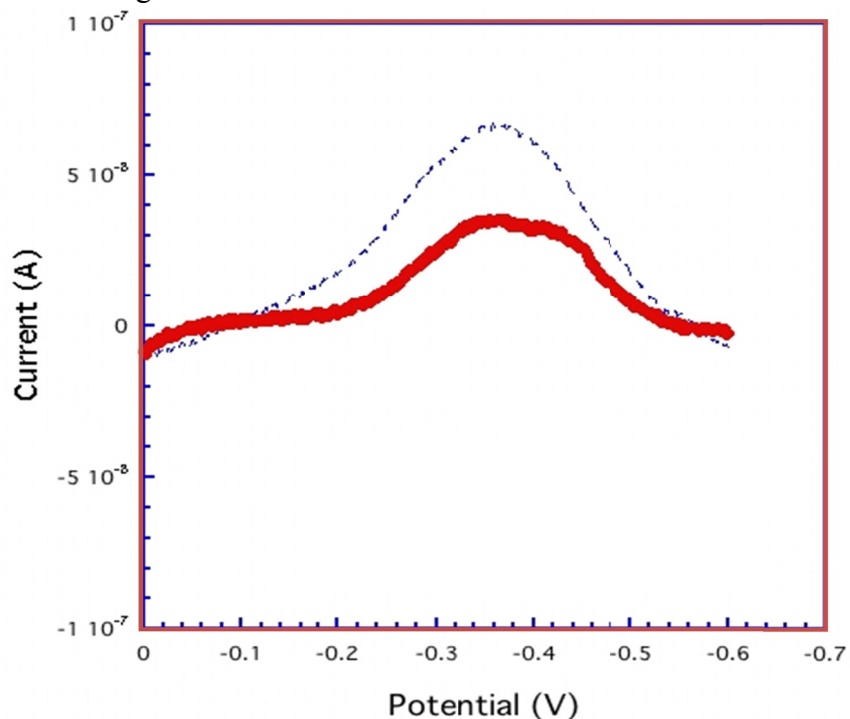


Figure 6.7. The same data as shown in **Figure 6.6**, but with the background signal subtracted to allow a clearer view of the details of each peak. The first scan is shown as solid line, and the second scan as dashes.

From **Figure 6.7** it can be seen that the peak shows similar fine structure as iNOS. A water molecule is loosely coordinated to the iron in the resting ferric state. Upon reduction, the water molecule rapidly dissociates. This explains the presence of two peaks for the reduction wave, but only a single peak for the re-oxidation wave of the voltammogram. However, while the potential is less positive (about -220 mV vs. Ag/AgCl or 0 vs. NHE) it is still well positive of the potential measured in aqueous solution. Due to the complicated synthesis of the molecule used for this SAM and its inability to improve upon issues seen with other films, this method was abandoned in favor of DDAB films as used previously with iNOS. The voltammetric response of wild type gsNOS in a DDAB film on a basal plane graphite (BPG) electrode is shown in **Figure 6.8**, with clearly two distinct peaks in the reduction wave similar to results seen with mammalian iNOS.¹⁹

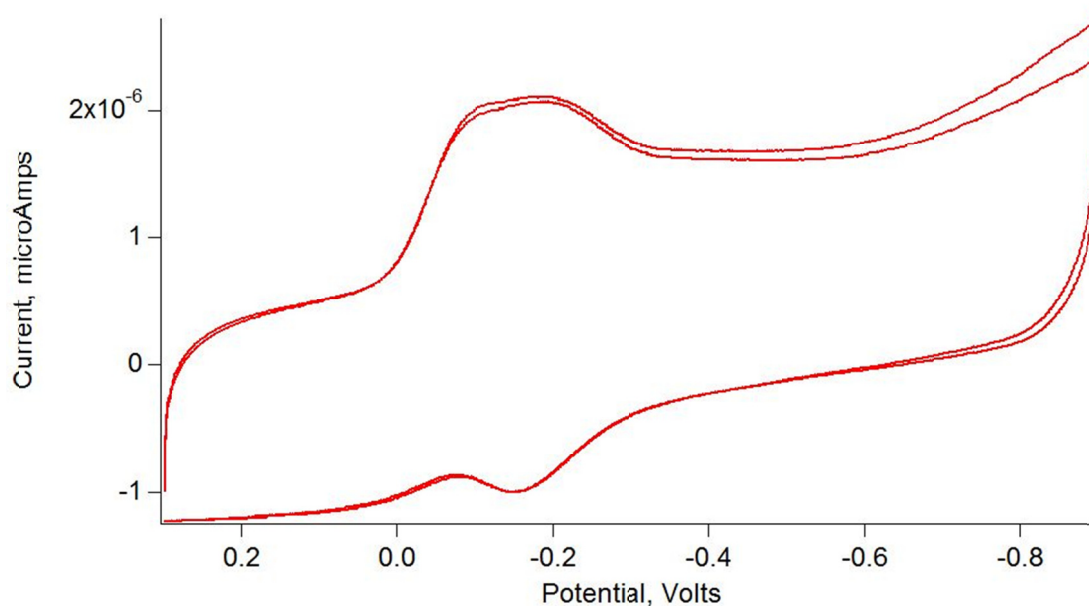


Figure 6.8. Cyclic voltammogram of wt gsNOS in DDAB film on a BPG electrode, showing two peaks in the reduction wave as was seen with iNOS.

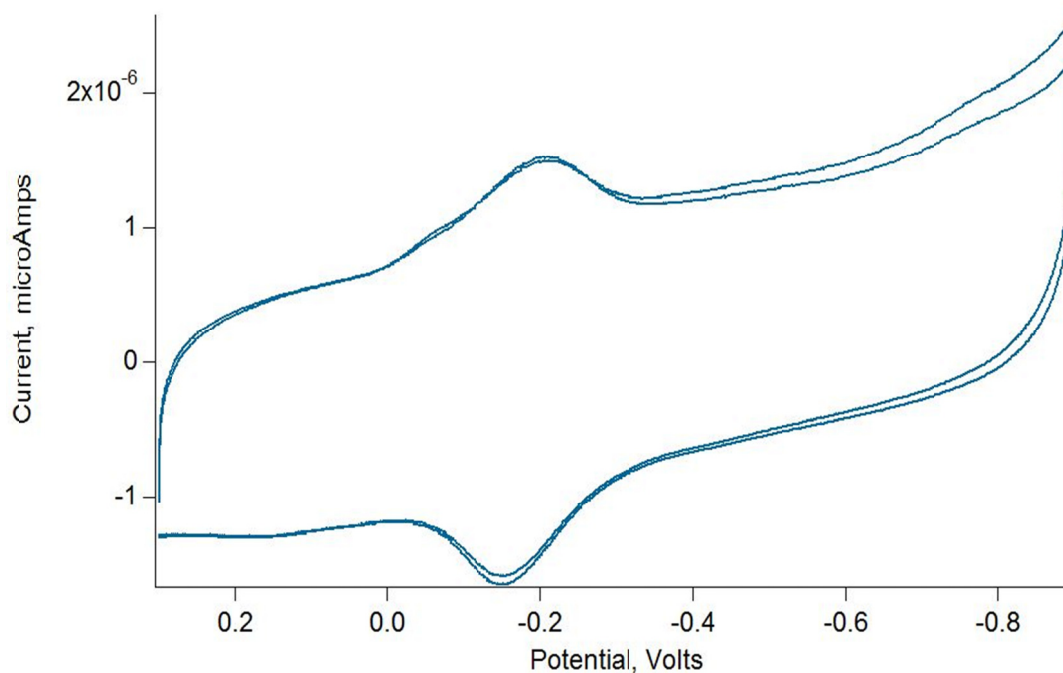


Figure 6.9. Cyclic voltammogram of W70F gsNOS in DDAB film on a BPG electrode, showing the presence of only one peak in the reduction wave.

The use of DDAB films on BPG electrodes gave large signals from gsNOS. Due to the ease of fabrication and the large signals, on-going studies are investigating the electrochemistry of mutant forms of gsNOS by this method. Initial values for the measured reduction potentials are shown in **Table 6.2**.

Table 6.2. The measured reduction potentials of 4 mutants (at position 70) of gsNOS.

Sample	$E_{(1/2)}$, mV vs. Ag/AgCl
WT	-178
His	-172
Phe	-216
Tyr	-209

Interesting features can be observed in the voltammograms, such as differing interactions with the axial water ligand (see **Figure 6.9**) due to altered electronics of the heme site. The trend in measured reduction potentials matches that observed by redox titration. Experiments were also carried out with the wild type enzyme at increased pH and indicated a shift of approximately 60 mV per pH unit, as is consistent with a proton-coupled electron transfer event. Given the presence of the water molecule that coordinates the heme in the Fe(III) state, but not the Fe(II) state and the possible protonation of the axial thiolate ligand, this result was expected. Studies are on-going in an effort to characterize the equilibrium for water ligation in each enzyme and the effect of the substrate arginine on these kinetics.

6.5 References

1. Anderson, J. L., Coury, L. A., and Leddy, J. (1998) Dynamic electrochemistry: Methodology and application, *Anal. Chem.* **70**, 519R.
2. Armstrong, F. A., Hill, H. A. O., Oliver, B. N., and Walton, N. J. (1984) Direct electrochemistry of redox proteins at pyrolytic-graphite electrodes, *J. Am. Chem. Soc.* **106**, 921.
3. Armstrong, F. A. (2005) Recent developments in dynamic electrochemical studies of adsorbed enzymes and their active sites, *Curr. Opin. Chem. Biol.* **9**, 110.
4. Rusling, J. F. (1998) Enzyme bioelectrochemistry in cast biomembrane-like films, *Accounts Chem. Res.* **31**, 363.
5. Fourmond, V., Burlat, B., Dementin, S., Sabaty, M., Arnoux, P., Etienne, E., Guigliarelli, B., Bertrand, P., Pignol, D., and Leger, C. (2010) Dependence of catalytic activity on driving force in solution assays and protein film voltammetry: Insights from the comparison of nitrate reductase mutants, *Biochemistry* **49**, 2424.
6. Hirst, J. (2006) Elucidating the mechanisms of coupled electron transfer and catalytic reactions by protein film voltammetry, *Biochim. Biophys. Acta-Bioenerg.* **1757**, 225.
7. Leger, C., and Bertrand, P. (2008) Direct electrochemistry of redox enzymes as a tool for mechanistic studies, *Chem. Rev.* **108**, 2379.
8. Blair, E., Greaves, J., and Farmer, P. J. (2004) High-temperature electrocatalysis using thermophilic p450 cyp119: Dehalogenation of ccl4 to ch4, *J. Am. Chem. Soc.* **126**, 8632.
9. Udit, A. K., Hill, M. G., and Gray, H. B. (2006) Electrochemistry of cytochrome p450bm3 in sodium dodecyl sulfate films, *Langmuir* **22**, 10854.
10. Sligar, S. G., Cinti, D. L., Gibson, G. G., and Schenkman, J. B. (1979) Spin state control of the hepatic cytochrome-p450 redox potential, *Biochem. Biophys. Res. Commun.* **90**, 925.
11. Zhang, J. D., Welinder, A. C., Hansen, A. G., Christensen, H. E. M., and Ulstrup, J. (2003) Catalytic monolayer voltammetry and in situ scanning tunneling microscopy of copper nitrite reductase on cysteamine-modified au(111) electrodes, *J. Phys. Chem. B* **107**, 12480.
12. Chi, Q. J., Zhang, J. D., Jensen, P. S., Christensen, H. E. M., and Ulstrup, J. (2006) Long-range interfacial electron transfer of metalloproteins based on molecular wiring assemblies, *Faraday Discuss.* **131**, 181.
13. Marshall, N. M., Garner, D. K., Wilson, T. D., Gao, Y. G., Robinson, H., Nilges, M. J., and Lu, Y. (2009) Rationally tuning the reduction potential of a single cupredoxin beyond the natural range, *Nature* **462**, 113.
14. Pascher, T., Karlsson, B. G., Nordling, M., Malmstrom, B. G., and Vanngard, T. (1993) Reduction potentials and their ph-dependence in site-directed-mutant forms of azurin from pseudomonas-aeruginosa, *Eur. J. Biochem.* **212**, 289.
15. Yokoyama, K., Leigh, B. S., Sheng, Y. L., Niki, K., Nakamura, N., Ohno, H., Winkler, J. R., Gray, H. B., and Richards, J. H. (2008) Electron tunneling through pseudomonas aeruginosa azurins on sam gold electrodes, *Inorg. Chim. Acta* **361**, 1095.

16. Yue, H. J., and Waldeck, D. H. (2005) Understanding interfacial electron transfer to monolayer protein assemblies, *Curr. Opin. Solid State Mat. Sci.* 9, 28.
17. Fujita, K., Nakamura, N., Ohno, H., Leigh, B. S., Niki, K., Gray, H. B., and Richards, J. H. (2004) Mimicking protein-protein electron transfer: Voltammetry of pseudomonas aeruginosa azurin and the thermus thermophilus cu-a domain at omega-derivatized self-assembled-monolayer gold electrodes, *J. Am. Chem. Soc.* 126, 13954.
18. Udit, A. K., Hagen, K. D., Goldman, P. J., Star, A., Gillan, J. M., Gray, H. B., and Hill, M. G. (2006) Spectroscopy and electrochemistry of cytochrome p450bm3-surfactant film assemblies, *J. Am. Chem. Soc.* 128, 10320.
19. Udit, A. K., Belliston-Bittner, W., Glazer, E. C., Nguyen, Y. H. L., Gillan, J. M., Hill, M. G., Marletta, M. A., Goodin, D. B., and Gray, H. B. (2005) Redox couples of inducible nitric oxide synthase, *J. Am. Chem. Soc.* 127, 11212.
20. Udit, A. K., and Gray, H. B. (2005) Electrochemistry of heme-thiolate proteins, *Biochem. Biophys. Res. Commun.* 338, 470.
21. Liu, G. Z., and Gooding, J. J. (2006) An interface comprising molecular wires and poly(ethylene glycol) spacer units self-assembled on carbon electrodes for studies of protein electrochemistry, *Langmuir* 22, 7421.
22. Presta, A., Weber-Main, A. M., Stankovich, M. T., and Stuehr, D. J. (1998) Comparative effects of substrates and pterin cofactor on the heme midpoint potential in inducible and neuronal nitric oxide synthases, *J. Am. Chem. Soc.* 120, 9460.
23. Tender, L., Carter, M. T., and Murray, R. W. (1994) Cyclic voltammetric analysis of ferrocene alkanethiol monolayer electrode-kinetics based on marcus theory, *Anal. Chem.* 66, 3173.
24. Devaraj, N. K., Decreau, R. A., Ebina, W., Collman, J. P., and Chidsey, C. E. D. (2006) Rate of interfacial electron transfer through the 1,2,3-triazole linkage, *J. Phys. Chem. B* 110, 15955.

Chapter 7

Conclusions and Future Work

7.1 Roles of the Hydrogen-Bond Donating Groups in Tuning the Axial Thiolate

The thermodynamics of wild type and three mutants of gsNOS were characterized by various methods. Data from circular dichroism spectroscopy shows that mutations at position 70 do not decrease the overall stability of the protein fold. The evidence from multiple techniques is clear, however, that these mutations significantly affect the electronics of the heme center. It was shown using binding assays, generation of the ferrous-CO species, and redox titrations that the σ -donating abilities of the thiolate are increased after removal of the hydrogen bonding group in the Trp. Both chemical redox titrations and instability of ferrous-CO complexes of the two mutants lacking this key hydrogen bond (W70F and W70Y) suggest that they have more negative reduction potentials than the two mutants with this hydrogen bond (wild type and W70H). Evans Methods NMR was used to confirm the results of UV-visible spectroscopy which suggest that removal of this hydrogen bond shifts the heme center toward the high-spin state due to strengthening of the Fe-S bond, as seen in the binding assays.

It can be concluded that this universally-conserved tryptophan residue serves several roles, but positioning of the heme within the protein (as has been suggested for cyt. P450s) is not one of them. In order to produce NO the electronics of the heme center must be tuned in such a way as to stabilize high-valent iron species for the oxidation of substrate. During catalysis, the site must also be tuned not only to support the six-coordinate ferrous-oxy complex, but promote release of NO \cdot from the heme in the end. If the 3/2+ reduction potential of the site is too negative, the ferrous-oxy may be unstable or the high-valent iron species too stable to perform the desired reactivity. If too negative, release of NO will be disfavored and decrease the rate of release to undesirable levels.

Stopped-flow coupled with UV-visible spectroscopy was employed to characterize wild type gsNOS and these three new mutant enzymes. It was shown that their autoxidation rates correlate with reduction potential data discussed in Chapter 3. The histidine mutant has an elevated reduction potential and the slowest autoxidation rate relative to the other three. The wild type is more negative by approximately 20 mV with a potential of -362 mV vs. NHE. This reduction potential is similar to that of mammalian inducible NOS, but these two are then more negative than other NOS enzymes by 100 mV. The reason for this behavior in gsNOS is unknown, but in iNOS the presence of the substrate sterically excludes a water molecule that coordinates the heme and this binding event shifts the reduction potential into the normal range for NOSs. The two mutants lacking this conserved hydrogen bond, W70F and W70Y, have significantly more negative potentials and were found to have very fast rate constants for autoxidation, consistent with more negative potentials.

The production of NO_x species of all four enzymes was characterized by the Griess Assay. The wild type produces nitrogen oxide species at a rate similar to other NOSs. The W70H mutant has an elevated rate of NO_x release/formation. The two mutants without this hydrogen bond have significantly decreased rates of NO_x production. Clearly this hydrogen bond plays a role in controlling the rate of NO release from the enzyme or the speed with which it is formed (as all four should react sufficiently rapidly with hydrogen peroxide for reduction not to be a factor in this assay).

Finally, stopped-flow was once again employed in order to determine if the Griess Assay was indeed detecting NO^\bullet or rather NO^- which are indistinguishable by that method. The ferric-NO complex, the immediate precursor to the nitric oxide product, was

observed for three of the four enzymes. Interestingly, this could not be observed for the W70H mutant. This mutant most likely releases NO^- .

The conserved proximal hydrogen-bond donating group found near the axial thiolate ligand in all nitric oxide synthases plays a key role in tuning the electronics of the active site. This is a uniquely long hydrogen bonding interaction between this tryptophan and the thiolate, at just 3.7 Å. Without this interaction, the enzyme is still capable of producing NO, as found for both the W70F and W70Y mutants by single turnover experiments. Their reduction potentials, however, are incredibly negative and most likely fall far below the biologically relevant window. The replacement of this tryptophan with a histidine results in an enzyme with a more elevated potential, however it cannot release NO radical. The histidine residue, lacking the aryl ring, most likely cannot π -stack with the porphyrin ring, giving it more flexibility. This may allow it to move closer to the thiolate to improve this hydrogen bonding interaction. If this interaction is too strong, NO^- is released.

In the second turnover of the catalytic cycle, an electron from the heme center must be shuttled back into the tetrahydrobiopterin cofactor to re-reduce it. The potentials of both the heme and the pterin must be tuned perfectly to allow forward electron transfer into the ferrous-oxy complex followed by back electron transfer into the pterin. This back electron transfer allows release of NO^\bullet and not NO^- . If the potential of the heme center is too high, this back electron transfer cannot occur, preventing NO^\bullet release. Thus, the hydrogen bonding interaction is necessary for tuning the reduction potential high enough for the reduction of the heme by a reductase domain/enzyme. However, when too strong,

the potential is tuned too high to send an electron back into the pterin after catalysis, which is necessary for formation of the product NO.

7.2 Gating of Diatomics in Nitric Oxide Synthase

First, CO is a valuable diatomic mimic for the more reactive dioxygen and nitric oxide, however with a caveat. One must remember the conditions under which experiments are performed. For CO photolysis, systems are under saturating conditions with large excesses of carbon monoxide. This is a good system for comparison with oxygen binding to hemoglobin in the lungs. Nitric oxide formation, on the contrary, involves the production of a single molecule of NO per protein, far from saturating conditions. Further, NO reacts rapidly in aerated aqueous solution, further preventing its buildup and keeping the system from reaching equilibrium. Also, the driving force ultimately behind each of these processes involves formation or cleavage of two distinct bonds. CO is very similar to NO, but on a fundamental level an Fe-N bond is not an Fe-C bond. While experiments with CO provide a wealth of information about the overall kinetics model for reactivity with diatomics, for an NO release rate one must perform the single turnover experiments.

With these experiments, we have confirmed that the isoleucine residue at position 223 does gate NO release in gsNOS, slowing the decay of the ferric-NO species. We have also demonstrated that position 134, occupied by a histidine in wild type gsNOS, also gates NO release, with smaller residues at this position corresponding to faster release rates. Together, these two positions can account for the majority of the differences in rate between any two NOS enzymes.

Further, we have used a new, more accurate five-state model to fit our data showing rapid equilibrium between the bound and unbound NO, and another unidentified species. This species has been previously observed in a mammalian enzyme by another group. It was called Compound I. The Compound I in cytochromes P450 has a much more blue-shifted Soret band with a maximum near 365 nm and it reacts much more quickly. It is of note that this species with absorbance at 420 nm has now been observed in both turnovers. This species could possibly be some form of the P420 species in NOS, which has either lost thiolate ligation or the thiolate has become protonated, becoming a neutral thiol ligand. Unfortunately, its exact identity remains uncertain.

7.3 Future Directions

Several experiments remain in order to fully characterize the set of mutants probing the role of the hydrogen bonding to the axial thiolate. First, redox titrations must be conducted with a different chemical titrant. The $3/2+$ couple of $\text{Ru}(\text{acac})_3$ is too positive to determine the potential of the W70F and W70Y mutants. Another reagent, such as benzyl viologen with a reduction potential of -374 mV vs. NHE, might prove more appropriate for observing the equilibrium between oxidized and reduced species. Further, these titrations should be carried in the presence of the substrate arginine as well, in order to determine if the presence of substrate shifts the potential as was seen with mammalian inducible NOS.

The full effect of mutating this hydrogen bond donor cannot be understood until structural data is collected. Crystallography would answer questions about the distance of each residue from the thiolate and from the porphyrin ring, as well as the positioning of

the sulfur atom with respect to the iron for each sample. It would also reveal any other unexpected effects on the fold of the protein. Samples have been sent to the lab of Brian Crane at Cornell, an expert in NOS crystallography. This family of enzymes, however, is notoriously difficult and slow to crystallize. Efforts to obtain these three-dimensional structures are underway.

Work on protein film voltammetry with gsNOS is still ongoing in the lab of Michael Hill at Occidental College. In addition to measuring reduction potentials, the interaction of each sample with the axial water ligand will be investigated by studying the scan rate dependence. The iron centers will also be probed in the presence of arginine, which should shift all potentials and remove any interaction with water at the heme. These experiments are expected to be completed within the next couple of months.

Finally, electron transfer pathways in NOS should be studied using more traditional Gray group laser-induced flash/quench techniques. Attempts have been made at connecting a Ru-trisdiimine photosensitizer to the enzyme in order to induce ET to/from the heme (see Appendix II). The iodoacetamidophenanthroline ligand should be used to tether Ru(bpy)₂ to the enzyme at position 115. Initial studies show quenching of the Ru excited state and formation of Ru(III), but no oxidation of the heme despite rapid loss of the Ru(III). These results suggest that possibly another residue in the enzyme is being oxidized. gsNOS has more than a dozen oxidizable Trp and Tyr residues. Mutations may be required in order to promote oxidation of the heme center rather than another residue. Further studies should be able to produce high-valent heme species in this enzyme. The characterization of any high-valent species in NOS would be of incredible interest to the field, as the active oxidants are still unknown.

Appendix I

Wires Review in the Journal of Porphyrins and Phthalocyanines

Reproduced with permission from: *J. Porphyrins Phthalocyanines* (2008) **12**: 971.

Probing the heme-thiolate oxygenase domain of inducible nitric oxide synthase with Ru(II) and Re(I) electron tunneling wires

Charlotte A. Whited, Wendy Belliston-Bittner, Alexander R. Dunn, Jay R. Winkler* and Harry B. Gray*

Beckman Institute, California Institute of Technology, Pasadena, 91125, USA

ABSTRACT: Nitric oxide synthase (NOS) catalyzes the production of nitric oxide from L-arginine and dioxygen at a thiolate-ligated heme active site. Although many of the reaction intermediates are as yet unidentified, it is well established that the catalytic cycle begins with substrate binding and rate-limiting electron transfer to the heme. Here we show that Ru(II)-diimine and Re(I)-diimine electron tunneling wires trigger nanosecond photoreduction of the active-site heme in the enzyme. Very rapid generation of a reduced thiolate-ligated heme opens the way for direct observation of short-lived intermediates in the NOS reaction cycle.

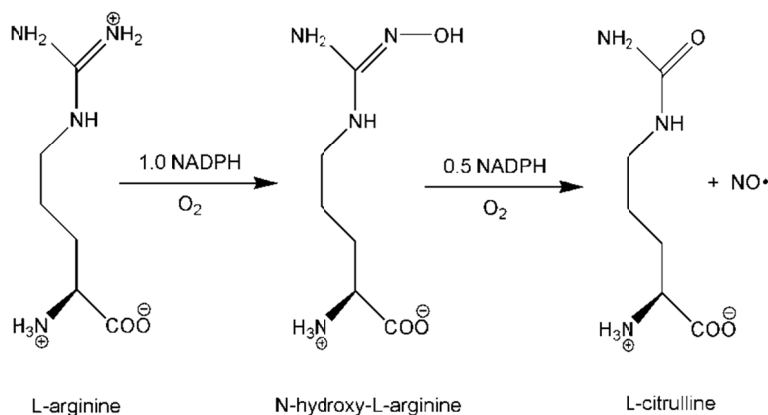
INTRODUCTION

Salvador Moncada and colleagues reported in 1987 that the molecule responsible for relaxation of blood vessels is nitric oxide (NO).¹ This publication marked the beginning of a new area of chemical and biological research, with thousands of articles published each year. Long known as a cytotoxic agent in pathological processes,² NO now is recognized as a key signaling molecule in the cardiovascular, immune, and nervous systems.³

Nitric oxide synthases (NOSs) are responsible for the production of NO in living systems.⁴ The three (mammalian) isoforms of the enzyme are named for the tissues in which they are found: endothelial NOS (eNOS), neuronal (nNOS), and an inducible form found in macrophages (iNOS). The functions of eNOS and nNOS are regulated by calcium ions and a

* Correspondence to: J. R. Winkler; winklerj@caltech.edu; H. B. Gray; hbgray@caltech.edu

calmodulin linker, while the inducible isoform is calcium ion independent.⁵ NOSs catalyze the oxidation of L-arginine (Arg) to L-citrulline in two turnovers, with N^ω-hydroxy-L-arginine (NHA or ArgOH) as an enzyme-bound intermediate (the product of the first turnover).⁶ The overall reaction is shown in **Scheme 1**.



Scheme 1: The five-electron oxidation of arginine to form NO and citrulline.⁷

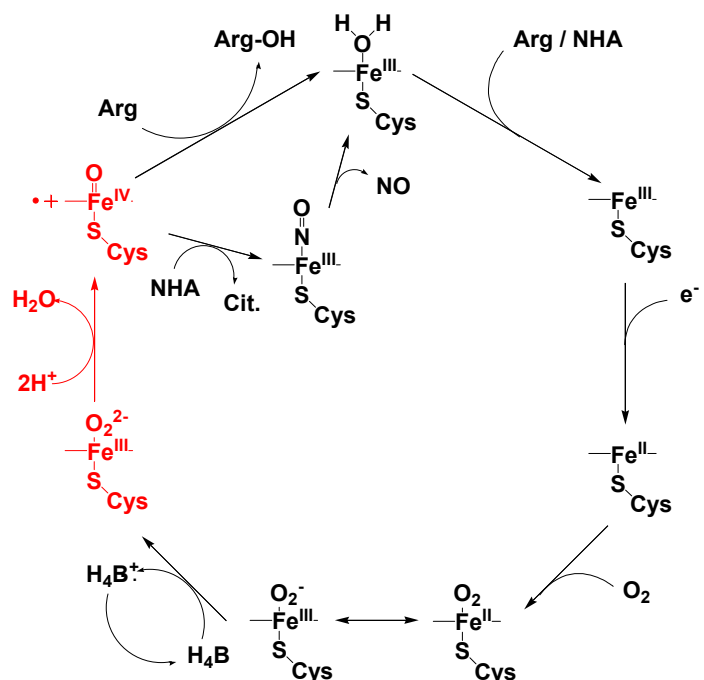
All three isoforms are found as homodimers, each monomer consisting of an oxygenase and a reductase domain.⁸ The reductase domain binds flavin adenine dinucleotide (FAD) and flavin mononucleotide (FMN), cofactors that shuttle electrons from nicotinamide adenine dinucleotide phosphate (NADPH),⁹ the ultimate source of electrons for the reaction, to the oxygenase domain where substrate oxidation occurs. The oxygenase domain contains a thiolate-ligated heme (protoporphyrin IX, or P-IX) as in cytochromes P450 (P450) and (6R)-5,6,7,8-tetrahydrobiopterin (pterin, H₄B).⁸ NO is produced when this domain is supplied with electrons from the reductase domain to activate dioxygen,¹⁰ and in the presence of fully reduced pterin cofactor.^{11, 12} Although structural characterization of full-length NOS has not been reported to date, structures of individual domains are known.^{13, 14}

The mechanism of NO production is incompletely understood.¹⁵ The resting state of the enzyme is a six-coordinate ferric heme with a water molecule occupying the sixth ligand position (four positions are occupied by N donors from the porphyrin, one by a sulfur atom from an axial cysteine, Cys194).¹⁶ Although neither Arg nor ArgOH ligates the heme, substrate binding shifts

both the Soret absorption maximum and the heme spin state.^{7, 17} One-electron reduction of the NOS:substrate complex gives a five-coordinate ferrous that readily binds dioxygen, forming a ferrous-oxy species (equivalent to ferric superoxide),⁸ the last observed intermediate in the catalytic cycle.^{8, 18}

The role of pterin has been extensively investigated.^{11, 16, 19} This molecule binds in a pocket alongside the heme, forming hydrogen bonds with a P-IX carboxylate, thereby coupling it to the active site.¹³ It is known that a pterin-based radical forms and is reduced during the catalytic cycle, as determined by analysis of results from rapid-freeze EPR experiments.^{12, 20} Turnover has never been observed without fully reduced pterin cofactor.²¹

The NOS reaction cycle bears many similarities to that of P450s. P450s contain thiolate-heme active sites and hydroxylate substrates via two-electron oxidation processes.^{22, 23} The P450 cycle also begins with substrate binding followed by heme reduction, dioxygen binding, and another reduction step leading to the formation of a high-valent iron-oxo complex (Compound I) that hydroxylates the substrate (**Scheme 2**).²³ Separate enzymes serve as reductases for P450s, but substrate hydroxylation can be driven using external sources of electrons.²⁴ Owing to these similarities, the mechanism of the first turnover of NOS is postulated to be the same as that of P450s.²⁵ However, the second turnover, a three-electron oxidation, is thought to employ a unique mechanism.²⁶ It has been suggested that a protonated ferric hydroperoxide may act as the nucleophile in the second turnover¹⁸ rather than Compound I, which is a ferryl P-IX radical cation.⁸



Scheme 2: Proposed NOS catalytic cycle; active-site intermediates that have not been observed are shown in red.

Steps in the mechanistic cycle borrowed from P450 are shown in **Scheme 2**. Although several intermediates in the P450 cycle already have been observed, there can be no doubt that “the hunt for an unambiguous experimental identification of the ephemeral active oxygen species will most certainly continue.”²² If that is the case for P450, then we may conclude that work on the NOS catalytic cycle is just beginning.

A long-standing goal in our group is the development of methods to generate and observe high-valent iron-oxo complexes that are believed to play key roles as intermediates in the catalytic cycles of heme enzymes.²⁷ Direct observation during turnover would allow definitive identification of the active oxidant. Drawing on studies of similar enzymes and using EPR under cryogenic conditions and X-ray crystallography, investigators have amassed a large body of evidence that strongly indicates that Compound I (**Scheme 2**, the ferryl P-IX radical cation shown in red) is the active species.²⁸ The steps leading to formation of this highly reactive species are slow, making its observation problematic, as at best it is present in very low concentrations during catalysis.

We have investigated the redox photochemistry of two heme enzymes, microperoxidase-8 (MP-8, a heme octapeptide fragment of cytochrome *c*) and horseradish peroxidase (HRP).²⁹ Visible excitation of $\text{Ru}(\text{bpy})_3^{2+}$ (bpy is 2,2'-bipyridine) in the presence of oxidative quenchers in solution generates a powerful Ru(III)-diimine oxidant, which reacts rapidly with P-IX to form the P-IX radical cation, which then oxidizes Fe(III) to give high-valent iron-oxo complexes of MP-8 and HRP.^{29, 30} Attempts to generate high-valent hemes in P450s in reactions with uncomplexed photogenerated oxidants were not successful so we changed course, as discussed in the following section.

CHANNEL-BINDING WIRES

Since 1999 we have developed sensitizer-linked electron tunneling wires that are able to deliver electrons and holes rapidly to and from deeply buried active sites of heme enzymes.^{31, 32} Attaching the photosensitizer to the substrate promotes a close interaction between the two, and increases the probability of ET (**Figure 1**). A selection of such molecules developed for the oxygenase domain of iNOS is shown in **Chart 1**.

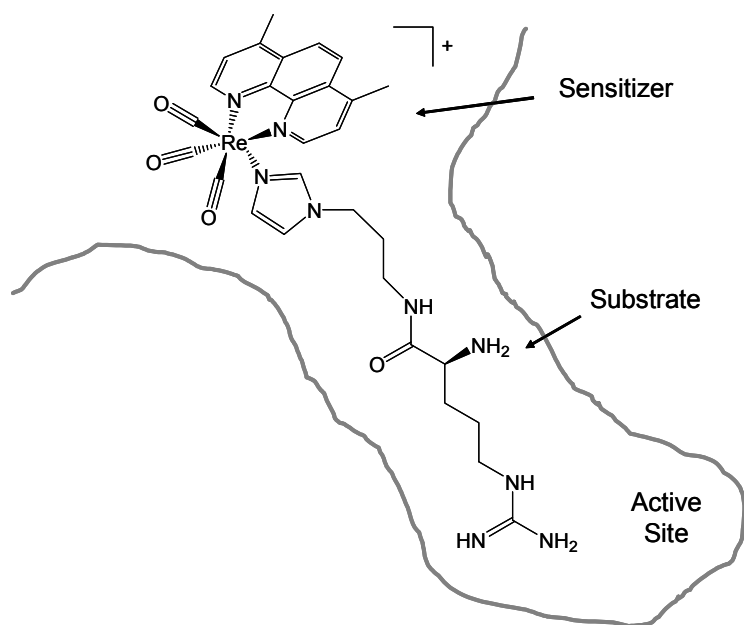


Figure 1: Substrates linked to sensitizers target active-site channels of enzymes.

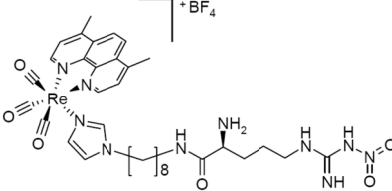
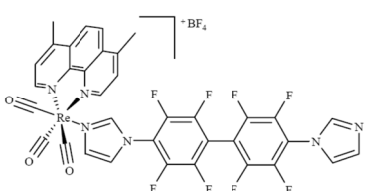
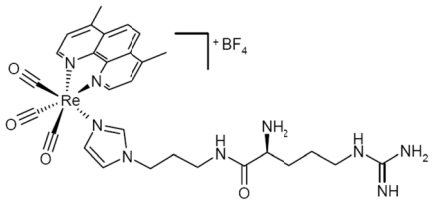
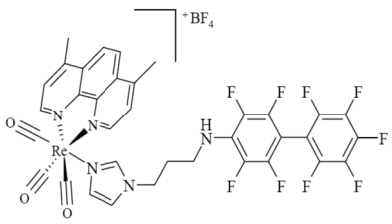
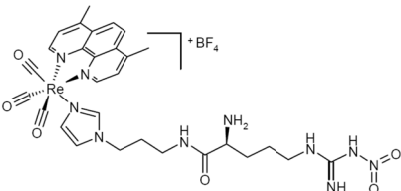
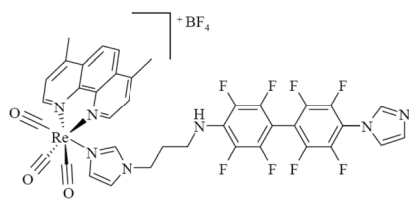
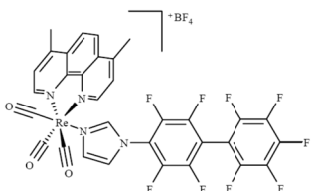
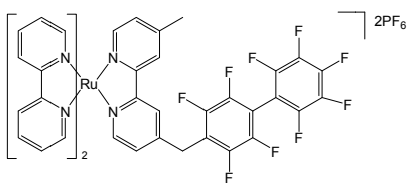
<i>Channel-Binding Wires</i>	
 <p>1: 3 μM</p>	 <p>5: 0.13 μM</p>
 <p>2: 2 μM</p>	 <p>6: < 10 μM</p>
 <p>3: 7 μM</p>	 <p>7: < 10 μM</p>
 <p>4: 1.4 μM</p>	 <p>8: 6.5 μM</p>

Chart 1: Ru(II) and Re(I) electron tunneling wires bind to the oxygenase domain of murine inducible nitric oxide synthase (iNOSoxy).^{18, 33}

The dissociation constants of complexes that contain wires in the substrate channels of enzymes can be determined from analysis of shifts in Soret absorptions. Examples of these shifts in the case of iNOSoxy are shown in **Figure 2**.³⁴

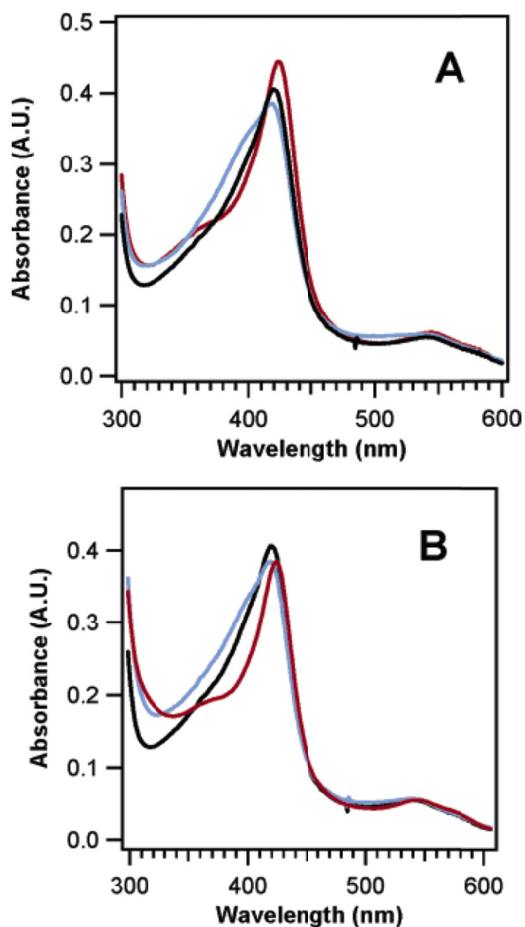


Figure 2: UV-visible absorption spectra of iNOSoxy: wire complexes. (A) iNOSoxy alone (5 μ M; black) and bound to 1 equivalent each of **5** (red) and **4** (blue). (B) iNOSoxy alone (5 μ M; black) and bound to 1 equivalent each of **7** (red) and **6** (blue).

The wires luminesce upon 355 nm (Re(I)) or 480 nm (Ru(II)) excitation. The emission overlap with heme absorptions triggers Förster energy transfer (FET), which accounts for the steady-state emission quenching observed upon binding of wires to iNOSoxy (**Figure 3**).³⁴

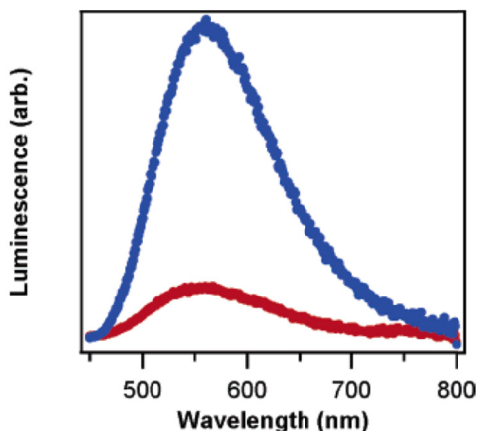


Figure 3: Steady-state luminescence spectra of **5** (2 μ M; blue) and a 1:1 mixture of **5** and iNOSoxy (2 μ M; red) with $\lambda_{\text{ex}} = 355$ nm.

Transient absorption measurements demonstrate that these wires reduce iNOSoxy upon 355 or 480 nm excitation. Reduction is indicated by a bleach near 420 nm, corresponding to the disappearance of the six-coordinate Fe(III) resting state and the formation of a new species (with absorption near 445 nm) assigned to six-coordinate Fe(II). Difference spectra were constructed from single-wavelength transient absorption traces 80 ns after excitation of the protein-bound wire **7** (**Figure 4**, blue) and 3 μ s after excitation of protein-bound wire **5** (**Figure 4**, red).

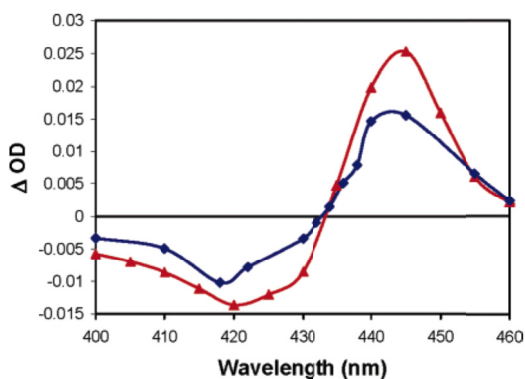


Figure 4: Difference spectra of a 1:1 mixture of **7** and iNOSoxy (5 μ M, 80 ns after 355 nm excitation, blue squares) and a 1:1 mixture of **5** and iNOSoxy (11 μ M, 3 μ s after 355 nm excitation, red triangles) showing a bleach of a six-coordinate Fe(III) Soret (420 nm) and the appearance of a six-coordinate Fe(II) Soret (445 nm). Individual points were taken from single-wavelength transient absorption traces.

Picosecond transient absorption measurements demonstrate rapid formation of Fe(II) in the presence of wires **5** and **7**. By pumping with 70 ps, 355 nm pulses and probing with 442 nm radiation from a continuous wave He:Cd laser, we obtained transient absorbance traces that

document the formation of a ferrous heme on very short timescales (**Figure 5**). The traces were fit to a single exponential to give $k_f = 7(3) \times 10^9 \text{ s}^{-1}$ for formation of Fe(II).

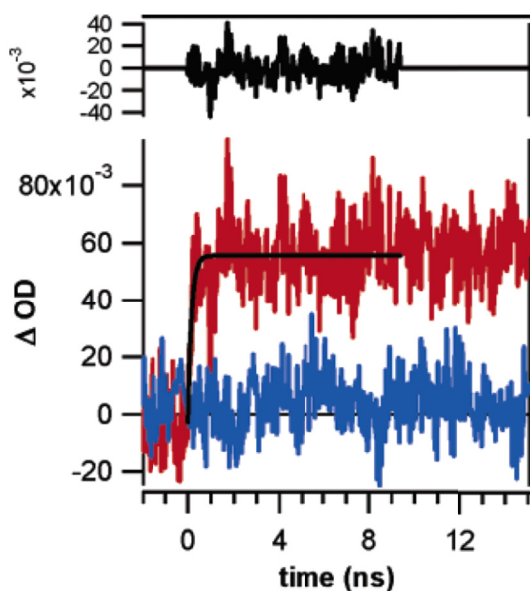


Figure 5: Transient absorbance at 442 nm of iNOSoxy alone (8 μM , blue) and in the presence of excess **5** (red) with $\lambda_{\text{ex}} = 355 \text{ nm}$. The red trace shows the rapid formation of ferrous heme fit to one exponential ($k_f = 7(3) \times 10^9 \text{ s}^{-1}$, black) with the residual shown above.

Although the demonstration of very rapid electron transfer to a heme active site represents a step toward the goal of observing high-valent intermediates, our electron delivering wires block access to substrate channels (**Figure 6**).³³ We have exploited this property of channel binders in the construction of highly selective amine oxidase inhibitors by manipulation of the linker elements of wire structures.³⁵

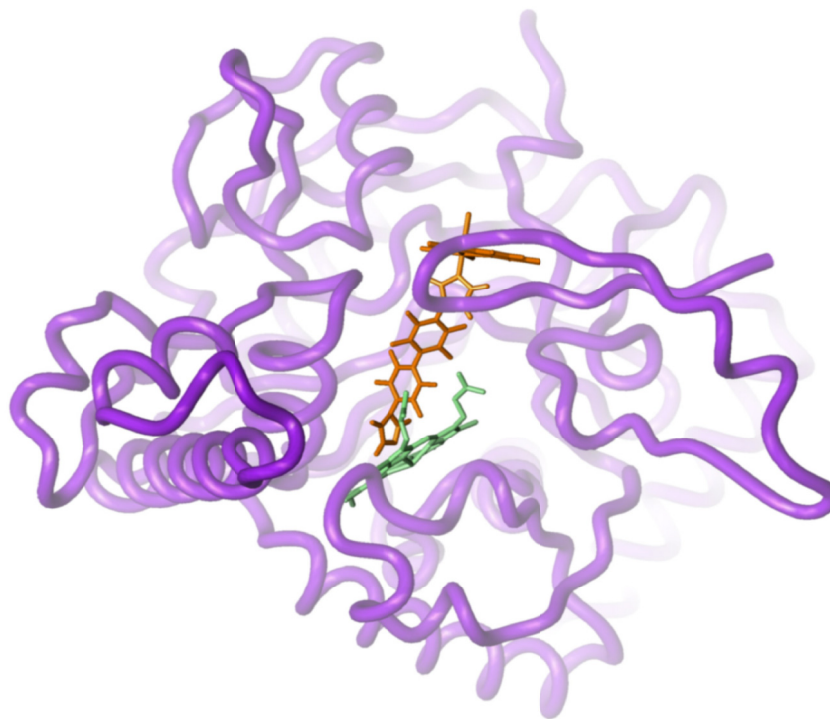


Figure 6: Structural model of Re-perfluorobiphenyl wire **5** in the substrate channel of iNOSoxy.³⁶

SURFACE-BINDING WIRES

We are investigating wires that bind on enzyme surfaces, as they are much less likely to impede substrate binding (**Chart 2**). The luminescence of wire **9** is quenched upon binding to iNOSoxy (**Figure 7**), and addition of channel binder **5** does not alter the decay rate.

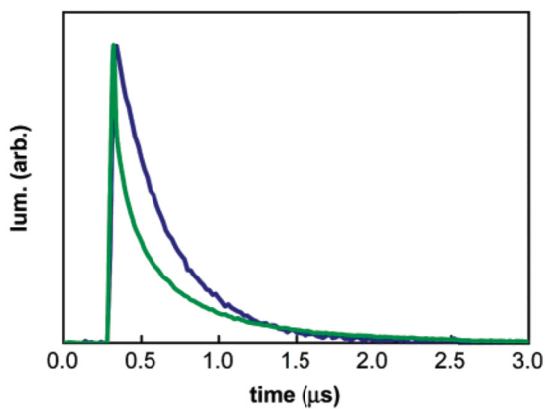


Figure 7: Transient decay data for **9** (blue) and a 1:1 mixture of **9** and iNOSoxy (1.8 μM; green). The fast component of the luminescence decay is assigned to the complex between **9** and iNOSoxy.

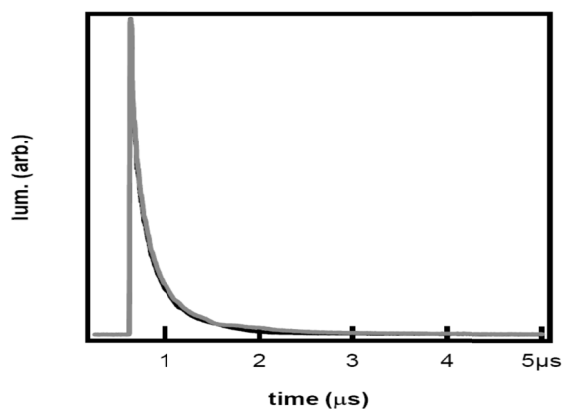


Figure 8: Transient luminescence decay data for a 2:1 mixture of **9** with iNOSoxy (black) and a 2:1:1 mixture of **9**, **5**, and iNOSoxy (gray). In the second mixture, **5** was shown by UV-visible absorption spectroscopy to be bound in the active site. Since the luminescence decay of **9** was not disturbed by the binding of **5**, these traces indicate that **9** does not bind in the active-site channel.

Upon electronic excitation, surface binders **9-12** trigger ET without blocking substrate or cofactor binding, maintaining the potential for enzymatic turnover.

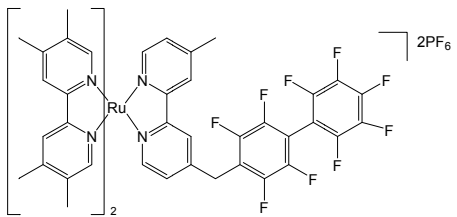
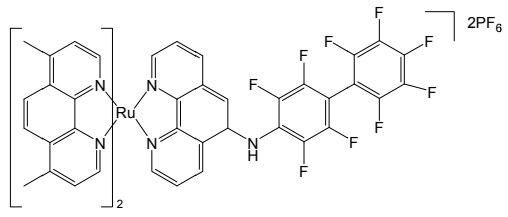
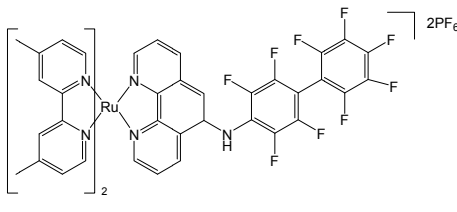
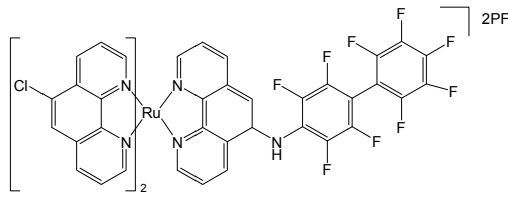
<i>Surface-Binding Wires</i>	
 <p>9: 0.58 μM</p>	 <p>11: 5 μM</p>
 <p>10: 0.5 μM</p>	 <p>12: 10 μM</p>

Chart 2: Four wires that bind on iNOSoxy surfaces.

We have shown that **9** binds to iNOSoxy independently of substrate and pterin with a dissociation constant of $< 1 \mu\text{M}$.³⁴ Binding distant from the active site is demonstrated by the

finding that a known channel binder does not displace **9** from the enzyme.³⁴ While the precise binding site has not been definitively established, FET measurements indicate that it may be in the hydrophobic pocket thought to be the docking site for the iNOS reductase domain.^{34, 37} Experiments with $\text{Ru}(\text{bpy})_3^{2+}$ show that the sensitizer alone does not bind to the enzyme, suggesting that the perfluorobiphenyl unit is largely responsible for the association of the wire with a hydrophobic iNOSoxy surface region.

Single-wavelength transient absorbance measurements with imidazole-bound iNOSoxy in the presence of one equivalent of **9**, 10 mM ascorbate, and saturated tetramethylphenylenediamine (TMPD) confirm that Fe(II) forms within 50 ns of excitation at 480 nm (**Figure 9**).³⁸ A difference spectrum constructed from the single-wavelength data at 2 μs (**Figure 10**) shows the bleach of the imidazole-Fe(III) Soret absorption peak at 428 nm and the development of the imidazole-Fe(II) feature at 445 nm. Control experiments with $\text{Ru}(\text{bpy})_3^{2+}$ demonstrate that the perfluorobiphenyl moiety of **9** is required for heme reduction. In the presence of $\text{Ru}(\text{bpy})_3^{2+}$ and quenchers, transient absorbance traces show only the production of $\text{Ru}(\text{I})$.³⁸

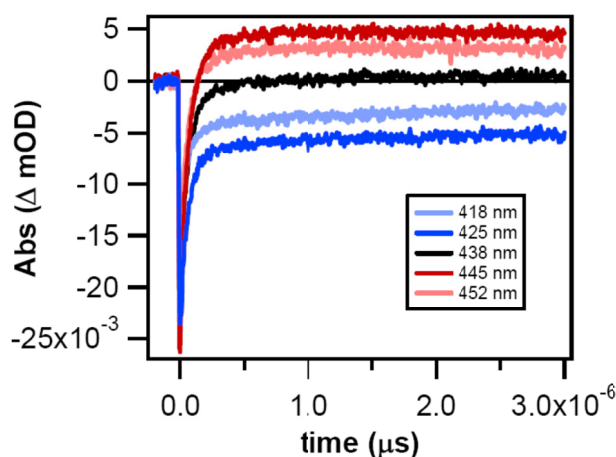


Figure 9: Transient absorbance of imidazole-iNOSoxy bound to 1 equivalent of **9** (11 μM with 10 mM ascorbate and saturated TMPD). $\lambda_{\text{ex}} = 480 \text{ nm}$.

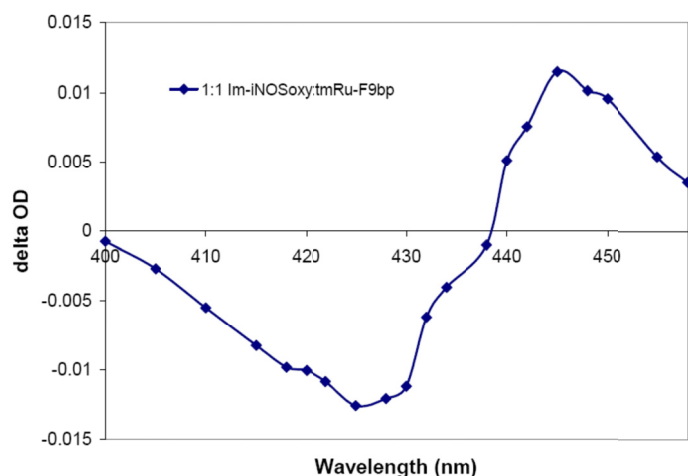


Figure 10: Transient absorbance of a 1:1 mixture of imidazole-iNOSoxy and **9** (22 μM with 10 mM ascorbate and saturated TMPD) showing a characteristic Fe(III/II) difference spectrum. Individual points were taken from single-wavelength transient absorbance traces, 2 μs after 480 nm excitation.

To estimate the specific rate of Fe(II) formation, $^*\text{Ru(II)}$ contributions were subtracted from the transient absorbance data.³⁸ Representative traces are shown in **Figure 11**. The traces were fit to a single-exponential function to obtain $k_{\text{ET}} = 2(1) \times 10^7 \text{ s}^{-1}$.

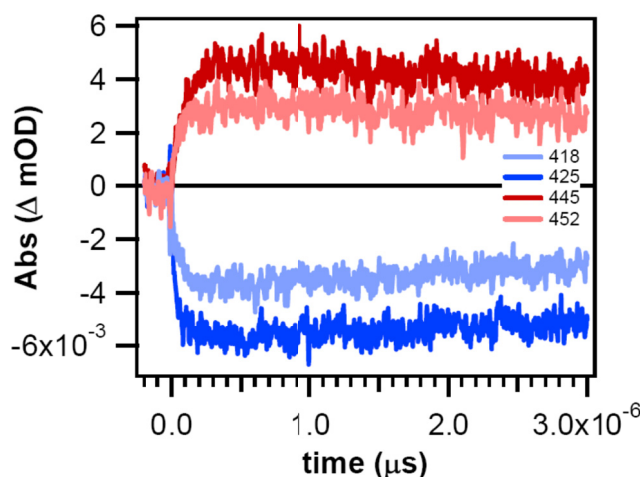


Figure 11: Transient absorbance of imidazole-iNOSoxy bound to 1 equivalent of **9** (11 μM with 10 mM ascorbate and saturated TMPD) corrected for absorbance due to $^*\text{Ru(II)}$ to reveal $k_{\text{ET}} = 2(1) \times 10^7 \text{ s}^{-1}$.

This is a remarkably fast reduction given the estimated Ru-Fe distance of 20.2 \AA ³⁴ and the absence of a through-bond pathway to the heme. Given its slim profile, hydrophobicity, and potential to π -stack with aromatic residues, the perfluorobiphenyl moiety of **9** could penetrate into the protein interior, leaving open the possibility of a through-wire hopping mechanism.¹⁸

CONCLUSIONS

We have developed a system in which the heme of inducible nitric oxide synthase can be photoreduced rapidly without interfering with substrate or cofactor binding. Employing flash-quench experiments with a surface-binding Ru-diimine wire in combination with reductive quenchers, we observed ET to the imidazole-bound heme of iNOSox fully seven orders of magnitude faster than the natural reduction. This finding represents an important step toward our goal of identifying reactive intermediates in the catalytic cycles of heme oxotransferases.

ACKNOWLEDGEMENTS

Our work is supported by the NIH (DK19038 and GM070868 to HBG; GM068461 to JRW); the Ellison Medical Foundation (Senior Scholar Award in Aging to HBG); an NSF graduate fellowship (CAW); the Fannie and John Hertz Foundation (ARD); the Parsons Foundation (WBB); and the Arnold and Mabel Beckman Foundation.

References

1. Palmer RMJ, Ferrige AG and Moncada S. *Nature*. 1987; **327**: 524-526.
2. Xie QW, Cho HJ, Calaycay J, Mumford RA, Swiderek KM, Lee TD, Ding AH, Troso T and Nathan C. *Science*. 1992; **256**: 225-228.
3. Sagami I, Sato Y, Noguchi T and Miyajima M. *Coord. Chem. Rev.* 2002; **226**: 179-186.
4. Li HY, Igarashi J, Jamal J, Yang WP and Poulos TL. *J. Biol. Inorg. Chem.* 2006; **11**: 753-768.
5. Stuehr DJ, Santolini J, Wang ZQ, Wei CC and Adak S. *J. Biol. Chem.* 2004; **279**: 36167-36170.
6. Marletta MA. *J. Biol. Chem.* 1993; **268**: 12231-12234.
7. Hurshman AR and Marletta MA. *Biochemistry*. 1995; **34**: 5627-5634.
8. Alderton WK, Cooper CE and Knowles RG. *Biochem. J.* 2001; **357**: 593-695.
9. Stuehr DJ, Cho HJ, Kwon NS, Weise MF and Nathan CF. *Proc. Nat. Acad. Sci. USA*. 1991; **88**: 7773-7777.
10. Hurshman AR and Marletta MA. *Biochemistry*. 2002; **41**: 3439-3456.
11. Hevel JM and Marletta MA. *Biochemistry*. 1992; **31**: 7160-7165.
12. Hurshman AR, Krebs C, Edmondson DE, Huynh BH and Marletta MA. *Biochemistry*. 1999; **38**: 15689-15696.
13. Crane BR, Arvai AS, Ghosh DK, Wu CQ, Getzoff ED, Stuehr DJ and Tainer JA. *Science*. 1998; **279**: 2121-2126.
14. Garcin ED, Bruns CM, Lloyd SJ, Hosfield D, Tiso M, Stuehr DJ, Tainer JA and Getzoff ED. *J. Biol. Chem.* 2004; **279**: 37918-37927.
15. Zhu Y and Silverman RB. *Biochemistry*. 2008.
16. Presta A, Weber-Main AM, Stankovich MT and Stuehr DJ. *J. Am. Chem. Soc.* 1998; **120**: 9460-9465.
17. Lippard SJ, Berg, J. M. *Principles of Bioinorganic Chemistry*. Mill Valley, CA: University Science Books; 1994.
18. Belliston-Bittner W, Dunn AR, Nguyen YHL, Stuehr DJ, Winkler JR and Gray HB. *J. Am. Chem. Soc.* 2005; **127**: 15907-15915.
19. Wang ZQ, Wei CC, Santolini J, Panda K, Wang Q and Stuehr DJ. *Biochemistry*. 2005; **44**: 4676-4690.
20. Wei CC, Wang ZQ, Hemann C, Hille R and Stuehr DJ. *J. Biol. Chem.* 2003; **278**: 46668-46673.
21. Ghosh DK, Wu CQ, Pitters E, Moloney M, Werner ER, Mayer B and Stuehr DJ. *Biochemistry*. 1997; **36**: 10609-10619.
22. Denisov IG, Makris TM, Sligar SG and Schlichting I. *Chem. Rev.* 2005; **105**: 2253-2277.
23. Meunier B, de Visser SP and Shaik S. *Chem. Rev.* 2004; **104**: 3947-3980.
24. Udit AK, Hill MG and Gray HB. *Langmuir*. 2006; **22**: 10854-10857.
25. Udit AK, Belliston-Bittner W, Glazer EC, Le Nguyen YH, Gillan JM, Hill MG, Marletta MA, Goodin DB and Gray HB. *J. Am. Chem. Soc.* 2005; **127**: 11212-11213.
26. Martin NI, Woodward JJ, Winter MB, Beeson WT and Marletta MA. *J. Am. Chem. Soc.* 2007; **129**: 12563-12570.

27. Green MT, Dawson JH and Gray HB. *Science*. 2004; **304**: 1653-1656.
28. Wang R and de Visser SP. *J. Inorg. Biochem.* 2007; **101**: 1464-1472.
29. Berglund J, Pascher T, Winkler JR and Gray HB. *J. Am. Chem. Soc.* 1997; **119**: 2464-2469.
30. Low DW, Winkler JR and Gray HB. *J. Am. Chem. Soc.* 1996; **118**: 117-120.
31. Wilker JJ, Dmochowski IJ, Dawson JH, Winkler JR and Gray HB. *Angew. Chem. Int. Edit.* 1999; **38**: 89-92.
32. Dmochowski IJ, Dunn AR, Wilker JJ, Crane BR, Green MT, Dawson JH, Sligar SG, Winkler JR and Gray HB. *Method. Enzymol.* 2002; **357**: 120-133.
33. Nguyen YHL. *Wiring Inducible Nitric Oxide Synthase*. Pasadena, CA: Department of Chemistry, California Institute of Technology; 2006.
34. Dunn AR, Belliston-Bittner W, Winkler JR, Getzoff ED, Stuehr DJ and Gray HB. *J. Am. Chem. Soc.* 2005; **127**: 5169-5173.
35. Langley DB, Brown DE, Cheruzel LE, Contakes SM, Duff AP, Hilmer KM, Dooley DM, Gray HB, Guss JM and Freeman HC. *J. Am. Chem. Soc.* 2008; **130**: 8069-8079.
36. Belliston-Bittner W. *Ultrafast Photoreduction of Nitric Oxide Synthase by Electron Tunneling Wires*. Pasadena, CA: Chemistry, California Institute of Technology; 2005.
37. Garcin ED, Bruns CM, Lloyd SJ, Hosfield DJ, Tiso M, Gachhui R, Stuehr DJ, Tainer JA and Getzoff ED. *J. Biol. Chem.* 2004; **279**: 37918-37927.
38. Belliston-Bittner W, Dunn AR, Winkler JR and Gray HB. *submitted*. 2008.

Appendix II

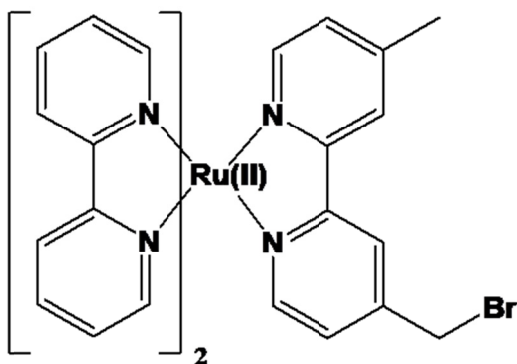
Labeling gsNOS with Ru-diimine Photosensitizers

AII.1 Introduction and Summary

The Gray group's interest in NOS focuses on the nature of the putative high-valent intermediates in the catalytic cycle. To study these, we have expressed a mutant with a single solvent-exposed cysteine residue and attached a ruthenium tris-diimine complex as a photosensitizer. We use the Ru complex and a laser-induced flash/quench scheme to pull electrons out of the active site to generate high-valent species, which we characterize by transient absorption spectroscopy.

In order to photochemically generate high-valent species of the heme center in nitric oxide synthase, mutant forms of the enzyme from *Geobacillus stearothermophilus* were expressed.* The enzyme contains more than a dozen surface-exposed histidine residues, so cysteine labeling is the preferred method for attaching the photosensitizer. There are four native cysteine residues in gsNOS at positions 76, 161, 227, and 269. Cys76 ligates the iron center and is necessary for enzymatic function. Cys161 is fully buried within the core of the protein and inaccessible to solution. Positions 227 and 269 were mutated to serine residues in order to prevent them from interfering with labeling reactions. First, a cysteine was installed close to the heme at position 84 (only 8 residues from the axial thiolate ligand). This position failed to label. Another position, K115, was mutated to a cysteine and this mutant was successfully labeled on two occasions (K115C/C227S/C269S). All of these plasmids can be found in the -20 alumni freezer in the box labeled Charlotte NOS.

The first molecule synthesized for labeling purposes was the photosensitizer shown below in **Scheme 1**. This molecule was attached to the mutant gsNOS protein on two occasions. Labeling conditions and synthetic details can be found below.



Scheme 1. The ruthenium photosensitizer used for labeling gsNOS.

AII.2 Materials and Methods

4-(bromomethyl)-4'-methyl-2,2'-bipyridine was synthesized according to published methods: Gould *et al.*, *Inorg. Chem.* **1991**, 30, 2942–2949, Strouse *et al.* *Inorg. Chem.* **1995**, 34, 473–487, and Geren *et al.*, *Biochem.* **1991**, 30, 9450–9457.

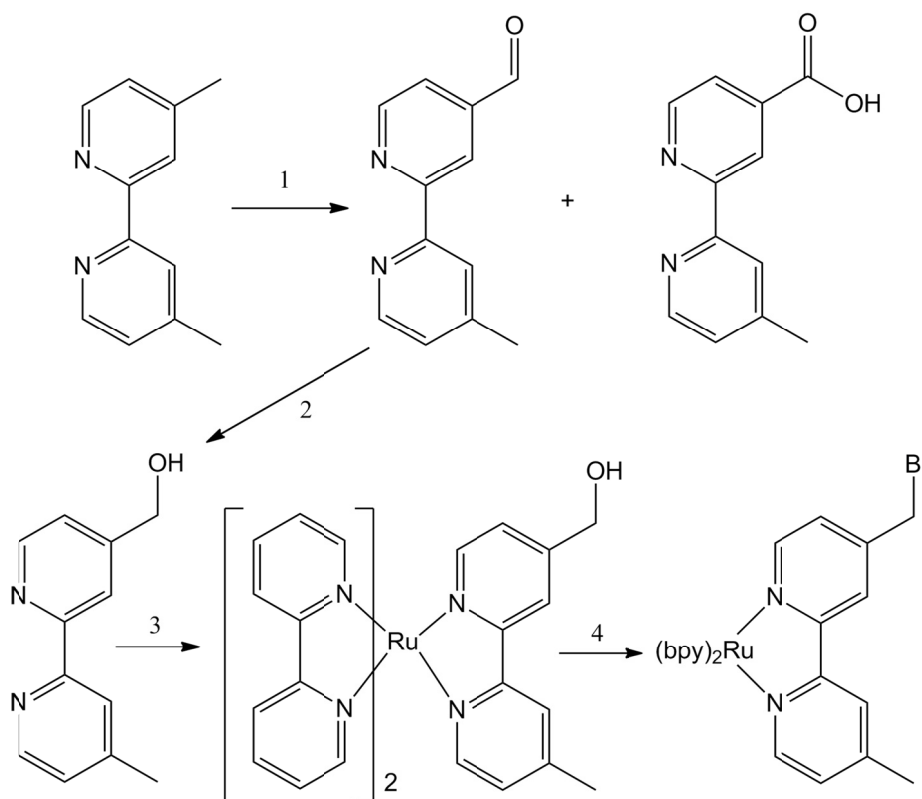
(1) 2g (0.011 mol) of 4,4'-dimethyl-2,2'-bipyridine were dissolved in 120 mL of dioxane (warm the mixture a little if it doesn't all dissolve). 2g of SeO₂ (0.018 mol) were added to this solution and it was refluxed for 24 hours. After cooling, the solution was filtered to remove the black precipitate. (The papers say to filter while hot to remove the black precipitate, let it cool, then again to collect a yellow precipitate. I found this unnecessary as no yellow precipitate ever crashed out.) The dioxane was removed by rotovapping and then the residue was redissolved in chloroform. The solution was again filtered to remove anything insoluble in chloroform. The chloroform was removed and the residue was redissolved in 200 mL of ethyl acetate. The ethyl acetate solution was extracted with 1 x 25 mL of 0.1 M NaCO₃ (aqueous) to remove the carboxylic acid product (see **Scheme 2**) which was discarded. The ethyl acetate solution was again extracted, this time with 3 x 30 mL of 0.2 M NaHSO₃ (aqueous sodium bisulfate solution). It turned pink. The pink aqueous fractions were then combined and extracted

with 4 x 25 mL of dichloromethane. The pink color remains in the aqueous fraction. The DCM is then rotovapped to give pure product. Yield, 20%. For NMR characterization see Strouse et al.

(2) 0.249 g of the product from (1) was dissolved in 15 mL of methanol. This solution was submerged in an ice bath. 6 mL of a solution of 0.2 M NaOH was prepared, and 55 mg of sodium borohydride (NaBH_4) was added to the NaOH solution. After ample time for cooling of the methanol, the borohydride was added dropwise to it. This mixture was allowed to stir on ice for a few minutes before removal of the ice bath and stirring for another hour at room temperature. The methanol was removed leaving a suspension of white solid in the aqueous fraction of the reaction. To this 6 mL of saturated Na_2CO_3 aqueous solution was added. This aqueous mixture was then extracted 4 times with 15 mL of chloroform. The chloroform was dried using MgSO_4 and then filtered and rotovapped to yield a white solid in > 90% yield.

(3) 193.6 mg (0.40 mmol) of cis-dichloroRu(bpy)₂ and 100 mg (0.50 mmol) 4-hydroxymethyl-4'-methylbipyridine (product of (2)) were added to a round bottom flask. This was dissolved in 100 mL of water and refluxed for 1 hour. It was then cooled, filtered, the liquid collected, and a solution of saturated NH_4PF_6 (aq.) was used to crash out the product. This was filtered and the product dried on a vacuum line.

(4) Once dry, the product from (3) was dissolved in 10 mL HBr and 1 mL H_2SO_4 and refluxed for approximately 5–6 hours. It was cooled and the product was precipitated using saturated NH_4PF_6 (aq.) again to precipitate the product. This was filtered and washed with ether and dried under vacuum to yield pure product.



Scheme 2. Synthesis of bromo-bpyRu(bpy)₂ photosensitizer.

This complex, the bromo-bpyRu(bpy)₂ photosensitizer, was used to label K115C/C227S/C269S gsNOS. Protein from 6L of growth was concentrated immediately after purification by gel filtration column (see Chapter 3). The entirety of clean gsNOS fractions was concentrated to under 10 mL in Tris buffer and desalted into 50 mM sodium phosphate buffer pH 8.0 (and 22 mL of roughly 10 μ M NOS was collected). 45 mg of the labeling complex was dissolved in 3 mL of DMSO and then 5 mL of water was added to this, making a stock solution of approximately 6.7 mM. 0.44 mL of this Ru-containing solution was added to the 10 mL of protein along TCEP to a final concentration of 1 mM (22 L in μ 22 mL). This solution was shaken in the cold room in the dark overnight (15 hours). A desalting column was used to remove the excess Ru complex. The solution was then loaded onto a HiTrap Q column. Buffer A = 50 mM

NaPi at pH 8.0, buffer B = 50 mM NaPi, pH 8.0 and 500 mM NaCl. A gradient was run from 0–70% B over 60 minutes at a rate of 2.5 mL/min (150 mLs or 30 column volumes). Elution was monitored at 280 nm (protein side chains), 400 nm (Soret band), and 460 nm (predominantly the Ru complex). Two large bands and one smaller shoulder came off the column, in that order, between 10 and 50% B. The mass spec of the first fraction corresponds to the mass of the protein (43863.6, calculated) plus the Ru complex (44460.8, calculated).

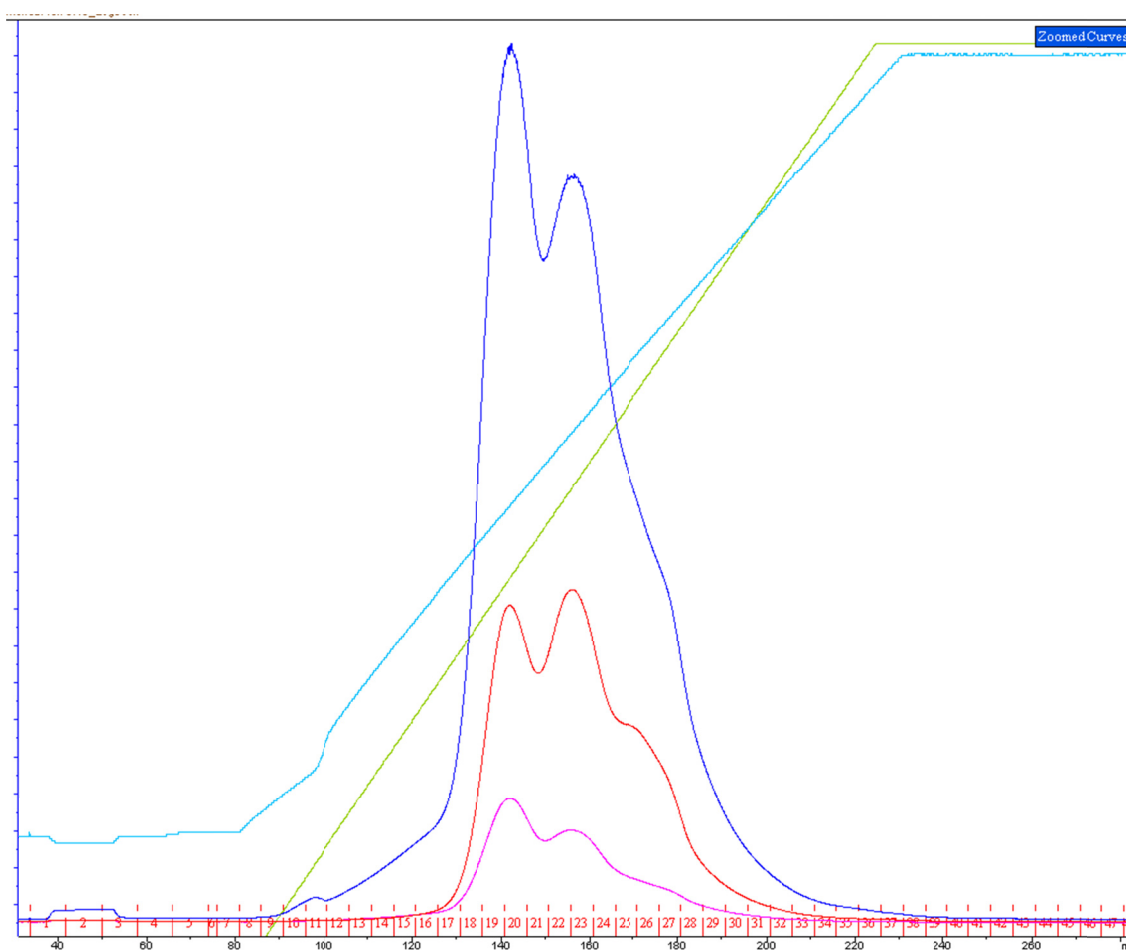


Figure 1. FPLC trace for labeled protein, the labeled fraction elutes first followed by unlabeled and another shoulder (mass corresponds to unlabeled as well).

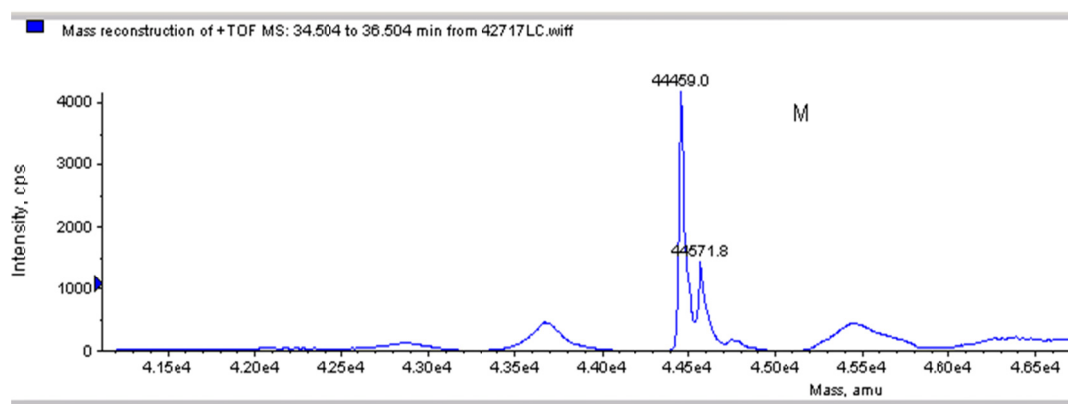


Figure 2. Mass spec of the first band to elute from Q column.

AII.3 Results

The presence of the label on the protein was confirmed by UV-vis and steady-state fluorescence spectroscopies.

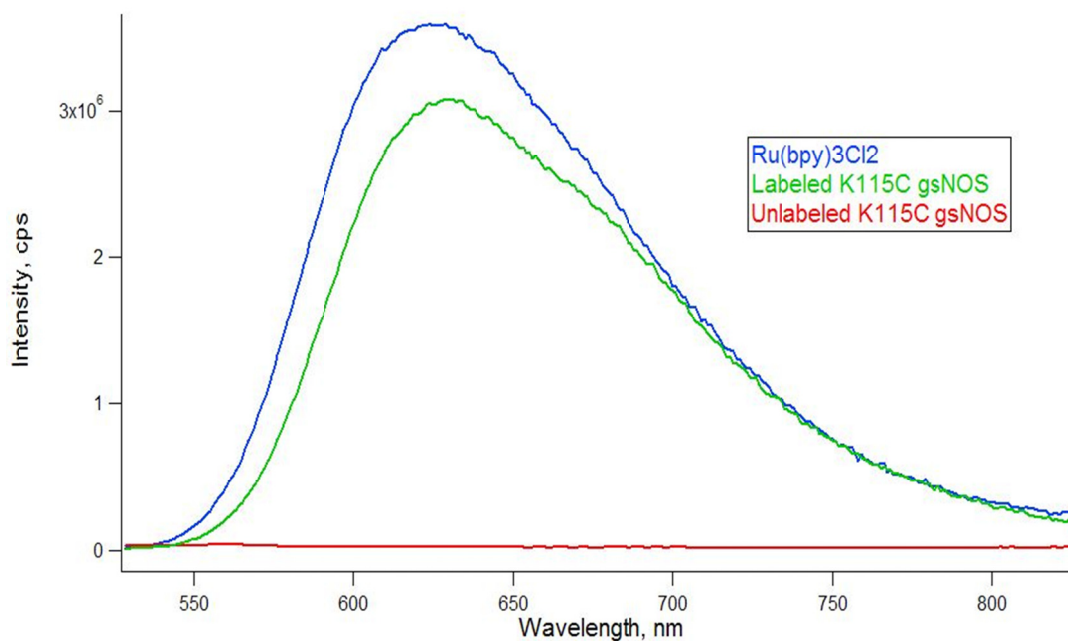


Figure 3. SSFL of labeled gsNOS in comparison with a comparable concentration of the model complex. A small amount of quenching is observed due to fluorescence resonant energy transfer to the heme in the enzyme.

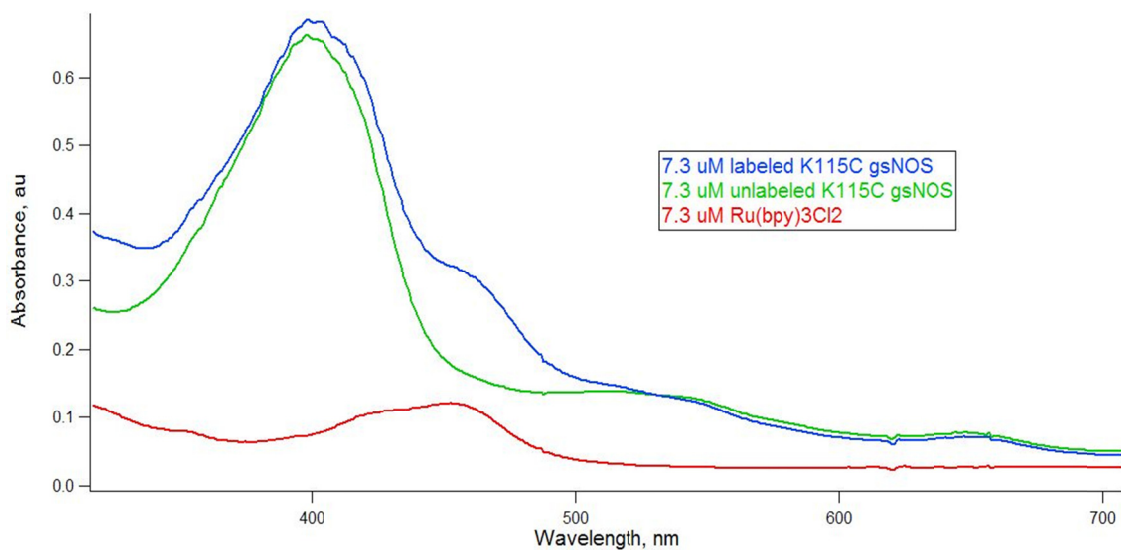


Figure 4. UV-vis spectra of model complex, unlabeled protein and the labeled protein.

The labeled NOS was then used in laser studies, with Ru-hexaammine as an oxidative quencher and Ru(bpy)₃ as a model complex for comparison.

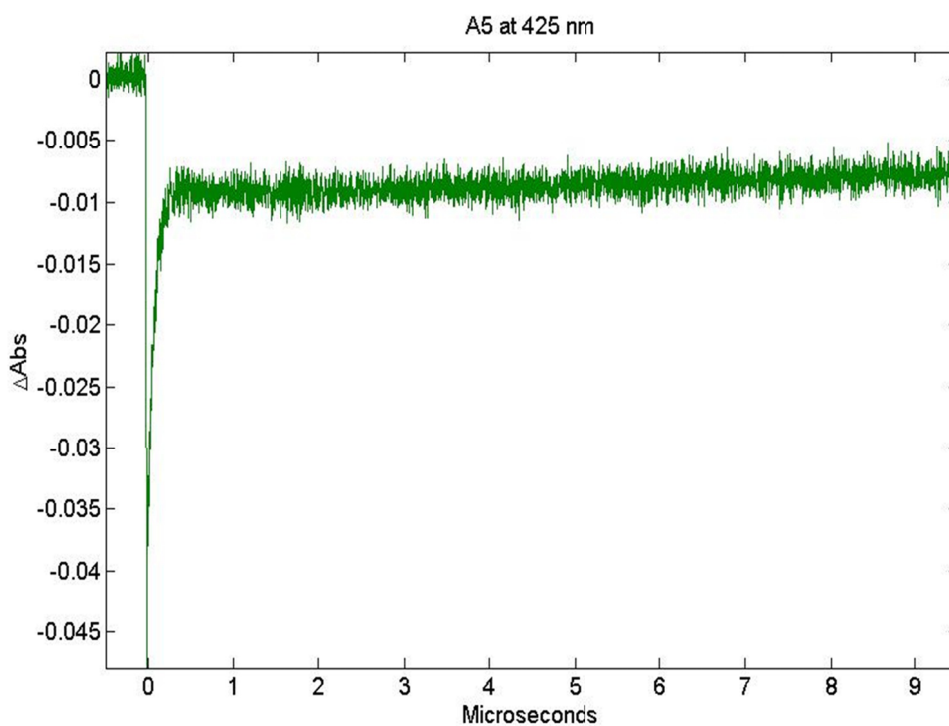


Figure 5. 8 μM Ru(bpy)₃²⁺ + 5 mM Ru(NH₃)₆³⁺ at 425 nm showing formation of Ru(III).

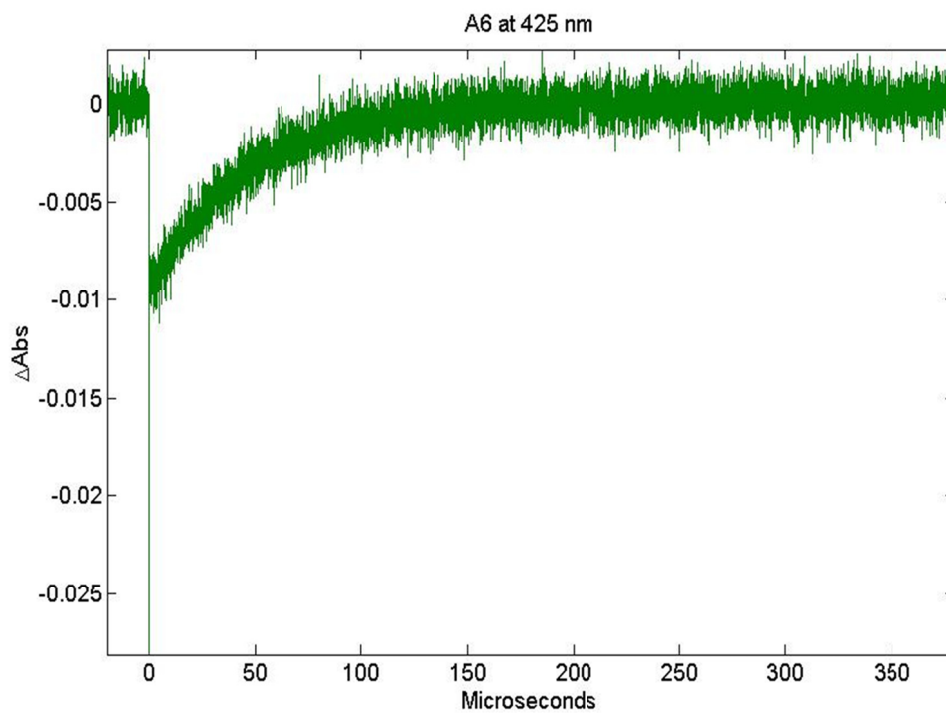


Figure 6. $8\ \mu\text{M}\ \text{Ru}(\text{bpy})_3^{2+} + 5\ \text{mM}\ \text{Ru}(\text{NH}_3)_6^{3+}$ at 425 nm showing decay of Ru(III).

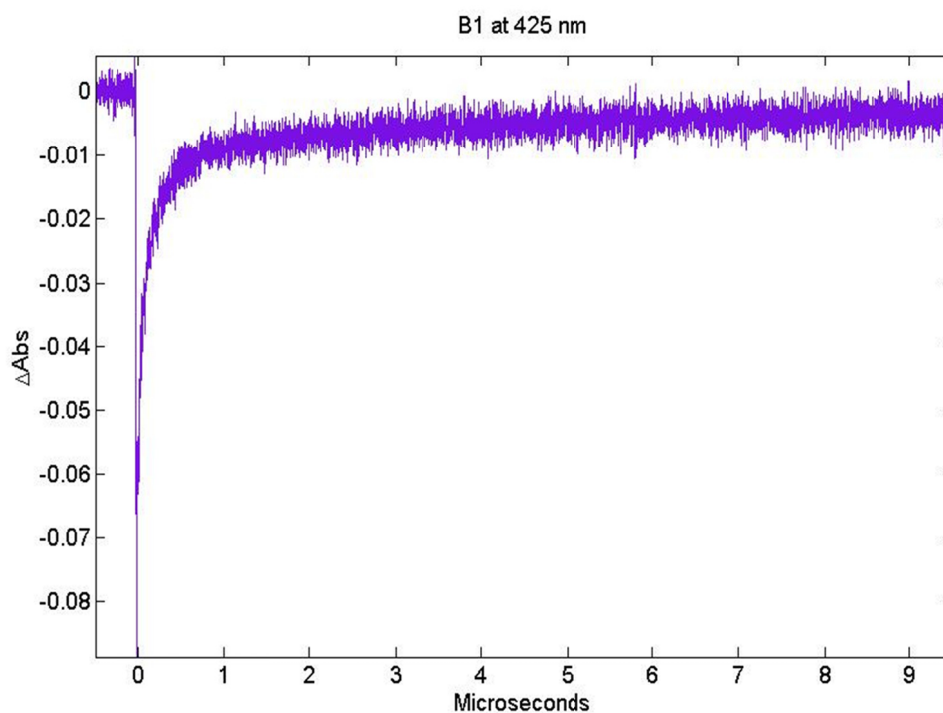


Figure 7. $8\ \mu\text{M}$ labeled gsNOS + $5\ \text{mM}\ \text{Ru}(\text{NH}_3)_6^{3+}$ at 425 nm showing formation of Ru(III) again.

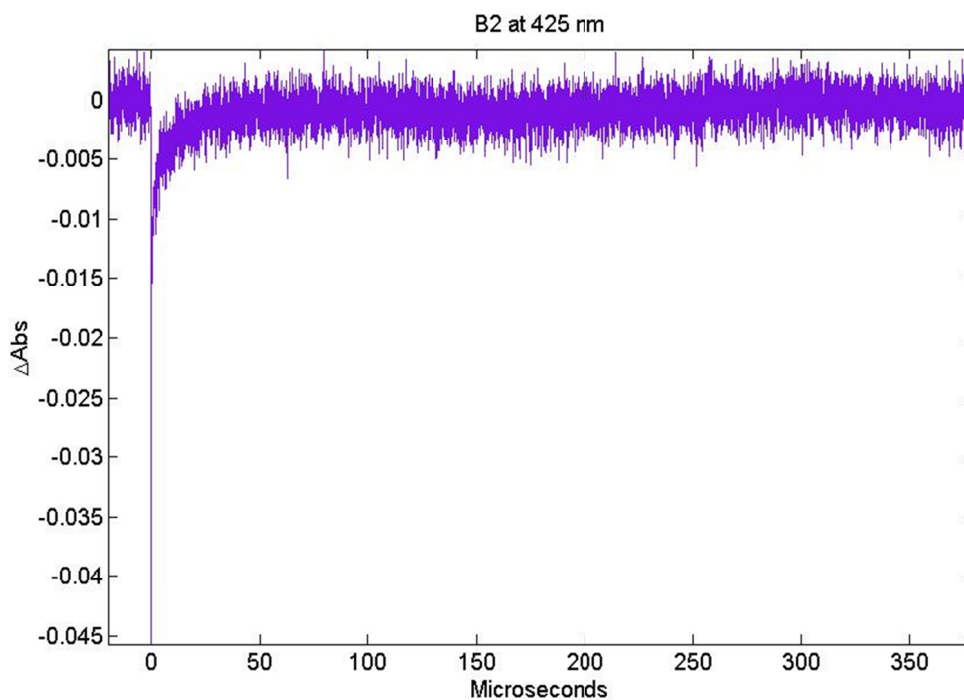


Figure 8. 8 μM labeled NOS + 5 mM $\text{Ru}(\text{NH}_3)_6^{3+}$ at 425 nm showing more rapid decay of Ru(III) in the presence of protein.

Unfortunately, no changes were observed in the Soret region, however, the Ru^{2+} signal recovers too quickly. Most likely, the strongly oxidizing Ru^{3+} is pulling an electron from another source, perhaps a tryptophan or tyrosine residue. A model was made (thanks to Kyle Lancaster) of the labeled protein, shown in **Figure 9**.

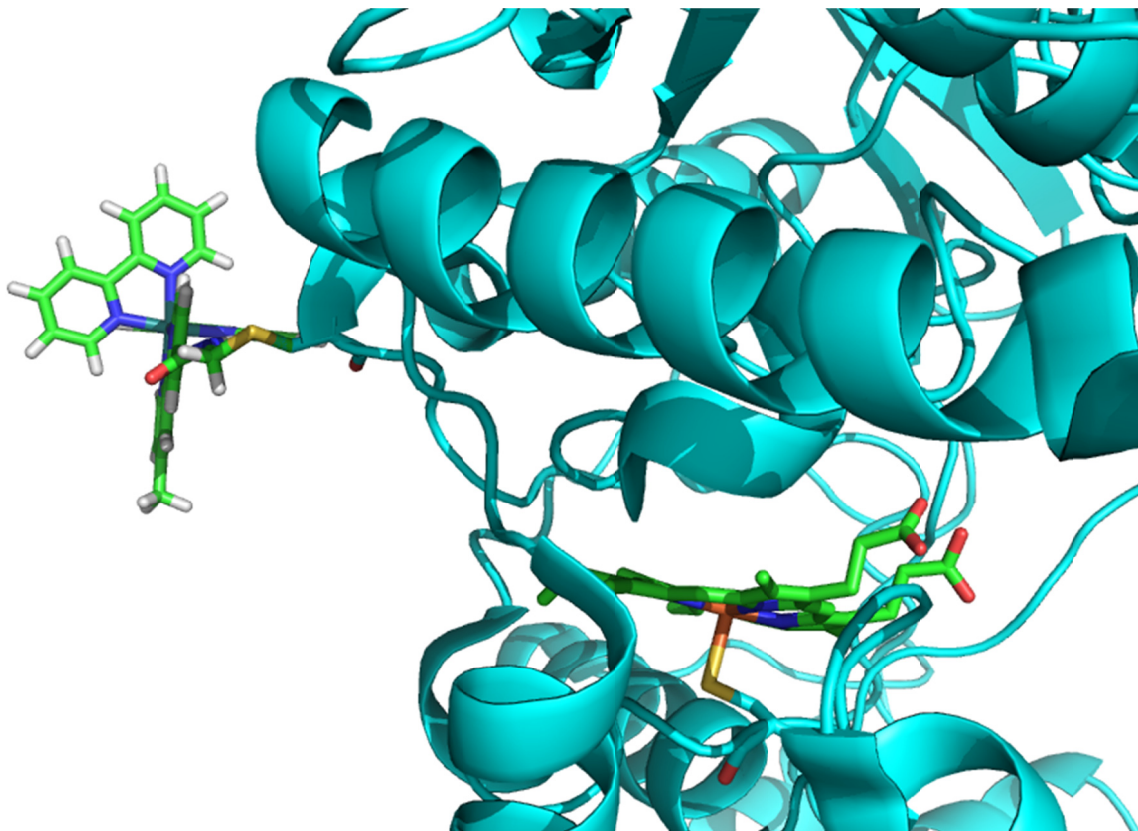


Figure 9. Model of the labeled protein showing proximity of the Ru to the heme.

Upon closer examination of the protein, we find 28 Trp and Tyr residues, including a tightly packed cluster, shown in **Figure 10**, including a patch that seems particularly close and easy to oxidize that contains a cluster of three of these residues (**Figure 11**). On its way to the heme, the hole may get side-tracked by these easily oxidized amino acids.

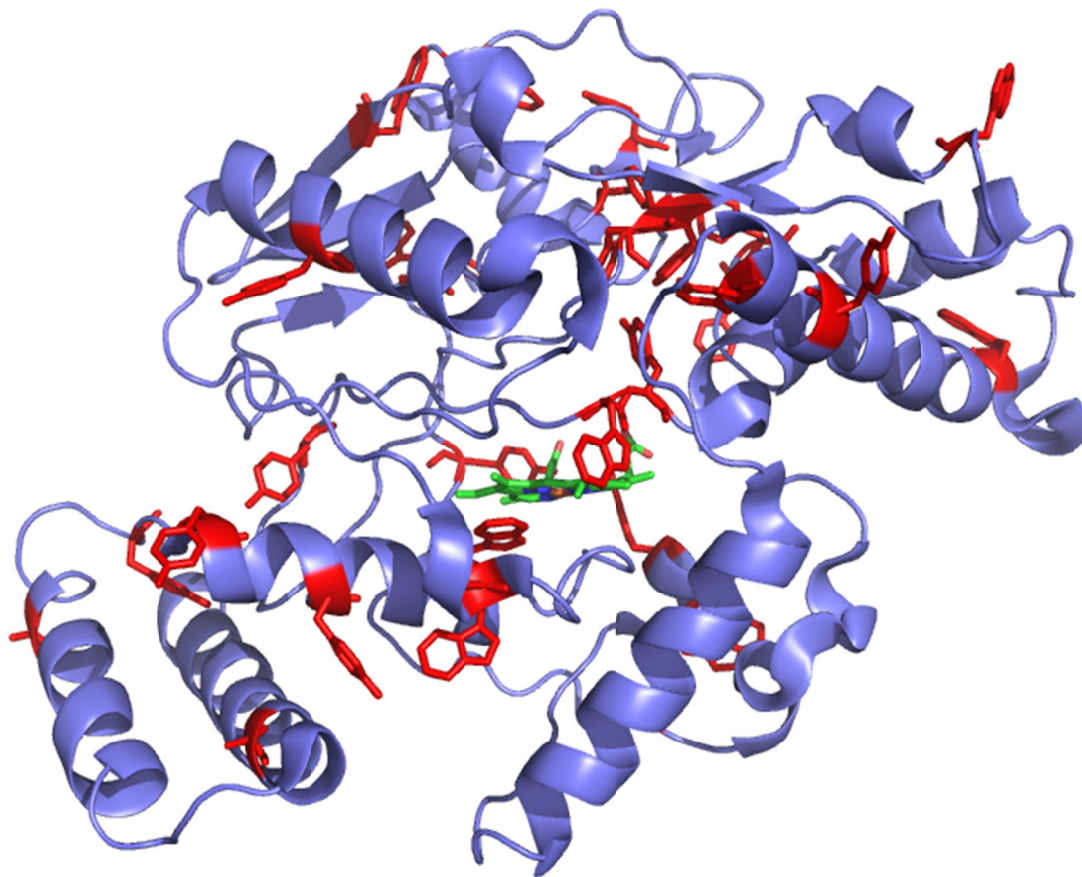


Figure 10. Wild type gsNOS showing all 28 Trp and Tyr residues in red.

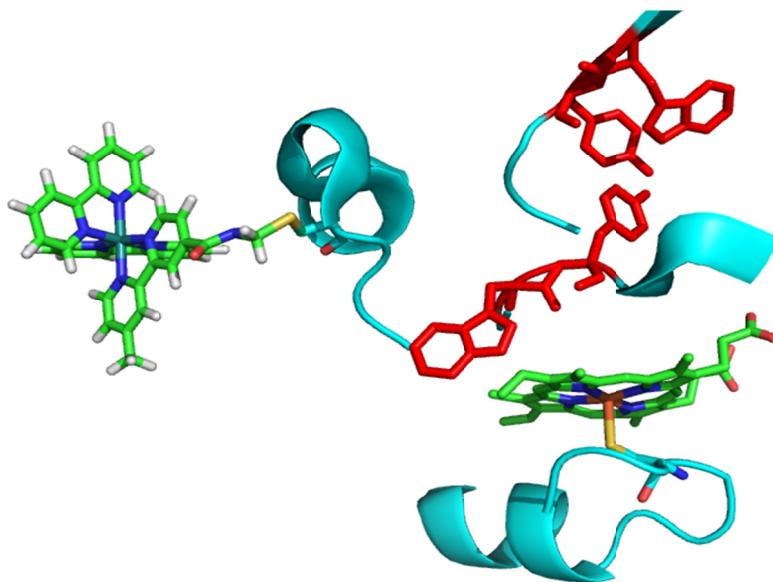


Figure 11. Model of labeled protein showing the location of several Trp and Tyr residues immediately between the label and the heme.

AII.4 Future Directions

This project was abandoned due to poor reproducibility of the labeling reaction and the lack of oxidation of the heme, as shown in the laser studies. We now know that reproducibility of the labeling reaction can be avoided by using an iodoacetamido-phenanthroline to label rather than an aryl bromide. See Ener *et al.*, *PNAS*, **2010**, *107*, 18783–18786. A note on synthesis of this new label: isolation was simplified by attaching aminophenanthroline to Ru(bpy)₂Cl₂ first (by a similar procedure used for step (3) above), and then mixing this complex with iodoacetic anhydride (1:1) in DCM and extracting this with an aqueous solution to remove iodoacetic acid. The product is light sensitive, so store it under foil. When this complex is used under the same labeling conditions as above or those published by Ener and coworkers, the labeling proved more reliable.

* Attempts were made to photochemically oxidize the heme with Ru(bpy)₃²⁺ in the presence of both reversible and irreversible oxidative quenchers. In neither case were any oxidative products observed, therefore covalent attachment was deemed necessary.